ADVANCED TESTING AND A NUMERICAL TOOL FOR SWELL EQUILIBRIUM LIMIT OF EXPANSIVE SOILS

Tests Avancés et un Outil d'analyse Numérique pour la limite de gonflements à l'équilibre des argiles expansives.

A Thesis Submitted to the Division of Graduate Studies
of the Royal Military College of Canada
by

Bee Fong Lim

In Partial Fulfillment of the Requirements for the Degree of
Doctor of Philosophy

October, 2014

ABSTRACT

Swelling-induced stresses and deformations have caused damage to buildings and infrastructure constructed in expansive soils. The cost of remediation and repairs on swelling-induced damages exceeds billions of dollars annually. The conventional swelling test has some limitations on measuring swelling pressures and volume changes that affect the analysis of swelling soils.

The swelling behavior of expansive clays is investigated through hydraulic mechanical advanced testing in the Swell Equilibrium Limit (SEL, Siemens and Blatz 2009) context. The SEL encompasses an upper bound limit of swelling-induced stresses and deformations under prescribed boundary conditions along with the applied pressure ranges from low stress to high confining stresses. A complete SEL is established from interpretation of triaxial and unconfined swelling tests. The unconfined swelling test is carried out in a newly developed testing apparatus. The maximum swelling deformation is determined by a non-contact method that incorporates digital image correlation. Various specimen aspect ratios are examined to determine the efficient test duration to achieve swelling equilibrium.

The SEL is used as a unifying framework to characterize swelling behavior of expansive soils in terms of swelling-induced stresses and volume change. A SEL catalogue is established with four tested materials that consist of a natural soil, two different recompacted soils and an engineered buffer. The index properties of each soil are studied in conjunction with the SEL curve fitting parameters. The developed correlation is used to calculate the preliminary SEL of Regina clay.

A numerical tool is developed to model swelling behavior in the SEL context. The numerical model used is the Sheng, Fredlund and Gens (SFG) model that requires two additional input parameters, including soil compressibility and saturation suction. The other input variables in the SFG model are based on the initial states of the soil and the applied boundary condition. A parametric study of the model is carried out to determine the sensitivity of the input parameters and the initial soil state. An example of a basement constructed in swelling soil is presented to demonstrate the model applicability to analyze swelling-induced stresses and deformations.

RESUME

Les contraintes et déformations induites par gonflement causent annuellement des dommages qui totalisent plusieurs milliards de dollars aux bâtiments et infrastructures construits dans les argiles expansives. Au présent, la conception et la construction des bâtiments sont guidés par les tests conventionnels du laboratoire et les stratégies d'analyse pour mesurer et prédire les pressions de gonflement et les changements de volume. Clairement il existe un écart entre l'état de la pratique pour caractériser les matériaux expansifs et l'analyse des applications d'ingénierie qui sont construites utilisent les sols expansifs. Cette thèse répond à ce besoin grâce à une nouvelle technique pour les tests du laboratoire, l'établissement d'un catalogue des résultats des tests de gonflement et le développement d'un outil d'analyse numérique pour prédire les contraintes et les déformations induites par gonflement.

Le comportement de gonflement de l'argile expansive est examiné par les tests avancés d'hydromécanique et est interprété dans le contexte de la limite de gonflements à l'équilibre (SEL, Siemens et Blatz, 2009). La SEL englobe une limite supérieure des contraintes et déformations induites par gonflement dans les conditions aux limites prescrites, avec la gamme de pression appliquée à partir de la contrainte nominale à la contrainte de confinement élevé. La limite de gonflement à l'équilibre complète est étayée par des tests triaxiaux et de gonflement non-confiné. Le test de gonflement non-confiné est accompli dans un laboratoire avec un nouvel appareil d'expérimentation. La déformation de gonflement maximale est déterminée par une méthode de non-contact qui intègre la corrélation des images numériques analysées avec le software geoPIV. Divers rapports d'aspects des spécimens sont testé pour déterminer le rapport de hauteur-

à-diamètre optimal qui permet l'achèvement de gonflement équilibre dans une période de test raisonnable.

La SEL est utilisé comme un cadre d'unification pour caractériser et prédire le comportement de gonflement dans les sols expansifs en fonction des contraintes induites par gonflement et le changement de volume. Un catalogue de SEL est établi par des tests sur quatre sols; ces sols consistent d'un sol naturel, deux sols différents qui sont ré-compacté et d'un tampon ingénierie. Les deux sols ré-compactés, spécifiquement l'argile ré-compacté de Bearpaw et l'argile de Lac Agassiz, ont été testés dans le gonflement triaxiaux et le gonflement non-confiné pour leur SEL interprétation. Les propriétés de l'index et les limites Atterberg de chaque sol sont rapportés en conjonction avec les paramètres d'ajustement de la courbe obtenus par le changement de volume de la SEL – la contrainte moyenne et la pression de gonflement – et les graphes EMDD. Le développement de cette corrélation est utilisé pour prédire la SEL de l'argile du Regina, qui est en accorde avec les données publiées.

Un outil d'analyse numérique est développé pour modéliser le comportement de gonflement dans le contexte de la SEL. L'outil d'analyse numérique est fondé sur le modèle de Sheng, Fredlund et Gens (SFG) qui a besoin de deux paramètres additionnels; la compressibilité du sol en gonflement et la succion de saturation. Ces paramètres sont en plus des propriétés des matériaux qui sont traditionnellement associés avec l'état critique. Les variables qui restent pour le modèle SFG sont basées sur les conditions du sol initial et les conditions aux limites appliquées pendant gonflement. Le modèle est appliqué avec succès aux résultats triaxiaux et de gonflement non-confiné sur un tampon ingénierie et un sol ré-compacté. Une étude paramétrique du modèle était aussi menée pour déterminer la

sensibilité des paramètres d'entrée et l'état du sol initial. Finalement, un exemple d'un mur de sous-sol construit dans le sol expansif est présenté pour démontrer l'applicabilité du modèle SFG pour prédire les contraintes et déformation induite par gonflement.

CO-AUTHORSHIP

The thesis from Chapter 1 through 5 is entirely the original work by the author under the supervision of her advisor, Dr. G.A. Siemens.

Chapter 2
A new unconfined swelling testing apparatus and methodology was designed and developed by the author. A series of unconfined swelling tests on two recompacted expansive soils were carried out by the author. The work has been published in *ASTM Geotechnical Testing Journal*:
Lim, B.F. and Siemens, G.A. (2013). An unconfined swelling test for clayey soils that incorporates digital image correlation. Geotechnical Testing Journal, 36(6), 1-11.

Chapter 3
The triaxial swelling apparatus was used by Siemens 2006 and Powell 2010 in their research. The author designed a modification to the triaxial apparatus to allow for novel installation of a suction measurement instrument at the base of the pedestal. A series of triaxial swelling tests were carried out by the author on two recompacted soils for the Swell Equilibrium Limit (SEL) interpretation (Siemens and Blatz 2009). A total of four test soils were examined for their swelling potential characterization in the SEL context. A SEL database was initiated and the SEL for Regina clay was calculated.

Chapter 3 is a draft manuscript prepared for consideration by *Canadian Geotechnical Journal*:
Lim, B.F. and Siemens, G.A. (2014) A unifying framework to characterize and model swelling behavior using advanced testing. *To be submitted to Canadian Geotechnical Journal*. November 2014.

Chapter 4
In Chapter 4, the research is on a numerical tool to model swelling behavior within the SEL context. The base constitutive model is the Sheng, Fredlund and Gens (SFG) model that requires two additional input parameters. The author formulated the SFG numerical model and calibrated it with advanced testing results in order to model swelling soil behavior in the SEL framework for expansive soils. Chapter 4 is a draft manuscript prepared for consideration *by Journal of Geotechnical and Geoenvironmental Engineering*:

Lim, B.F. and Siemens, G.A. (2014) A numerical tool for modelling swelling behavior of expansive soils. *To be submitted to Journal of Geotechnical and Geoenvironmental Engineering*. December 2014.

Other contributions
During the course of the research, the author was also involved in projects as a research assistant in the geotechnical laboratory at RMC under contract with Nuclear Waste Management Organization (NWMO). The author performed a series of triaxial tests to characterize material properties of light backfill saturated with $CaCl_2$ solution from year 2007 to 2010. In year 2011 to 2013, the author performed a series of triaxial tests on 70:30 bentonite-sand backfill saturated with saline solution (SR-270-PW) and de-ionized water. The results and interpretation from this project formed the basis for the following journal publication included in Appendix K:

Siddiqua, S., Siemens, G., Blatz, J., Man, A. and Lim, B.F. (2014).Influence of pore fluid chemistry on the mechanical properties of clay-based materials. Geotechnical and Geological Engineering, 32(4), 1029-1042.

References

Lim, B.F. and Siemens, G.A. 2013. An unconfined swelling test for clayey soils that incorporates digital image correlation. Geotechnical Testing Journal 36 (6): 1-11.

Powell, J. S. 2010. Geotechnical characterization of the bearpaw shale. Ph.D. Thesis., Department of Geological Sciences & Geological Engineering, Queen's University, Kingston, Ont.

Siddiqua, S., Siemens, G., Blatz, J., Man, A. and Lim, B.F. 2014. Influence of pore fluid chemistry on the mechanical properties of clay-based Materials. Geotechnical and Geological Engineering 32 (4): 1029-42.

Siemens, G. A. 2006. The influence of boundary conditions on the hydraulic-mechanical behavior of an unsaturated swelling soil. Ph.D. thesis., Department of Civil Engineering, University of Manitoba.

Siemens, G.A. and Blatz, J.A. 2009. Evaluation of the influence of boundary confinement on the behavior of unsaturated swelling clay soils. Canadian Geotechnical Journal (46): 339-56.

ACKNOWLEDGEMENTS

My gratitude goes to my advisor, Dr. Greg Siemens for his tireless effort in supporting me as a supervisor, mentor and encourager. His friendliness has made our communication and interaction a lot easier especially to someone like me who was foreign to this land.

Many thanks to the faculty members, supporting staffs, and friends from Civil Engineering Department, GeoEngineering Centre and RMC campus. Thank you for the conversations we had at the lunch room which has been very enriching to me. Not forgetting the kind and helpful technologists, Joe Dipietrantonio, Dexter Gaskin and Kristine Mattson for their precious technical support and endless patience.

To my dear parents and family in Malaysia, I'm very grateful for your understanding, moral support and love.

Last but not least, my spiritual family in Kingston. Thank you for your acceptance, forgiveness, prayers and love.

What a journey! Finishing this program took a little longer and harder than what I had expected but I have no regret of walking through this journey and having known all of you.

TABLE OF CONTENTS

LIST OF SYMBOLS AND ABBREVIATIONS

Symbols

A, B	- fitting parameters in V= A + B ln p
C, D	- fitting parameters in $p_{swell} = C^*e^{(D^*EMDD)}$
Δ	- change
ε_a	- axial strain
ε_r	- radial strain
ε_v	- volumetric strain
ν	- Poisson's ratio
ρ_w	- density of fluid (water)
ρ_d	- dry density
C_h	- suction compression index
C_s	- corrected swelling index
C_w	- suction modulus ratio
d	- day
d	- diameter of specimen
d_0	- initial diameter of specimen
e	- void ratio =(volume of voids)/(volume of solids)
f	- lateral restraint factor
f_c	- clay fraction
f_m	- montmorillonite fraction of clay
ρ_b	- bulk density
ρ_d	- dry density
γ_h	- suction compression index
G_s	- specific gravity
	- also specific gravity of non-clay material
G_n	- specific gravity of non-swelling clay

H	- height of specimen
λ_{vp}	- slope of the NCL for normally consolidated soils
λ_{vs}	- soil compressibility due to suction
λ_{ws}	- slope of main drying curve
I_p	- plasticity index
K	- correction parameter
κ_{ws}	- slope of scanning curve
p	- mean stress $=(\sigma_1+2\sigma_2)/3$
$\overline{p}$	- net mean stress $=(p-u_a)$
p_{equil}	- equilibrium mean stress
p_{swell}	- swelling pressure
p^c	- BBM model parameter
θ_w	- volumetric water content
R	- universal gas constant
R^2	- coefficient of determination
r	- radius of specimen
r_0	- initial radius of specimen
σ_1	- major stress
σ_2	- radial or minor stress
s	- coefficient for load effect
s	- suction $(=u_w-u_a)$
s_{sa}	- saturation suction
S_r	- degree of saturation
s_{ini}	- initial suction
s_{eot}	- end-of-test suction
t	- time
T	- absolute temperature
u_a	- pore air pressure

u_w	- pore water pressure
υ_{w0}	- specific volume of water
V (or v)	- specific volume =(1+e)
Vol	- volume
Vol_0	- initial volume
w	- gravimetric water content
ω_υ	- molecular mass of water vapor
Ψ_t	- total soil suction

Abbreviations

1-D - one dimensional

A - activity (=I_p / %f_c)

AEV - air-entry value

AR - aspect ratio (=Height/Diameter)

BBM - Barcelona Basic Model

BExM - Barcelona Expansive Model

BSB - bentonite sand buffer

CCD - charge coupled device (of digital camera)

CMS - constant mean stress

CS - constant stiffness

CV - constant volume

EOT - end-of-test

EMDD - effective montmorillonite dry density

LI - liquidity index

LL - liquid limit

MEBM - modulus of elasticity-based method

PI - plasticity index

PL - plastic limit

RH - relative humidity

SEL - swell equilibrium limit

SFG - Sheng, Fredlund and Gens

SLR - single-lens reflex

SWCC - soil water characteristic curve

LIST OF TABLES

LIST OF FIGURES

CHAPTER 1: INTRODUCTION

1.1 General Overview

Unsaturated soil mechanics has been developed as an extension of saturated soil mechanics in order to understand soil behavior under negative pore pressure (suction). The theoretical basis and framework used in saturated soil mechanics cannot be extended for unsaturated soils. The presence of suction changes the conventional saturated soil behavior and its characteristics. In nature, the change in suction corresponds to the seasonal fluctuation of the ground water table in the soil. As a result, additional stress state variables such as suction need to be included in soil deformation and stress-strain relationships.

Expansive soils provide a unique challenge in the field of unsaturated soil mechanics. These soils can be beneficial if their intrinsic soil behavior is designed for and managed. For example, the swelling potential of expansive soils can be used to construct an evapo-transpirative cover system, landfill liner and an engineered buffer for an underground waste repository (Siemens 2006). These systems make use of the self-healing capacity of the soil to reduce the permeability and hence control contamination initiating from the waste. On the other hand a substantial amount of dollars are spent annually on damage due to swelling. Swelling nature can cause excessive deformations and swelling-induced stresses on adjacent structures. This damage can be prevented with a better understanding of the soil behavior under both unsaturated and saturated conditions.

1.2 Analysis Methods for Swelling Soil

Developing practical tools that can be used in engineering design is the main motivation of many researchers in unsaturated soils. A literature review on the previous research works to develop an analysis tool for swelling soil behavior is presented in the following.

Briaud et al. (2003) mentioned a few existing methods that are used to estimate vertical deformation of swelling soil. These methods include the potential vertical rise (PVR) method (McDowell 1956), suction methods (McKeen 1992) and the Clod test (Miller et al. 1995). The PVR method does not calculate vertical heave directly but the relative volume change is estimated from the field water content and Atterberg limits instead. The vertical deformation estimated would be the upper bound swelling potential. The suction method proposed in McKeen (1992) requires inputs such as, suction compression index (C_h), lateral restraint factor (f), coefficient for load effect (s) and initial as well as final suction in the soil. The other approach of swelling soil analysis is the Clod method (Miller et al. 1995). The advantage of using Clod method is that it leads to site-specific values of suction compression index. Besides that, Clod method uses resin that could hold fractured soil together whereas it would not be possible on a trimmed sample. However, this method does not calculate vertical deformation directly.

Vanapalli et al. (2012) proposed an empirical equation that can estimate swelling pressure with respect to the soil-water characteristic curve for sand-bentonite mixtures. This method is an extension of the semi-empirical technique developed in estimating swelling pressure of natural expansive soils that requires plasticity index and the variation of moisture content of the soil (Vanapalli et al. 2010). The application of SWCC in estimating swelling pressure needs more comprehensive understanding of the effect from compaction method and compaction water content.

Vanapalli and Lu (2012) have made a comprehensive review on various techniques to estimate swelling pressure and one-dimensional (1-D) deformation for expansive soils. According to Vanapalli and Lu (2012), the analysis for swelling soil could be generalized into three main groups, namely empirical method (Vanapalli et al. 2010), oedometer test method (Fredlund 1983, Sridharan et al. 1986) and suction method (McKeen 1992).

The empirical method relates swelling potential to classification and index property of the expansive soils. Vanapalli et al. (2010) proposed an empirical estimation equation which requires three inputs, such as corrected swelling index (C_s), suction modulus ratio (C_w) and correction parameter, K (function of water content and plasticity index, I_p). The widely used oedometer test method in swelling soil is given by Fredlund (1983) where vertical heave is calculated from free swell test and swelling pressure is obtained from "corrected" pressure from a swell-load curve. The suction methods incorporate suction measurement or correlation as a stress state input in swelling behavior.

Adem and Vanapalli (2014) have performed a study on soil-environment interactions in modelling for expansive soils where the overall volume changes (due to shrinkage or swelling) is attributed to water content and matric suction changes in unsaturated expansive soils. They have used a modulus of elasticity-based method (MEBM, Adem and Vanapalli 2013) to model the soil-environment interactions with an expansive soil.

1.3 Swelling in Expansive Soils

Swelling mechanisms in expansive unsaturated soil are dependent on the clay mineralogy, stress history, loading condition and change in suction. Among these factors the intrinsic soil property is its clay mineralogy. Various types of clay minerals that can be found in clayey soils; namely, kaolinite, chrolite, illite, smectite (e.g. montmorillonite) and others (Mitchell and Soga 2005). Most of the expansive soils have a significant montmorillonite component. Montmorillonite is a high plasticity swelling clay material with high liquid limit and its clay mineral is made up of 2:1 structure. Swelling in montmorillonite is due to the diffused double layer between the clay platelets. The clay surface is negatively-charged and the hydroxyls (cation) from water molecules are easily attracted to the clay surface. Replacement of the interlayer cations by water molecules results in only partial satisfaction of the net negatively charged surface since the water molecule has a net neutral charge. The net increase in repelling forces causes swelling at the microscopic level. The major contributor to swelling is the interaction between montmorillonite particles. Therefore it is essential to investigate the swelling characteristic under the influence of montmorillonite content.

Research that has contributed to the study of swelling behavior in terms of mineralogy or geo-chemistry interaction is included in the papers published by Katti and Shanmugasundaram (2001), Komine and Ogata (2004), Tripahty et al. (2004) and Thakur and Singh (2005).

1.4 Numerical Models for Unsaturated soils

Numerical studies in unsaturated soils are typically developed with reference to the models used in saturated soils. The extended application of saturated soil model in unsaturated soils requires additional stress variables and hardening equation to capture the suction-induced changes on soil behavior. Some of the commonly used unsaturated soil models are summarized in the following section.

Barcelona Basic Model (BBM) developed by Alonso et al. (1990) is one of the most widely used constitutive models in unsaturated soils. This model was initially studied with slightly or moderately expansive soils that are represented by a compacted kaolin and a sandy clay with suction control. In developing the BBM model, an elasto-plastic hardening model using two independent sets of stress variables was established. In simulating unsaturated soils behavior with respect to effects of suction, a total of nine input parameters are required in the model. Wheeler et al. (2002) made some comments on the use of BBM model. Their comments include a suggestion for a practical approach of selecting model parameter, p^c from test data.

Wheeler and Sivakumar (1995) developed an unsaturated soil elasto-plastic critical state framework that is based on BBM model (Alonso et. al 1990). The model is applied to a series triaxial test on compacted speswhite kaolin with suction-control. In addition to nine input parameters required in BBM model, a new parameter is introduced, specific water volume, v_w. They have suggested that the future development of unsaturated soil model should consider the simplification on model input requirement that would be more practical for design analysis.

Alonso et al. (1999) developed an unsaturated expansive soil model that is based on the earlier BBM (Alonso et al. 1990). This model is named, Barcelona Expansive Model (BExM) that considers two levels of structure, micro-structure and macro-structure. BExM is applied to simulate test data obtained from oedometer tests with suction-control on compacted Boom clay. The model includes the effect of cyclic behavior on drying-wetting paths. In micro-macrostructure interaction, swelling occurs when suction cycles are applied at low stress; compression is observed when suction cycles are applied at high stress.

Blatz and Graham (2003) proposed an elastic-plastic model for compacted high plasticity sand-clay mixture. The compacted clay is tested in a new triaxial apparatus with suction control. The suction device is buried in the triaxial specimen. The study is focused on the influence of suction on yield stress and shear strength. The future works recommended is the possibility of coupling suction-induced yielding and loading-induced yielding resulted from plastic hardening.

Sheng et al. (2008) developed an unsaturated soil model, namely Sheng, Fredlund and Gens (SFG) model that relates two independent stress-strain variables in terms of net stresses and suction. The model is a new volume-stress-suction relationship that accommodates effects of hysteresis of wetting-drying cycles. Various stress paths can be defined with this model. SFG equations model the unsaturated soil behavior of various tested soils. The test data includes compacted bentonites with suction change (Lloret et al. 2003), compacted Pearl clay (Sun et al. 2007) and initial slurry soil (Fredlund 1964). The advantage of this new model is that it requires only two additional input parameters of soil compressibility and saturation suction. The numerical analysis studied in Chapter 4 is based on SFG model.

1.5 Objectives

The main objective of this research program is to further understand swelling soil behavior through advanced experimental work and develop an engineering analysis tool with a numerical model for expansive soils. These objectives can be achieved through the following steps:

a. Develop a new testing apparatus and methodology for unconfined swelling test as an extended study of SEL curve at low stress levels. The program includes a new apparatus design (humidity-confined chamber), selection of suitable digital camera and lenses, testing methodology and digital image analysis software.

The triaxial swelling apparatus requires a modification at the pedestal to allow for relative humidity measurement at the specimen (Appendix E). The relative humidity is correlated to total suction for unsaturated analysis.

b. Apply SEL as an unifying framework to characterize swelling soils and calculate a SEL of an expansive soil with the correlation to the initial soil condition and index properties. Two additional expansive soils are tested for the SEL interpretation. A SEL catalogue is developed, which allows analysis of SELs of expansive soils.

c. Develop an engineering analysis tool for swelling-induced stresses and deformation. A numerical model is investigated for its applicability to utilize experimental data obtained from advanced testing in practical design analysis.

1.6 Organization of Thesis

This thesis is presented in a manuscript format in accordance to the outline given by Division of Graduate Studies and Research at Royal Military College of Canada – Thesis Preparation Guidelines (version 3 December 2013).

Chapter 1 consists of a general introduction, research objectives and organization of the thesis. Chapter 2 through Chapter 4 is original manuscripts of the research work. The overall conclusions drawn from the research are presented in Chapter 5.

Chapter 2 presents the development of a new testing apparatus and methodology of an unconfined swelling test. The free state of swelling boundary condition allows for SEL curve to be interpreted at low stress levels. The innovation of this new apparatus employs non-contact measurement of swelling deformation which is correlated with digital image interpretation. The maximum swelling deformation under unconfined boundary condition is quantified successfully. The result from digital image correlation is in good agreement with caliper measurement at the end of tests.

Chapter 3 extends the application of SEL curve in characterizing expansive soils. The SEL is used as a unifying framework to investigate swelling-induced stresses and deformation under prescribed boundary conditions ranging from free swelling to rigid constant volume swelling. A catalogue of expansive clays is established with four tested soil materials. The correlation of SEL curves with a soil's initial state and index properties allows for a SEL calculation to be made.

Chapter 4 presents the applicability and development of an unsaturated numerical tool for swelling soil analysis. The experimental data from advanced testing is modelled successfully with SFG model. The applicability of SFG model in swelling soil analysis makes it an attractive tool in practical design because of its simple requirement of input parameters.

The overall conclusions of the thesis are summarized in Chapter 5.

1.7 Research Novelty

High quality of swelling deformation measurement on unconfined swelling test specimen is presented in Chapter 2. This work has improved the measurement quality on the soil specimen that swells under no confining boundary condition.

Chapter 3 establishes the database of expansive soils swelling behavior that is interpreted in SEL concept. The database is developed from high quality experimental result tested using the advanced triaxial and unconfined swelling apparatuses.

SFG modelling in Chapter 4 offers geotechnical practitioners a simple analysis tool to calculate swelling-induced stresses and deformations with two calibrated input parameters from SEL test data.

1.8 References

Adem, H. and Vanapalli, S. 2014. Soil-environment interactions modelling for expansive soils. Environmental Geotechnics: 1-10.

Adem, H. and Vanapalli, S.K. 2013. Constitutive modeling approach for estimating the 1-D heave with respect to time for expansive soils. International Journal of Geotechnical Engineering 7 (2): 199-204.

Aitchison, G. D. 1973. The quantitative description of the stress-deformation behavior of expansive soils – preface to set of papers. Proceedings of the 3rd International Conference on Expansive Soils 2 : 79-82.

Alonso, E.E., Gens, A., and Josa, A. 1990. A constitutive model for partial saturated soils. Géotechnique 40 (3): 405-30.

Alonso, E.E., Vaunat, J. and Gens, A. 1999. Modelling the mechanical behavior of expansive clays. Engineering Geology 54 : 173-83.

Blatz, J.A. and Graham, J. 2003. Elastic-plastic modelling of unsaturated soil using results from a new triaxial test with controlled suction. Géotechnique 53 (1): 113-22.

Briaud, J.L., Zhang, X., and Moon, S. 2003. Shrink test–water content method for shrink and swell predictions. Journal of Geotechnical & Geoenvironmental Engineering 129 (7): 590-600.

Fredlund, D. G. 1983. Prediction of ground movements in swelling clays. 31st Annual Soil Mechanics and found Engineering Conference. University of Minnesota, Minneapolis: 1-48.

———. 1964. Comparison of soil suction and one-dimensional consolidation characteristic of a highly plastic clay. Technical Report no. 245, Division of Building Research, National Research Council, Ottawa, Ont.

Katti, D.R. and Shanmugasundaram, V. 2001. Influence of swelling on the microstructure of expansive clays. Canadian Geotechnical Journal 38 : 175-82.

Komine, H., and Ogata, N. 2004. Predicting swelling characteristics of bentonites. Journal of Geotechnical & Geoenvironmental Engineering 130 (8): 818-29.

Lloret, A., Villar, M. V., Sànchez, M., Gens, A., Pintado, X., and Alonso, E. E. 2003. Mechanical behavior of heavily compacted bentonite under high suction changes. Géotechnique 53 (1): 27-40.

Lytton, R. L. 1994. Prediction of movement in expansive clays. Proc., Settlement' 94 Conf., Geotechnical Spec. Publ. no. 40, ASCE, Reston, Var. 2 : 1827-45.

McDowell, C. 1956. Interrelationships of loads, volume change, and layer thickness of soils to the behavior of engineering structures. Highway Research Board, Proc., 35th Annual Meetings, Publ. no. 426, Transportation Research Board, Washington, D.C.: 754-72.

McKeen, G. R. 2001. Investigating field behavior of expansive clay soils. Paper presented at Proceedings of Expansive Clay Soils and Vegetative Influence on Shallow Foundations, Houston, Texas.

Miller, D. J., Durkee, E. B., Chao, K. C., and Nelson, J. D. 1995. Simplified heave prediction for expansive soils. Proc., 1st Int. Conf. on Unsaturated Soils, Balkema, Rotterdam, the Netherlands: 891-7.

Mitchell, J.K. and Soga, K. 2005. Fundamentals of soil behavior. 3rd Edition ed. Canada: John Wiley & Sons.

Seed, H.B., Woodward, R.J., Jr and Lundgren, R. 1962. Prediction of swelling potential for compacted clays. Journal of Soil Mechanics and Foundation Engineering Division ASCE 88 : 53-87.

Sheng, D., Fredlund, D.G. and Gens, A. 2008. A new modelling approach for unsaturated soils using independent stress variables. Canadian Geotechnical Journal(45): 511-34.

Sridharan, A., Rao, A. and Sivapullaiah, P.V. 1986. Swelling pressure of clays. Geotechnical Testing Journal 9 (1): 24-33.

Sun, D., Sheng, D. and Xu, Y. 2007. Collapse behavior of unsaturated compacted soil with different initial densities. Canadian Geotechnical Journal 44 : 673-86.

Thakur, V.K.S. and Singh, D.N. 2005. Rapid determination of swelling pressure of clay minerals. Journal of Testing and Evaluation 33 (4): 239-45.

Tripathy, S., Sridharan, A. and Schanz, T. 2004. Swelling pressures of compacted bentonites from diffuse double layer theory. Canadian Geotechnical Journal 41 : 437-50.

Vanapalli, S.K. and Lu, L. 2012. A state-of-the art review of 1-D heave prediction methods for expansive soils. International Journal of Geotechnical Engineering 6 (15): 41.

Vanapalli, S.K., Lu, L. and Oh, W.T. 2010. Estimation of swelling pressure and 1-D heave in expansive soils. Unsaturated Soils, Barcelona, Spain. September 6-8, 2010. Eds: Alonso, E & Gens, A., CRC Press 2 : 1201-7.

Vanapalli, S.K., Lu, L., Sedano, J.A.I. and Oh, W.T. 2012. Swelling characteristics of sand-bentonite mixtures. Unsaturated Soils: Research and Applications: 77-84.

Wheeler, S. J. and Sivakumar, V. 1995. An elasto-plastic critical state framework for unsaturated soil. Géotechnique 45 (1): 35-53.

Wheeler, S.J., Gallipoli, D. and Karstunen. 2002. Comments on use of the Barcelona basic model for unsaturated soils. International Journal for Numerical and Analytical Methods in Geomechanics 26 : 1561-71.

CHAPTER 2: AN UNCONFINED SWELLING TEST FOR CLAYEY SOILS THAT INCORPORATES DIGITAL IMAGE CORRELATION

2.1 Introduction

The characterization of swelling potential is of critical importance in the analysis and design of infrastructure founded in swelling soil. The behavior of expansive soil is complicated by excessive volume changes during swelling and the development of swelling-induced stresses when expansion is restrained. Damage to infrastructure founded in swelling soil due to excessive deformation is measured in billions of dollars every year (Keller 2008, Puppala and Cerato 2009). The swelling ability of soil also provides self-healing qualities, which can also be utilized in waste isolation applications. Design optimization requires accurate analysis of swelling potential and swelling pressures.

Traditionally, the swelling potential and swelling pressures are measured using an oedometer apparatus as shown schematically in Figure 2.1a (ASTM D4546-96). Specimens are subjected to wetting under free swell or constant volume conditions. The test results provide the maximum vertical swelling strain or vertical swelling pressure. Recently the standard test was revised (ASTM D4546-08), and it now calls for the application of constant vertical stress conditions followed by wetting. Several tests are completed at increasing vertical stresses until the stress that inhibits swelling is determined. The test method imposes laterally constrained conditions on the swelling behavior, but these conditions rarely persist in the field. Numerous researchers and practitioners have successfully used these, or similar, test methods to characterize expansive soils (Komine and Ogata 1994, Dixon et al. 2002, Rao and Tripathy 2003, DiMaio et al. 2004, Rao et al. 2004, Imbert and Villar 2006, Peng and Horn 2007, Cerato et al. 2009, Nagaraj et al. 2009, Baille et al. 2010, Ito and Azam 2010, Singhal et al. 2011, Kodikara 2012, Lee et al. 2012 and Powell et al. 2012a, 2012b, 2013). Micro-porosity effects on the behavior of swelling materials have also been examined (Siemens et al. 2007 and Vallejo 2011). Vallejo (2011) studied the influence of pore micro geometry on the slaking of shale and concluded that smoother and smaller pores have a reduced resistance to slaking.

Rojas et al. (2011) reported a test methodology and apparatus for measuring wetting and drying water-retention curves using the vapor equilibrium technique, and they also included digital image analysis to measure deformations. Compacted bentonite specimens were subjected to constant relative humidity environments and the specimens either shrank or swelled in response to the imposed suction level. Soil images were captured during the test with a digital single-lens reflex (SLR) camera and strains were interpreted using commercial photo-editing software. Their results confirm the effectiveness of the vapor equilibrium method for applying wetting and drying conditions and non-contact measurement techniques to measure soil strains.

Siemens and Blatz (2009) reported a unifying framework for the behavior of swelling soils. Termed the Swell Equilibrium Limit, the framework can be used to analyze swelling-induced pressures and swelling strains based on the initial conditions and the boundary conditions during swelling. The soil is characterized, as illustrated in Figure 2.1b, with constant mean stress, constant stiffness, or constant volume boundary conditions imposed during triaxial swelling tests (Siemens and Blatz 2007). The end points of the swell tests are then connected to form the Swell Equilibrium Limit. The Swell Equilibrium Limit was developed for a highly swelling engineered barrier with 50% bentonite (Siemens and Blatz 2009) and later was applied to a natural soil (Powell et al. 2013). The Swell Equilibrium Limit framework works well at stress conditions found in many applications and may have several uses within a single engineering application.

Figure 2.1c displays a retaining wall system that provides multiple boundary conditions to the surrounding swelling soil. Below the cantilever wall, the swelling soil is under a constant mean stress boundary imposed by the constant vertical stress from the overlying soil and concrete. Under wetting conditions, the soil underneath the wall footing swells along a vertical stress path in a specific volume–mean stress (V-p) space. Adjacent to the retaining wall, the soil swells against the wall, which leads to displacement. This complex soil–structure interaction has been idealized as a constant stiffness boundary, which is a spring-like boundary condition. In V-p space, the stress path plots along a sloped line, with the slope angle being a function of the wall stiffness. The other boundary condition would be a perfectly stiff wall that would plot as a horizontal stress path in V-p space (not shown).

Few studies have focused on swelling soil behavior at low stresses. The Swell Equilibrium Limit framework has been characterized using triaxial swelling tests, but its use at low stress levels has not been investigated. Continuing with the retaining wall example [Figure 2.1c], the soil underneath the road in front of the retaining wall will swell against a pseudo-unconfined condition at a shallow depth. In this location, free swell conditions persist; however, one-dimensional conditions do not. Given the significant non-linearity in the Swell Equilibrium Limit [Figure 2.1b and Figure 2.1c], accurate analysis of the potential vertical deformations at these low stresses is very difficult. This motivated the author to develop a new test apparatus and methodology for characterizing the swelling potential at low stresses under true free swell boundary conditions.

Herein we propose an unconfined swelling test for measuring the maximum swelling potential for direct water access. The swell measurements obtained from the unconfined swelling test allow the Swell Equilibrium Limit framework to be applied at low stresses where significant non-linearity is expected [Figure 2.1b and Figure 2.1c]. The soil specimen is given free access to water and allowed to deform without any restraining boundary condition upon swelling. The test method uses digital image correlation or particle image velocimetry (GeoPIV) (White et al. 2003), which has been used in many geotechnical applications to measure soil deformations. Test results are presented to verify the apparatus and methodology, and then preliminary interpretation is provided in the Swell Equilibrium Limit framework.

2.2 Test Apparatus

The unconfined test apparatus provides water uptake and a high humidity environment to soil specimens to enable measurement of their unrestrained swelling potential. A photograph of an overall view of the unconfined swelling test setup is shown in Figure 2.2a. Plan and cross-section drawings are included in Figure 2.2b and 2.2c. The configuration allows for five unconfined swelling tests to be completed simultaneously. The apparatus is constructed from 25.4-mm-thick Perspex and includes a sealed box that is 1.00 m wide, 0.24 m tall, and 0.20 m deep. The box is designed with a removable cover to allow digital images to be captured without obstruction and to allow water to be applied during the test. A rubber seal is placed around the edge of the removable cover, and vacuum grease is applied to ensure that the box is sealed during the swelling tests. Soil specimens are given direct access to water via spraying and wicking action from filter paper strips dipped into the reservoir. At the beginning of the test, six 10-mm-wide wicking strips are secured radially around the soil specimens with the ends placed in the water reservoir. The reservoir also maintains a high humidity level in the airspace within the box.

The process for making manual measurements of specimen height and diameter during the test is difficult because of the size of the specimens and the size constraints within the box. Unconfined swelling test durations can range from a few weeks to a few months depending on the size of the specimen. Thus a noncontact displacement measurement technique is incorporated into the apparatus. Digital images of the soil specimens are recorded using a digital SLR camera. Figure 2.3 illustrates typical deformations that are recorded during an unconfined swelling test. The camera is attached to a custom mount, and the mount is placed into a slot to position the camera in front of a soil specimen [see Figure 2.2a, 2.2b, and 2.2c for camera, mount, and slot locations]. Soil deformations during the unconfined swelling test are measured by interpreting digital images using GeoPIV (White et al. 2003). A rigid frame with black circular targets is positioned around each pedestal. The locations of the targets are measured in a local coordinate system. The software uses the targets on the frame to correct digital images for small differences in the location of the camera and as reference locations to calculate soil deformations within a local coordinate system. Targets are also secured to the top of the soil specimen along its center plane. Soil specimen targets are used to track soil deformations during the unconfined swelling test.

The choice of a suitable digital camera and lens was made during the design stage. Of the possible suitable combinations, a Canon EOS Digital Rebel XTi with an EFS60mm f/2.8 Macro USM Lens was selected to record digital images of the soil specimens. The camera has a CCD that is 14.8 mm by 22.2 mm in size with an image resolution of 2592 pixels by 3888 pixels. The focal length of the macro lens is 60 mm. The camera is located 0.69 m in front of the center plane of each soil specimen, giving an average resolution of 0.04 mm/pixel. The camera is relocated from one slot to another slot to take images of soil specimens at each location. To prevent undesired movement while recording a digital image, a remote control with a self-timer setting of 2s is used.

2.3 Test Methodology and Analysis

Unconfined swelling tests may be performed on natural or remolded specimens. A series of tests was carried out in the same or similar configuration to assess the repeatability of the testing method. According to the test method, test specimens are prepared and their initial mass, dimensions, and water content are recorded. Six 10-mm-wide wicking strips are installed along the side of the specimen. Figure 2.3 displays the wicking strips and illustrates typical deformations recorded during an unconfined swelling test. Two GeoPIV targets are pinned diametrically on the top surface of the specimen for image analysis. The soil specimen, with the wicking strips and targets, is then placed on a pedestal inside the sealed box. The specimen is located in such a way that the specimen targets face the camera and are in the same plane as the frame of the GeoPIV targets. Once the compacted soil specimen is placed on the pedestal, an initial photograph is recorded and the legs of the wicking strips are submerged in the water reservoir. To maintain the specimens in a pseudo-submerged state, de-ionized water is sprayed at the specimens on a daily basis. Water is sprayed all around each specimen until the wicking strips and soil specimen are visibly wet. The cover of the humidity box normally remains closed to prevent the loss of humidity through evaporation. The cover is opened only when an image is to be captured or when the specimens are sprayed. Periodically, digital images are taken of the soil specimen, which also requires opening of the sealed box. Between spraying events, the wicking strips effectively retain moisture in the soil specimen. In our tests, a relative humidity probe within the box airspace confirmed that the relative humidity was greater than 9 9%.

Unconfined swelling tests continue until the specimen equilibrates with the moist environment. Progressive swelling of compacted specimen 189_AR=0.15 at elapsed times of 1 day, 1.8 days, and 9.7 days is shown in Figure 2.3. The dashed box in the figure indicates the original size of the soil specimen prior to wetting. Significant swelling deformations can be observed in this series of images. At the end of the test, the final dimensions, mass, and moisture contents of swelled specimens are measured. The spatial distribution of the moisture content is measured by dividing specimens vertically using a knife and then radially using two circular cutting rings with diameters of 36.4 mm and 13.6 mm. The soil specimen is divided to the outermost diameter, middle diameter, and core section. This division allows for the moisture content distribution to be measured radially across the specimen.

2.3.1 Deformation analysis

Soil deformation is measured using a non-contact method employing the image-based software GeoPIV (White et al. 2003), which allows for real-time measurements. The software calculates soil deformation over a series of digital images by searching for characteristic patches of pixels in consecutive digital images and calculating the displacement. Vertical and horizontal displacements are inferred from the measured movement of GeoPIV targets installed on diametrically opposite sides of the top of specimens (Figure 2.3). A secondary option is to select a patch of pixels at the intersection between the bottom of the target holder and the edge of the specimen, as illustrated in Figure 2.3a. From the vertical and horizontal displacement measurements at the top edges of the specimen, axial strain and radial strain are calculated to determine the volume strain of the specimen during the test. The results obtained from the GeoPIV analysis are then compared with the caliper measurements taken at the end of the test. Strain analysis of soil deformation in the test uses the following equations:

[2.1] $$\varepsilon_a = \frac{\Delta H}{H_o}$$

[2.2] $$\varepsilon_r = \frac{\Delta r}{r_o} = \frac{\Delta d}{d_o}$$

[2.3] $$\varepsilon_v = \frac{\Delta Vol}{Vol_o}$$

where $\varepsilon_a =$ axial strain, $\Delta H =$ change in height, $H_o =$ initial height, $\varepsilon_r =$ radial strain, $\Delta r =$ change in radius, $r_o =$ initial radius, $\Delta d =$ change in diameter, $d_o =$ initial diameter, $\varepsilon_v =$ volumetric strain, $\Delta Vol =$ change in volume, and $Vol_o =$ initial volume.

In geotechnical analysis, small strains are normally assumed; however, this assumption is invalid in the analysis of unconfined swelling tests because of the large deformations. Therefore, the volume strain is calculated from axial and radial strains as (Ehrgott 1971)

[2.4] $$\frac{\Delta Vol}{Vol_o} = \varepsilon_a + 2\varepsilon_r - 2\varepsilon_r\varepsilon_a + \varepsilon_r^2(\varepsilon_a - 1)$$

2.4 Results and Interpretation

The material used to verify the capabilities of the unconfined swelling test was Bearpaw clay-shale, which was obtained from Southern Saskatchewan (Powell et al. 2012a, 2012b, 2013). Bearpaw is classified as high-plasticity clay with liquid and plastic limits ranging from 99% to 145% and 22% to 29%, respectively, and is composed of 39% clay. The profile consists of high plasticity soil from depths of 30 to 90 m, and remolded specimens from sample with ID189 were used for the testing program. Remolded specimens were prepared from dried and pulverized soil that was mixed to a target water content using the method described by Siemens (2006). The moistened soil was double-bagged and stored in a refrigerator for 48 h to allow for moisture equilibrium and a confirmatory measurement of the moisture content. The soil was removed and compacted into 50-mm-diameter specimens in lifts. Initial testing focused on optimizing the aspect ratio while holding the diameter constant. The aspect ratio (AR) is defined as

[2.5] $$AR = \frac{Height}{Diameter}$$

2.4.1 Unconfined swelling test results

An unconfined swelling test on specimen ID189 with AR=0.15 is presented as a typical test to display the capabilities of the unconfined swelling test apparatus and methodology. The specimen was compacted to a target initial state of modified Proctor optimum, which was determined to have a gravimetric water content of 15% and a dry density of 1.74 Mg/m^3. Table 2.1 highlights the initial conditions of the test specimens. Following preparation, the specimen was installed and given access to water. The swell results in terms of axial, radial, and volumetric strain versus time, plotted on both linear and logarithmic axes, are shown in Figure 2.4a and 2.4b, respectively. The specimen swelled at a high initial rate, and then the swell rate decreased after a few days. The volumetric strains of the soil specimen were 60% and 61% after 14 and 21 days, respectively (Figure 2.4). The specimen expanded radially more than axially, and both expansions equilibrated with the moisture conditions at similar times. When the same data are re-plotted on a semi-log scale [Figure 2.4b], the result resembles an unloading curve on a consolidation plot. Peng and Horn (2007) investigated the anisotropic behavior of some organic and inorganic soils that underwent shrinkage and swelling processes. They found that a typical swelling curve consists of two distinctive parts, the virgin swelling and the residual swelling curves. The virgin swelling curve contributes more than 80% of the total soil volume expansion. The semi-log plot [Figure 2.4b] also shows two distinctive swelling slopes, a primary swelling slope and a secondary swelling slope. The secondary swelling slope represents a decreasing rate of volume change over time. The primary swells at a gradient of 80%/cycle and decreases to 9%/cycle along the secondary swelling curve [Figure 2.4]. The intersection of the two curves indicates the end of primary swelling. For specimen 189_AR=0.15, the end of primary swelling occurred at t=2.5 d, which is very efficient for this type of test. Overall, primary swelling contributes more than 80% of the total swelling strains (volumetric strain at t=2.5 is 54%, and final total swell is 63%), which is consistent with results from Peng and Horn (2007). After four days, the specimen swelled at a log-linear rate for the remainder of the test. The test was completed after 27 days.

Test results for four specimens, which varied in their target ARs (AR=0.15, 0.25, 0.75, and 2.0), are presented in Figure 2.5 on linear and logarithmic time scales. The four specimens had identical initial dry densities of 1.7 Mg/m^3, except for the specimen with AR=0.25, which had a density of 1.6 Mg/m^3. The varying ARs enabled an interpretation of the dimensional effect on swelling behavior. The test results show similar trends with high initial swelling rates that decreased over time. The specimens with smaller ARs (0.15, 0.25, and 0.75) reached equilibrium in less than 20 days and achieved similar overall swelling magnitudes. The initial rate of swelling is related to the AR of a specimen; the smaller the AR, the higher the rate of swelling. The specimen with AR=2.0 had a significantly lower initial swelling rate and, based on Figure 2.5a, achieved a significantly lower swelling magnitude at the end of the test.

Re-plotting the time-dependent swell data on a semi-log plot [Figure 2.5b] shows similar results for the specimens with lower ARs and different behavior for the larger AR (AR=2.0). The three lower AR specimens showed distinctive primary and secondary swelling curves with progressively increasing equilibration times ranging from 2.5 days for AR=0.15 to 19 days for AR=0.75. Even after almost 70 days of testing, a secondary swelling curve was not evident in the AR=2.0 specimen. If the primary swelling curve is projected to the equilibrium strains for the smaller specimens, the end of primary swelling may arrive at between 120 and 250 days. A swelling test of this length is not feasible for normal site characterizations.

The time required in order to achieve the end of primary swelling is directly related to the AR and the associated drainage length of the specimen.

Unconfined swelling test results are summarized in Table 2.2 in terms of the duration needed to reach the end of primary swelling, primary swelling slope, secondary swelling slope, and initial swelling rate. Smaller ARs are associated with higher surface-area-to-volume ratios. Holding the initial diameter constant and increasing the height from 7.6mm (AR=0.15) to 101.9mm (AR=2.0) resulted in a 100-fold increase in the time to the end of primary swelling. The specimens that arrived at the end of primary swelling showed consistent swell magnitudes relative to their initial conditions. Thus, reducing the size decreases the overall testing time without having a significant effect on the final results.

The use of image analysis allows the measurement of axial and radial deformations that can be used to study potential anisotropic swelling behavior. Axial and radial strains are plotted against time in Figure 2.4a, and further data are presented in Figure 2.6, which shows radial strain versus axial strain. Also plotted in Figure 2.6 are triaxial swelling results from constant mean stress swelling tests, performed at 200 kPa and 400 kPa mean stress, on Bearpaw clay (Powell et al. 2013). The unconfined swelling test results initiate at the origin and plot into the lower left quadrant. The four swelling tests show internal variability in terms of the relative anisotropy; however, broadly speaking, swelling occurs along the 1:1 line. Figure 2.6b shows a close-up view of the higher stress swelling data. During swelling, the deformations occur along similar slopes in the higher stress tests, indicating that the swell properties are consistent with what is observed in the unconfined swelling tests.

2.4.2 End-of-test measurements

The end-of-test measurements display the consistency of the results, as well as the benefits of using smaller test specimens. The end-of-test volume strain is plotted in Figure 2.7 and summarized in Table 2.3 versus the AR. The GeoPIV and caliper end-of-test measurements are in good agreement, as plotted in Figure 2.7. The difference between the caliper measurement and GeoPIV analysis is within 2 mm, as presented in Table 2.3. The effect of the discrepancy was analyzed, and it contributes to a difference in volumetric strain of +4% to -19% depending on the original size of the specimens. Caliper measurements are generally different, as the soil specimen will have become very soft by the end of the test. Extreme care is needed when taking caliper measurements on the softened soil. The average swelling deformation from the caliper measurement and GeoPIV analysis is around 70%. This deformation is considered as the maximum volumetric strain upon wetting. The two types of volume measurements show general agreement with similar end-of-test volume strains and changes in height and diameter.

After the unconfined swelling tests are complete, the spatial distribution of the moisture content is measured radially. The gravimetric water content is measured at three different radial locations (R1, R2, and R3, moving from the center to the perimeter of the specimen) using cutters with diameters of 36.4 mm and 13.6 mm. The results in Figure 2.8 show that the water content decreased toward the inner core of the specimen. The water content at the outer area of the specimen was the highest relative to the other two locations. The outer area of the soil specimen has the most direct access to water; water needs to permeate a longer path through the soil particles toward the core of the specimen.

Summaries of the end-of-test measurements are plotted in Figure 2.9 and listed in Table 2.4. Figure 2.9a demonstrates the results for the gravimetric water content of the specimens at the beginning and the end of swelling tests. The target initial compacted state was optimum water content and dry density. By the end of the test, the water content had increased to a range of 46% to 67%. The final degree of saturation reached more than 90% [refer to Figure 2.9b], which indicates high saturation, especially considering that there was no external confining stress or back pressure applied to the specimens. The initial and the end-of-test specific volumes are plotted in Figure 2.9c. The soil specimens had relatively homogeneous compaction because the initial specific volume was in the range of 1.57 to 1.61, except in the specimen with AR=0.25, which had a slightly larger void (V=1.72) and a slightly lower initial dry density (ρ_d=1.60 Mg/m^3).

In order to demonstrate that the specimens had achieved a satisfactory degree of saturation by the end of the test, data are presented in a plot of dry density versus gravimetric water content. In Figure 2.10, the initial compacted soil specimens are close to the optimum point. By the end of the test, the soil specimens had reached the line above S_r=90%, which indicates a high degree of saturation. The extent to which the soil swelled from its compacted state demonstrates the high swelling potential of the Bearpaw clay-shale.

2.5 The Swell Equilibrium Limit of Compacted Bearpaw Soil

The Swell Equilibrium Limit is a unifying concept used to analyze the maximum swelling potential which may be realized as expansion or swelling induced pressure. Powell et al. (2013) reported a Swell Equilibrium Limit for natural Bearpaw, which is presented in Figure 2.11 along with the unconfined swell data from the current study. Powell et al. (2013) reported triaxial swelling and oedometer swelling pressure test results and showed the influence of sample depth on the Swell Equilibrium Limit. The data from the unconfined swelling tests are plotted along the y-axis in the linear scale and at 0.1 kPa (arbitrary value) in the semi-log plot [Figure 2.11b]. There is noted variation in the final specific volume values for the unconfined swelling tests; however, this is in line with the variation noted by Beddoe et al. (2011) in swelling tests on geosynthetic clay liners performed at 2 kPa vertical stress. A Swell Equilibrium Limit for sample 189 is interpreted from the oedometer tests and unconfined swelling tests. With the low-stress data points, the upper-bound limit of swelling potential in this framework is measured experimentally. The data points at very low stress represent the worst-case scenario in which a soil would expand to its full potential at low confining stress.

2.6 Conclusions

An unconfined swelling test apparatus and methodology are presented for measuring the maximum swelling deformation of a soil under true free stress conditions. The methodology includes a non-contact method using digital image analysis to measure deformations. The in-test results indicate that primary and secondary swelling behavior and anisotropic swelling can be measured using the employed non-contact deformation method. The soil swelling deformation calculated with GeoPIV analysis is also in general agreement with end-of-test measurements. The effect of the AR on the swelling behavior is noted regarding the initial swelling rate and the time needed to reach equilibrium with the applied wetting conditions. The end-of-test measurements indicate consistent behavior for the specimens tested and that a high degree of saturation was achieved during the test. The maximum swelling deformation for Bearpaw soil is in the range of 60% to 70% volumetric strain under unconfined swelling conditions. The results are interpreted in the Swell Equilibrium Limit framework to allow of swelling soil deformations. This extends the use of the Swell Equilibrium Limit framework down to low stress levels.

2.7 References

Aiban, S. A. 2006. Compressibility and swelling characteristics of Al-khobar palygorskite, Eastern Saudi Arabia. Engineering Geology 87 : 205-19.

ASTM D4546. Standard test methods for one-dimensional swell or settlement potential of cohesive soils. In . Philadephia, Pennsylvania: ASTM.

Baille, W., Tripathy, S., and Schanz, T. 2010. Swelling pressures and one-dimensional compressibility behaviour of bentonite at large pressures. Applied Clay Science 48 : 324-33.

Beddoe, R.A., Take, W.A. and Rowe, R.K. 2011. Water-retention behavior of geosynthetic clay liners. Journal of Geotechnical & Geoenvironmental Engineering 137 (11): 1028-38.

Cerato, A.B., Miller, G.A. and Hajjat, J.A. 2009. Influence of clod-size and structure on wetting-induced volume change of compacted soil. Journal of Geotechnical & Geoenvironmental Engineering 135 (11): 1620-8.

Cuisinier, O. and Masrouri, F. 2004. Testing the hydromechanical behavior of a compacted swelling soil. Geotechnical Testing Journal 27 (6): 1-9.

DiMaio, C., Santoli, L., Schiavone, P. 2004. Volume change behaviour of clays: The influence of mineral composition, pore fluid composition and stress state. Mechanics of Materials 36 : 435-51.

Dixon, D.A., Chandler, N.A. and Baumgartner, P. 2002. The influence of groundwater salinity and influences on the performance of potential backfill materials. Paper presented at Proceedings of the 6th International Workshop on Design and Construction of Final Repositories, Backfilling in Radioactive Waste Disposal, Brussels.

Ehrgott, J. Q. 1971. Calculation of stress and strain from triaxial test data on undrained soil specimens. Defense Atomic Support Agency., Report No. S-71-9.

Ferber, V., Auriol, J., Cui, Y. and Magnan, J. 2008. Wetting-induced volume changes in compacted silty clays and high-plasticity clays. Canadian Geotechnical Journal 45 : 252-65.

Gokhale, K.V.G.K. and Jain, K.K. 1972. Anisotropic swelling in black cotton soil. Bulletin of the International Asscociation of Engineering Geology 5 (1): 63-71.

Imbert, C. and Villar, M.V. 2006. Hydro-mechanical response of a bentonite pellets/powder mixture upon infiltration. Applied Clay Science 32: 197-209.

Ito, M. and Azam, S. 2010. Determination of swelling and shrinkage properties of undisturbed expansive soils. Geotechnical and Geological Engineering 28 : 413-22.

Keller, E. A. 2008. Environmental Geology. 8th ed. USA: Prentice hall.

Kodikara, J. 2012. New framework for volumetric constitutive behaviour of compacted unsaturated soils. Canadian Geotechnical Journal 49 (1227): 1243.

Komine, H. and Ogata, N. 1994. Experimental study on swelling characteristics of compacted bentonite. Canadian Geotechnical Journal 31 (4): 478-90.

Lee, J. O., Lim, J.G., Kang, I.M. and Kwon, S. 2012. Swelling pressures of compacted Ca-bentonite. Engineering Geology 129-130 : 20-6.

Likos, W. J. 2004. Measurement of crystalline swelling in expansive clay. Geotechnical Testing Journal 27 (6): 1-7.

Mishra, A.K., Ohtsubo, M., Li, L. and Higashi, T. 2011. Controlling factors of the swelling of various bentonites and their correlations with the hydraulic conductivity of soil-bentonite mixtures. Applied Clay Science 52 : 78-84.

Nagaraj, H.B., Munnas, M.M. and Sridharan. 2009. Critical evaluation of determining swelling pressure by swell-load method and constant volume method. Geotechnical Testing Journal 32 (4): 1-10.

Peng, X. and Horn, R. February 2007. Anisotropic shrinkage and swelling of some organic and inorganic soils. European Journal of Soil Science 58 : 98-107.

Powell, J. S. 2010. Geotechnical characterization of the bearpaw shale. Ph.D. Thesis., Department of Geological Sciences & Geological Engineering, Queen's University, Kingston, Ont.

Powell, J.S., Siemens, G., Take, W.A. and Remenda, V. 2013. Characterizing the swell potential of bearpaw shale. Engineering Geology 158 : 89-97.

———. 2012. Influence of specimen geometry on sample disturbance observed in oedometric testing of clay shales. Geotechnical Testing Journal 35 (5): 1-13.

Prakash, K. and Sridharan, A. 2004. Free swell ratio and clay mineralogy of fine-grained soils. Geotechnical Testing Journal 27 (2): 1-6.

Puppala, A.J., Manosuthikij, T., Nazarian, S., Hoyos, L.R. and Chittoori, B. 2011. In situ matric suction and moisture content measurements in expansive clay during seasonal fluctuations. Geotechnical Testing Journal 35 (1): 1-9.

Puppala, A. J. and Cerato, A.B. 2009. Heave distress problems in chemically-treated sulfate laden materials. Geostrata: 28-32.

Rao, A.S., Phanilumar, B.R. and Sharma, R.S. 2004. Prediction of swelling characteristics of remoulded and compacted expansive soils using free swell index. Quarterly Journal of Engineering Geology and Hydrogeology 37 : 217-26.

Rao, K.S.S. and Tripathy, S. 2003. Effect of aging on swelling and swell-shrink behavior of a compacted expansive soil. Geotechnical Testing Journal 26 (1): 1-11.

Robinson, R.G., Dasari, G.R., and Tan, T.S. 2004. Three-dimensional swelling of clay lumps. Geotechnique 54 (1): 29-39.

Rojas, J.C., Gallipoli, D. and Wheeler, S.J. 2010. Image analysis of strains in soils subjected to wetting and drying. Geotechnical Testing Journal 35 (1): 1-14.

Siemens, G. and Blatz, J.A. 2007. Triaxial apparatus for applying liquid infiltration with controlled boundary conditions and internal suction measurement. Journal of Geotechnical & Geoenvironmental Engineering 133 (6): 748-52.

Siemens, G. A. 2006. The influence of boundary conditions on the hydraulic-mechanical behaviour of an unsaturated swelling soil. Ph.D. thesis., Department of Civil Engineering, University of Manitoba.

Siemens, G.A. and Blatz, J.A. 2009. Evaluation of the influence of boundary confinement on the behaviour of unsaturated swelling clay soils. Canadian Geotechnical Journal(46): 339-56.

Singhal, S., Houston, S.L. and Houston W.N. 2011. Effects of testing procedures on the laboratory determination of swell pressure of expansive soils. Geotechnical Testing Journal 34 (5): 1-13.

Vallejo, L. E. 2011. Mechanics of the slaking of shales. Geomechanics and Engineering: An International Journal 3 (3): 219-31.

White D.J., Take W.A. and Bolton M.D. 2003. Soil deformation measurement using particle image velocimetry (PIV) and photogrammetry. Géotechnique 53 (7): 619-31.

Wray, W.K., El-Garhy, B.M. and Youssef, A.A. 2005. Three-dimensional model for moisture and volume changes prediction in expansive soils. Journal of Geotechnical & Geoenvironmental Engineering 131 (3): 311-24.

Table 2.1. Initial conditions for unconfined swelling tests.

Test ID	Target aspect ratio, H/d	Height, H (mm)	Diameter, d (mm)	Bulk density, ρ_b (Mg/m^3)	Dry density, ρ_d (Mg/m^3)	Water content, w (%)	Void ratio, e (-)	Specific volume, V (-)	Degree of saturation, S_r (%)
189_AR=0.15	0.15	7.6	51.2	2.02	1.71	17.8	0.61	1.61	81.0
189_AR=0.25	0.25	13.7	51.4	1.85	1.60	15.6	0.72	1.72	59.5
189_AR=0.75	0.75	38.9	51.5	2.02	1.75	15.2	0.57	1.57	73.8
189_AR=2.0	2.0	101.9	51.6	2.00	1.74	15.3	0.58	1.58	72.4

Table 2.2. Swelling rate for unconfined swelling.

Test ID	Target aspect ratio, H/d	Surface-area / volume (m^2/m^3)	Time to end of primary swelling (d)	Primary swelling slope (%/cycle)	Secondary swelling slope (%/cycle)	Initial swelling rate (%/d)
189_AR=0.15	0.15	0.34	2.5	-80	-9	0.227
189_AR=0.25	0.25	0.22	4	-35	-7	0.147
189_AR=0.75	0.75	0.13	19	-39	-20	0.081
189_AR=2.0	2.0	0.10	120-250[1]	-37	-	0.045

[1]Projected

Table 2.3. Comparison of caliper and GeoPIV of end-of-test measurements for unconfined swelling tests.

Test ID	Target aspect ratio	Caliper		GeoPIV		Difference between caliper and GeoPIV		
	H/d	Height, H (mm)	Diameter, d (mm)	Height, H (mm)	Diameter, d (mm)	Height, H (mm)	Diameter, d (mm)	ΔEOT Volumetric strain (%)
189_AR=0.15	0.15	9.7	61.3	8.7	61.3	-1.0	0.0	-19
189_AR=0.25	0.25	15.7	60.9	15.8	59.4	0.1	-1.5	-7
189_AR=0.75	0.75	45.7	61.3	46.4	61.3	0.7	0.0	4
189_AR=2.0	2.0	117.5	59.3	117.4	57.3	-0.1	-2.0	-10

$\Delta EOT = \varepsilon_{V(GeoPIV)} - \varepsilon_{V(Caliper)}$

Table 2.4. End-of-test results for unconfined swelling.

Test ID	Height, H (mm)	Diameter, d (mm)	Bulk density, ρ_b (Mg/m^3)	Dry density, ρ_d (Mg/m^3)	Water content, w (%)	Void ratio, e (-)	Specific volume, V (-)	Degree of saturation, S_r (%)	Volumetric strain, ε_v (%)
189_AR=0.15	9.7	61.3	1.56	0.97	61.4	1.84	2.84	91.8	-62.5
189_AR=0.25	15.7	60.9	1.68	1.01	66.5	1.72	2.72	106.4	-54.4
189_AR=0.75	45.7	61.3	1.66	1.08	53.8	1.54	2.54	96.0	-71.4
189_AR=2.0	117.5	59.3	1.70	1.16	46.7	1.38	2.38	93.4	-45.1

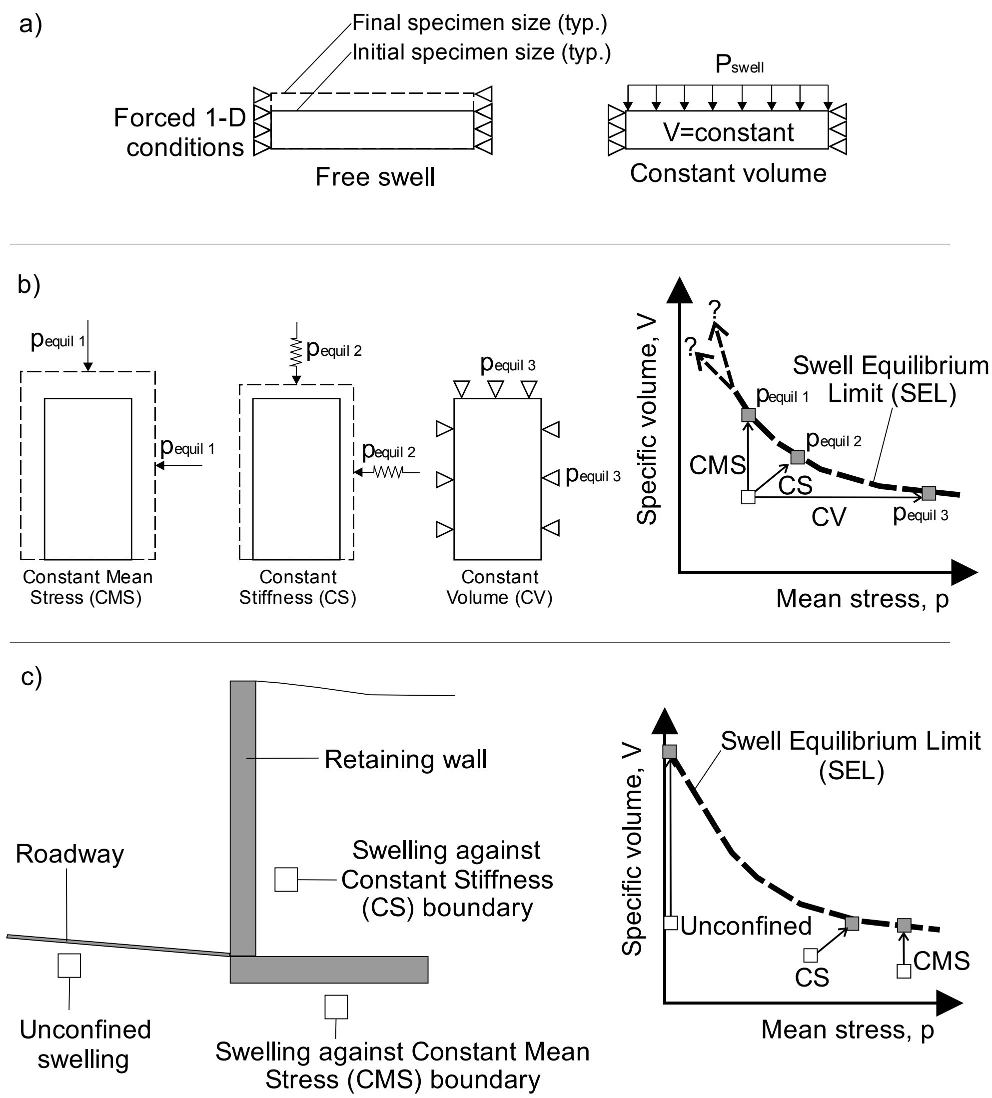

Figure 2.1. (a) Traditional swelling tests: free swell and swelling pressure tests. (b) Triaxial swelling tests: boundary conditions during swell tests and Swell Equilibrium Limit (SEL) schematic. (c) Practical application of SEL: unconfined swelling under a roadway, swelling under foundation (constant mean stress), and swelling against a retaining wall (idealized as constant stiffness).

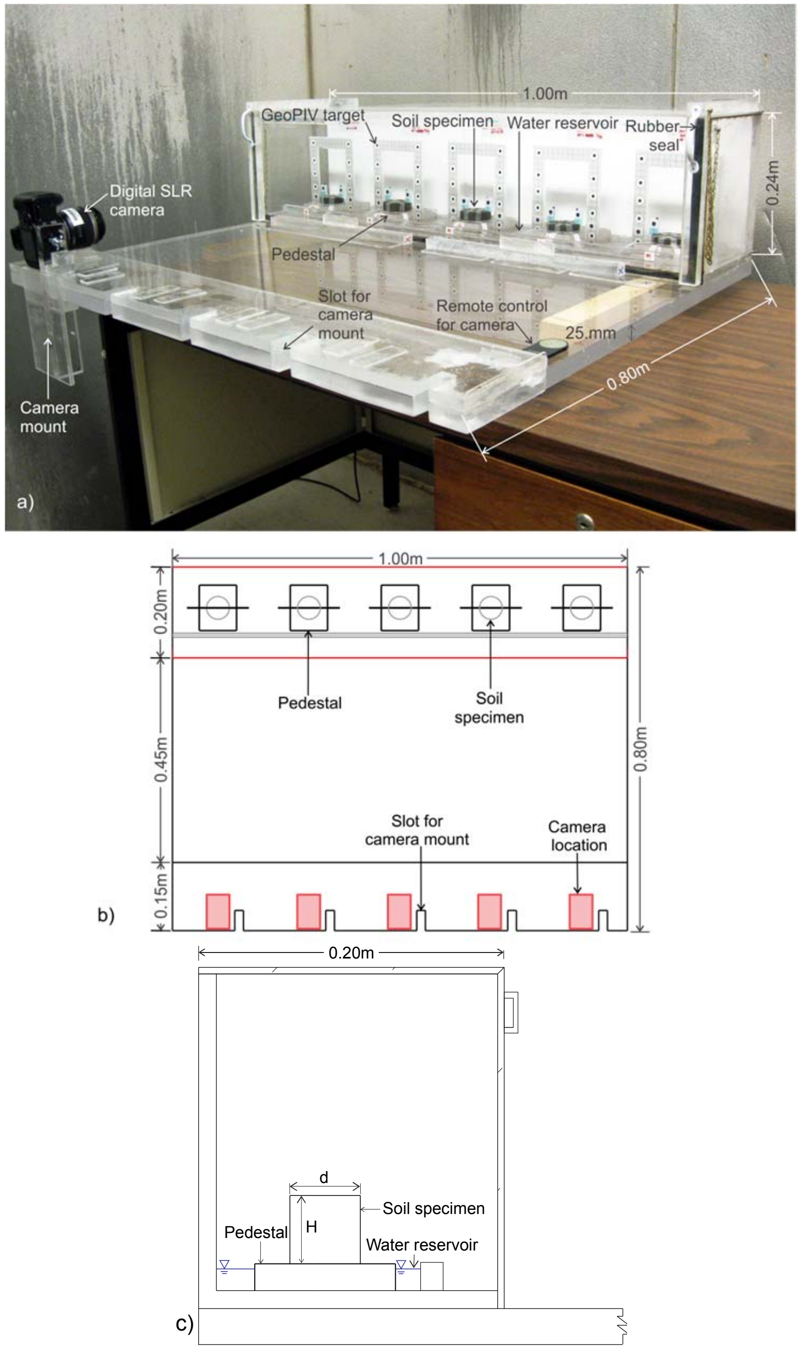

Figure 2.2. Unconfined swelling test apparatus: (a) photograph; (b) plan view drawing; and (c) side view.

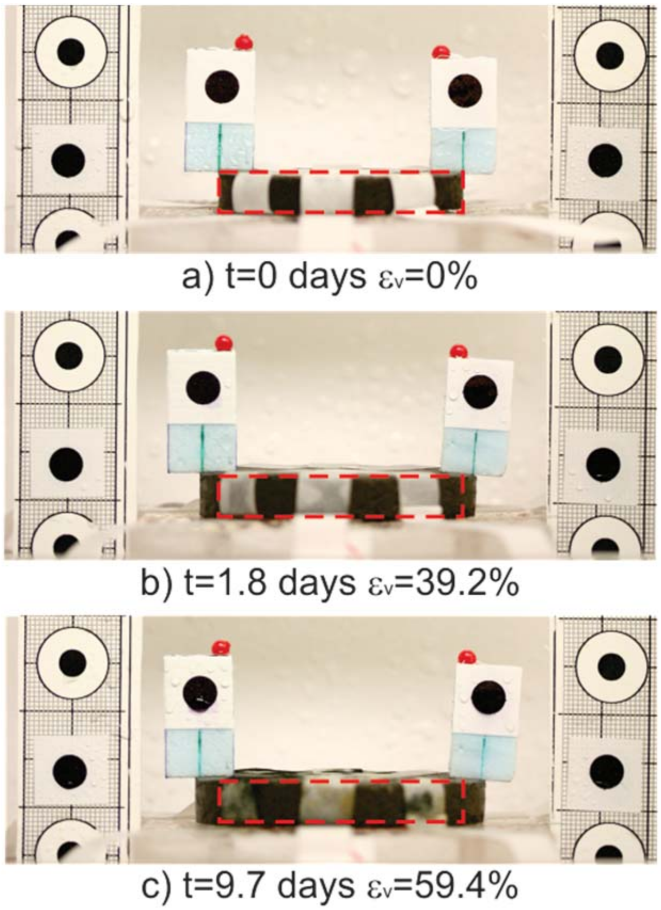

a) t=0 days ε_v=0%

b) t=1.8 days ε_v=39.2%

c) t=9.7 days ε_v=59.4%

Figure 2.3. Progressive swelling of specimen 189_AR=0.15.

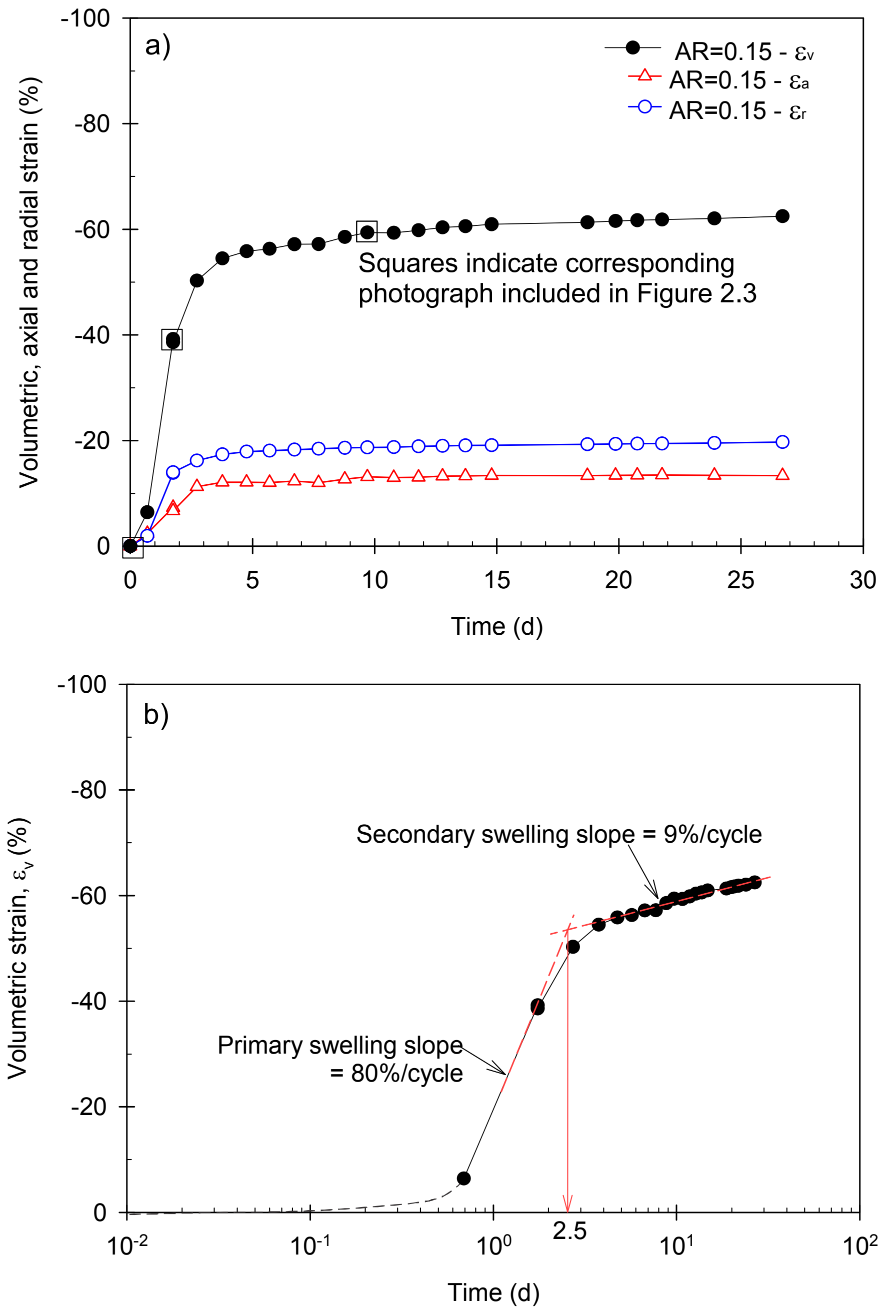

Figure 2.4. Volumetric, axial, and radial strain versus time for 189_AR=0.15 upon wetting plotted versus time on (a) a linear scale and (b) a logarithmic scale.

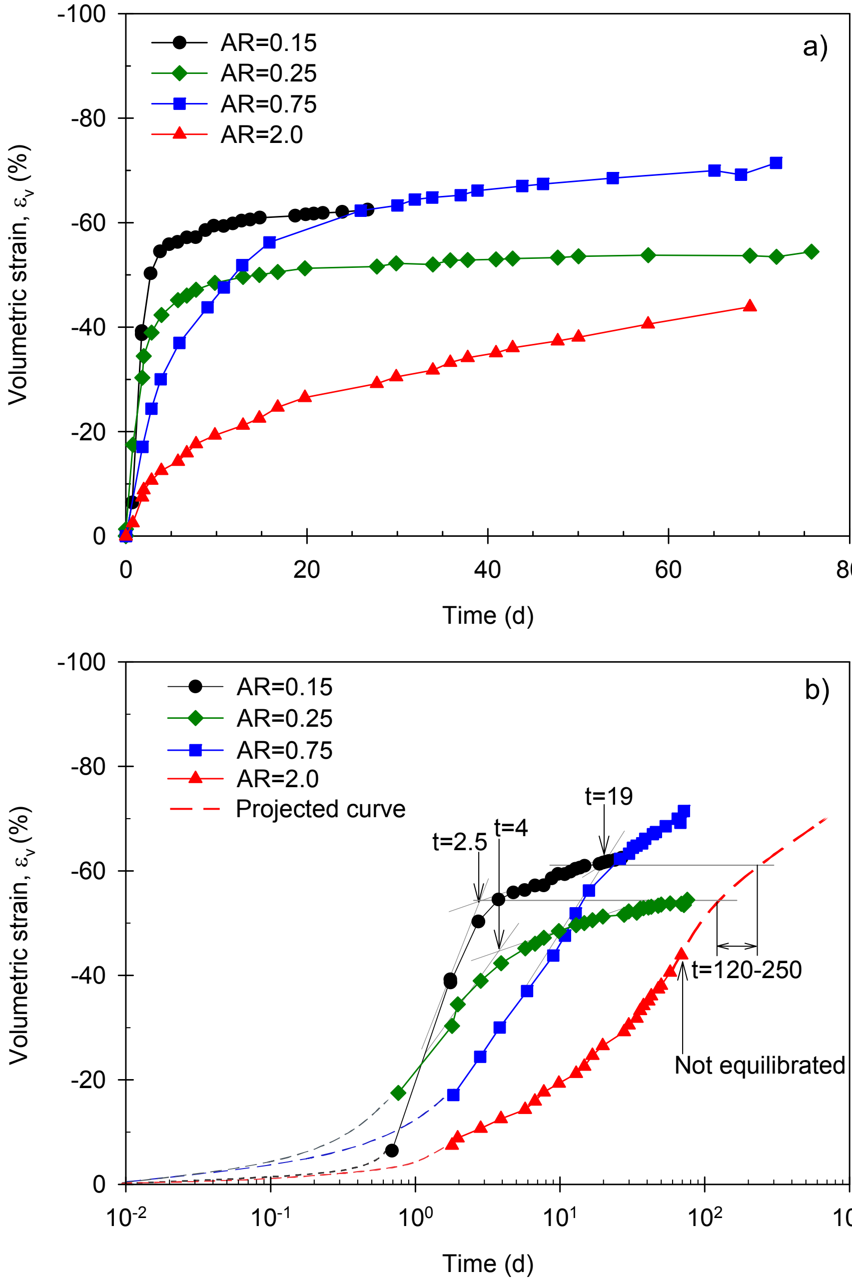

Figure 2.5. Volumetric strain versus time for varied aspect ratios plotted on (a) a linear scale and (b) a logarithmic scale.

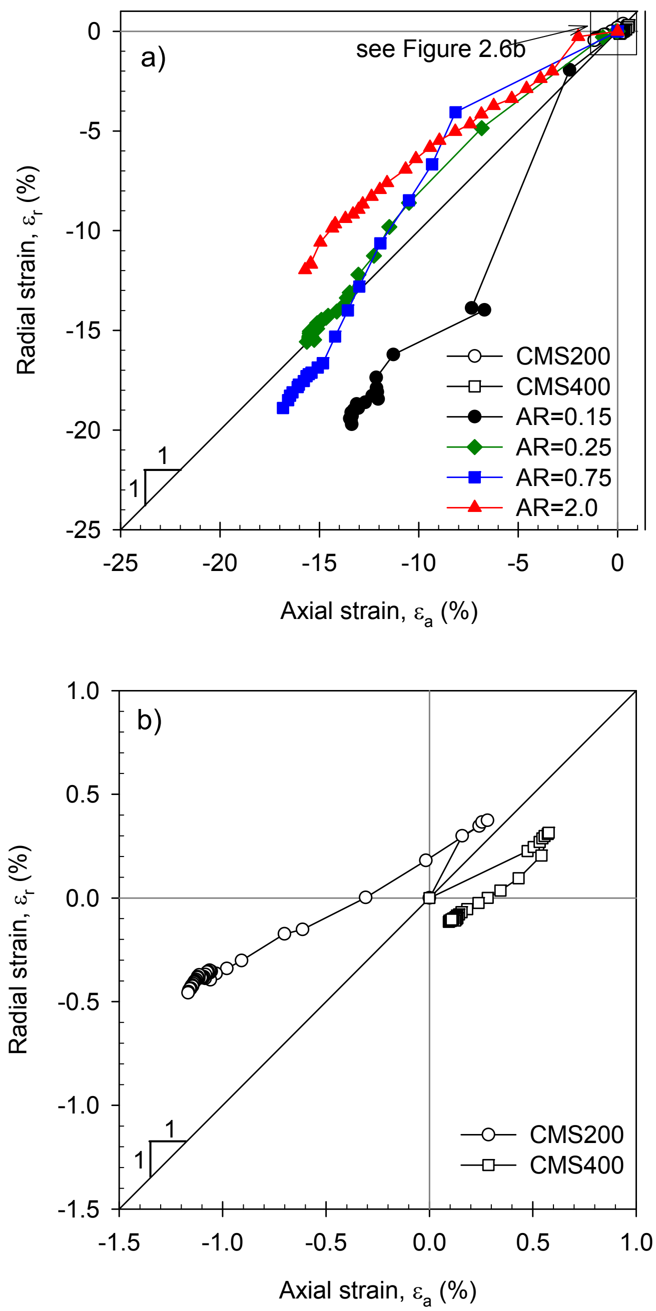

Figure 2.6. Radial strain versus axial strain upon swelling highlighting the similarity to triaxial swelling tests in part (b).

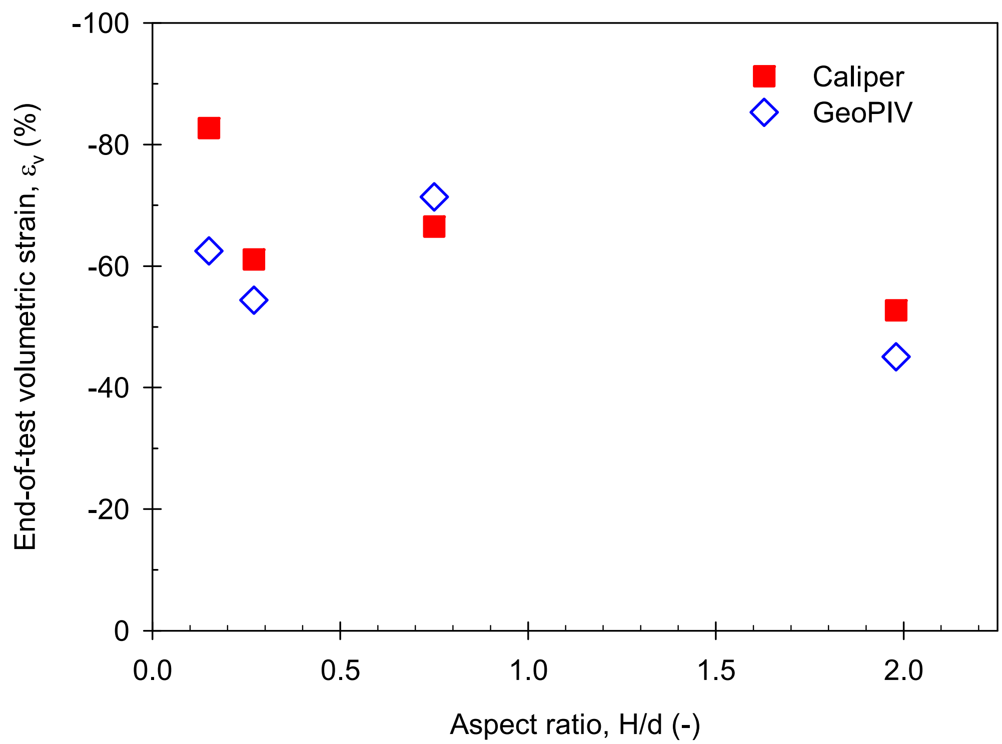

Figure 2.7. End-of-test volumetric strain versus aspect ratio (H/d) for caliper and GeoPIV methods.

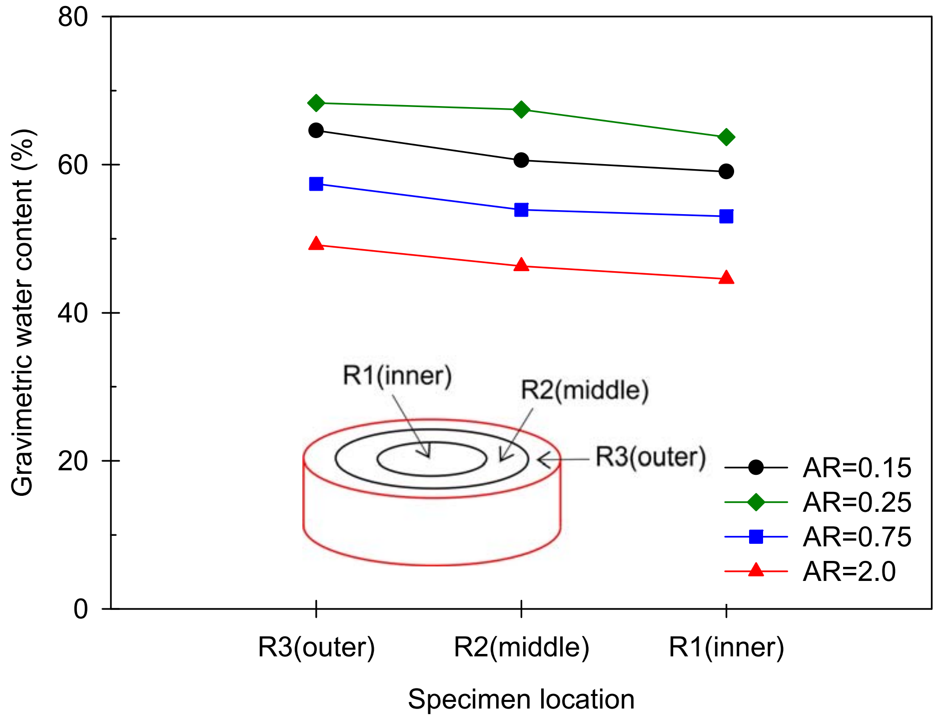

Figure 2.8. Spatial distribution of end-of-test moisture content.

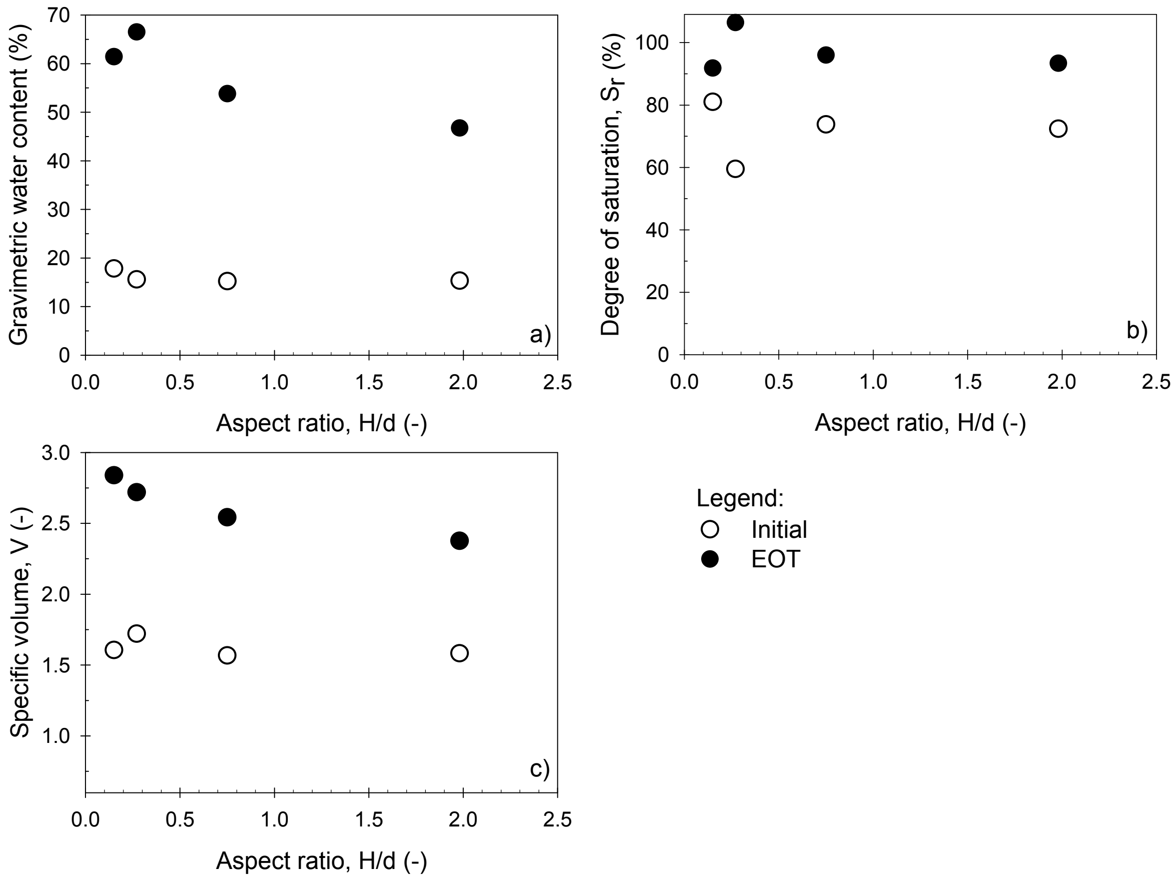

Figure 2.9. Initial and end-of-test (EOT) of (a) gravimetric water content, (b) degree of saturation, and (c) specific volume versus aspect ratio (H/d).

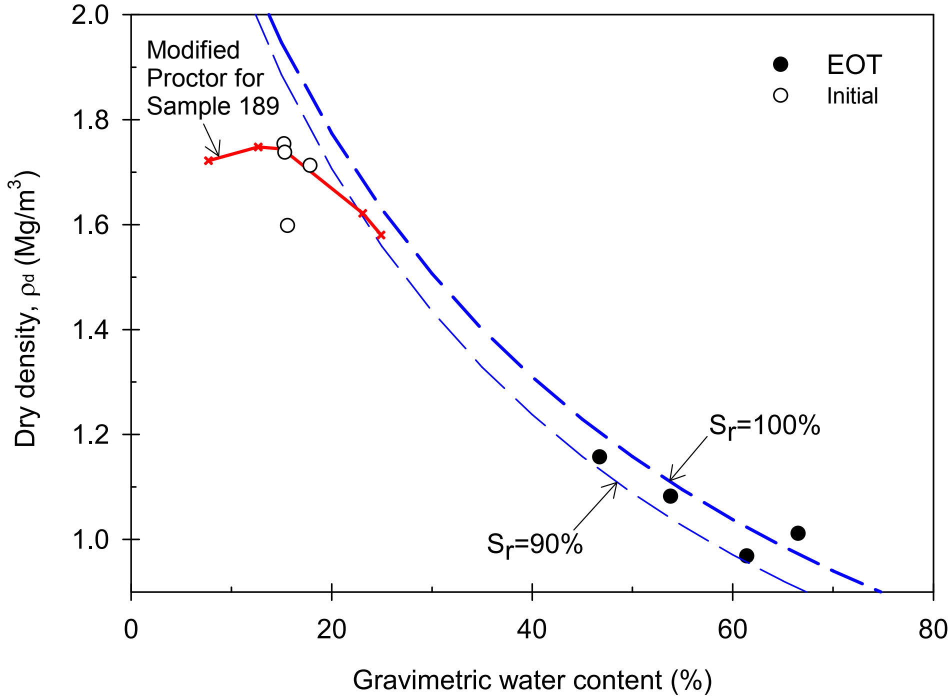

Figure 2.10. Initial and end-of-test (EOT) dry density versus water content and modified Proctor results for sample 189.

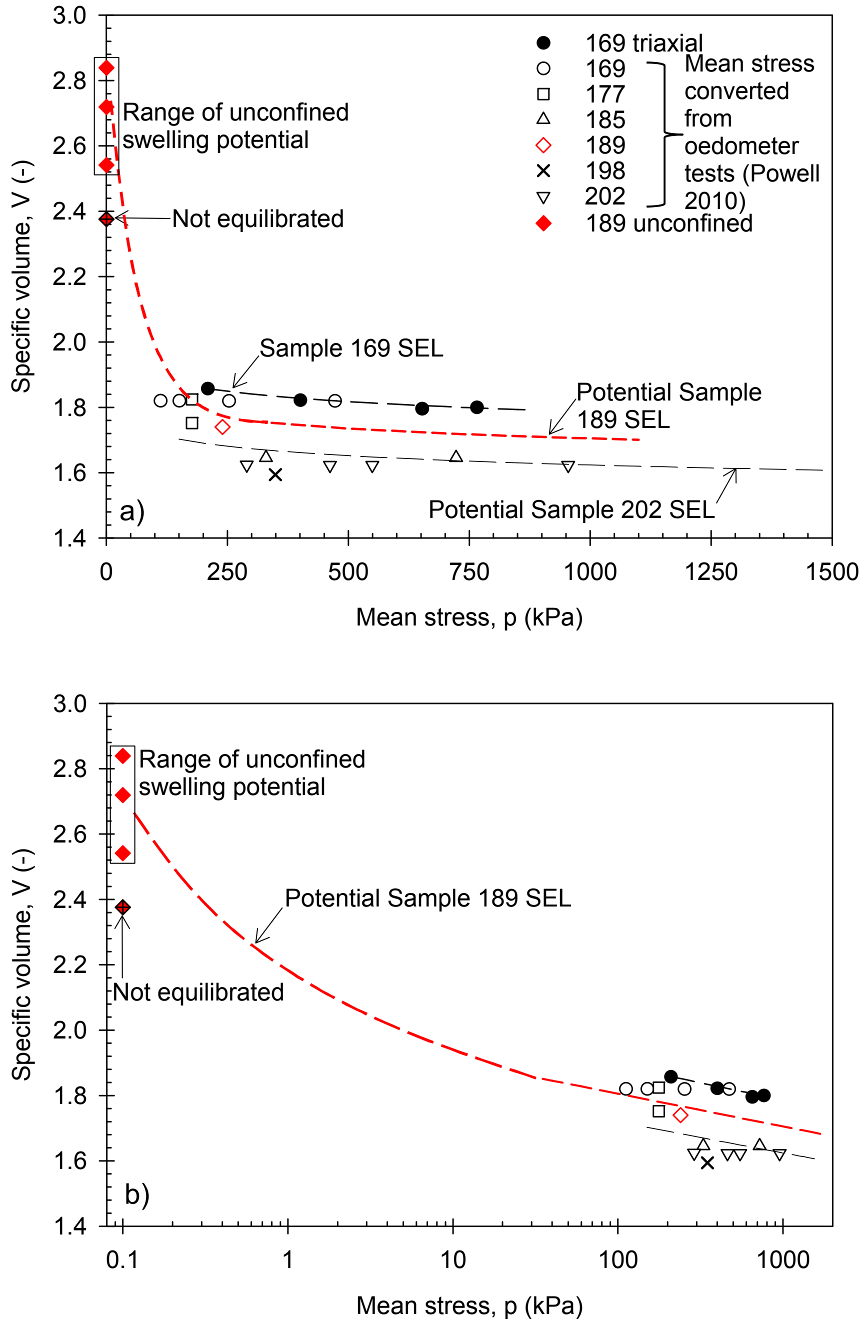

Figure 2.11. Swell equilibrium limit from unconfined swelling, triaxial swelling, and oedometer swelling pressure tests.

CHAPTER 3: A UNIFYING FRAMEWORK TO CHARACTERIZE AND MODEL SWELLING BEHAVIOUR USING ADVANCED TESTING

3.1 Introduction

Swelling-induced damage on public and private infrastructure has cost billions of dollars in repair and remediation. In some cases damage is accepted, as remediation is too expensive. On the positive side, in environmental applications, such as a landfill, swelling ability gives the containment barrier self-healing abilities. Significant research has focused on dealing with challenges in understanding and design using swelling soils. Therefore, the swelling potential of expansive clay is of interest of many researchers and practitioners (Komine and Ogata 1994, 2004; Yilmaz 2006; Nagaraj et al. 2009; Siemens and Blatz 2009; Kayabali and Demir 2011; Rao et al. 2011; Powell et al. 2013). As challenges associated with swelling soils are still being encountered, a unifying framework for swelling behavior would be a valuable tool for practitioners.

In order to model swelling behavior in design, the field boundary conditions should first be examined. A retaining wall constructed in swelling soil is illustrated in Figure 3.1. Three conditions are highlighted on the retaining wall cross-section and their stress-volume paths are plotted schematically on the graph in specific volume-mean stress (V-p) space. A worse-case condition of extended duration rain event or snow melt causing ponding at the surface is used to illustrate the three swelling conditions. Near the surface at soil element 1, unconfined swelling conditions prevail as the soil is at a low stress and there are no constraints on swelling. On the plot the stress-volume path is vertical starting at zero stress and the initial specific volume. The second condition is swelling at depth under constant mean stress (CMS). The soil element has an initial V-p state and again swells along a vertical stress-volume path. Under CMS conditions no additional confinement is provided during swelling. Finally the third condition is behind the retaining wall. As the soil element swells confinement is provided by the retaining wall. Thus, as the soil swells it expands and encounters swelling-induced stresses, which is termed constant stiffness (CS). The stiffer the wall material and construction, the flatter the stress-volume path. For perfect confinement a horizontal stress-volume path is followed, termed constant volume (CV).

Much effort has been invested in advanced laboratory testing on swelling soils in order to obtain a comprehensive understanding of the behavior of swelling soils (ASTM D4546; Wiebe et al. 1998; Yong 1999; Aversa and Nicotera 2002; Al-Shamrani et al. 2000; Sanchez et al. 2008; Wang et al. 2012; Cui et al. 2014; Liu et al. 2014). Laboratory test methods aim to represent field conditions as closely as possible. Siemens and Blatz (2007) proposed a new swelling test which allows for general boundary conditions to be applied including CMS, CS and CV. Chapter 2 also presented a new unconfined swelling test that incorporates non-contact method to measure soil deformations. Thus, the range of field boundary conditions presented in Figure 3.1 can be applied with varying stress-volume paths in a laboratory setting.

Additionally, swelling potential has been related successfully to the soil's index properties (Shi et al. 2002; Komine and Ogata 2003; Prakash and Sridharan 2004; Rao et al. 2004; Ito and Azam, 2010; Cui et al. 2012; Ito and Azam, 2013). Siemens and Blatz (2009) proposed a unifying framework to describe swelling behavior as illustrated on the graph in Figure 3.1. In V-p space, the three swelled states are connected with a line termed the Swell Equilibrium Limit (SEL). The SEL is an upper bound limit to swelling under general boundary conditions varying from constant mean stress to constant volume. During wetting, regardless of the boundary conditions, the soil element will swell until it lies on the SEL. Currently the SEL for a compacted 50:50 bentonite-sand mixture (named Bentonite-Sand-Buffer or BSB) and natural Bearpaw shale have been characterized by Siemens and Blatz (2009) and Powell et al. (2013), respectively. Conceptually, the swelled state for the entire retaining wall, illustrated in Figure 3.1, can be captured using the SEL. Following construction, the initial state for all elements would be below the SEL. During a long-term infiltration event, all elements would swell towards the SEL. Thus the swelling-induced pressures on the retaining wall and the swelling deformations can be analyzed using the SEL.

The SEL provides a unifying framework to understand swelling soil behavior based on advanced laboratory testing results. Additionally, relating swelling behavior to index properties gives practitioners an additional method to model swelling-induced stresses and deformations. In this Chapter, the swelling results for two additional swelling soils, recompacted Lake Agassiz clay and Bearpaw shale, are presented and the SELs are interpreted. This is the first step towards creating a database of SELs for modelling of swelling behavior. The SEL equation parameters for the characterized soils are successfully related to the index properties of the soils. Finally the SEL for Regina clay is calculated from the database which agrees with the published data.

3.2 Materials

Four different types of expansive soils are studied in this research. The grain-size distributions are plotted in Figure 3.2 and the plasticity chart is given in Figure 3.3. A series of laboratory work have been carried out on two natural recompacted soils, one on cored natural soil and one on compacted bentonite. The two recompacted soils are recompacted Lake Agassiz clay and recompacted Bearpaw clay, which are specimens recompacted from dried pulverized grains. The Bearpaw shale (Powell 2012 and Powell et. al. 2013) represents the cored natural soil. Bentonite-sand-buffer (BSB, Siemens and Blatz 2009) is categorized as compacted bentonite that is proposed to be used as a sealing material in a deep geological repository. The index properties of each soil are listed in Table 3.1.

Lake Agassiz clay used in this study is from southern Manitoba, Canada where its origin formation is of glaciation sedimentation. Lake Agassiz clay is classified as a plastic freshwater clay (Graham et al. 1983). Soil specimens are recompacted to a target of modified optimum dry density and water content, which was measured to be 1.62 Mg/m^3 initial dry density and 20% moisture content. The liquid limit (LL), plastic limit (PL) and plasticity index (PI) of the recompacted Lake Agassiz clay are, 85%, 34% and 51%, respectively. The grain size distribution can be referred to Figure 3.2 where the soil consists of 74% clay and 20% silt.

Bearpaw shale is originated from Bearpaw formation found near Sasktatoon, Canada. Bearpaw shale formation is predominately marine silty clays and sands (Powell 2012). The particular core sample was taken from a depth of 43 m below ground level. The Bearpaw shale in its natural state has been tested for its SEL (Powell et. al. 2013). The same soil is re-used in this research. The pulverized dried Bearpaw clay is compacted to a target dry density and moisture content that is nominally similar to its insitu state. The targeted initial condition is 1.50 Mg/m^3 dry density and 30% moisture content. The Atterberg limits of the recompacted Bearpaw clay used in this research consists of 67% LL, 26% PL and 41% PI. The LL 145% and PI 122% of Bearpaw shale are higher than the recompacted one. The clay fraction and montmorillonite content for Bearpaw shale is 39% and 72%, respectively (Peterson and Peters 1963).

The compacted bentonite, BSB studied by Siemens and Blatz (2009) consists of 50% of sand and 50% of Wyoming bentonite by mass. The LL and PL of Na-bentonite are 555% and 43%, respectively. The sand content of BSB is an angular material mixed to a standard grain-size (Dixon et al 1994). The well-graded sand mixed in BSB has the properties of C_u = 4, C_c = 0.84, d_{10} = 0.12mm and d_{50} = 0.38mm (Siemens and Blatz 2009). The LL and PL for BSB is 265% and 21%, respectively. Sridharan and Rao (2004) identified that the ratio of plastic limit to liquid limit remains constant as long as the clay mineral type in the mixture of clay minerals is the same and the measurements support this finding. Both silt and sand fraction act as a dilution factor in the sand-bentonite mixture.

3.3 Methods

3.3.1 Triaxial swelling test method

The results from the triaxial swelling tests allow for interpretation of a SEL for the tested soil. In order to interpret a SEL curve, a number of triaxial swelling tests (Siemens and Blatz 2007) and unconfined swelling tests (Lim and Siemens 2013) is performed. A triaxial swelling test is performed on a triaxial specimen under pre-determined boundary conditions using a modified triaxial apparatus. The pre-determined boundary condition is defined in mean stress – volumetric strain space and simulates field conditions (Figure 3.1). The boundary conditions are imposed with an automated algorithm in the data acquisition system. A constant mean stress (CMS) stress-volume path can be specified where the specimen is given access to water and swells under a constant stress. The stress path is set to move vertically along y-axis in a V-p plot (Figure 3.1b). A CMS test measures the maximum swelling deformation at that stress level. In the second scenario, a constant volume (CV) test, the total volumetric change of the specimen is kept constant by increasing the applied confining pressure. The confining pressure is increased to counteract the swelling deformation upon infiltration. The stress path followed by a CV test moves horizontally parallel with the x-axis in a V-p plot.

Test specimens are prepared to a target dry density and water content condition following with the procedure detailed in Siemens 2006. A required amount of dry mass of pulverized soil is weighted. The dry pulverized soil is moistened thoroughly with a targeted amount of de-ionized water using a mixing bowl. The moist soil is kept in a double-layered sealed plastic bag and left in the refrigerator for 24 hours for moisture equilibrium. After 24 hours, the moist soil in the plastic bag is used for specimen compaction in a 50.8mm diameter compaction mold. The compacted triaxial specimen is installed in the modified triaxial infiltration apparatus (see Figure 3.4 for a schematic). A typical triaxial infiltration test consists of three phases, namely isotropic compression, equilibration, and water infiltration. Isotropic compression and equilibration occurs as the cell pressure is raised up to a target stress level and remains constant for 24 hours. After 24 hours, the equilibration of suction (measured with a relative humidity sensor) at the specimen is achieved. To initiate the water infiltration phase, the back pressure is raised and the plumbing and geotextile are flooded (Figure 3.4). As soon as small deformations are detected by the data acquisition system, the algorithm engaged to apply the specified stress-volume path. During the water infiltration phase, the partially saturated specimen continually takes up water until the soil achieves its swelling equilibrium. The completion of a swelling test is indicated by ± 2% changes of water added to the specimen, pressure or volumetric strain over a one-day period.

The triaxial swelling apparatus previously used by Siemens and Blatz (2007, 2009) and Powell et al. (2013) is modified for suction measurement device installation within the triaxial pedestal. Previously a suction measurement probe was installed at the center of the compacted specimen. However, the Xeritron probe is out of production and an extensive search did not turn up sensors that met small size and high accuracy requirements. Blatz (2000) noted that total suction measurements taken near the top cap gave similar readings as those taken at the center of the specimen. Locating the sensor within the pedestal allows for probe installation prior to the test, which is, operationally, a simpler method compared with compaction at the center of test specimens. In conjunction with this, a grooved pedestal cap replaces a porous stone installation at the pedestal. The water flows through the fanning groove at the pedestal cap, through the geotextile and infiltrates the specimen. The chamber beneath the cap contains a RH sensor tip. On the top of the infiltration cap, a tiny perforated cylindrical tip protrudes from the cap. The triaxial specimen is installed on the pedestal with the tiny tip inserts to a pre-bored hole at the bottom of the specimen. The specimen equilibrates with the vapor inside the confined chamber where the RH tip is housed.

The measured relative humidity is interpreted as total suction with the following equation (Lu and Likos 2004):

$$[3.1] \qquad \Psi_t = -\frac{RT}{\upsilon_{w0}\omega_\upsilon} ln(RH)$$

where Ψ_t = total soil suction, R = universal gas constant (8.314 J/mol K), T = absolute temperature (K), υ_{w0} = specific volume of water (m^3 /kg), ω_υ is the molecular mass of water vapor (18.016 kg/kmol) and RH= relative humidity.

3.3.2 Unconfined Swelling Test

An unconfined swelling test (Lim and Siemens 2013) represents the scenario where the swelling soil is free to expand at essentially zero confinement (notwithstanding the self-weight of the specimen). The measured swelling deformation from unconfined swelling test defines the maximum volumetric deformation on the y-axis of a V-p plot at zero stress. Details regarding the test set-up and procedure have been described in Lim and Siemens 2013 (Chapter 2) and a brief summary is given here. The unconfined swelling test is carried out in a humidity-controlled chamber. The moisture content of the specimen is increased through spraying of water on the specimen periodically and wicking action from a reservoir. The wetted specimen swells under its own self-weight in the absence of external applied pressure. The swelling deformation is measured with non-contact method by using digital image analysis. The digital photographs are analyzed with GeoPIV (White et al. 2003) software that is capable of tracing deformation using image analysis.

3.4 Swelling Test Results and SEL Interpretation

3.4.1 Typical CV test

A typical CV 150 kPa test for recompacted Lake Agassiz clay is presented in Figure 3.5 in terms of mean stress and volumetric strain versus time (Figure 3.5a) as well as water added to specimen and total suction versus time (Figure 3.5b). Following preparation and installation, the specimen was subjected to 150 kPa of isotropic compression. After 24 hours, the RH at the specimen was measured at 93.3% which represents a total suction of 9.6 MPa. A total volumetric strain of 0.74% was measured from the isotropic compression. The test was continued with the infiltration stage.

The back pressure was raised up to 100 kPa to infiltrate the specimen. When the specimen was infiltrated, it started to expand a small, but detectable, amount. The stress-volume path control was activated and automatically increased cell pressure to suppress expansion. The cell pressure was increased from 150 kPa during the infiltration stage. On Day 5, the mean stress gradually levelled off at 750 kPa. At the same time, the total volumetric strain was kept constant within ±0.05%. The curve of water added to specimen (Figure 3.5b) qualitatively resembles the mean stress plot. The rate of change for both curves are relatively high at the beginning and then slower down gradually. The total suction curve reacted at slower rate compared to the mean stress or water added to specimen plot. The total suction reduced to 0.8 MPa after 5 days of infiltration. The total amount of water added to specimen was measured at 24.5 mL. The CV 150 kPa test reached its swelling equilibrium in 25 days.

3.4.2 Typical CMS test

Figure 3.6 shows a typical CMS 150 kPa test result for recompacted Lake Agassiz clay in terms of mean stress and volumetric strain versus time (Figure 3.6a) as well as water added to specimen and total suction versus time (Figure 3.6b). The mean stress was raised up to 150 kPa in isotropic compression stage. After 24 hours, the equilibrium of moisture content at the specimen was achieved. The equilibrated relative humidity was measured at 96.0% RH which represents 6 MPa of total suction. The total volumetric strain from isotropic compression was 0.6%. At the infiltration stage, the back water pressure was increased at 100 kPa. This stress level was maintained constant throughout the whole test duration. The volumetric strain versus time (Figure 3.6a) closely resembles the water added to specimen plot (Figure 3.6b). The rate of change for both curves was relatively high at the beginning and then tapered off. On Day 6, total volumetric strain swelled up to 13%, water added to specimen reached 52.0 mL and total suction was reduced to 1.7 MPa. Later on, the rate of change in these measurements levelled off gradually until the end-of-test criteria were satisfied. At the end of test, the total volumetric strain was measured at 14.5%. A total of 62.0 mL of de-ionized water was added to the specimen and the total suction approached zero. The test duration for CMS 150 kPa was approximately 35 days.

3.4.3 Typical unconfined swelling test

Figure 3.7a presents the unconfined swelling test results for recompacted Lake Agassiz clay and recompacted Bearpaw clay, respectively. As shown in Figure 3.7a, the recompacted Lake Agassiz clay swelled at a high rate within the first two days after water application. On Day 2, the volumetric strain obtained 80% of the total change over the test. Subsequently, the rate of change in swelling levelled off gradually over time. For recompacted Lake Agassiz clay, the final total volumetric strain was -70% (in swelling).

The recompacted Bearpaw clay specimen behavior similarly to the recompacted Lake Agassiz clay but at lower magnitudes for both total swelling and initial swelling rate. Figure 3.7a shows that the recompacted Bearpaw clay has a gentler slope in strain versus time. The rate of change was slower within the first 6 days. On Day 6, the volumetric strain was measured at -42% while at the end of test, the volumetric strain was -46%.

The volumetric strain versus log time is plotted in Figure 3.7b, which shows that a swelling curve consisting of both primary and secondary slopes. The recompacted Lake Agassiz clay measured a higher final volumetric strain at -70% and reached the end of primary swelling at t=0.95 day. In the same plot, the recompacted Bearpaw clay had the final volumetric strain at -46% and achieved the end of primary swelling at t= 6.9 day.

3.4.4 Summary result of triaxial infiltration tests on recompacted Lake Agassiz clay

A series of five triaxial infiltration tests have been performed on the recompacted Lake Agassiz clay. The test series consist of CMS 150, CMS 300, CMS 600, CV 150 and CV 300 tests. Figure 3.8a shows a summary test result of mean stress versus time for the five tests. Means stress in CMS 600, CMS 300 and CMS 150 is kept at a constant level, eg, at 600 kPa, 300 kPa and 150 kPa, respectively throughout the infiltration test. Specimen CV 300 requires the highest mean stress of 1200 kPa to counteract against the swelling deformation in the constant volume test. The second highest mean stress is measured in CV 150 which requires p =753 kPa to keep the specimen volume constant.

The summary of total volumetric strain versus time is plotted in Figure 3.8b. The highest swelling strain of 14.5% was measured in CMS 150 as it has the lowest mean stress. The volumetric strain of CMS 300 was measured at 7.3 %. CMS 600 had a final total volumetric deformation of 3.8%. The volumetric strain is kept constant at ε_v= -0.06% for CV 150 and ε_v= 1.2% in CV 300.

In general, a constant mean stress (CMS) test requires longer duration for its swelling equilibrium compared to a constant volume (CV) test. For example, CMS 150 lasted the longest duration of 35 days (5 weeks) for completion. Both CV 150 and CV 300 reached the swelling equilibrium in a little over 3 weeks.

3.5 Interpreting SEL Curve for recompacted Lake Agassiz Clay

The triaxial swelling and unconfined swelling test results are plotted in Figure 3.9 in specific volume versus mean stress (V-p) space for interpretation of the SEL for Lake Agassiz clay. A SEL curve is formed by connecting the end-of-test points from triaxial infiltration and unconfined swelling test. The test paths start at a target specific volume of recompacted specimen of 1.73 and zero mean stress. The unconfined swelling test swelled along a vertical stress-volume path to the equilibrium value of V=3.0. The triaxial swelling tests initiate with an isotropic compression stage during which the specimen compresses (decrease in specific volume) along with increasing mean stress. During infiltration, the stress-volume path follows the specified boundary condition resulting in a vertical path for CMS and a horizontal path for CV tests. Tests continued until the swelling potential of the soil was satisfied by either expansion (CMS) or swelling-induced stresses (CV). CMS 150, CMS 300 and CMS 600 terminate at specific volumes of 1.99, 1.88 and 1.80, respectively. The CV 150 and CV 300 swelling tests follow horizontal stress-volume paths during infiltration. The test result shows that a higher mean stress is required in CV 300 (p= 1200 kPa) than CV 150 (p= 753 kPa) to keep the volume constant.

3.6 Swelling Test Results and SEL Interpretation

3.6.1 SEL curves for recompacted Lake Agassiz clay and Bearpaw shale/clay

A series of triaxial infiltration test result on recompacted Bearpaw clay (5 tests) and Lake Agassiz clay (5 tests) are summarized in Table 3.2 which consists of initial and post-infiltration measurement on triaxial specimen. The unconfined swelling test data on both soils is presented in Table 3.3. The data from these two tables are used to plot the SEL curves for the soils. Details of the individual test results and overall summary for the recompacted Bearpaw clay tests are provided in Appendix C.

The swelling test results for recompacted Lake Agassiz clay are re-plotted in Figure 3.10a along with the isotropic compression curve and the SEL. The compression line represents the condition after the specimen is subjected to isotropic compression and prior to wetting. The area between the isotropic compression curve and the SEL is highlighted as the swelling potential for each soil. The swelling potential can be realized as either expansion, swelling-induced stresses or both depending on the boundary conditions. Regardless, the soil will swell towards the SEL from the isotropic compression line during swelling. The final state (or upper bound limit) of swelling deformation and induced-pressure is represented with the SEL curve.

The SEL curve of recompacted Lake Agassiz clay is fitted with a natural logarithm equation:

[3.2] $$V_{SEL} = A + B \ln p$$

with A=2.691 and B=-0.141 being the fitted values as listed in Table 3.4a. Parameter 'A' represents the y-intercept at p=1 and parameter 'B' reflects the curvature of the SEL. Higher values of 'A' and 'B' are associated with greater swelling potential over a wider range of stresses.

Figure 3.10b plots a summary of the triaxial swelling and unconfined swelling tests for recompacted Bearpaw clay (individual test results and data breakdown provided in Appendix C) along with the isotropic compression curve and highlighted swelling potential. The maximum swelling potential under unconfined conditions is measured at V=2.89. Figure 3.10b shows that the SEL and isotropic compression line of recompacted Bearpaw clay intersect at approximately p= 300 kPa. This indicates recompacted Bearpaw clay swells at mean stress 300 kPa and less under CMS boundary conditions.

Compared with Lake Agassiz clay, the swelling potential of recompacted Bearpaw clay (Figure 3.10b) is relatively lower as the shaded area is smaller than the one in Figure 3.10a. The SEL curve of recompacted Bearpaw clay is fitted with a logarithm equation with fitting parameters A=2.596 and B=-0.127. Both the recompacted Lake Agassiz clay and Bearpaw clay have similar value of $f_c.f_m$ (refer Table 3.1) but the initial dry density of the recompacted Bearpaw clay is relatively lower than the recompacted Lake Agassiz clay. Therefore, it is reasonable to expect a smaller swelling potential in Bearpaw clay.

3.6.2 SEL catalogue

In addition to the SELs reported in this chapter, Figure 3.10 plots summaries of an additional two materials previously reported including bentonite-sand-buffer (BSB in Siemens and Blatz (2009), Figure 3.10c) and natural Bearpaw shale (Powell et al. 2013, Figure 3.10d). The plots include SELs, isotropic compression curves and the swelling potential of each soil is highlighted (area between the isotropic compression curve and the SEL). The parameters for the fitted SEL curves in the format of equation [3.2] are listed on the figure as well as in Table 3.4. The coefficient of determination, R^2 falls in the range of 0.92 to 0.97.

The summary results for BSB (plotted in Figure 3.10c and taken from Siemens and Blatz 2009) indicate the soil is expansive over a wider range of stresses than those examined. Even at 1500 kPa mean stress, expansion was measured under CMS boundary conditions and an additional 400 kPa of swelling-induced stress was required to maintain the initial volume for the CV 1500 test. The shaded area between the isotropic compression curve and the SEL for BSB covers the largest area in Figure 3.10, which indicates the greatest swelling potential of the four soils. As a compacted bentonitic material, the swelling potential of BSB correlates to the index properties such as liquid limit, plastic limit, plasticity index and activity. Associated with the high swelling potential the fitting parameter 'B' of in BSB is also the greatest absolute value (B=-0.214).

The swelling results for natural Bearpaw shale (Figure 3.10d) indicate the material is very stiff during isotropic compression and has limited swelling potential over the range tested. The isotropic compression curve is essentially flat which is consistent with the extremely high preconsolidation pressure of the sample of 10,000 kPa (Powell et al. 2012). Natural Bearpaw shale is an expansive soil that is highly structured and has an extensive stress history dating back to its deposition during the Cretaceous period approximately 71-72 million years ago (geologic history summarized in Powell et al. 2012). Although compacted to nominally the same density and water content, the soil fabric in natural intact shale and recompacted clay is different as its stress history has been erased during the specimen preparation process.

Comparing the natural shale and recompacted clay of Bearpaw swelling properties, although materials have the same constituents the swelling potential is rather different. The higher 'B' value in recompacted Bearpaw clay (eg, B=-0.127) covers a steeper curve from V=1.90 to V=2.89 over the range from 0-300 kPa mean stress. The 'B' value in natural Bearpaw shale is 0.0463 which covers a narrower range from V=1.80 to V=2.0 up to 800 kPa mean stress. The main difference is the change in structure of the materials from natural to recompacted. Another contributing factor is the change in liquid limit with the recompacted material. Peterson (1954) reported that drying Bearpaw shale caused a reduction in the liquid limit and this study found similar results. The natural Bearpaw shale has a higher liquid limit of 145% compared to LL=67% in the recompacted Bearpaw clay. Nonetheless, the structure of the natural Bearpaw shale is controlling the swelling behavior over the range of stresses tested.

Figure 3.11 plots the summary SEL for all the materials in ε_v-p space. In this plot the results are normalized to start at volumetric strain and mean stress equal to zero, which allows for direct comparison of the swelling potential. The swelling potential in a descending order is BSB, recompacted Lake Agassiz clay, recompacted Bearpaw clay and natural Bearpaw shale. The SEL generalizes the swelling potential in a unifying framework where different types of swelling soils could be compared together. It is evident that the SEL of each soil has close correlation to the soil index property and initial condition. In a practical application, the SEL of a swelling soil may be calculated if the index property and initial condition has been determined from a geotechnical investigation of a project. Whether the soil is a compacted or natural type, the calculated SEL could be plotted with the catalogue of SELs and made comparison accordingly. It is, therefore, beneficial to interpret the SEL of other swelling soils with the catalogue of swelling soils.

3.6.3 Interpreting swelling pressure with EMDD

The major clayey constituent that contributes to the swelling potential is the montmorillonite content in the clay (Michell 1993). Dixon et al. 2002 reported a database of 1D swelling pressures for compacted bentonitic materials, which is re-plotted in Figure 3.12. They reported swelling pressure versus Effective Montmorillonite Dry Density (EMDD), which is defined as the mass of montmorillonite divided by volume occupied by non-clay and non-swelling materials.

[3.3]
$$EMDD = \frac{f_m f_c \rho_d}{\left[1 - \frac{(1-f_c)\rho_d}{G_s \rho_w} - \frac{(1-fm)f_c\rho_d}{G_n \rho_w}\right]}$$

where f_m is the montmorillonite fraction of clay, f_c is the fraction of clay, ρ_d is the dry density of soil, ρ_w is the density of water, G_s is the specific gravity of nonclay soil, G_n is the specific gravity of non-swelling clay. Normalizing to the EMDD allows for comparison of different materials with variable montmorillonite contents and initial densities.

As the database is for laterally confined tests, the stresses in the triaxial swelling tests must be converted to equivalent swell pressures before plotting on Figure 3.12. Siemens and Blatz 2009 have proposed a swelling pressure conversion equation from 1D to mean stress (or vice versa) using an elasticity assumption. The derivation used for the stress conversion is as follow:

[3.4] $$p_{equil} = \frac{p_{swell}}{3}\left(\frac{1+\upsilon}{1-\upsilon}\right)$$

where p_{equil} is the equilibrium mean stress from end of the triaxial infiltration test, p_{swell} is the 1D swelling pressure and ν is the Poisson's ratio of the soil.

The converted swelling pressure for recompacted Lake Agassiz clay, recompacted Bearpaw clay and natural Bearpaw shale is plotted together with bentonite-sand-buffer (BSB, Siemens and Blatz 2009) as well as the de-ionized water data (DDW) from Dixon et al 2002 in Figure 3.12. Dixon et al. 2002 also reported a log-linear correlation between 1D swelling pressure and EMDD. The general fitting equation for the plot of swelling pressure (on a log scale) versus EMDD is in the form:

[3.5] $$p_{swell} = C * e^{(D * EMDD)}$$

where C and D are the fitting parameters of the equation. Value D represents the slope of the fitted line on a log-linear scale and C is the theoretical value of p_{swell} at EMDD=0. The fitted lines are plotted on Figure 3.12 for the four soils and the equations and coefficient of determination, R^2 are listed in Table 3.4b. The R^2 of the equations ranges from 0.93 to 0.95.

The fitting parameters follow anticipated trends based on their swelling potential. Ranking the materials in order of greatest to least values of parameter 'C' is BSB, recompacted Lake Agassiz clay, recompacted Bearpaw clay and natural Bearpaw shale. On the other hand, ranking the materials increasing order for parameter 'D' is BSB, recompacted Lake Agassiz clay, recompacted Bearpaw clay and natural Bearpaw shale. The highest swelling potential is represented by the highest 'C' (0.007609) value with lowest 'D' (4.56) value in BSB.

The natural and recompacted clays have a steeper slope compared to the compacted bentonites in Figure 3.12. The location of the EMDD lines for the natural and recompacted clays is found at the left of the BSB's EMDD line. Since the initial dry density of these clays are smaller in comparison, it is reasonable to have the EMDD lines located at the left of BSB's EMDD line. The steeper slope in the natural and recompacted clays is also an indication that these types of clays are more sensitive in the wetting-induced swelling pressure with the change in EMDD content.

3.7 Preliminary SEL for Regina Clay

Using the existing catalogue of swelling soils that have been characterized in terms of their SEL, a new method for establishing an estimated SEL for an uncharacterized material is proposed. The SEL curves can be represented with the fitted equations in V-p plot $V_{SEL} = A + B\,ln\,p$ or p_{swell} - EMDD plot $\log(\,p_{swell}\,) = C * e^{(D*EMDD)}$. The fitting parameters from these equations for four types of expansive soils are listed in Table 3.4. As mentioned in the introduction, numerous researchers have related swelling potential to various index properties. Thus a parametric study was initiated to investigate the correlation between the fitting parameters for the SELs with numerous index properties including clay fraction (f_c), montmorillonite content (fm), liquid limit (LL), plastic limit (PL), plasticity index (PI), liquidity index (LI), ratio of PI/LL and PL/LL, initial specific volume (or dry density). Each of these plots appears in Appendix D. Figure 3.13 and Figure 3.14 are a compilation of the plots that correlate the fitting parameters A and B with the selected index properties of the swelling soils. From these two figures, it can be seen that the natural soil is distinguished from the recompacted clays in the plots. The plots are correlated linearly with the compacted soils. The selected plots are the stronger correlated index properties such as initial specific volume, liquid limit, plasticity index, PL/LL, and PI/LL with a $R^2 \geq 0.83$.

The benefit of the catalogue is to allow for preliminary modelling of SEL curves for soils that have not been subjected to advanced swelling tests. Table 3.5 lists the index properties and initial condition of Regina clay (Fredlund 1975). The properties of Regina clay that have been selected to correlate to the parameters A and B include initial specific volume, LL, PI, PL/LL and PI/LL. These index properties of Regina clay are used to calculate the A and B value. Once the A and B value are calculated from all the correlations, the preliminary SEL for Regina clay takes the average value of A and B and result in A=2.667 and B=-0.138. Therefore the preliminary SEL for $V_{Regina} = 2.667 - 0.138\,ln\,p$. The SEL for Regina clay is plotted in Figure 3.15 compared with the test data from Fredlund 1975 and other established SEL curves of tested soils. The SEL of Regina clay is in good agreement with the test data and the line sits closely with other recompacted soils.

3.8 Conclusion

The destructive effect of swelling soil on surrounding infrastructure is one of the classic issues with unsaturated soils. Given the continuing challenges associated with swelling soils the need for a practical analysis tool is apparent. The SEL concept provides a unifying framework for understanding and modelling the behavior of swelling soils. It allows an upper bound swelling limit depending on the initial conditions and the stress-volume paths upon wetting. The SEL curve obtained from triaxial infiltration and unconfined swelling test encompasses a practical comprehensive scenario of swelling behavior from rigid boundary condition to free swelling without confinement.

This chapter presented SELs for two additional soils and related the SEL parameters to index properties of the compacted materials. Using the developed relationships allowed for a preliminary SEL of Regina clay to be calculated which agrees with published data. Further testing is required to build-up the triaxial swelling soil database to increase the range of applicability of the relationships. The unifying SEL framework is capable of characterizing expansive soil behavior in terms of the swelling deformation and wetting-induced stress. The development of SEL curve with advanced testing is potentially a practical estimation for soil swelling potential because it covers a wide range of boundary conditions and stress-paths upon wetting.

3.9 Reference

Al-Shamrani, M.A. and Al-Mhaidib, A.I. 2000. Swelling behavior under oedometric and triaxial loading conditions. Advances in Unsaturated Soil, Seepage, and Environmental Geotechnics (GSP 148) 148 : 344-60.

ASTM D4546. Standard test methods for one-dimensional swell or settlement potential of cohesive soils. In . Philadephia, Pennsylvania: ASTM.

Aversa S. and Nicotera M. 2002. A triaxial and oedometer apparatus for testing unsaturated soils. Geotechnical Testing Journal 25 (1): 3-15.

Blatz, J. A. 2000. Elastic-plastic modeling of unsaturated high plastic clay using results from a new triaxial test with controlled suction. Ph.D., Department of Civil and Geological Engineering, University of Manitoba, Winnipeg, Man.

Cui, S., Zhang, H. and Zhang, M. 2012. Swelling characteristics of compacted GMZ bentonite–sand mixtures as a buffer/backfill material in china. Engineering Geology 141-142 : 65-73.

Cui, Y., Saba, S.,Tang, A. M., and Barnichon, J. 2014 (in press). Investigation of the swelling behavior of compacted bentonite/sand mixture by mock-up tests. Canadian Geotechnical Journal(ja).

Dixon, D.A., Chandler, N.A. and Baumgartner, P. 2002. The influence of groundwater salinity and influences on the performance of potential backfill materials. Paper presented at Proceedings of the 6th International Workshop on Design and Construction of Final Repositories, Backfilling in Radioactive Waste Disposal, Brussels.

Dixon, D.A., Hnatiw, D.S.J. and Kohle, C.L. 1992. Preparation and quality control of materials used on the reference buffer material. Whiteshell Laboratories, Pinawa, Manitoba: Fuel Waste Technology Branch, Technical Record TR-575, COG-92-133.

Fredlund, D. G. 1975. Engineering properties of expansive clays. Paper presented at Seminar on Shallow Foundations on Expansive Clays, Regina, Saskatchewan.

Ito, M. and Azam, S. 2013. Engineering properties of a vertisolic expansive soil deposit. Engineering Geology 152 (1): 10-6.

———. 2010. Determination of swelling and shrinkage properties of undisturbed expansive soils. Geotechnical and Geological Engineering 28 : 413-22.

Kayabali, K. and Demir, S. 2011. Measurement of swelling pressure: Direct method versus indirect methods. Canadian Geotechnical Journal 48 : 354-64.

Komine, H., and Ogata, N. 2004. Predicting swelling characteristics of bentonites. Journal of Geotechnical & Geoenvironmental Engineering 130 (8): 818-29.

———. 2003. New equations for swelling characteristics of bentonite-based buffer materials. Canadian Geotechnical Journal 40 (2): 460-75.

Lim, B.F. and Siemens, G.A. 2013. An unconfined swelling test for clayey soils that incorporates digital image correlation. Geotechnical Testing Journal 36 (6): 1-11.

Liu, X.F., Buzzi, O.P. and Vaunat, J. 2014. Influence of stress-volume path on swelling behavior of an expansive clay. Paper presented at 6th International Conference on Unsaturated Soils: Research & Applications, Sydney, Australia.

Lu, N. and Likos, W.J. 2004. Unsaturated soils mechanics. Canada: John Wiley & Sons.

Mitchell, J.K. and Soga, K. 2005. Fundamentals of soil behavior. 3rd Edition ed. Canada: John Wiley & Sons.

Nagaraj, H.B., Munnas, M.M. and Sridharan. 2009. Critical evaluation of determining swelling pressure by swell-load method and constant volume method. Geotechnical Testing Journal 32 (4): 1-10.

Nowamooz, H. and Masrouri, F. 2012. Soil fabric of compacted and natural swelling soils studied by mercury intrusion porosimetry. In Unsaturated soils: Research and applications., ed. Mancusi, C., Jommi, C. and D'Onza, F., 131-136Springer Berlin Heidelberg.

Peterson, R. 1954. Studies of Bearpaw shale at a dam site in Saskatchewan. Proc. ASCE 80 (476).

Peterson, R. and Peters, N. 1963. Heave of spillway structures on clay shales. Canadian Geotechnical Journal 1 : 5-15.

Powell, J. S. 2010. Geotechnical characterization of the bearpaw shale. Ph.D. Thesis., Department of Geological Sciences & Geological Engineering, Queen's University, Kingston, Ont.

Powell, J.S., Siemens, G., Take, W.A. and Remenda, V. 2013. Characterizing the swell potential of Bearpaw shale. Engineering Geology 158 : 89-97.

———. 2012. Influence of specimen geometry on sample disturbance observed in oedometric testing of clay shales. Geotechnical Testing Journal 35 (5): 1-13.

Powell, J.S., Take, W.A., Siemens, G. and Remenda, V. 2012. Time-dependent behavior of the bearpaw Shale in oedometric loading and unloading. Canadian Geotechnical Journal 49 : 427-41.

Prakash, K. and Sridharan, A. 2004. Free swell ratio and clay mineralogy of fine-grained soils. Geotechnical Testing Journal 27 (2): 1-6.

Rao, A.S., Phanilumar, B.R. and Sharma, R.S. 2004. Prediction of swelling characteristics of remolded and compacted expansive soils using free swell index. Quarterly Journal of Engineering Geology and Hydrogeology 37 : 217-26.

Rao, B. H.,Venkataramana, K. and Singh, D.N. 2011. Studies on the determination of swelling properties of soils from suction measurements. Canadian Geotechnical Journal 48 (3): 375-87.

Sánchez, M., Villar, M.V., Gens, A., Gómez-Espina, R. and Lloret, A. 2008. Swelling pressure in compacted bentonite: Laboratory tests and modelling. Paper presented at 1st European Conference on Unsaturated Soils, Durham, UK.

Shi, B., Jiang, H., Liu, Z. and Fang H.Y. 2002. Engineering geological characteristics of expansive soils in china. Engineering Geology 67 : 63-71.

Siemens, G. and Blatz, J.A. 2007. Triaxial apparatus for applying liquid infiltration with controlled boundary conditions and internal suction measurement. Journal of Geotechnical & Geoenvironmental Engineering 133 (6): 748-52.

Siemens, G.A. and Blatz, J.A. 2009. Evaluation of the influence of boundary confinement on the behavior of unsaturated swelling clay soils. Canadian Geotechnical Journal(46): 339-56.

Sridharan, A. and Rao, R. P. 2004. Characterization of Ariake and other marine clays. Paper presented at International Symposium on Lowland Technology (ISLT-2004), Bangkok.

Wang, Qiong, Anh Minh Tang, Yu-Jun Cui, Pierre Delage, and Behrouz Gatmiri. 2012. Experimental study on the swelling behavior of bentonite/claystone mixture. Engineering Geology 124 : 59-66.

White D.J., Take W.A. and Bolton M.D. 2003. Soil deformation measurement using particle image velocimetry (PIV) and photogrammetry. Géotechnique 53 (7): 619-31.

Wiebe, B., Graham, J., Tang, G.X., and Dixon, D. 1998. Influence of pressure, saturation and temperature on the behavior of unsaturated sand-bentonite. Canadian Geotechnical Journal(35): 194-205.

Yilmaz, I. 2006. Indirect estimation of the swelling percent and a new classification of soils depending on liquid limit and cation exchange capacity. Engineering Geology 85 : 295-301.

Yong, R. N. 1999. Soil suction and soil-water potentials in swelling clays in engineered clay barriers. Engineering Geology 54 : 3-13.

Table 3.1. Index properties for multiple soils.

Soil Type	Specific gravity, G_s (-)	Clay fraction, f_c (%)	Montmo-rillonite fraction of clay, f_m (%)	$f_c.f_m$ (-)	Liquid Limit, LL (%)	Plastic Limit, PL (%)	Plastic Index, PI (-)	PL /LL (-)	PI /LL (-)	Activity, A=PI/% clay	Initial dry density, ρ_d (Mg/m3)	Initial specific volume, V_o (-)	Poisson's ratio, υ (-)
Recompacted Lake Agassiz clay	2.76	75	30*	0.225	85	34	51	0.40	0.60	0.64	1.59	1.742	0.33
Recompacted Bearpaw clay	2.75	39**	72**	0.281	67	26	41	0.39	0.62	1.05	1.45	1.894	0.34
**Natural Bearpaw shale	2.75	39	72	0.281	145	23	122	0.16	0.84	3.13	1.50	1.833	0.34
Bentonite –sand-buffer (BSB)	2.70	50^{Φ}	90^{Φ}	0.450	265	21	244	0.08	0.92	4.88	1.67	1.615	0.18
Regina clay (Fredlund 1975)	2.83	51	77	0.393	76	26	50	0.34	0.66	1.0	1.54	1.838	0.35

Note:
* Data obtained from Dixon (2002).
** Data obtained from Powell et al. (2013).
$^{\Phi}$ Data obtained from Siemens and Blatz (2009).

Table 3.2. Initial condition and end-of-test result of triaxial swelling test for recompacted Lake Agassiz and recompacted Bearpaw clays.

Soil type	Test ID	Initial (as-compacted)			End of triaxial swelling test							
		Gravimetric water content, w_o (%)	Specific volume, V_o (-)	Degree of saturation, S_r (%)	Gravimetric water content, w (%)	Specific volume, V (-)	*Volumetric strain, ε_V (%)	Mean stress, p (kPa)	Water uptake (mL)	Degree of saturation, S_r (%)	Dry density ρ_d (Mg/m^3)	Bulk density ρ_b (Mg/m^3)
Recompacted Bearpaw clay	CMS200	29.3	1.87	93	31.9	1.90	-1.21	204	23	98	1.45	1.91
	CMS400	27.8	1.88	87	31.6	1.87	0.99	401	1.8	100	1.47	1.94
	[1]CMS200	31.8	1.95	92	33.5	1.95	-0.22	187	8.9	97	1.41	1.88
	[2]CMS400	30.9	1.95	89	31.3	1.83	6.46	400	2.3	97	1.46	1.92
	CV400	29.6	1.91	90	30.8	1.83	4.18	410	1.82	102	1.50	1.97
Recompacted Lake Agassiz clay	CV150	21.6	1.76	79	29.0	1.76	-0.06	753	25	105	1.57	2.02
	CMS150	20.3	1.74	77	39.1	1.99	-14.6	143	62	109	1.39	1.93
	CV300	19.0	1.72	73	26.3	1.70	1.22	1200	25	103	1.62	2.05
	CMS300	21.1	1.75	78	32.4	1.88	-7.28	291	37	102	1.47	1.95
	CMS600	19.3	1.75	71	29.2	1.80	-3.80	606	33	101	1.53	1.98

All triaxial infiltration tests are saturated with water pressure at 100 kPa.
* negative value represents expansion; positive value represents compression
1: test begins with CMS200, then load up with 200 kPa at each stress increment up till 800kPa under CMS condition.
2: test begins with CMS400, then unload to 200 kPa under CMS condition.

Table 3.3. Initial condition and end-of-test result of unconfined swelling test for recompacted Bearpaw and recompacted Lake Agassiz clay.

Soil Type	Initial (as-compacted)			End of unconfined swelling test					
	Water content, w_o (%)	Specific volume, V_o (-)	Degree of saturation, S_r (%)	Water content, w (%)	Specific volume, V (-)	*Volumetric strain, ε_V (geoPIV) (%)	Degree of saturation, S_r (%)	Dry density, ρ_d (Mg/m^3)	Bulk density, ρ_b (Mg/m^3)
Recompacted Lake Agassiz clay	20.6	1.77	74.1	67.3	3.00	-70.3	92.7	0.92	1.54
Recompacted Bearpaw clay	30.0	1.88	93.8	61.8	2.74	-42.1	97.8	1.00	1.63

* negative value represents expansion; positive value represents compression

Table 3.4. Fitted SEL curves for BSB, recompacted Lake Agassiz clay, recompacted Bearpaw clay and natural Bearpaw shale.

a) Fitting parameters of A and B from V- p plot

Soil type	$V = A + B * \ln p$	R^2
BSB	$V = 3.023 - 0.214 \ln p$	0.9178
Recompacted Lake Agassiz clay	$V = 2.691 - 0.141 \ln p$	0.9634
Recompacted Bearpaw clay	$V = 2.596 - 0.127 \ln p$	0.9706
Natural Bearpaw shale	$V = 2.102 - 0.0463 \ln p$	0.9626

b) Fitting parameters of C and D from log (p_{swell}) – EMDD plot

Soil type	$p_{swell} = C * e^{(D*EMDD)}$	R^2
BSB	$p_{swell} = 0.007609e^{(4.56*EMDD)}$	0.9510
Recompacted Lake Agassiz clay	$p_{swell} = 0.0004966e^{(12.27*EMDD)}$	0.9903
Natural Bearpaw shale	$p_{swell} = 1.254E - 10e^{(31.45*EMDD)}$	0.9305

Table 3.5. Calculated fitting parameters of A and B for calculating preliminary Regina clay's SEL in V=A+B ln p.

Index property of Regina clay (Fredlund 1975)		Correlation equation used	Calculated A	Correlation equation used	Calculated B
V_o =	1.838	Fig 3.13(a)	2.638	Fig 3.14(a)	-0.133
LL =	76	Fig 3.13(b)	2.641	Fig 3.14(b)	-0.132
PI =	50	Fig 3.13(c)	2.653	Fig 3.14(c)	-0.135
PL/LL=	0.344	Fig 3.13(d)	2.702	Fig 3.14(d)	-0.146
PI/LL =	0.656	Fig 3.13(e)	2.702	Fig 3.14(e)	-0.146
		Average	2.667	Average	-0.138

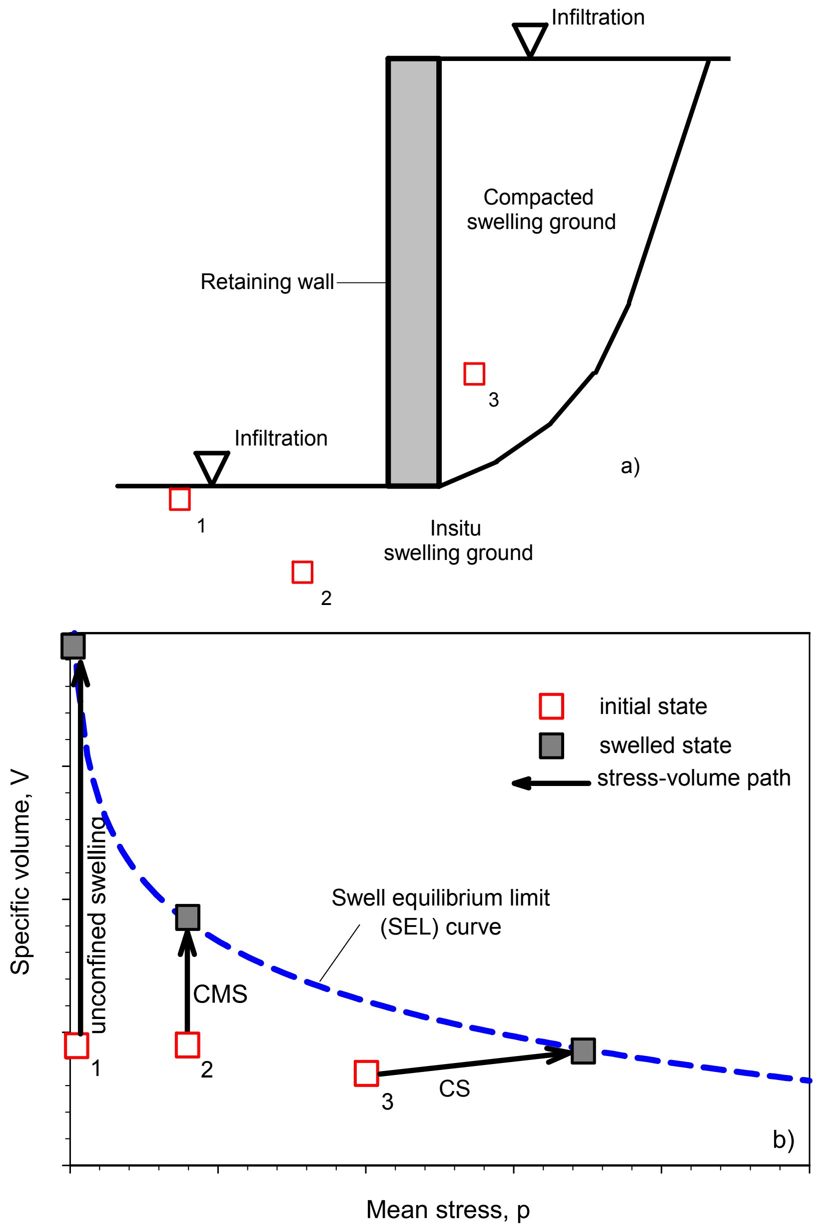

Figure 3.1. Illustrative concept of the Swell Equilibrium Limit indicating stress-volume paths for swelling around a retaining wall application.

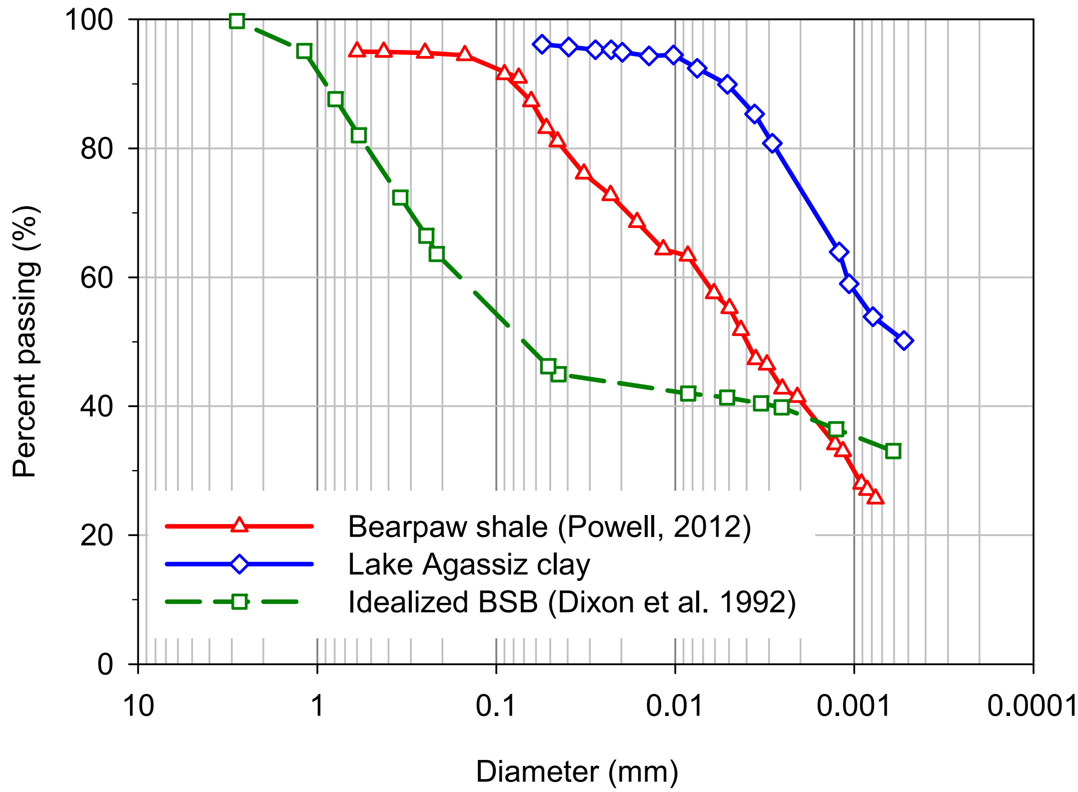

Figure 3.2. Grain size distribution for Bearpaw shale, bentonite-sand-buffer and Lake Agassiz clay.

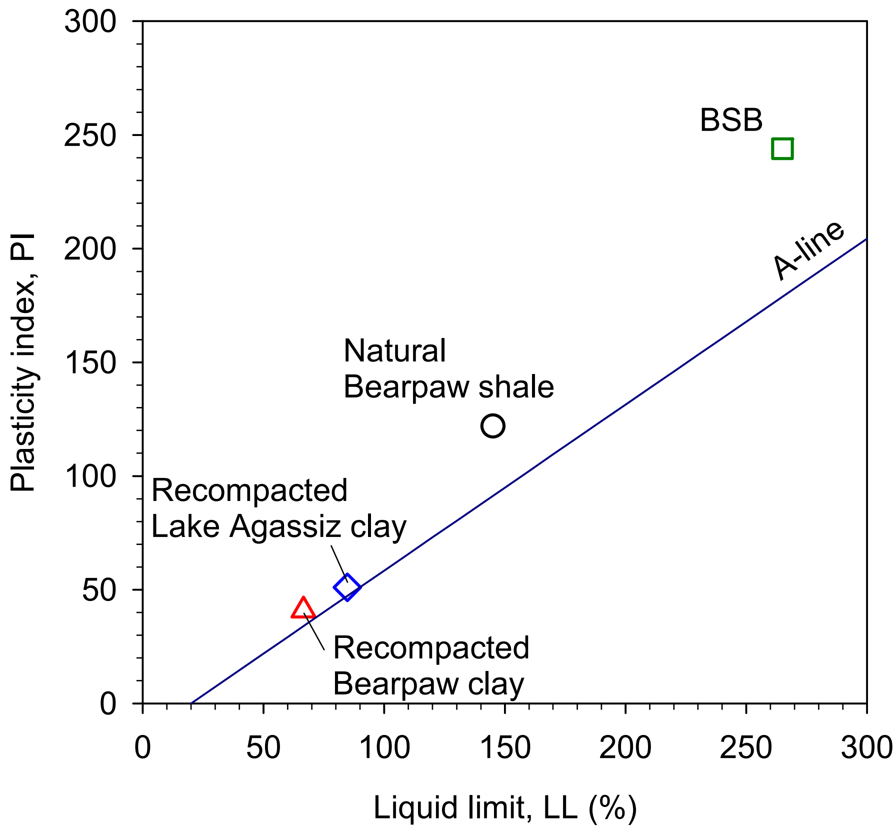

Figure 3.3. Plasticity chart for recompacted Lake Agassiz clay, recompacted Bearpaw clay, natural Bearpaw shale and BSB.

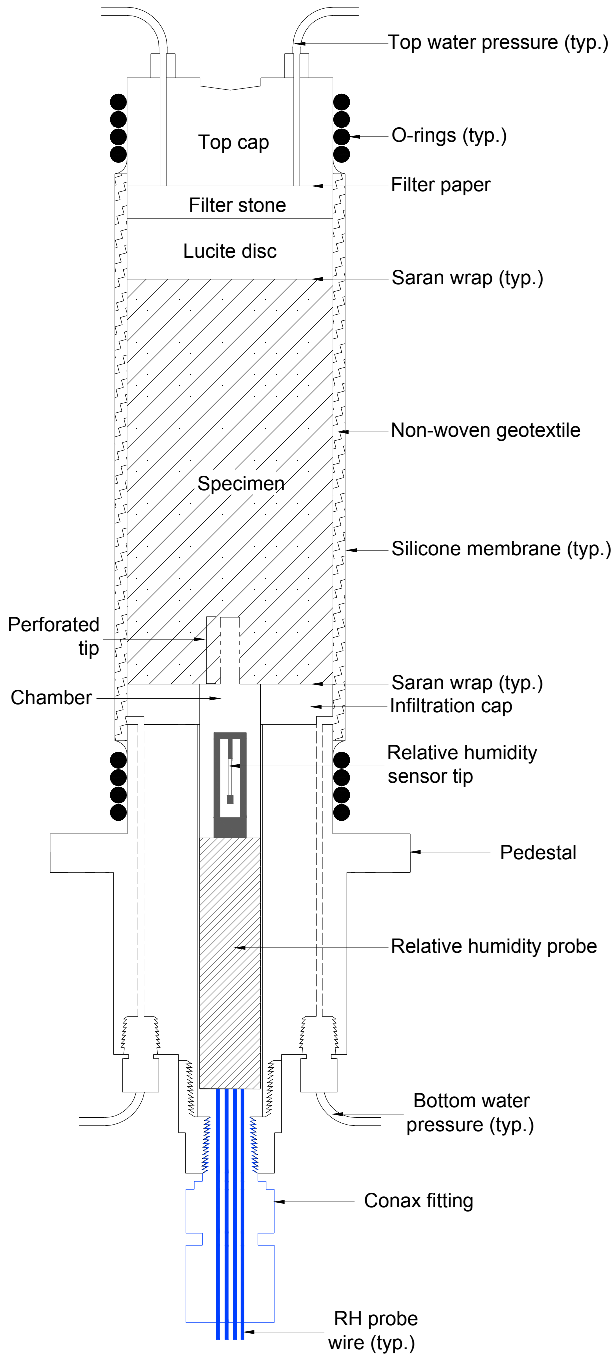

Figure 3.4. Schematic of triaxial pedestal highlighting modifications made to suction measurement location.

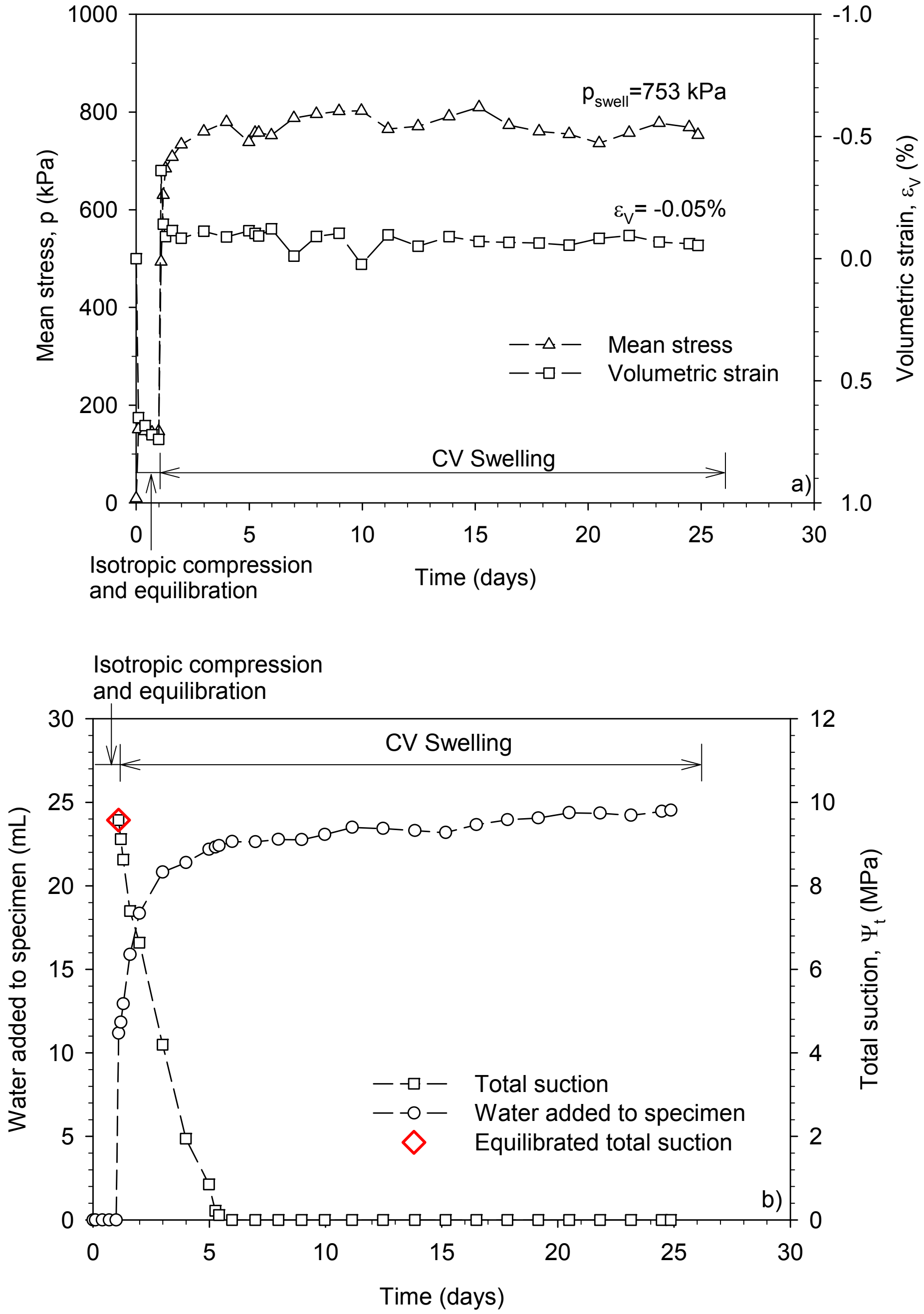

Figure 3.5. Triaxial swelling test of recompacted Lake Agassiz clay: CV 150kPa plotting a) mean stress and volumetric strain versus time, and; b) water added to specimen and total suction versus time.

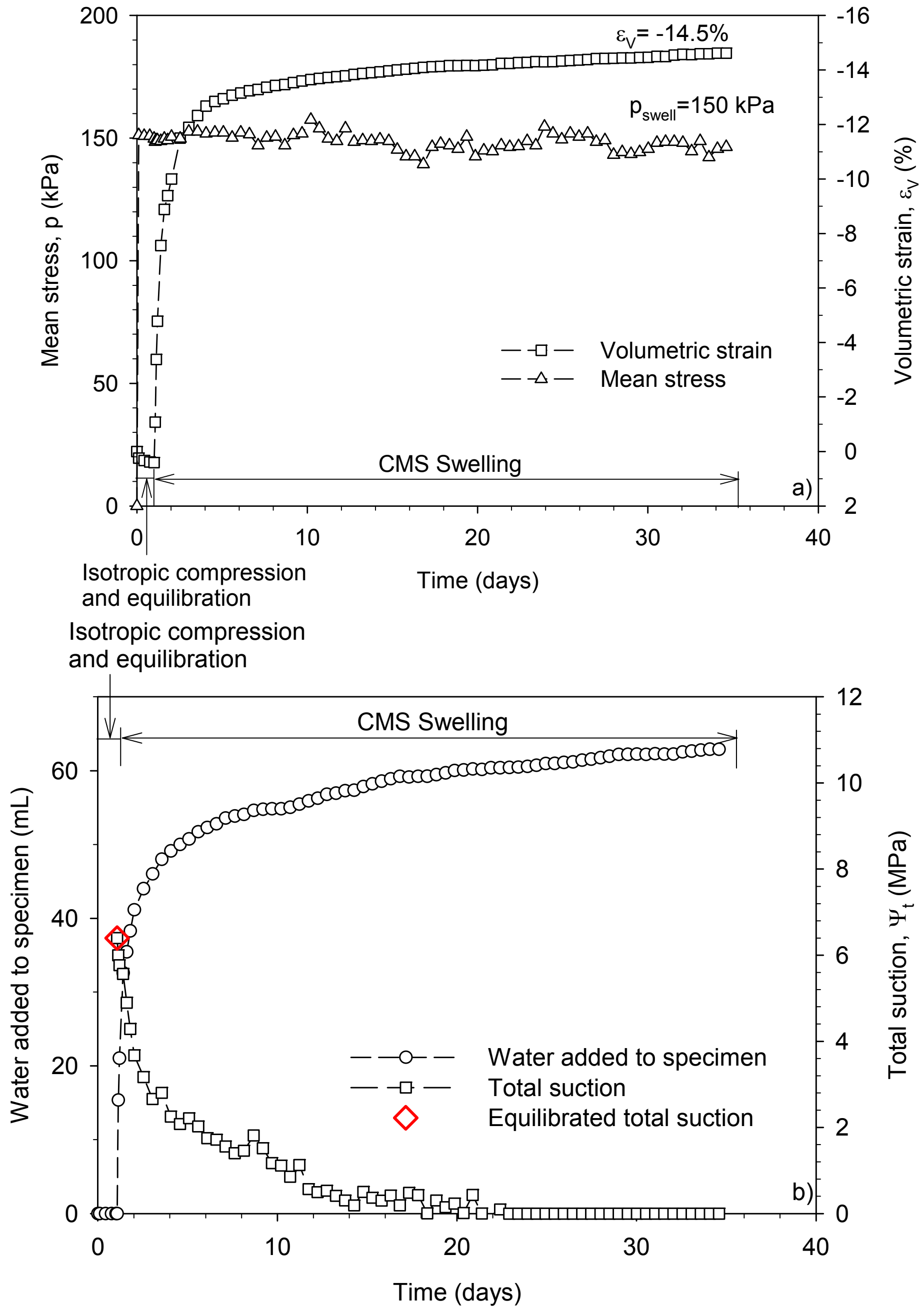

Figure 3.6. Triaxial swelling test of recompacted Lake Agassiz clay: CMS 150kPa plotting a) mean stress and volumetric strain versus time, and; b) water added to specimen and total suction versus time.

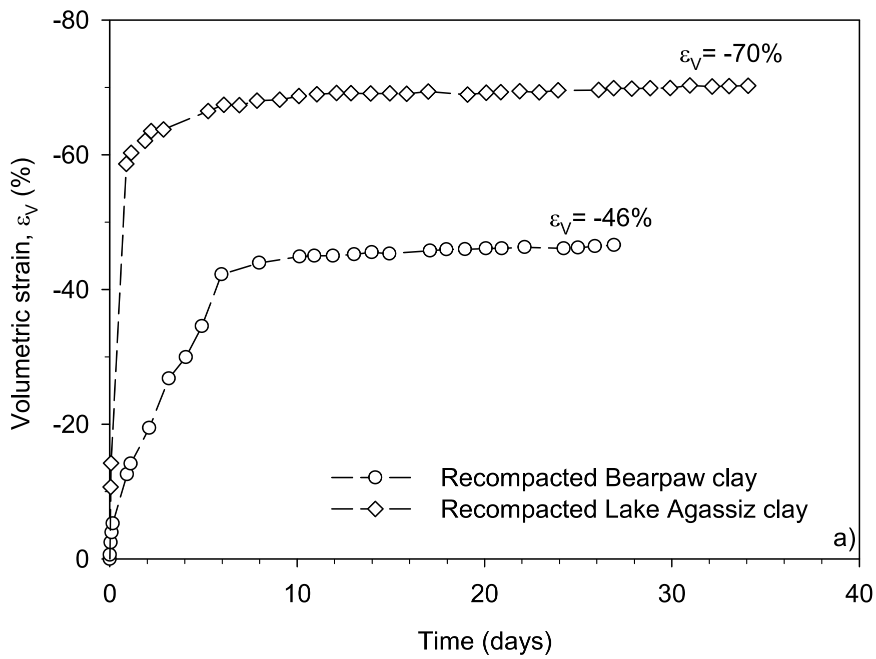

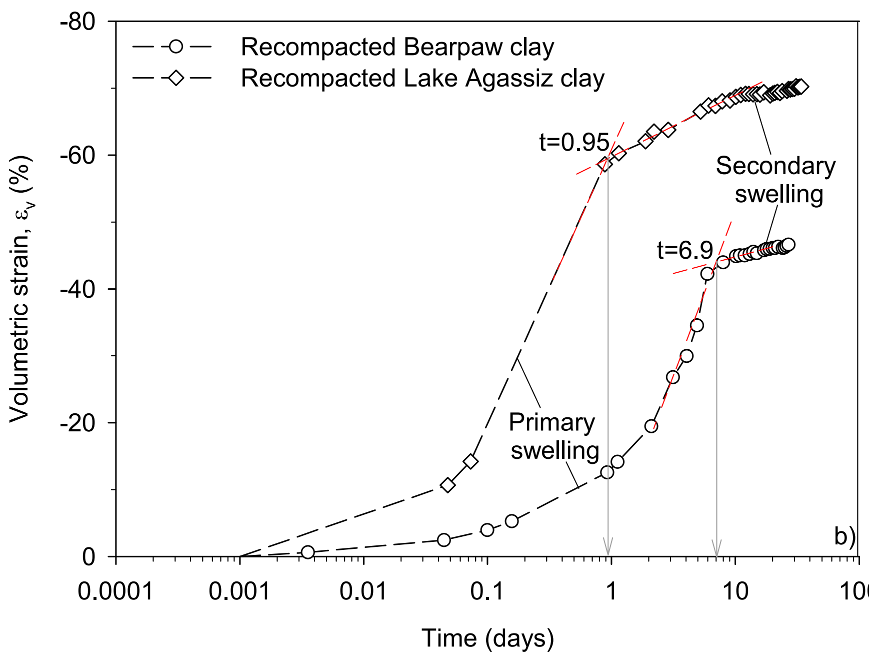

Figure 3.7. Unconfined swelling test summary for recompacted Lake Agassiz clay and Bearpaw clay plotted as volumetric strain versus time plotted on a) linear axis and b) log axis.

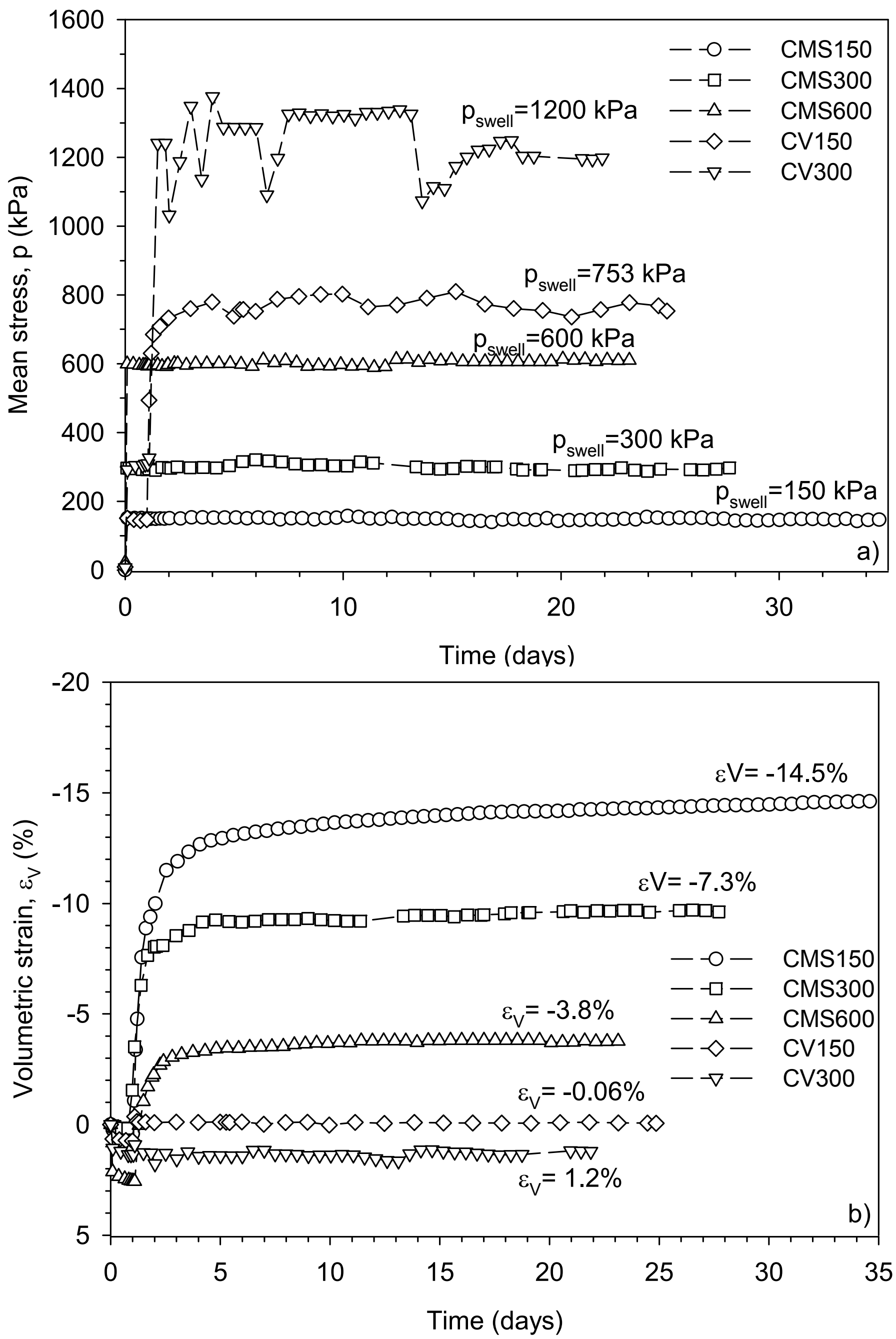

Figure 3.8. Swelling test summary for recompacted Lake Agassiz clay plotting a) mean stress versus time and b) volumetric strain versus time.

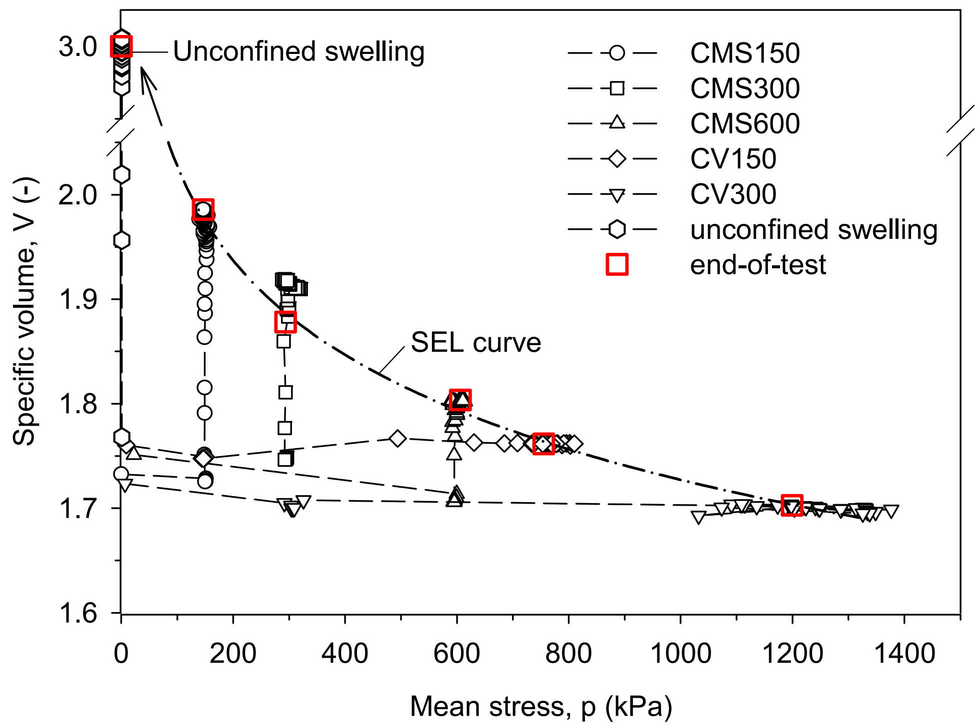

Figure 3.9. Swell equilibrium limit (SEL) for recompacted Lake Agassiz clay.

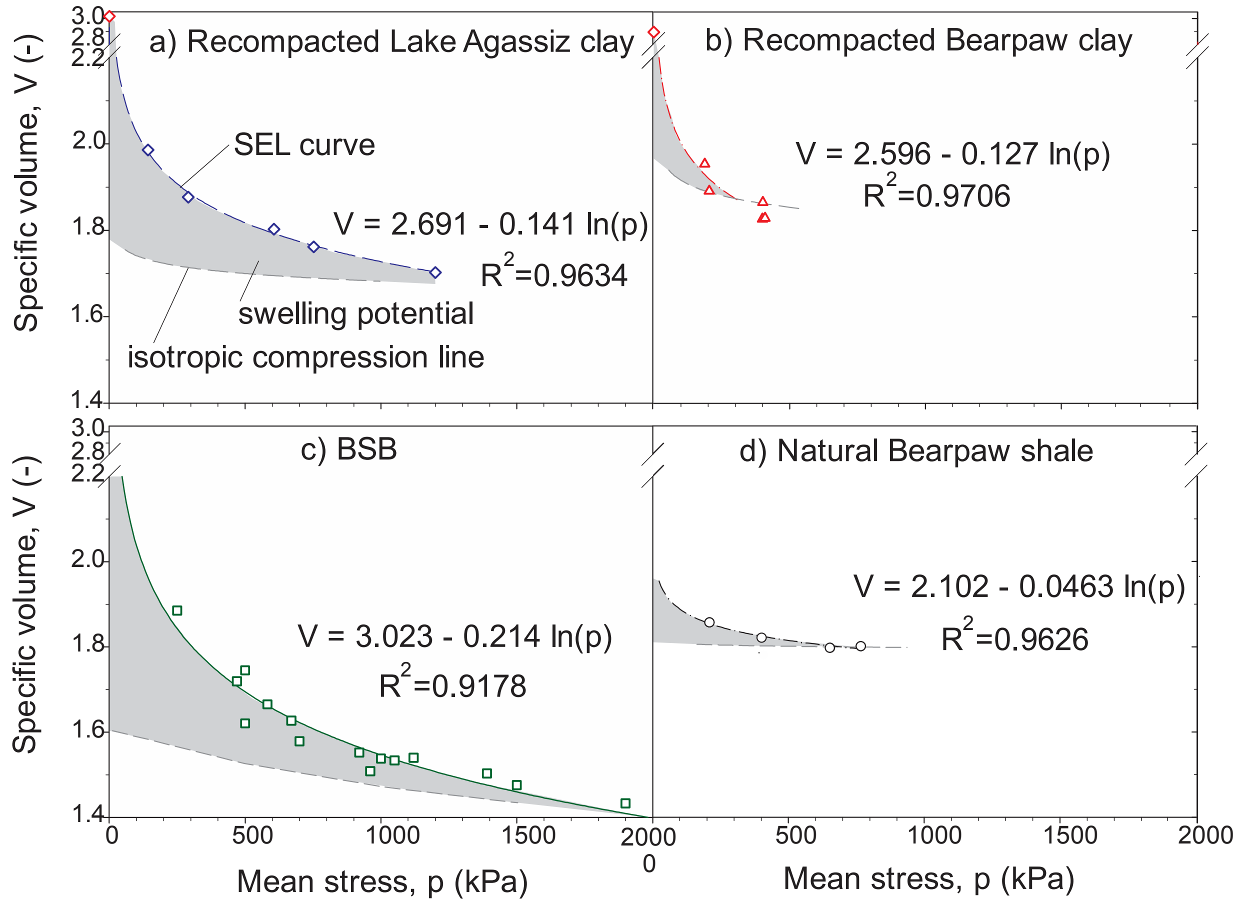

Figure 3.10. Swell equilibrium limit (SEL) for: a) Recompacted Lake Agassiz clay; b) Recompacted Bearpaw clay; c) Bentonite-sand-buffer and d) Natural Bearpaw shale.

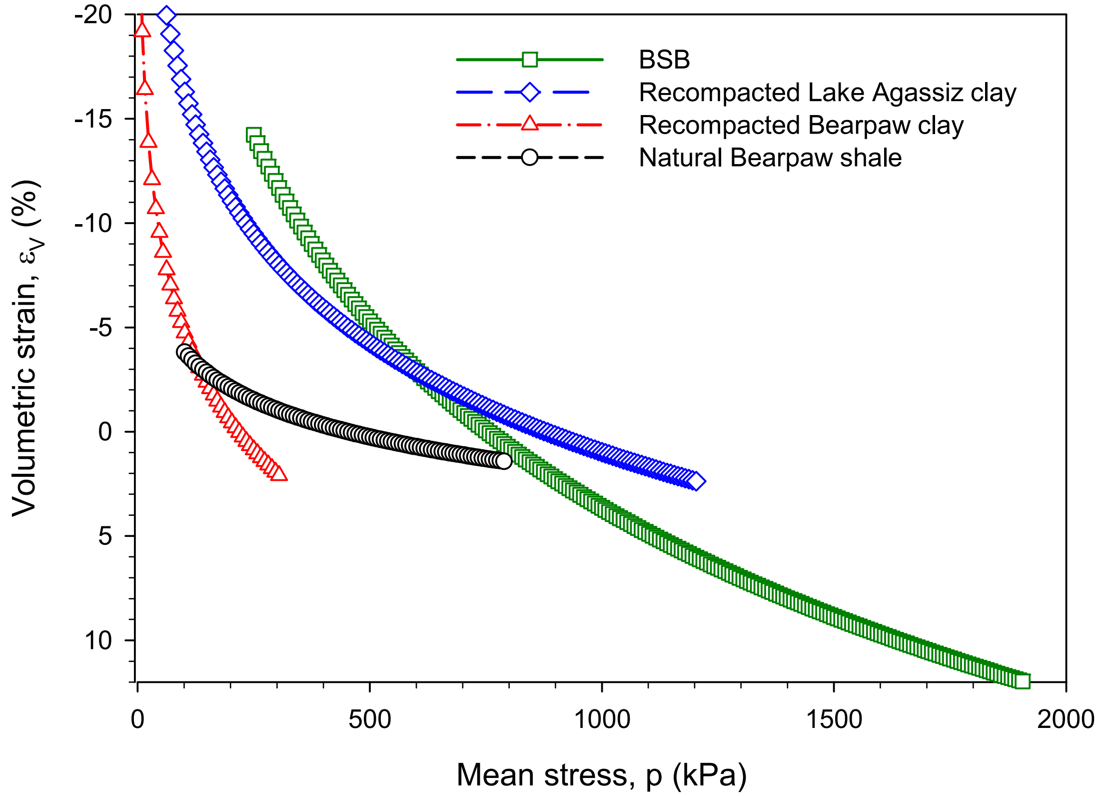

Figure 3.11. Swell equilibrium limits (SELs) in ε_v –p space.

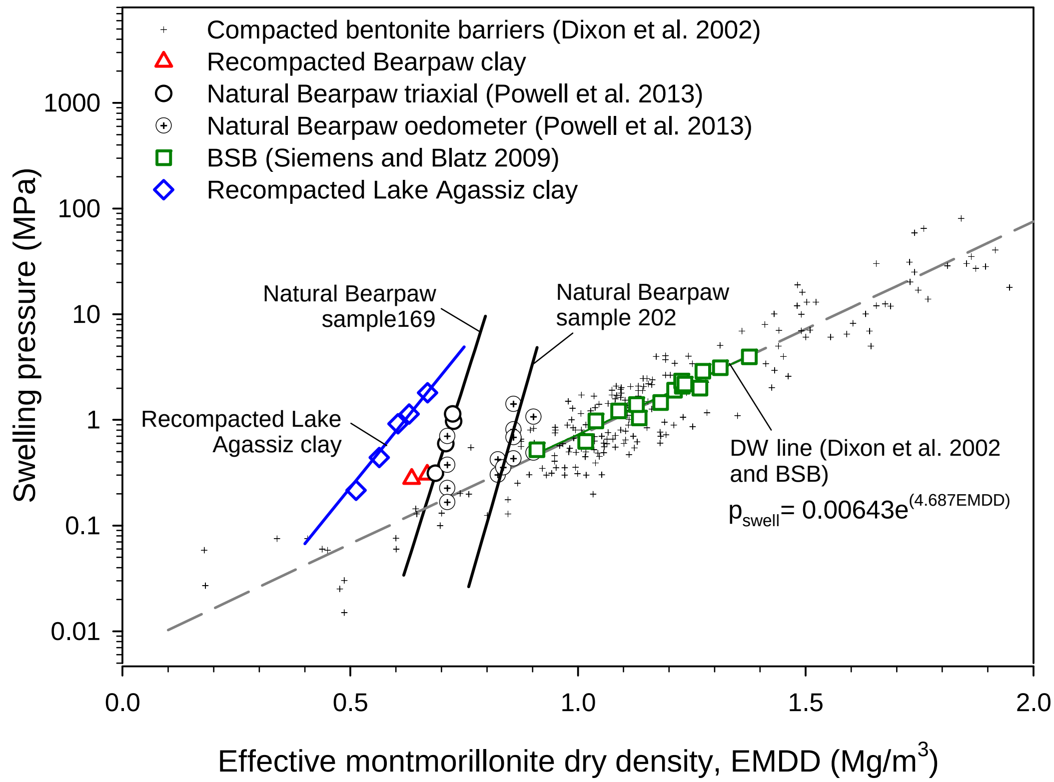

Figure 3.12. Swelling pressure versus effective montmorilllonite dry density of recompacted Lake Agassiz clay triaxial, natural Bearpaw triaxial and oedometer (Powell et al. 2013), BSB (Siemens and Blatz, 2009) and Dixon et al. (2002) swelling pressure data.

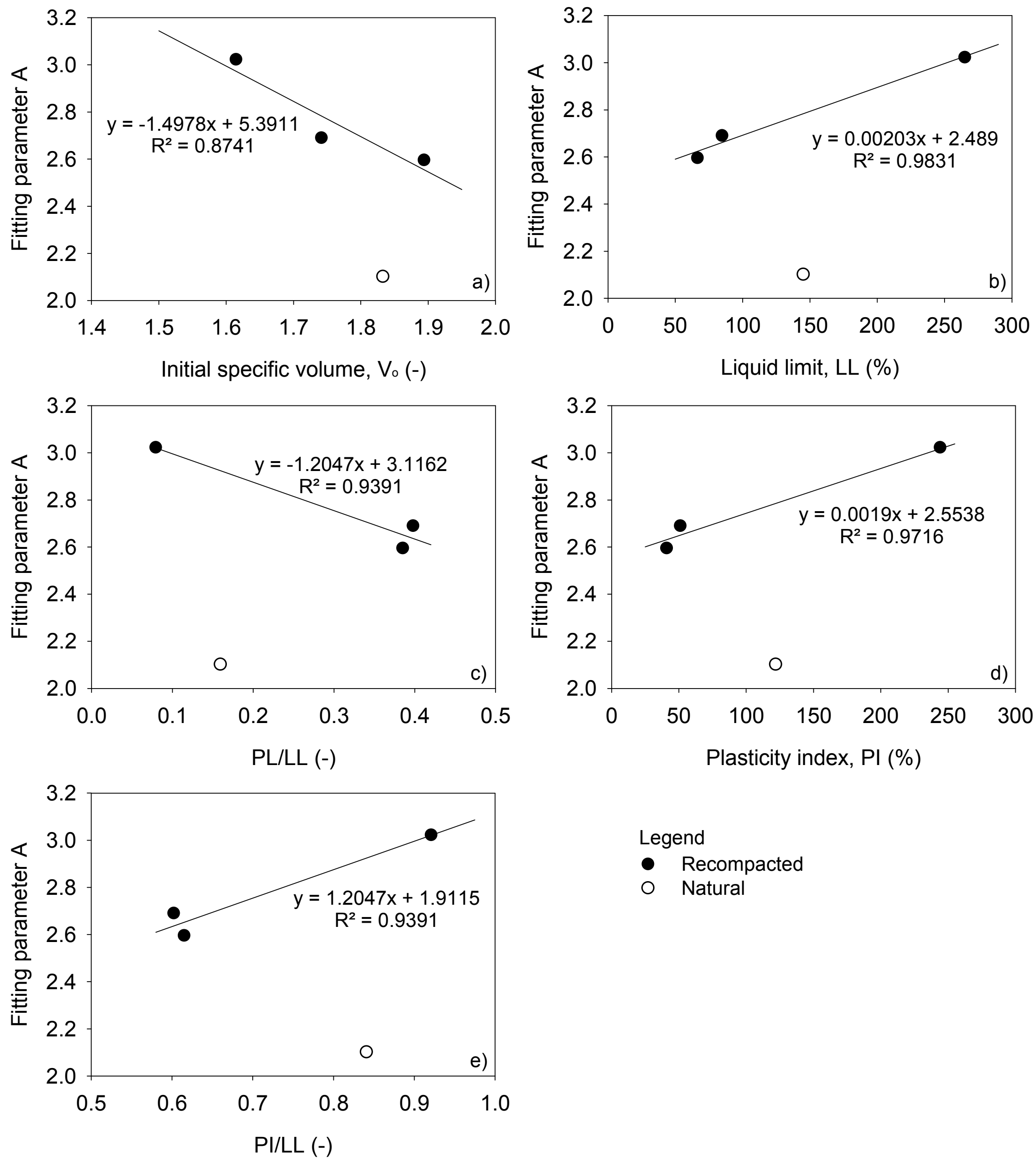

Figure 3.13. Correlation plots relating SEL fitting parameter A to soil index properties.

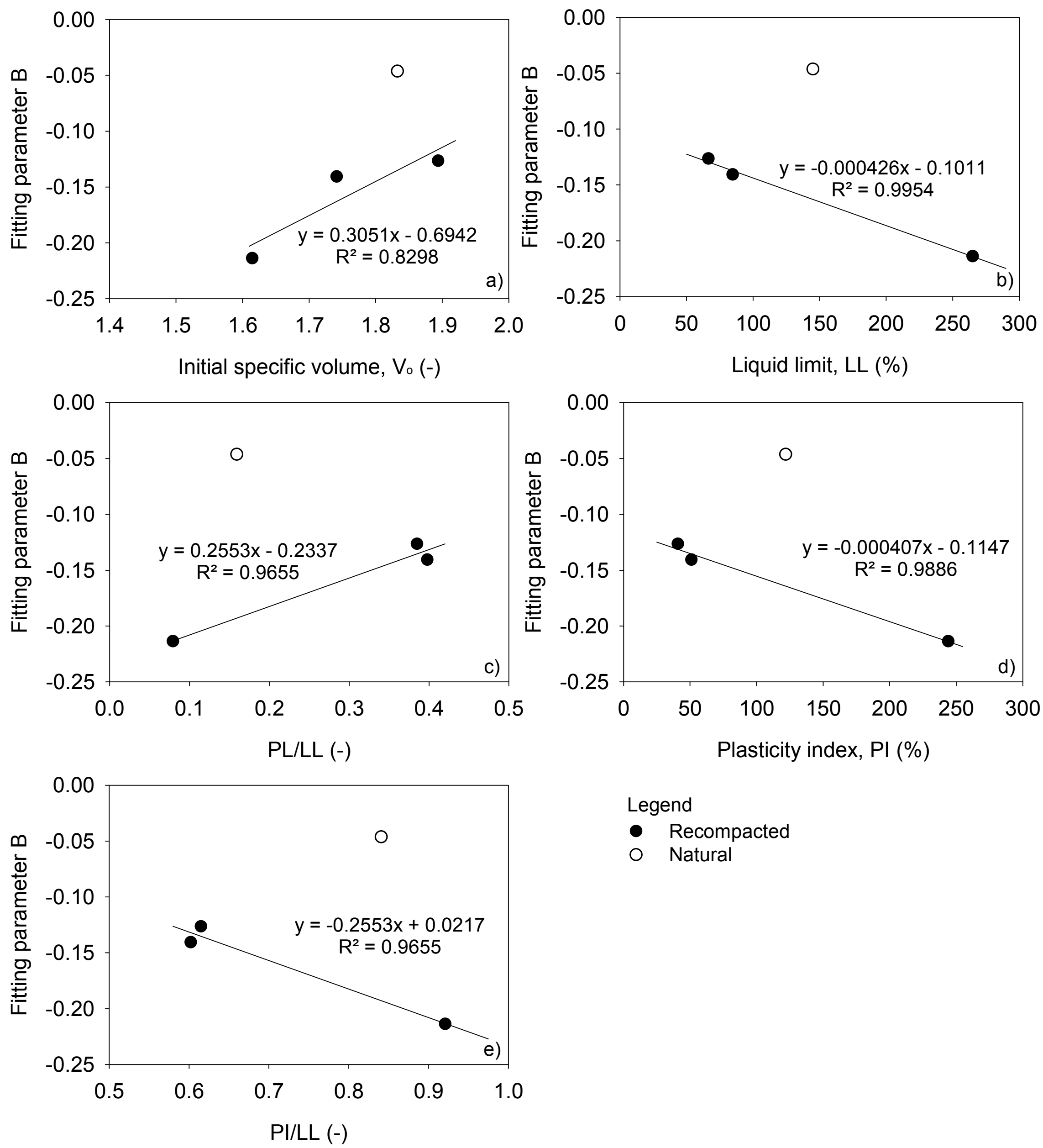

Figure 3.14. Correlation plots relating SEL fitting parameter B to soil index properties.

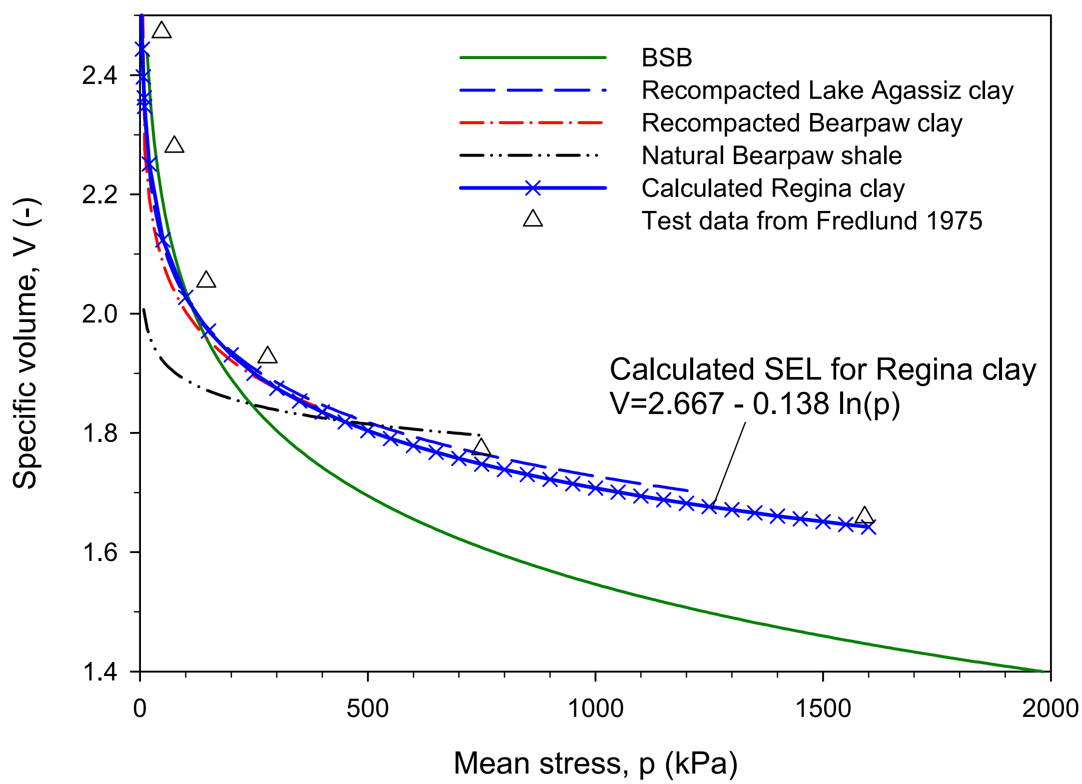

Figure 3.15. SEL curves for the tested soils and a calculated SEL for Regina clay compared with swelling data from Fredlund (1975).

CHAPTER 4: A NUMERICAL TOOL FOR MODELLING SWELLING BEHAVIOUR OF EXPANSIVE SOILS

4.1 Introduction

Unsaturated soil systems in the near-surface vadose zone are inherently challenging to model in the laboratory and numerically. In the vadose zone, soil behavior is significantly affected by daily and seasonal weather as well as changing groundwater conditions. Thus the challenge is to identify governing behavior mechanisms. Advanced testing allows for more complicated systems to be examined at the laboratory scale to attempt to isolate behavior, however the lessons learned need to be applied to a wider range of applications. Computing power has advanced to allow for complicated constitutive models to be applied to a wide range of applications, however, these must first be calibrated to high quality physical data.

Infrastructure constructed in expansive soils continues to suffer damage at the cost of billions of dollars per year (Keller, 2008, Puppala and Cerato, 2009) despite extensive research efforts. Expansive soil affects are inherently an unsaturated soils application that occurs in the vadose zone and are complicated by environmental effects. Numerous attempts have been made to develop analysis procedures to understand expansive behavior (Miller et al. 1995, Briaud et al. 2003, Vanapalli et al. 2010) however, damage continues to occur. Thus the need remains for an analysis tool to reliably model swelling behavior.

There has been a wide body of research focusing on developing constitutive models for unsaturated soils (Alonso et al. 1990, Cui and Delage 1996, Fredlund and Morgenstern 1977, Wheeler and Sivakumar 1995). The Barcelona Basic Model (BBM) developed by Alonso et al. 1990 has become a keystone in unsaturated soils literature and this model has provided a platform for many developments made in the more recent models. One of challenges in numerical model is to formulate the constitutive equations with appropriate input parameters. For instance, the BBM model may require nine input parameters or soil constants (Alonso et al. 1990). Another challenge is some models may work well only with a specific type of soil. These challenges may have posed some difficulty to a designer to use new soil models confidently as they are rarely used in practice. More recently an unsaturated constitutive model developed by Sheng et al. (2008) has shown good potential in numerical analysis of unsaturated soils (Sheng et al. 2004, Sheng et al. 2008, Zhou and Sheng 2009, and Sheng and Zhou 2011). The improvement made by SFG model is its simplicity in terms of input parameter requirement and the applicability to swelling as well as collapsible unsaturated soils.

The Swell Equilibrium Limit (SEL) concept developed by Siemens and Blatz (2009) provides a unifying framework to understand swelling behavior. The swelling-induced stresses and deformation obtained from the advanced swelling tests encompass a comprehensive range of scenarios on how swelling soil responds to a given wetting condition. The implementation of SEL concept in a swelling soil is illustrated in a shallow foundation application as shown in Figure 4.1. Three swelling scenarios occurring during long-term infiltration are illustrated in Figure 4.1 including: 1) free swell condition at the surface, 2) constant mean stress swelling under the basement slab and 3) constrained swelling adjacent to the stiff basement wall. In scenario 1, the soil at the ground surface experiences the greatest magnitude in swelling deformation upon wetting as there is no boundary constraint and very low stress. This scenario is represented by the unconfined swelling shown as stress-volume Path 1 in a schematic specific volume – net mean stress plot (Figure 4.1b). In scenario 2, soil at a certain depth experiences swelling deformation under a constant stress (see stress-volume Path 2 – Constant Mean Stress (CMS)). Finally in scenario 3, ground adjacent to a concrete basement wall, the soil is subjected to a rigid boundary condition. In this case, the soil will experience swelling-induced stresses as expansion is constrained by the stiff wall.

Previous chapters in this thesis have developed a new laboratory method to measure unconfined swelling behavior (Chapter 2, Lim and Siemens 2013) and reported further advanced swelling tests within the SEL context (Chapter 3). This research utilizes the experimental data in a numerical model that can be used as an analysis tool in engineering design. In this chapter, an analysis tool for modeling swelling behavior of expansive soils is developed based on the SFG constitutive model. Advanced swelling tests are simulated to determine the constitutive parameters for the model for two soils, namely BSB and recompacted Lake Agassiz clay. Finally an example is given to analyze swelling-induced pressures on a basement wall, swelling below a foundation as well as near-surface swelling.

4.2 Sheng, Fredlund and Gens (SFG) Constitutive Model

A constitutive model for unsaturated soils was reported by Sheng et al. (2008). The SFG model is an elastic-plastic constitutive model for volume change and shear strength of unsaturated soils, derived from a theoretical approach. The model has been derived for compacted and consolidated unsaturated soils. An additional capability of the model is to handle collapse mechanisms in unsaturated soil. The SFG model has been used successfully to model unsaturated soil behavior of clayey soil (Lloret et al 2003), compacted Pearl clay (Sun et al. 2007), silty soil (Jennings and Burland 1962), reconstituted silty clay (Cunningham et al. 2003), compacted soils (Sivakumar and Wheeler 2000), compacted kaolin specimen (Thu et al. 2007) and Brown London Clay (Marinho et al. 1995) as presented in Sheng et al. 2008 and Sheng and Zhou 2009. In this chapter, the model is used to simulate advanced swelling tests and, therefore, the background of those aspects of the model are introduced.

The SFG model isolates volume change of an unsaturated soil into suction-induced and stress-induced components. The volume change equations take the form:

[4.1] $$dv = -\lambda_{vp} \frac{d\bar{p}}{\bar{p}+s} - \lambda_{vs}(s)\frac{ds}{\bar{p}+s}$$

[4.2] $$\lambda_{vs}(s) = \begin{cases} \lambda_{vp} & s < s_{sa} \\ \lambda_{vs} \dfrac{s_{sa}+1}{s+1} & s \geq s_{sa} \end{cases}$$

where v = specific volume, $\bar{p}$ =p-u_a = net mean stress, u_a = pore-air pressure, s=u_a-u_w = suction, λ_{vp} = slope of the NCL for normally consolidated soils, λ_{vs} = suction compressibility , and s_{sa} = saturation suction.

The form of Equation [4.1] appears similar to a saturated soil. In fact the λ_{vp} term is the compressibility of a normally consolidated saturated soil. The first term calculates deformation based on change in net mean stress and the second term calculates deformation based on change in suction. The only additional required parameter to calculate volume change in the SFG model is the saturation suction, s_{sa}. Saturation suction is similar but distinct from the air entry value (AEV) as defined in Figure 4.2. The AEV is usually defined as the intersection between the main drying curve and the flat initial part of the SWCC. Whereas the saturation suction defines the suction at which the soil changes from a saturated soil to an unsaturated soil. In other words, the saturation suction is the highest suction where the soil maintains Sr=1.0. Therefore the saturation suction is less than the AEV (Sheng et al. 2008) as illustrated in Figure 4.2. For use in Equation [4.2], at suctions less than the s_{sa}, deformations are calculated as if the soil is saturated ($\lambda_{vs} = \lambda_{vp}$). At suctions greater than the s_{sa}, the compressibility is reduced by a factor $(s_{sa}+1)/(s+1)$. Thus compressibility due to suction variation is at a maximum at low suctions and reduces as suction increases due to the $(s+1)$ term in the denominator.

The soil compressibility termed as λ_{vp} is originally related to the slope of NCL line in saturated soils. However, in the application of SEL concept, λ_{vp} is related to the swelling potential. Therefore the conventional λ_{vp} value can be served as a reference to initiate the calibration procedure in the model. The appropriate λ_{vp} that needed to be used in SFG model is back-calculated from the SEL test data.

4.2.1 Constant Mean Stress (CMS) module in SFG model

The modules for simulating CMS and CV boundary conditions within the SFG framework are presented separately here. The test paths for constant mean stress (CMS) and constant volume (CV) swelling tests (Siemens and Blatz 2009, Chapter 3) are illustrated in Figure 4.3 in terms of suction-net mean stress space and specific volume-net mean stress plots. Following compaction the soil is at its initiation suction and specific volume at zero net mean stress. The first phase is isotropic compression where the specimen is brought to a specified stress state. As a result of increasing net mean stress, suction decreases along a straight line (Figure 4.3a, Blatz and Graham 2003) and specific volume decreases (Figure 4.3b). During a CMS swelling test, the net mean stress is maintained constant and the specimen given access to water. Thus the stress path in suction–net mean stress space is a vertical line moving down from the isotropic compression line to zero suction. In specific volume-net mean stress space the stress-volume path is vertically upward until equilibrium is achieved.

In the CMS module, volume change is calculated using Equations [4.1] and [4.2]. However, since net mean stress is constant throughout during swelling, (i.e. $d\bar{p} = 0$) the first term in Equation [4.1] is equal to zero. Thus volume change calculated in this module is only attributed to the reduction in suction. This isolates the suction contribution to deformation making it advantageous to model the CMS tests prior to the CV tests. Modeling of the unconfined test (Chapter 2) is performed in a similar manner except the isotropic compression phase is ignored and tests are assumed to occur at $\bar{p}$ =1 kPa as nominal pressure. Explicitly Equation [4.1] is reduced as follows:

$$dv = -\lambda_{vp}\frac{d\bar{p}}{\bar{p}+s} - \lambda_{vs}(s)\frac{ds}{\bar{p}+s}$$

$$dv = -\lambda_{vs}(s)\frac{ds}{\bar{p}+s} \qquad [4.3]$$

The CMS module proceeds by incrementally decreasing suction (ds=constant) and deformations are calculated for each increment. The module is complete once the equilibrium suction is attained.

4.2.2 Constant Volume (CV) module in SFG model

The CV module initiates similarly to the CMS module with isotropic compression defining the initial stress, suction and volume state of the soil. The test paths are again shown schematically in Figure 4.3a and Figure 4.3b. During swelling, Equation [4.1] is used in the calculations. However, at each increment the equation is set equal to zero (dv=0) to represent the constant volume boundary conditions. Thus the first term, stress-induced deformation, is equated to the second term of suction-induced deformation. Explicitly:

$$dv = -\lambda_{vp}\frac{d\bar{p}}{\bar{p}+s} - \lambda_{vs}(s)\frac{ds}{\bar{p}+s} = 0$$

$$-\lambda_{vp}\frac{d\bar{p}}{\bar{p}+s} = \lambda_{vs}(s)\frac{ds}{\bar{p}+s}$$

$$d\bar{p} = \frac{\lambda_{vs}(s)}{-\lambda_{vp}}ds \qquad [4.4]$$

If suction is lesser than s_{sa}, $\lambda_{vs}(s)=\lambda_{vp}$:

[4.5] $$d\overline{p} = \frac{\cancel{\lambda_{vs}(s)}}{-\cancel{\lambda_{vp}}} ds = ds$$

If suction is greater than s_{sa}, $\lambda_{vs}(s) = \lambda_{vp} \frac{s_{sa}+1}{s+1}$:

$$d\overline{p} = \frac{\cancel{\lambda_{vp}} \frac{s_{sa}+1}{s+1}}{\cancel{\lambda_{vp}}} ds$$

[4.6] $$d\overline{p} = \frac{s_{sa}+1}{s+1} ds$$

Therefore it is anticipated that saturation suction, s_{sa}, will have an influential impact on the modelled swelling pressure.

The CV module proceeds through swelling by reducing suction incrementally (ds=constant) and calculating the resulting increase in net mean stress (dp) using either Equation [4.5] or [4.6] depending if suction is greater or lesser than s_{sa}. In suction-net mean stress space (Figure 4.3a) the stress path is curved downward and in specific volume-net mean stress space (Figure 4.3b) the path is horizontal.

4.2.3 Materials

The two tested soils presented are the compacted bentonite-sand-buffer (BSB, Siemens and Blatz 2009) and the recompacted Lake Agassiz clay (Chapter 3). Index properties of these two soils are listed in Table 4.1. BSB is a type of engineered buffer consists of a mixture of equal parts Na-bentonite and sand. BSB has considerably high plasticity with LL of 265% and PI of 244%. The activity of BSB is as high as 4.88. The recompacted Lake Agassiz clay is a type of natural swelling soil taken from Southern Manitoba. The clay content of recompacted Lake Agassiz clay is higher at 75% but its Atterberg Limits are relatively lower than BSB's. The LL and PI of recompacted Lake Agassiz is 85% and 51%, respectively. The activity of recompacted Lake Agassiz clay is 0.64.

4.3 Model Development

4.3.1 Bentonite-sand-buffer (BSB)

The SFG model requires two model input parameters, thus giving it greater potential for use as a practical analysis tool. The model inputs for the swelling soil required are compressibility (λ_{vp}) and saturation suction (s_{sa}) and the initial suction state as defined by the ds/dp ratio for each material.

The range of plausible compressibility values for BSB was back analyzed from the laboratory test data. Compressibility parameter (λ_{vp}) was estimated from the CMS and CV tests in BSB (Siemens and Blatz 2009) assuming no contribution from suction. CMS and CV tests from a total of four different stress levels (p= 250, 500, 1000 and 1500 kPa). Soil compressibility, λ_{vp} is estimated from the end-of-test data of both CMS and CV tests. The initial and end-of-test data were analyzed and used in the preliminary calculation. The range indicated in Table 4.2 is from 0.074-0.542. The average value of 0.25 was selected as a starting point for model calibration.

The preliminary saturation suction, s_{sa} of BSB is assessed from existing SWCC data for compacted barriers as presented in Figure 4.4a (after Priyanto 2007). The data includes a number of bentonite barriers as well as the data for the BSB tests modeled presently. The data has a wide range of variability, which is common in these types of materials. Bounding SWCC curves as well as an average SWCC curve are included on the plot. As explained in earlier section, s_{sa} is the maximum suction for the flat initial portion of the SWCC and is less than the traditional AEV. The variability of the data necessitates interpretation of the s_{sa}. The plausible range for s_{sa} based on the laboratory data is 150-250 kPa (range indicated on the figure). Based on the shape of the SWCCs a preliminary value of 200 kPa was used in model development.

The SFG modules apply a constant suction increment to throughout the model. Thus the initial and final suction value of the soil sets the start and end points for the model. The initial and final suction measurements for the swelling tests in BSB are plotted in Figure 4.5a (Siemens 2006). As expected, suction decreases with increasing net mean stress owing to the compression of the soil resulting in a reduced void ratio and increased volumetric water content (Blatz and Graham 2003). The more reliable suction data is selected at each pressure level while the outliers are neglected. The average suction values at the relevant stress levels (250 kPa, 500 kPa, 1000 kPa and 1500 kPa) are plotted. A linear equation is fitted through the average suction values and a ratio of $\Delta s/\Delta p=-1.0$ is established. The value is comparable to $\Delta s/\Delta p=-0.83$ measured by Blatz and Graham (2003).

The end-of-test suction data (s_{eot}) is also plotted in Figure 4.5a. All s_{eot} values are in the range from 400 to 600 kPa. These measurements are made with an indirect method and, therefore, likely consist mainly (if not completely) of osmotic suction. For consistency in modelling, s_{eot} is taken as 400 kPa as the osmotic suction.

4.3.2 Recompacted Lake Agassiz clay

The soil compressibility is back-calculated from the triaxial swelling test of recompacted Lake Agassiz clay. Table 4.2b summarizes the end-of-test of CMS150, CV150, CMS300 and CV300 as well as the back-calculated soil compressibility. The range of soil compressibility is 0.23-0.331. The average value of 0.28 as used as the starting point for SFG model calibration.

The preliminary estimate of saturation suction for recompacted Lake Agassiz clay is estimated from Figure 4.4b. The initial equilibrated and end-of-test suctions of recompacted Lake Agassiz clay are plotted with the SWCC data from Pauls 1995. The measured data falls in a reasonable range of the data given by Pauls 1995. The plausible range of saturation suction is 70-200 kPa. As a starting value, s_{sa} = 200 kPa is used in SFG model.

Figure 4.5b presents the initial and post swelling test suctions plot for recompacted Lake Agassiz clay. Due to the scattered data points in suction measurement, the average suction at each pressure level (p=1, 150 and 300 kPa) is plotted. The average points are fitted through with a linear equation and this relation results in a ratio of $\Delta s/\Delta p=-1.0$. The fitted line in Figure 4.5b represents the initial equilibrated suction of recompacted Lake Agassiz clay in the model.

The end-of-test suction, s_{eot} of recompacted Lake Agassiz clay is measured to be zero. Therefore, the s_{eot} used in the model would be zero for recompacted Lake Agassiz clay.

4.4 Results

The modeling strategy utilized in the modelling the CMS and CV swelling tests included using consistent model inputs for the modelling program. In this section, typical experimental results are presented followed by the model calibration for BSB and Lake Agassiz clay.

4.4.1 Typical results of CMS and CV tests on BSB

Figure 4.6a shows a typical Constant Mean Stress (CMS) test result of BSB. The equilibration phase lasted three days. Then, the cell pressure was raised to p=500 kPa as isotropic compression resulted in volumetric compression of 5.4%. The swelling stage started when the water was supplied to the specimen. In a CMS test, the confining pressure was kept constant throughout the test. The water added to the specimen exhibited a higher gradient at the beginning and then levelled off asymptotically after about 12 days. The volumetric strain curve indicated swelling once the water was absorbed in the specimen. The trend of volumetric curve qualitatively resembles the curve of water added to specimen. The suction in the specimen decreased over time but the rate of suction change was slower compared to others. This is due to suction gradients within the specimen with the sensor being representative of suction at the center of the specimen. At the end of test, the relative volumetric expansion was 4.7% (final volume strain εv=0.7%), the total water added to specimen was 25 mL and the final suction was 0.7 MPa. The test duration lasted approximately three weeks.

Typical Constant Volume (CV) test results are given in Figure 4.6b as net mean stress, volumetric strain, suction and water added to specimen versus time. Similarly to the beginning of a CMS test, the suction in the specimen was left for equilibration (1 day in this case). Then, the cell pressure was increased to 500 kPa for isotropic compression. The compressed volumetric strain was 6.5%. Subsequently, the swelling stage was initiated by providing access of water. The water infiltrated rapidly at the beginning and then levelled off at t = 8.0 days. During swelling, suction decreased in response to water infiltration. The rate of suction change was slower than the rate of water added to specimen. The stress-volume path in a CV test is controlled in order to maintain zero total volume strain in the specimen. Additional cell pressure is applied to counteract the volume change during the CV swelling stage. The rate of change in net mean stress is a similar shape to the water infiltration curve. At 8.4 days, net mean stress stabilized at 980 kPa. At the end-of-test, the total water added to specimen was 16 mL and the final suction was 0.25 MPa. The CV 500 kPa test took approximately two weeks to complete.

Figure 4.8. presents a typical model simulation compared with experimental data for the test at stress = 500 kPa on BSB. The open squares are the result from swelling test while the ‘plus (+)’ symbol represents the model simulation. Figure 4.7a plots the total suction versus net mean stress for the tests of CMS500 and CV500. From as-compacted

state, the specimen is applied with 500 kPa of net mean stress. The application of net mean stress compresses the total volume of the specimen, hence the total suction of the specimen is decreased with a ratio of $\Delta s/\Delta p$ =-1.0 as presented in Figure 4.5a.

Once the infiltration stage begins, the test path of the CMS swelling moves vertically downward from a high initial suction to a low suction at constant stress at 500 kPa. Both experimental data and model agree well in CMS swelling. In the same plot, the suction of the CV swelling is also reduced from a high initial suction. The suction – stress path curves downward to the right of net mean stress axis. The swelling-induced stress is increased during the CV swelling test. The end-of-test of experimental data and simulation data match well at the final data point. Figure 4.7b plots the swelling strain versus net mean stress for these two tests. The CMS 500 test-path follows a vertical upward direction (volume expansion) while the CV 500 moves horizontally to the right of net mean stress-axis (increase in swelling-induced stress).

4.4.2 SFG model refinement for BSB and recompacted Lake Agassiz clay

The preliminary model inputs (Table 4.3a) were incorporated into a spreadsheet to simulate the CMS and CV tests in BSB. With these preliminary input values, the model calculated an over-estimate in volume change and an under-estimate in swelling-induced stresses. A systematic approach to input variation was undertaken to calibrate the model output to the laboratory results. The CMS simulations were found to be sensitive to the compressibility while the CV simulations were sensitive to the saturation suction. Therefore, the λ_{vp} value is decreased incrementally from 0.25 until the simulations captured the swelling deformation. Whereas the s_{sa} value is increased to match the measured swelling-induced stresses for the CV tests. Using constant input parameters (λ_{vp} =0.21 and s_{sa}=245 kPa), the CV and CMS tests were modeled within ±20 kPa in swelling pressure and ±1.5% in volumetric strain for the 500 kPa, 1000 kPa and 1500 kPa pressure levels. The model and laboratory test comparisons are plotted in Figure 4.8 in terms of volumetric strain versus net mean stress and suction versus net mean stress. Figure 4.9 demonstrates the comparison of data from experiment versus the model in total suction – net mean stress plot for BSB. The idealized equilibration suction line is the same relationship plotted in Figure 4.5a.

The SFG model simulates the CMS and CV swelling tests using constant input parameters except for the tests at lower net mean stress (see CMS250 and CV250 comparisons in Figure 4.8).

Table 4.4 lists the comparison between the testing measurement and model. With the same input parameter of λ_{vp} =0.21 and s_{sa}=245 kPa, the model for p=250 kPa has under-calculated the swelling pressure by 154 kPa and also under-calculated the swelling strain by 12.2%. In order to optimize the model at low stress, both of λ_{vp} and s_{sa} values are increased. The input parameter that accurately models the results low stress are λ_{vp} =0.55 and s_{sa}=320 kPa. The comparison of SFG model and the end-of-test data in BSB is shown in Figure 4.8.

Swelling strains at low stress are pronounced in the SEL context (Figure 4.8). Therefore, at low stress, the soil compressibility is likely to have a higher value. To justify the modification of the s_{sa} and λ parameters the SWCCs reported by Marcial et al. 2002 were considered. Marcial et al. 2002 reported unconfined SWCCs for 100% MX-80 bentonite. The results indicated significant swelling at low suction levels. The data allows direct interpretation of the λ_{vs} parameter as plotted in Figure 4.10. In Figure 4.10 the plot demonstrates that suction-induced soil compressibility is significantly higher at lower suction in 100% bentonite (Marcial et al. 2002). Therefore, it is reasonable to adopt a higher soil compressibility in the SFG model for swelling models at low stresses. Plotted on the same graph is the variation of the λ_{vs} parameter for BSB.

Table 4.5 listed the preliminary model inputs of recompacted Lake Agassiz clay that are used in SFG model spreadsheet. As a starting trial with the preliminary inputs, the model has under-calculated the swelling pressure but over-calculated the swelling strains. In order to calibrate the input parameters to the experiment data, the soil compressibility is reduced incrementally from 0.38 and the s_{sa} is increased incrementally from 200 kPa. The parameters of compressibility and s_{sa} are further refined incrementally to match the measured swelling strains and swelling-induced stresses. The final optimized inputs are λ_{vp} =0.17 and s_{sa}=215 kPa for the tests with p=150, 300 and 600 kPa, which are within the reasonable range. With these constant optimized inputs, the CV and CMS tests were modelled within ±30 kPa in swelling pressure and ±1% in swelling strains. The result of model calculation and experiment data for recompacted Lake Agassiz clay is presented in Figure 4.11.

Similar to BSB, the inputs required further refinement to model swelling behavior at low stresses in recompacted Lake Agassiz clay. For the test at p=150 kPa, the λ is increased from 0.17 incrementally to 0.28 and its s_{sa} is reduced incrementally from 215 kPa to 140 kPa. The modelled swelling pressure and volumetric strain for the test of p=150 kPa is 781 kPa and -15.2%, respectively. In the unconfined swelling tests, only the swelling deformation is measured and the average swelling deformation of recompacted Lake Agassiz clay is measured at -72.1%. It is necessary to further refine the model input for the unconfined swelling tests. The compressibility is increased incrementally from 0.17 to 0.73 while the s_{sa} is reduced incrementally from 215 kPa to 140 kPa. The modelled swelling strain is -72.8% for the unconfined swelling test and the difference is only 0.7% compared to the experimental data. Table 4.6 summarized the optimized model inputs and the comparison between the experimental data and the model for recompacted Lake Agassiz clay. The final compressibility versus suction relationship is presented in Figure 4.10.

4.4.3 Parametric study in SFG model

Following model calibration a parametric study was performed to assess the sensitivity of the model output to the relevant parameters. Consideration can then be emphasized on the more influential parameters when these values are used in an analysis. The tests selected for the parametric study for the SFG model are the CMS500 and CV500 tests on BSB. The benchmark case is labelled as Case 1 where its λ_{vp} and s_{sa} is 0.21 and 245 kPa, respectively. The modelled swelling pressure and deformation from various cases are then compared with the benchmark case's value of p_{swell} = 990 kPa and ε_V = -4.2%. The magnitude of the difference between the model and the laboratory data is calculated with the following equations:

$$[4.7] \quad \Delta p_{swell} = p_{model} - p_{test}$$

$$[4.8] \quad \Delta \varepsilon_v = \varepsilon_{v\_model} - \varepsilon_{v\_test}$$

Table 4.7a compiles the various categories of comparison of each input parameter. There are a total of five (5) categories of study involving variation in λ_{vp}, s_{sa}, ds, S_{ini} and S_{eot}. The various input parameters and the result of parametric analysis are listed in Table 4.7b.

Figure 4.12 presents the influence of each input parameter on the modelled swelling pressure (Δp_{swell}) with a fitted linear relation. Whereas the effect of each input parameter on the calculated volumetric strain ($\Delta\varepsilon_V$) is plotted in Figure 4.13.

Soil compressibility, λ_{vp}, shows no effect on swelling pressure (Figure 4.12a) as all three values of compressibility result in the same swelling pressure at 990 kPa. Soil compressibility (Figure 4.13a) influences directly the magnitude of deformation that is induced either by suction or pressure or both. As indicated, Case 2 with a higher λ_{vp} (λ_{vp} =1.0) results in higher deformation of -20.1% and the lower λ_{vp} (λ_{vp} =0.068) yields smaller deformation of -1.4%. The sensitivity of soil compressibility on volume change is $\frac{\Delta\varepsilon_V}{\Delta\lambda_{vp}} = 20.1\ \frac{\%}{(-)}$.

The effect of varying saturation suction is plotted in Figure 4.12b and Figure 4.13b with the specific cases listed in Table 4.7b. Case 4 is with higher s_{sa} = 500 kPa while Case 5 has a lower s_{sa} of 50 kPa. Case 5 has over-calculated the swelling pressure by 503 kPa but Case 4 has under-calculated the pressure by -389 kPa instead. The sensitivity in s_{sa} is $\frac{\Delta p_{swell}}{\Delta s_{sa}} = 2\ \frac{kPa}{kPa}$. This sensitivity is considered high among other parameters. The modelled volume strain is -8.5% and -0.9% in Case 4 and Case 5, respectively. The effect of s_{sa} value on volume change is small as the sensitivity is $\frac{\Delta\varepsilon_V}{\Delta s_{sa}} = 0.02\ \frac{\%}{kPa}$.

Suction increment (drying) or reduction (wetting) is represented by ds in the model. For suction reduction, ds is a negative value. There are two different increments applied in the study, namely, -150 kPa and -25 kPa compared with Case 1 of -50 kPa. The difference in the modelled swelling pressure and volume change is less than ± 30 kPa and ± 0.5%, respectively. The sensitivity is $\frac{\Delta \mathrm{p_{swell}}}{\Delta(\mathrm{ds})} = 0.2\ \frac{kPa}{kPa}$ and $\frac{\Delta\varepsilon_V}{\Delta(\mathrm{ds})} = 0.004\ \frac{\%}{kPa}$. Therefore, the effect of suction increment on the calculated results is considered marginal.

The laboratory measurements indicated some variability in the initial and final suction measurements. The variability in measurements is due to sensitivity in the instrument calibration at low suctions and the non-linear relationship between relative humidity (which the sensor is measuring) and total suction. Nonetheless the initial and final suction values are included in the parametric analysis. Case 8 has a higher initial suction at 3600 kPa; the lower initial suction in Case 9 is at 2600 kPa. The sensitivity of the initial suction on the swelling pressure is $\frac{\Delta\, p_{swell}}{\Delta\, s_{ini}} = 0.1\ \frac{kPa}{kPa}$. For the influence of initial suction on volume change, the sensitivity is $\frac{\Delta\ \varepsilon_V}{\Delta\ s_{ini}} = 0.0003\ \frac{\%}{kPa}$ which is considered a less dominant input in the model.

The end-of-test suction is the final suction measured at the soil following wetting. Higher S_{eot} indicates the soil is dryer at end-of-test. The S_{eot} in Case 10 is 500 kPa; the difference in swelling pressure and deformation is -52 kPa and -0.7%, respectively. The s_{eot} in Case 11 is 300 kPa; the modelled swelling pressure is 1056 kPa while the swelling deformation is -5.3%. The study has shown that when the soil has more moisture or higher degree of saturation, more swelling potential is developed in the soil. Among the input parameters, the end-of-test suction could be considered relatively influential with the sensitivity of $\frac{\Delta p_{swell}}{\Delta s_{eot}} = -0.6 \frac{kPa}{kPa}$ on the calculated swelling pressure and $\frac{\Delta\varepsilon_V}{\Delta s_{eot}} = -0.01\ \frac{\%}{kPa}$ on the deformation.

From this parametric analysis, the SFG model responds with decreasing sensitivity on the swelling pressure for the inputs: s_{sa}, s_{eot}, ds, s_{ini} and λ_{vp}. The decreasing effect on the modelled swelling deformation is λ_{vp}, s_{sa}, s_{eot}, ds and s_{ini}.

4.5 Application of SFG model

In Canada, the Lake Agassiz clay is classified as a swelling clay and the structures built in this region are prone to swelling soil problem. In arid regions, seasonal changes in water table are also very common. The suction in the soil is higher when it is in a dry season, however, the suction in the soil dissipates due to thawing of snow or extended rainfall events. When the swelling soil is given access of water, the soil is expected to swell against the local infrastructure. The moisture-induced swelling stresses and deformations along various boundary conditions can be simulated with the SFG model as the soil input parameters are established.

Figure 4.14 depicts a basement of a house with 3.5m height that is typically constructed in swelling ground. The ground in the vicinity of the basement would be backfilled and considered similar to the recompacted Lake Agassiz soil reported in this chapter. The moisture content of Lake Agassiz clay deposit was measured by Baracos 1957 and Thiessen 2010 in their research. Both of their measurement data on gravimetric water content is comparable.

The basement is analyzed with 6 increasing depths which are 0.5m, 0.1m, 1.5m, 2.0m, 2.5m and 3.0m below the ground level. The initial moisture content at the basement is based on the measurement from Thiessen 2010 (Figure 4.15a). The initial suction at the basement is correlated from the soil-water characteristic curve presented in Figure 4.4b based on the gravimetric water content. The correlated total suction profile is presented in Figure 4.15b. A higher suction of 1500 kPa is at the location closer to the ground surface and the suction profile reduces with depth. The final suction is assumed at the worst case scenario where the suction is reduced to zero. Such condition may happen after an extended heavy rainfall event causes ponding and saturates the ground near the foundation. The total unit weight of the clay is taken as 20 kN/m^3 and the net mean stress (p) at each depth is calculated and plotted as triangle open symbol in Figure 4.15c. The cross symbol in Figure 4.15c represents the lateral earth stress applied to the basement wall that is calculated with the effective frictional angle of 17.5^o (Pathak 2009).

For the soil at depth of 0.5m, the CMS condition is anticipated to occur because the soil is subjected to a 10 kPa of net mean stress and the soil deformation is not constrained rigidly at near ground surface. For the soil at the middle of the wall (soil depth at 1.5m and 2.0m), the anticipated condition would be between CMS and CV conditions because the soil deformation could be observed as bulging or cracking at the basement wall. The swelling –induced stresses calculated from CV condition would develop and exerted on the basement wall. For the greater depth at 2.5m and 3.0m, the soil may experience a CV condition as the soil deformation is restrained by the stiff footing of the wall. Thus, the wall toe may experience swelling-developed stresses.

The input parameters of soil compressibility, λ_{vp}= 0.28 and saturation suction, s_{sa}= 140 kPa obtained from Section 4.4.2 are used in the swelling analysis. The initial soil states and suction level as plotted in Figure 4.15b and Figure 4.15c are input into SFG model for calculation (Appendix I). The calculated swelling-induced stresses and deformations at each soil depth are plotted in Figure 4.15c and Figure 4.15d. The highest swelling-induced stresses and swelling deformation are calculated at 461 kPa and -36.2 %, respectively at the depth of 0.5m. Both of the swelling stresses and deformations reduce with depth. SFG model input parameters, initial and final states of suction profile, applied net mean stress and model calculated result is summarized in Table 4.8.

An envelope of the calculated swelling-induced stresses and deformations at each depth is plotted in Figure 4.16. An engineer requires applying his practical judgment to determine the most possible scenario that may occur to the basement using the result presented in Figure 4.16. The engineer needs to consider the calculated swelling-induced stresses in additional to the lateral earth pressure at the wall. A typical retaining wall design guideline given in Canadian Foundation Engineering Manual considers either at-rest condition or active lateral earth pressure that would be applied to a retaining wall.

Figure 4.15c has clearly shown that the lateral earth pressure in a typical wall design analysis is significantly lower compared to the magnitude of swelling-induced stresses calculated by SFG model. Many home owners may potentially suffer from the basement damage caused by swelling soil because the typical wall design has not considered the additional swelling stresses in the analysis. Therefore, the swelling soil behavior modelled with SFG equation provide a more realistic and practical estimation to the design of structures constructed in swelling ground.

The advantage of using SFG model in swelling soil design is its simplicity of requiring two additional soil input parameters, namely, soil compressibility and saturation suction. These two inputs can be calibrated with high quality experimental result obtained from the advanced SEL testing. Geotechnical engineer may consider using SFG model in designing structures in swelling ground.

4.6 Conclusion

Advanced numerical tools provide the ability to simulate and understand complex systems. At the same time experimental apparatuses continue to become more multifaceted and able to better represent field behavior. The temptation of these tools is that the ability to add complexity sometimes makes them too difficult to use in practice. A numerical tool, that is based in theory but only needs a very few number of input parameters, has the opportunity to be used in practice.

The SEL concept provides a unifying framework to understand swelling behavior of expansive soils. The SFG constitutive model is based on theoretical unsaturated soil mechanics and can be used with the addition of two soil input parameters. Namely soil compressibility for swelling (λ_{vp}) and saturation suction (s_{sa}). In this chapter, the SFG model is successfully applied to advanced swelling experiments for two swelling soils, namely BSB and recompacted Lake Agassiz clay. A parametric analysis is performed to examine the sensitivity of the model output to the input parameters. Finally an example model for calculating swelling strains and swelling-induced stresses on a basement foundation application are presented. The simplicity and the accuracy given by the SFG model calculation have made it an attractive tool for modelling in unsaturated swelling soil. Further work will address transient effects and environmental interactions.

4.7 Reference

Canadian Foundation Engineering Manual 2006. 4th ed. Alberta, Canada: The Canadian Geotechnical Society.

Alonso, E.E., Gens, A., and Josa, A. 1990. A constitutive model for partial saturated soils. Géotechnique 40 (3): 405-30.

Alonso, E.E., Vaunat, J. and Gens, A. 1999. Modelling the mechanical behavior of expansive clays. Engineering Geology 54 : 173-83.

Baracos, A. 1957. The foundation failure of the Transcona grain elevator. The Engineering Journal 40 : 973-7.

Blatz, J.A. and Graham, J. 2003. Elastic-plastic modelling of unsaturated soil using results from a new triaxial test with controlled suction. Géotechnique 53 (1): 113-22.

Briaud, J.L., Zhang, X., and Moon, S. 2003. Shrink test–water content method for shrink and swell predictions. Journal of Geotechnical & Geoenvironmental Engineering 129 (7): 590-600.

Cui, Y.J. and Delage, P. 1996. Yielding and plastic behavior of an unsaturated compacted silt. Geotechnique 46 (2): 291-312.

Cunningham, M .R., Ridley, A. M., Dineen, K. and Burland, J. B. 2003. The mechanical behavior of a reconstituted unsaturated silty clay. Geotechnique 53 (2): 183-94.

Fredlund, D.G. and Morgenstern, N.R. 1977. Stress state variables for unsaturated soils. Journal of the Geotechnical Engineering Division, Proceedings of the ASCE 103 (GT5): 447-67.

Gens, A. and Alonso, E.E. 1992. A framework for the behavior of unsaturated swelling clays. Canadian Geotechnical Journal 29 : 1013-32.

Jennings, J.E.B. and Burland, J.B. 1962. Limitations of the use of effective stresses in partly saturated soils. Geotechnique 12 (1): 125-44.

Keller, E. A. 2008. Environmental Geology. 8th ed. USA: Prentice hall.

Lim, B.F. and Siemens, G.A. 2013. An unconfined swelling test for clayey soils that incorporates digital image correlation. Geotechnical Testing Journal 36 (6): 1-11.

Lim, B.F., Siemens, G., Boyle, J.S., Remenda, V. and Take, A. 2008. Numerical analysis of expansive soil behavior using the swell equilibrium limit. The 61st Canadian Geotechnical Conference, Edmonton, Alberta (September 21-24, 2008): 176-81.

Liu, X.F., Buzzi, O.P. and Vaunat, J. 2014. Influence of stress-volume path on swelling behavior of an expansive clay. Paper presented at 6th International Conference on Unsaturated Soils: Research & Applications, Sydney, Australia.

Lloret, A., Villar, M. V., Sànchez, M., Gens, A., Pintado, X., and Alonso, E. E. 2003. Mechanical behavior of heavily compacted bentonite under high suction changes. Géotechnique 53 (1): 27-40.

Marcial, D., Delage, P. and Cui, Y.J. 2002. On the high stress compression of bentonites. Canadian Geotechnical Journal 39 : 812-20.

Marinho, F.A.M., Chandler, R.J., and Crilly, M.S. 1995. Stiffness measurements on an unsaturated high plasticity clay using bender elements. Paper presented at Proceedings of the 1st International Conference on Unsaturated Soils, Paris, France, 6-8 September 1995. A.A. Balkema, Rotterdam, the Netherlands. Paris, France.

Miller, D. J., Durkee, E. B., Chao, K. C., and Nelson, J. D. 1995. Simplified heave prediction for expansive soils. Proc., 1st Int. Conf. on Unsaturated Soils, Balkema, Rotterdam, the Netherlands: 891-7.

Pathak, Y. P. 2009. Experimental and numerical studies of geosynthetic-reinforced clays and silts under environmental-induced swelling. PhD., Department of Civil Engineering, University of Manitoba, Winnipeg, Man.

Pauls, G. J. 1995. The relationship between slope stability and pore-water pressure in highly plastic clay in the carrot river basin. M.Sc., Department of Civil Engineering, University of Saskatchewan, Saskatoon.

Priyanto, D. G. 2007. Development and application of new constitutive models to simulate the hydraulic-mechanical behavior of unsaturated swelling clay. Ph.D. thesis., Department of Civil Engineering, University of Manitoba, Winnipeg, Man.

Puppala, A. J. and Cerato, A.B. 2009. Heave distress problems in chemically-treated sulfate laden materials. Geostrata: 28-32.

Sheng, D., and Zhou, A.N. 2011. Coupling hydraulic with mechanical models for unsaturated soils. Canadian Geotechnical Journal 48 : 826-40.

Sheng, D., Fredlund, D.G. and Gens, A. 2008. A new modelling approach for unsaturated soils using independent stress variables. Canadian Geotechnical Journal(45): 511-34.

Sheng, D., Sloan, S.W. and Gens, A. 2004. A constitutive model for unsaturated soils. Computational Mechanics 33 :453-465.

Sheng, D., Sloan, S.W., Gens, A. and Smith, D.W. 2003. Finite element formulation and algorithms for unsaturated soils. part I: Theory. International Journal for Numerical and Analytical Methods in Geomechanics 27 (9): 745-65.

Sheng, D., Zhang, S. and Yu, Z. 2013. Unanswered questions in unsaturated soil mechanics. Science China Technological Sciences 56 : 1257-72.

Siemens, G. A. 2006. The influence of boundary conditions on the hydraulic-mechanical behavior of an unsaturated swelling soil. Ph.D. thesis., Department of Civil Engineering, University of Manitoba.

Siemens, G.A. and Blatz, J.A. 2009. Evaluation of the influence of boundary confinement on the behavior of unsaturated swelling clay soils. Canadian Geotechnical Journal(46): 339-56.

———. 2008. Numerical modelling of shallow foundations on swelling clay soil using the swelling equilibrium limit. Paper presented at Proceedings of the First European Conference on Unsaturated Soils, Durham, UK.

———. 2008. Numerical modelling of shallow foundations on swelling clay soil using the swelling equilibrium limit. Paper presented at Proceedings of the First European Conference on Unsaturated Soils, (Unsaturated Soils: Advances in Geo-Engineering), Durham, UK.

Sivakumar, V. and Wheeler, S.J. 2000. Influence of compaction procedure on the mechanical behavior of an unsaturated compacted clay. part 1: Wetting and isotropic compression. Geotechnique 50 (4): 259-368.

Sun, D., Sheng, D. and Xu, Y. 2007. Collapse behavior of unsaturated compacted soil with different initial densities. Canadian Geotechnical Journal 44 : 673-86.

Thiessen, K. 2010. Stabilization of natural clay riverbanks with rockfill columns: A full-scale field test and numerical verification. PhD., Department of Civil Engineering, University of Manitoba, Winnipeg, Man.

Thu, T.M., Rahardjo, H. and Leong, E.C. 2007. Soil-water characteristic curve and consolidation behavior for a compacted silt. Canadian Geotechnical Journal 44 : 266-75.

Vanapalli, S.K., Lu, L. and Oh, W.T. 2010. Estimation of swelling pressure and 1-D heave in expansive soils. Unsaturated Soils, Barcelona, Spain. September 6-8, 2010. Eds: Alonso, E & Gens, A., CRC Press 2 : 1201-7.

Wheeler, S. J. and Sivakumar, V. 1995. An elasto-plastic critical state framework for unsaturated soil. Géotechnique 45 (1): 35-53.

Zhou, A. and Sheng, D. 2009. Yield stress, volume change and shear strength behaviour of unsaturated soils: The validation of the SFG model. Canadian Geotechnical Journal 46 : 1034-45.

Table 4.1. Index properties for BSB and recompacted Lake Agassiz clay.

Soil Type	Specific gravity, G_s (-)	Clay fraction, f_c (%)	Montmori-llonite fraction of clay, f_m (%)	Liquid Limit, LL (%)	Plastic Limit, PL (%)	Plastic Index, PI (%)	Activity, A =PI/ % clay	Initial dry density, ρ_d (Mg/m^3)	Initial specific volume, V (-)
$^{\Phi}$Bentonite – sand-buffer	2.70	50	90	265	21	244	4.88	1.67	1.615
Recompacted Lake Agassiz clay	2.76	75	30*	85	34	51	0.64	1.58	1.742

Note:
$^{\Phi}$ Data obtained from Siemens and Blatz (2009)
* Data obtained from Dixon (2002)

Table 4.2. Estimated preliminary soil compressibility for a) BSB and b) Recompacted Lake Agassiz clay.

a) BSB

Test data					Back-calculate	
			CV	CMS		
p (kPa)	V_{ini} (-)	s_{eot} (kPa)	p_{eot} (kPa)	ε_V (%)	dV (-)	λ_{vp} (-)
250	1.585	400	915	-17.3	0.274	0.542
500	1.534	400	980	-5.1	0.078	0.225
1000	1.506	400	1440	-2.5	0.038	0.157
1500	1.454	400	1905	-0.9	0.013	0.074
					Average	0.250

b) Recompacted Lake Agassiz clay

Test data					Back-calculate	
			CV	CMS		
p (kPa)	V_{ini} (-)	s_{eot} (kPa)	p_{eot} (kPa)	ε_V (%)	dV (-)	λ_{vp} (-)
150	1.753	0	753	-15.1	0.265	0.331
300	1.741	0	1198	-9.9	0.172	0.230
600	1.729	0	N/A	-5.7	0.099	N/A
					Average	0.280

N/A: not available

Table 4.3. Input parameter of SFG and initial condition of SEL test for BSB.

p (kPa)	*λ_{vp} (-)	*s_{sa} (kPa)	s_{ini} (kPa)	s_{eot} (kPa)	ds (kPa)
250	0.25	200	3365	400	-50
500	0.25	200	3102	400	-50
1000	0.25	200	2577	400	-50
1500	0.25	200	2052	400	-50

*Preliminary value for optimization of modelling

Table 4.4. SFG model results for BSB's SEL.

SFG model input parameter			Experiment data		Model		Comparison	
p (kPa)	λ_{vp}	s_{sa} (kPa)	p_{swell} (kPa)	ε_V (%)	p_{swell} (kPa)	ε_V (%)	Δp_{swell} (kPa)	$\Delta\varepsilon_V$ (%)
250	$^{\Phi}$0.55	$^{\Phi}$320	915	-17.3	917	-17.4	2	0.1
250	0.21	245	915	-17.3	761	-5.1	-154	12.2
500	0.21	245	980	-5.1	993	-4.2	13	0.9
1000	0.21	245	1440	-2.5	1450	-3.2	10	-0.6
1500	0.21	245	1905	-0.9	1899	-2.3	-6	-1.4

$^{\Phi}$Optimized input for test at low stress

Table 4.5. Input parameter of SFG and initial condition of SEL test for recompacted Lake Agassiz clay.

p (kPa)	*λ_{vp} (-)	*s_{sa} (kPa)	s_{ini} (kPa)	s_{eot} (kPa)	ds (kPa)
1	0.28	200	7899	0	-150
150	0.28	200	7750	0	-150
300	0.28	200	7600	0	-150
600	0.28	200	7300	0	-150

*Preliminary value for optimization of modelling

Table 4.6. SFG model results for recompacted Lake Agassiz clay's SEL.

SFG model input parameter			Experiment data		Model		Comparison	
p (kPa)	λ_{vp}	s_{sa} (kPa)	p_{swell} (kPa)	ε_V (%)	p_{swell} (kPa)	ε_V (%)	Δp_{swell} (kPa)	$\Delta\varepsilon_V$ (%)
1	$^{\Phi}0.73$	$^{\Phi}140$	no data	-72.8	no data	-72.1	no data	0.7
150	$^{\Phi}0.28$	$^{\Phi}140$	753	-15.1	781	-15.2	28	-0.1
150	0.17	215	753	-15.1	1064	-12.1	311	3.1
300	0.17	215	1198	-9.9	1210	-9.1	12	0.8
600	0.17	215	no data	-5.7	no data	-6.4	no data	-0.7

$^{\Phi}$Optimized input for tests at low stress

Table 4.7. Parametric analysis of SFG model.

a) Various categories of model input parameters.

Case/Category		*1	2	3	4	5	6	7	8	9	10	11
a	Higher λ_{vp}	✓	✓									
	Lower λ_{vp}	✓		✓								
b	Higher s_{sa}	✓			✓							
	Lower s_{sa}	✓				✓						
c	Higher ds	✓					✓					
	Lower ds	✓						✓				
d	Higher s_{ini}	✓							✓			
	Lower s_{ini}	✓								✓		
e	Higher s_{eot}	✓									✓	
	Lower s_{eot}	✓										✓

*Benchmark for comparison

b) Input parameters and the result of parametric study.

Case	Variation in model input parameter (highlighted) λ_{vp} (-)	s_{sa} (kPa)	ds (kPa)	s_{ini} (kPa)	s_{eot} (kPa)	SFG model p_{swell} (kPa)	ε_V (%)	Comparison with Case 1 Δp_{swell} (kPa)	$\Delta\varepsilon_V$ (%)	Sensitivity	
*1	0.21	245	-50	3100	400	990	-4.2	0	0		
2	1.0	245	-50	3100	400	990	-20.1	0	15.9	$\frac{\Delta p_{swell}}{\Delta\lambda} = 0\ \frac{kPa}{(-)}$	$\frac{\Delta\varepsilon_V}{\Delta\lambda} = 20.1\ \frac{\%}{(-)}$
3	0.068	245	-50	3100	400	990	-1.4	0	-2.9		
4	0.21	500	-50	3100	400	1493	-8.5	503	4.3	$\frac{\Delta p_{swell}}{\Delta s_{sa}} = 2\ \frac{kPa}{kPa}$	$\frac{\Delta\varepsilon_V}{\Delta s_{sa}} = 0.02\ \frac{\%}{kPa}$
5	0.21	50	-50	3100	400	602	-0.9	-389	-3.4		
6	0.21	245	-150	3100	400	966	-3.8	-24	-0.4	$\frac{\Delta p_{swell}}{\Delta(ds)} = 0.2\ \frac{kPa}{kPa}$	$\frac{\Delta\varepsilon_V}{\Delta(ds)} = 0.004\ \frac{\%}{kPa}$
7	0.21	245	-25	3100	400	997	-4.3	6	0.1		
8	0.21	245	-50	3600	400	1027	-4.4	36	0.1	$\frac{\Delta p_{swell}}{\Delta s_{ini}} = 0.1\ \frac{kPa}{kPa}$	$\frac{\Delta\varepsilon_V}{\Delta s_{ini}} = 0.0003\ \frac{\%}{kPa}$
9	0.21	245	-50	2600	400	947	-4.1	-43	-0.2		
10	0.21	245	-50	3100	500	938	-3.5	-52	-0.7	$\frac{\Delta p_{swell}}{\Delta s_{eot}} = -0.6\ \frac{kPa}{kPa}$	$\frac{\Delta\varepsilon_V}{\Delta s_{eot}} = -0.01\ \frac{\%}{kPa}$
11	0.21	245	-50	3100	300	1056	-5.3	66	1.0		

*Benchmark for comparison

Table 4.8. Calculated swelling pressure and deformation for a basement constructed in swelling soil.

Case	Depth (m)	SFG model input parameter: p (kPa)	λ_{vp} (-)	s_{sa} (kPa)	Estimated suction: s_{ini} (kPa)	s_{eot} (kPa)	SFG model: p_{swell} (kPa)	ε_V (%)
1	0.5	10	0.28	140	1500	0	461	-36.2
2	1.0	20	0.28	140	1200	0	440	-32.7
3	1.5	30	0.28	140	600	0	335	-28.6
4	2.0	40	0.28	140	400	0	311	-25.0
5	2.5	50	0.28	140	250	0	260	-20.8
6	3.0	60	0.28	140	400	0	242	-18.0

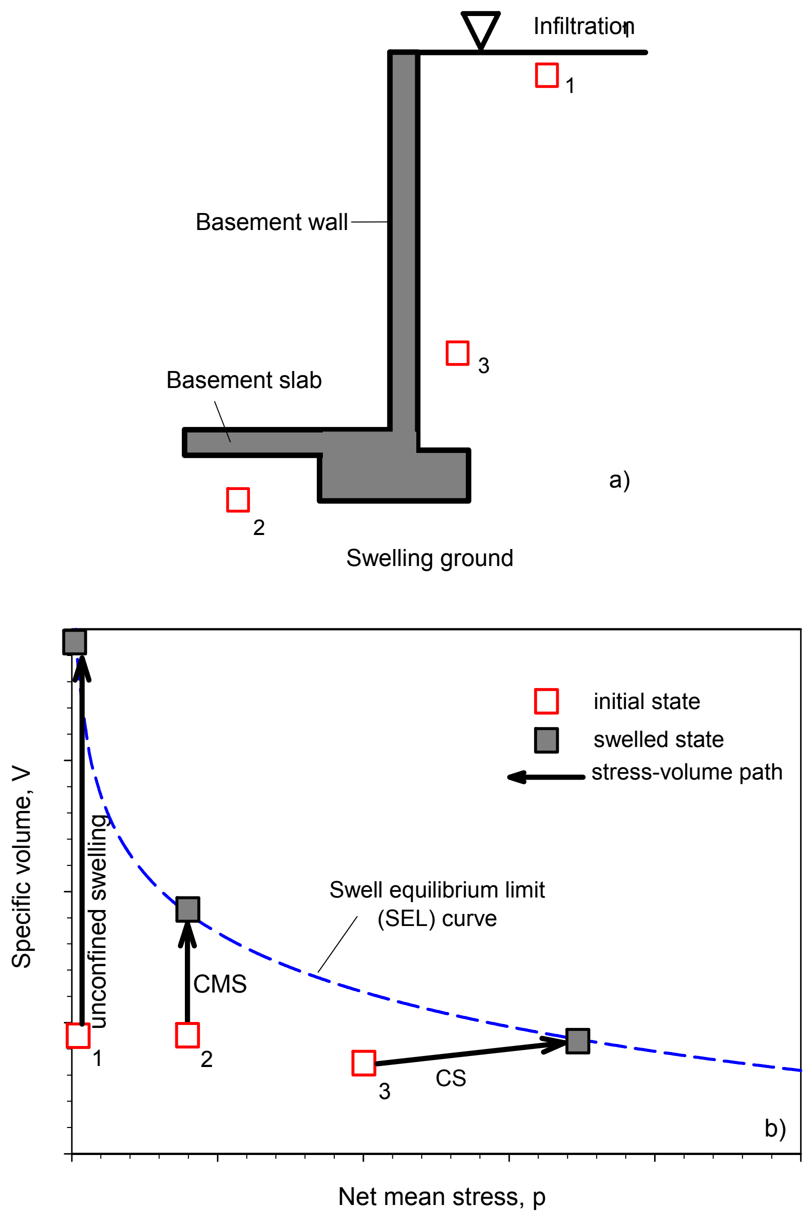

Figure 4.1. Illustrative concept of the Swell Equilibrium Limit illustrating stress-volume paths for swelling at a basement wall application.

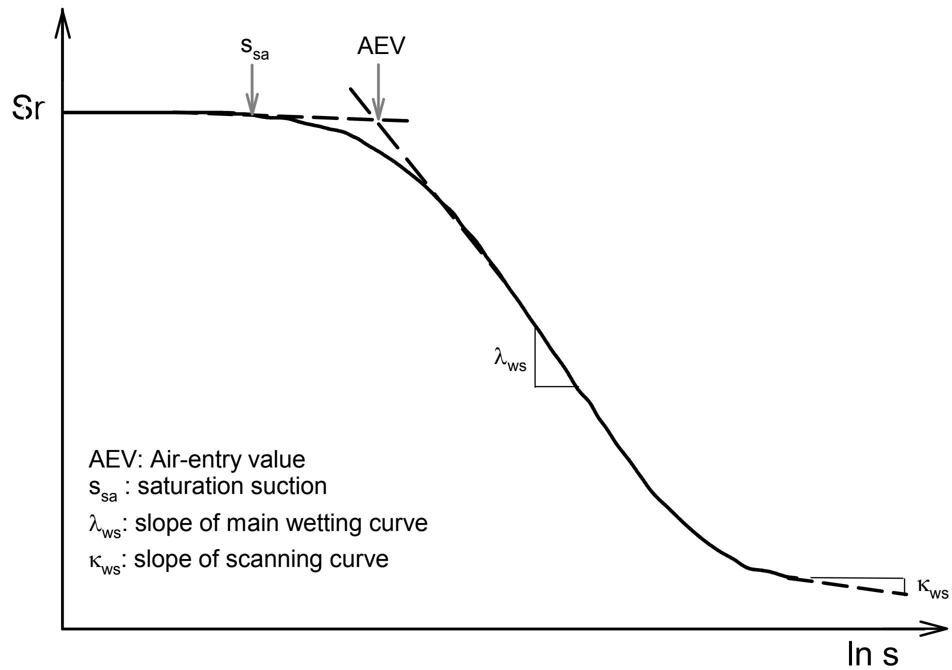

Figure 4.2. Schematic of SWCC illustrating SFG parameter definition including saturation suction, s_{sa} (Sheng at al. 2008)

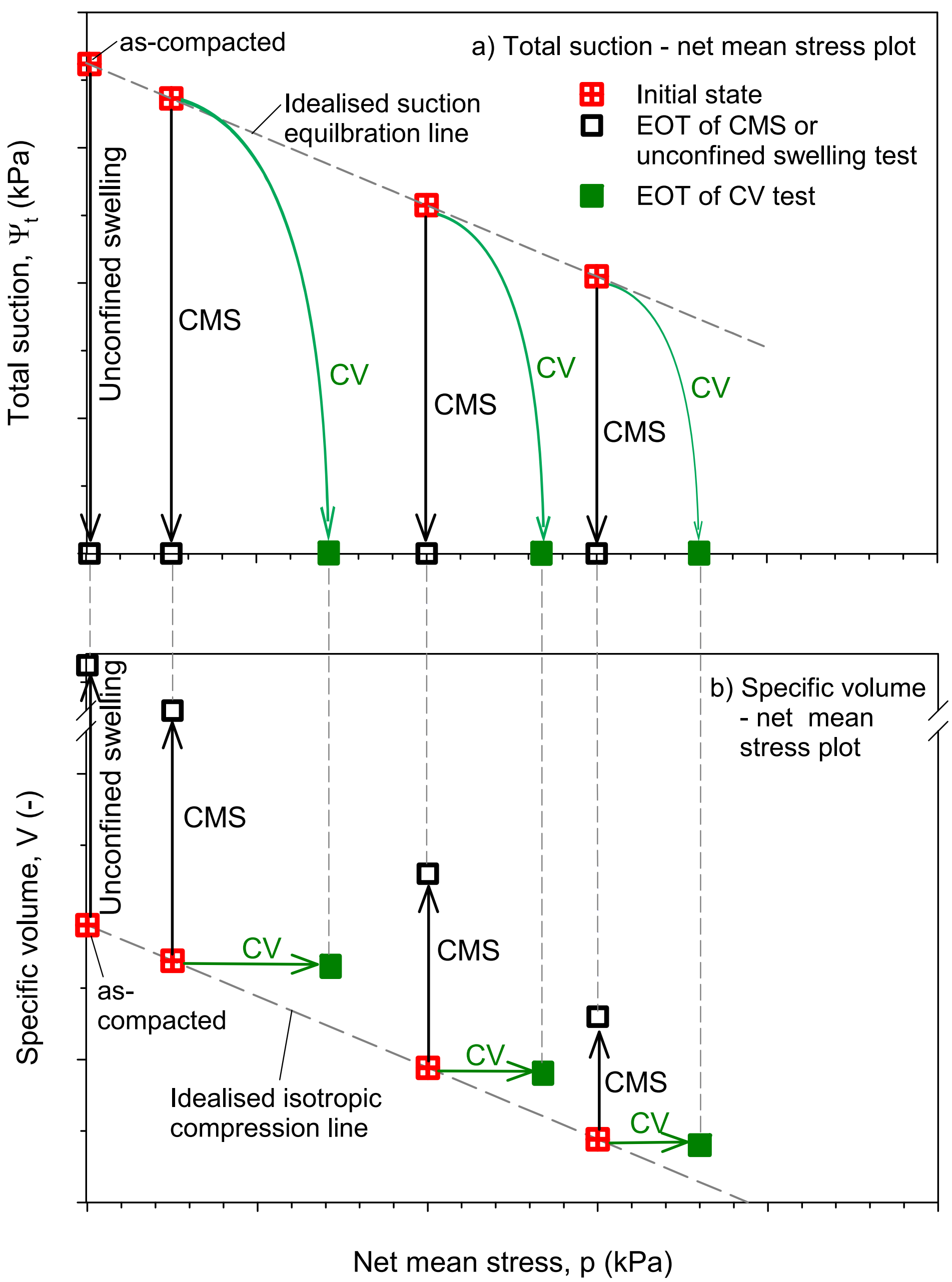

Figure 4.3. Schematic of isotropic compression, constant net mean stress and constant volume stress-volume paths: a) Suction-net mean stress plot and b) Specific volume- net mean stress plot.

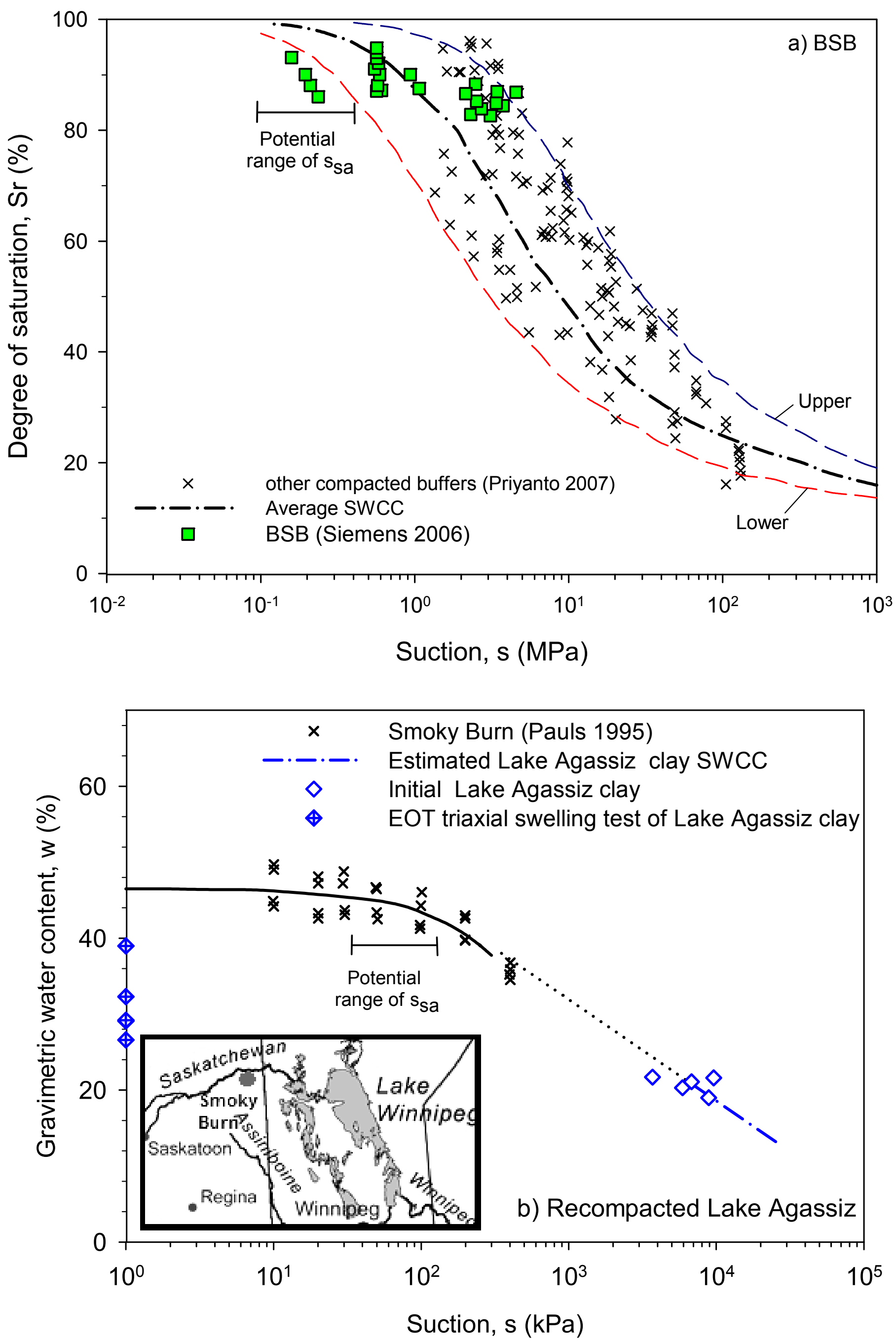

Figure 4.4. Soil-water characteristic curve: a) BSB and other compacted bentonites (after Priyanto 2007) and b) Recompacted Lake Agassiz clay.

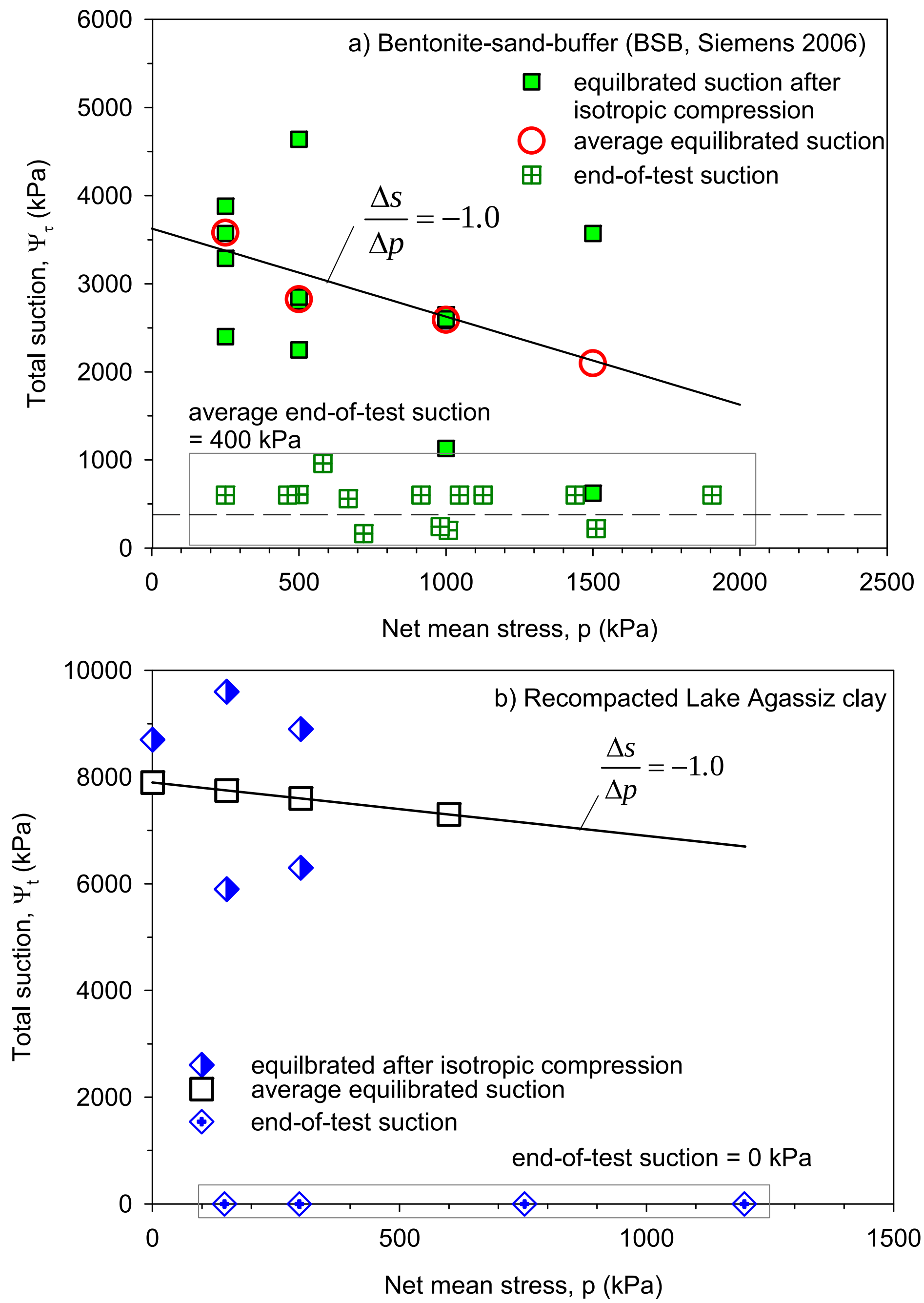

Figure 4.5. Initial equilibrated and end-of-test suction for a) bentonite-sand-buffer (BSB, Siemens 2006) and b) Recompacted Lake Agassiz clay.

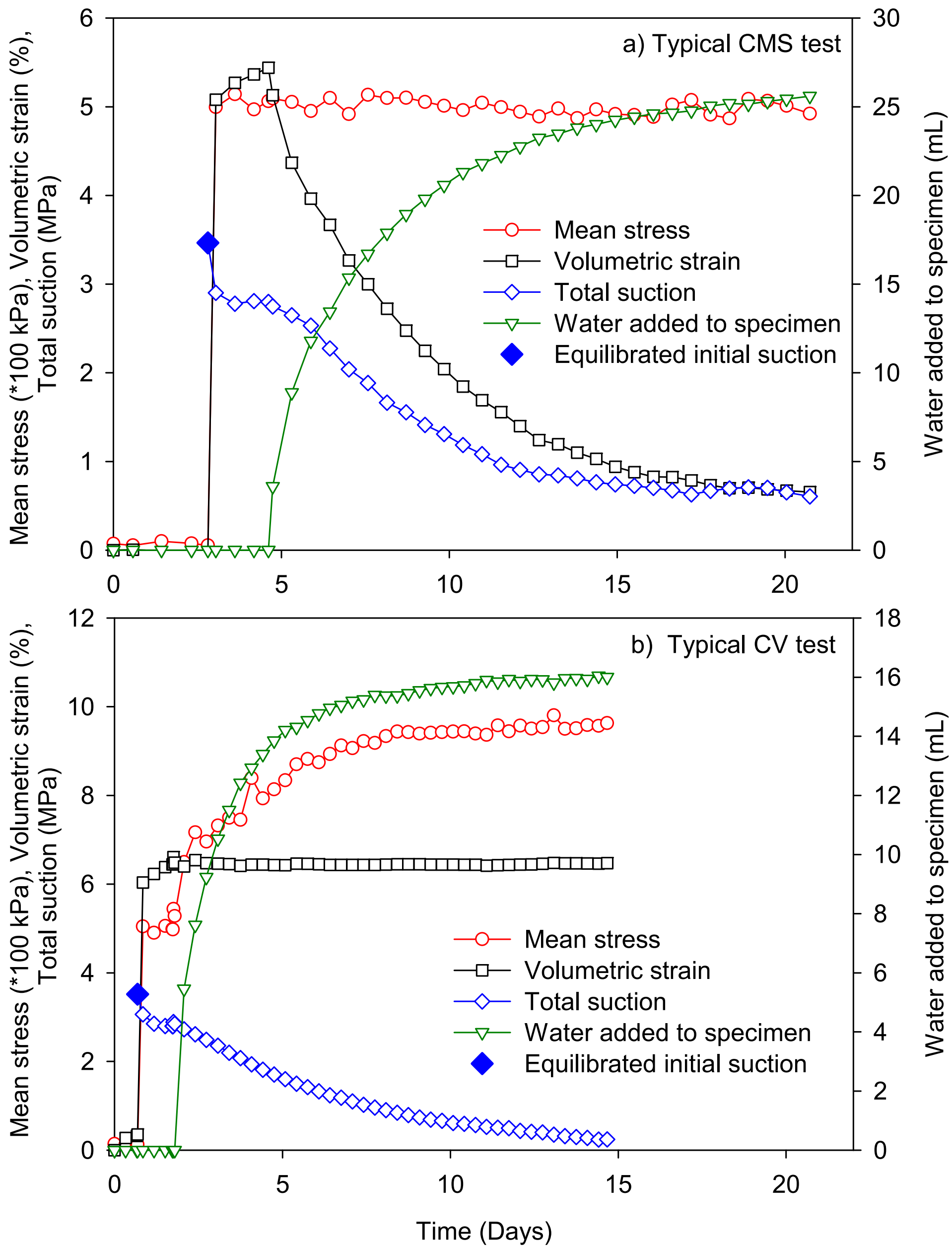

Figure 4.6. Typical SEL test result in a) 500 kPa constant mean stress (CMS); b) 500kPa constant volume (CV): net mean stress, volumetric strain, suction, and water added to specimen versus time (after Blatz and Siemens 2004).

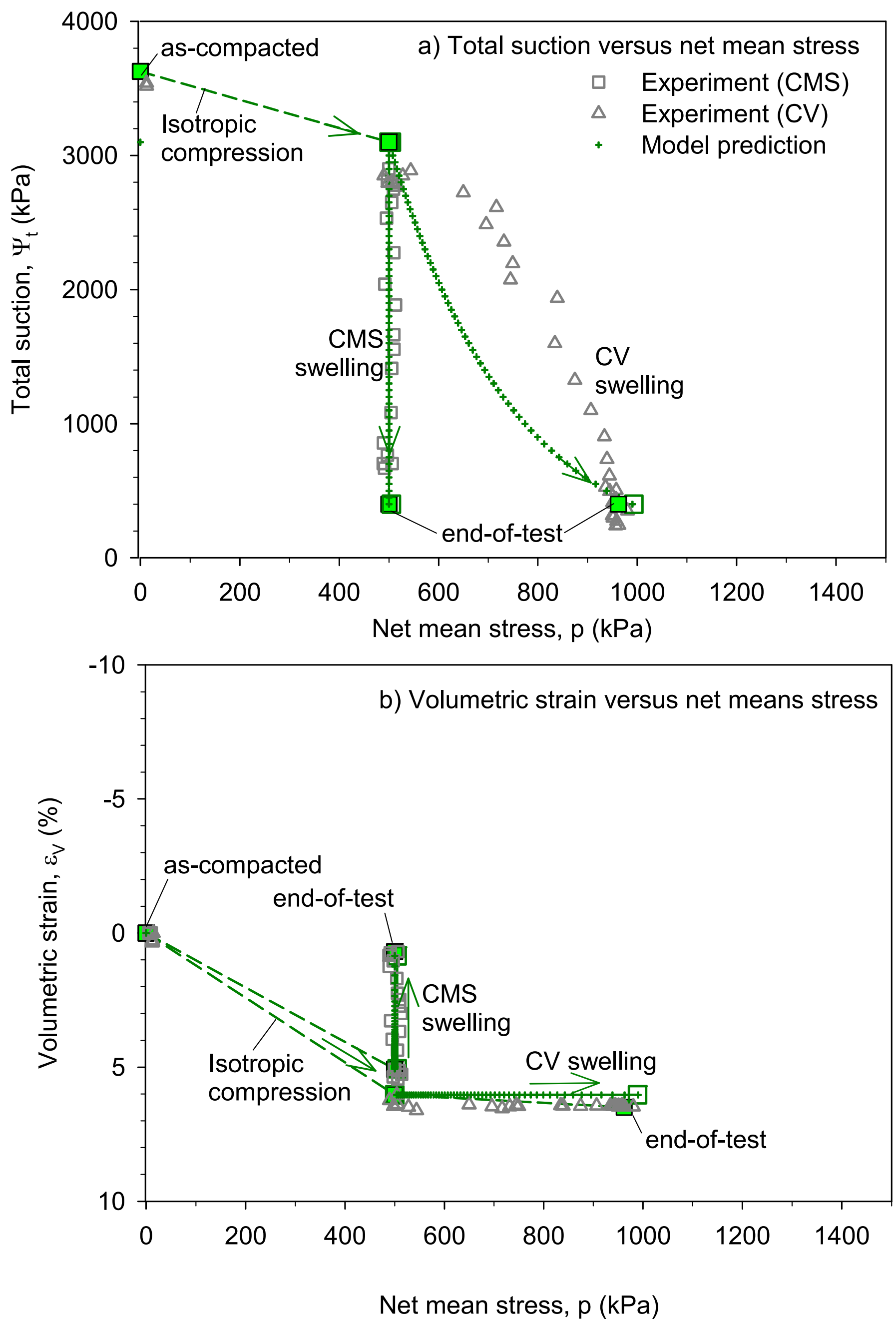

Figure 4.7. Typical experimental and modelled paths for CMS 500 and CV 500 swelling test: a) Total suction versus net mean stress plot and b) Volumetric strain versus net mean stress plot

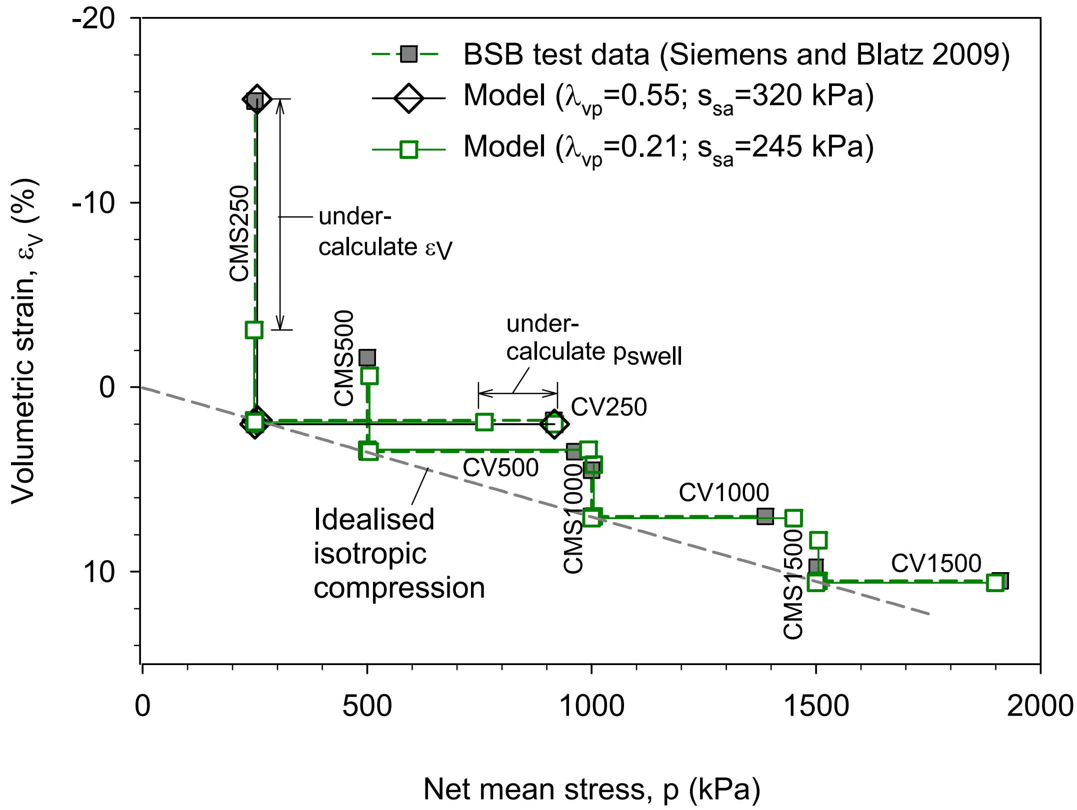

Figure 4.8. Comparison of SFG model and test data for BSB in volumetric strain versus net mean stress.

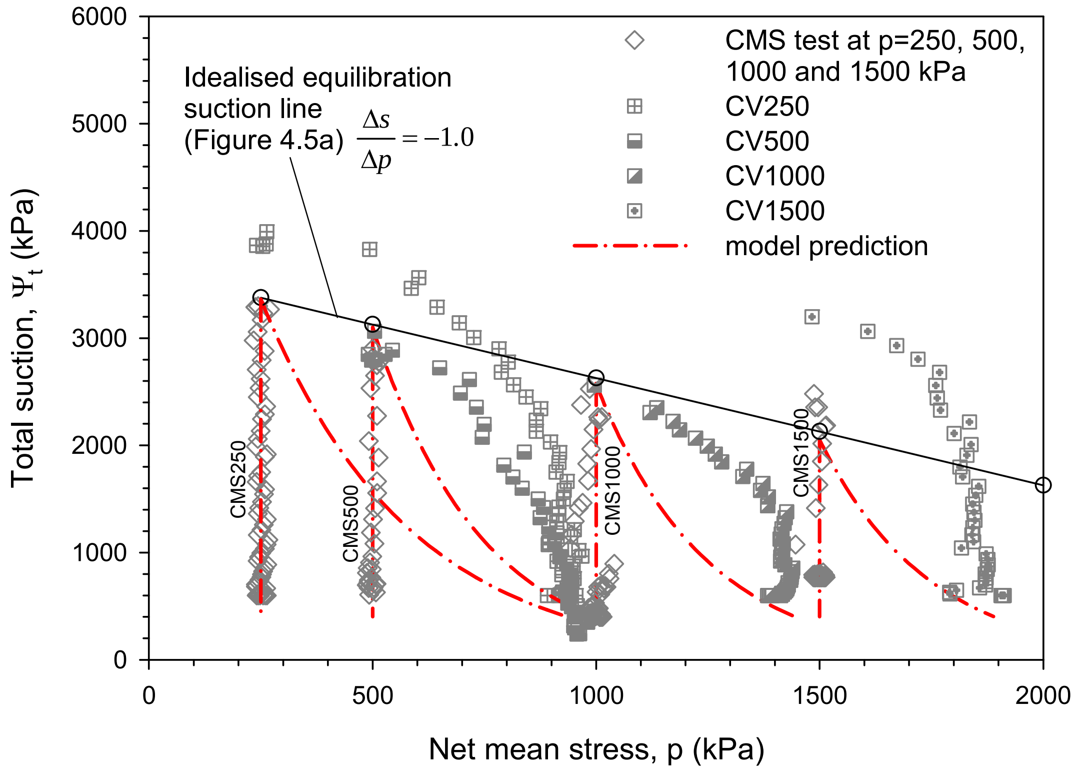

Figure 4.9. Comparison of BSB experiment data versus SFG model.

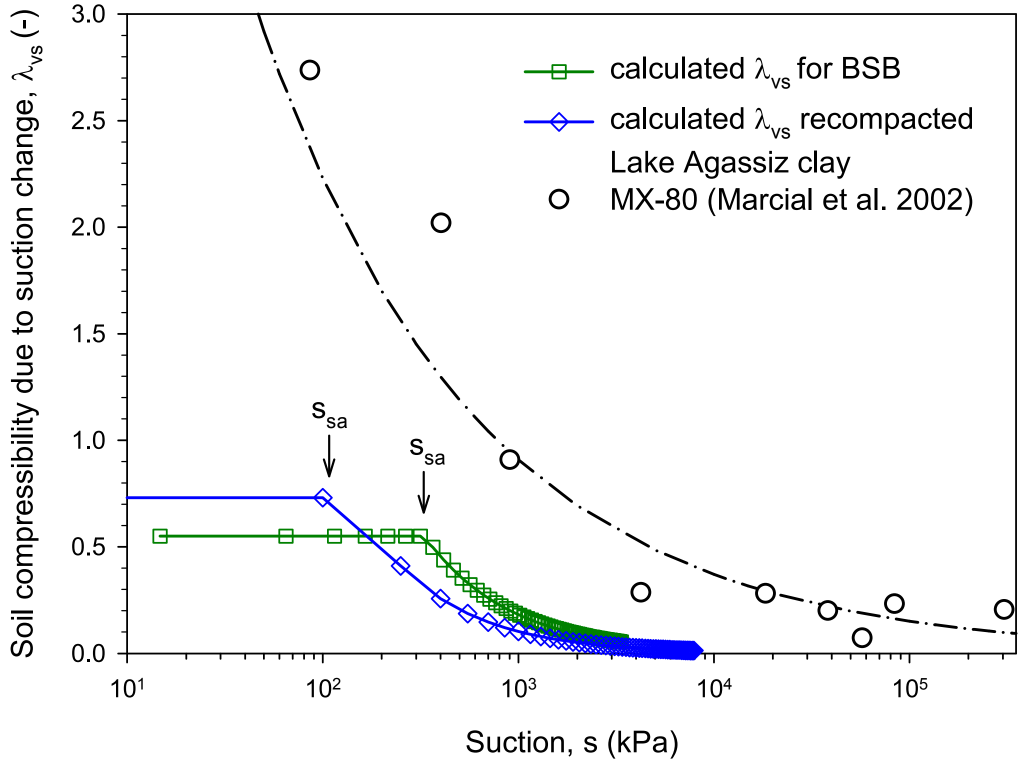

Figure 4.10. Suction-induced soil compressibility, λ_{vs} for BSB, recompacted Lake Agassiz clay and compacted bentonite MX-80 (after Marcial et al. 2002).

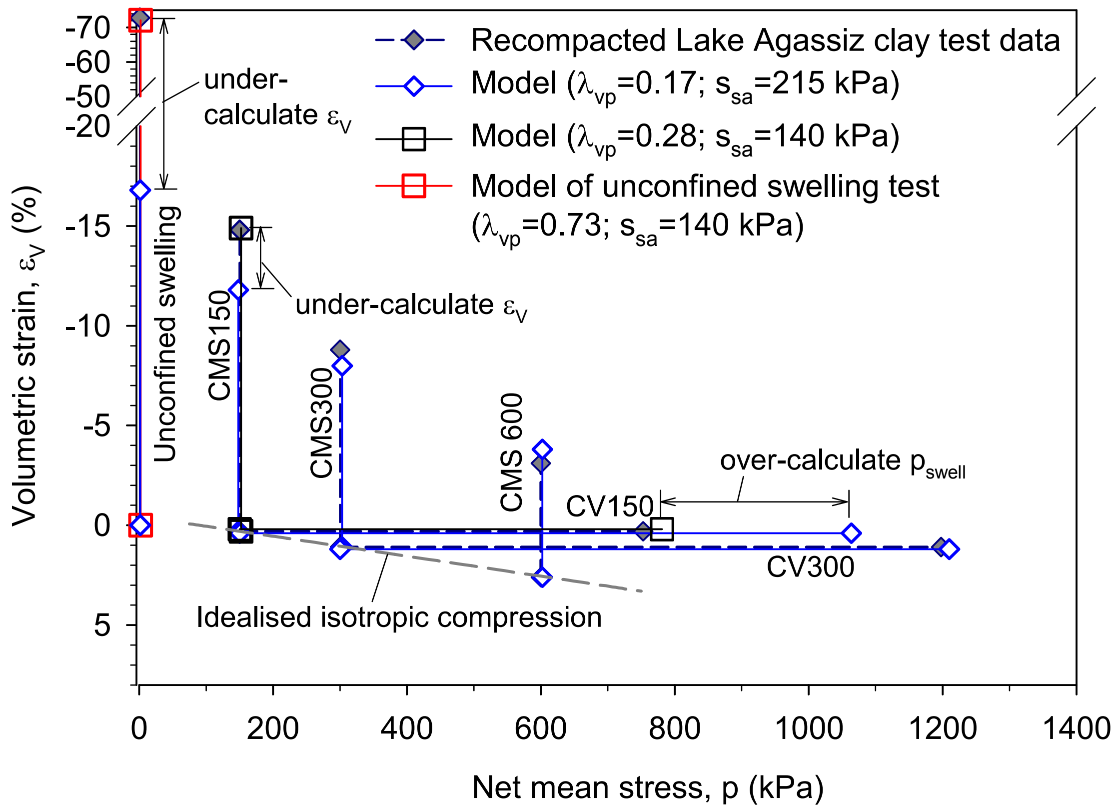

Figure 4.11. Comparison of SFG model and test data for triaxial swelling tests of recompacted Lake Agassiz clay.

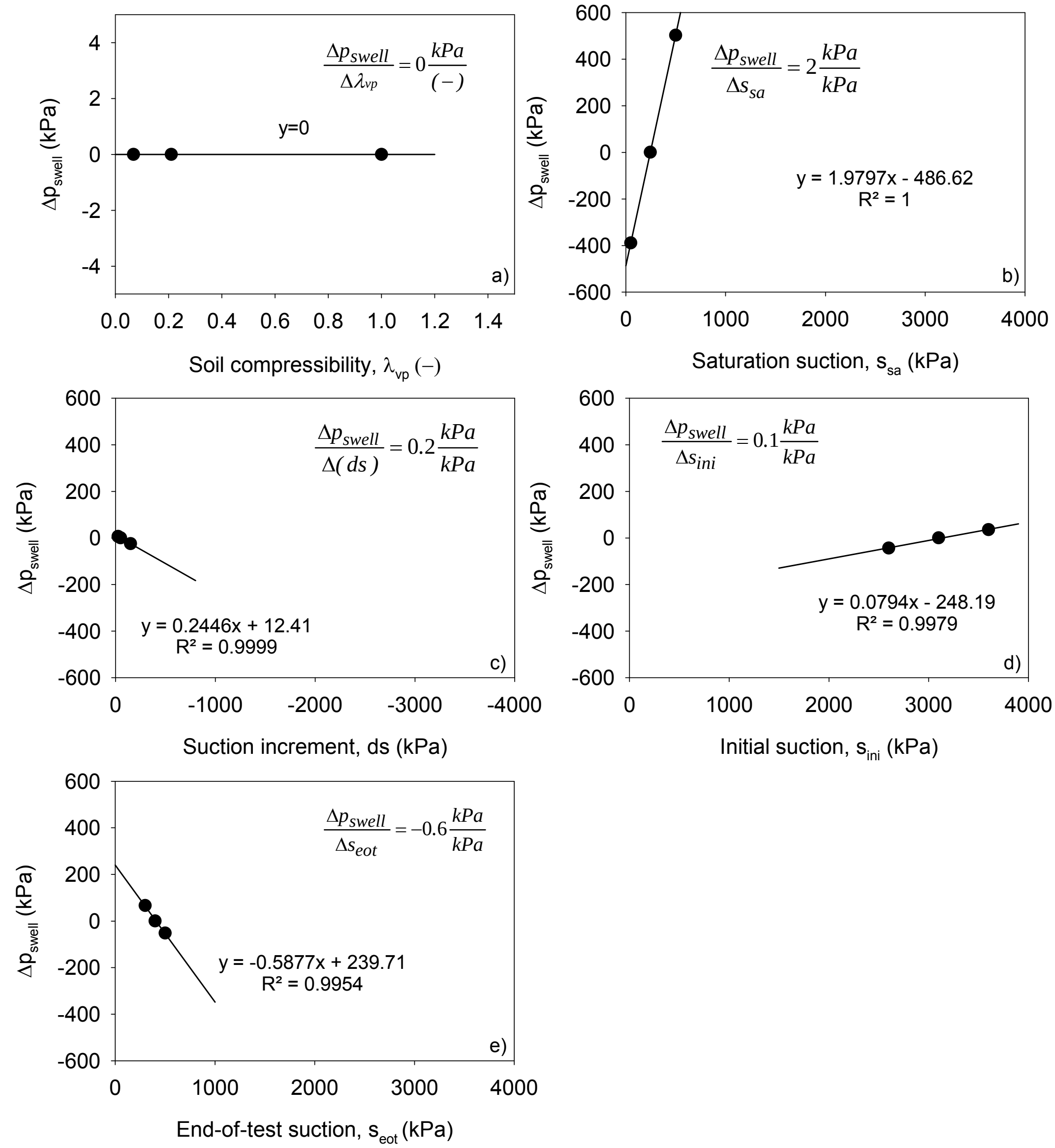

Figure 4.12. Parametric analysis of SFG model input parameters and initial condition on the swelling pressure.

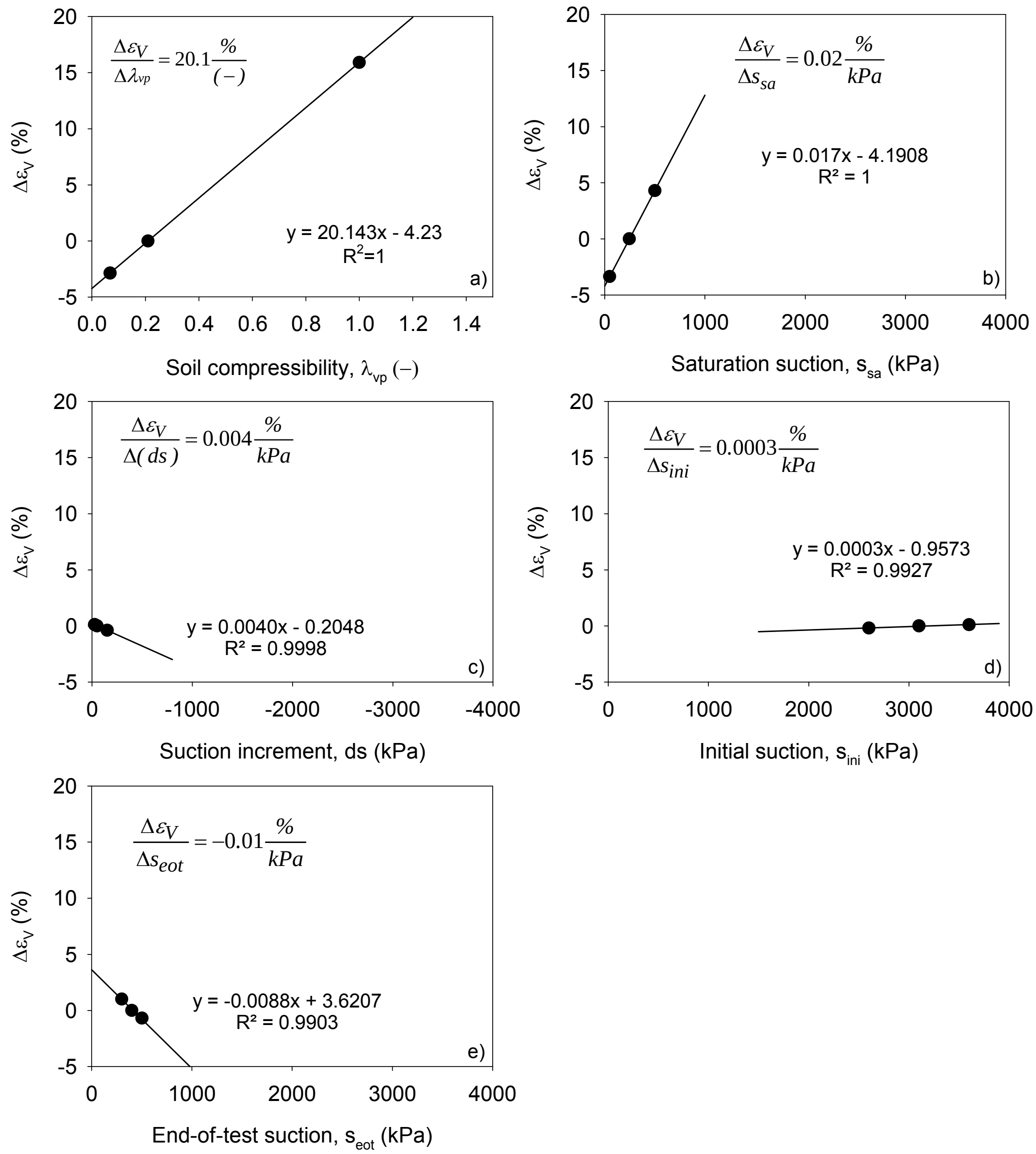

Figure 4.13. Parametric analysis of SFG model input parameters and initial condition on the swelling strain.

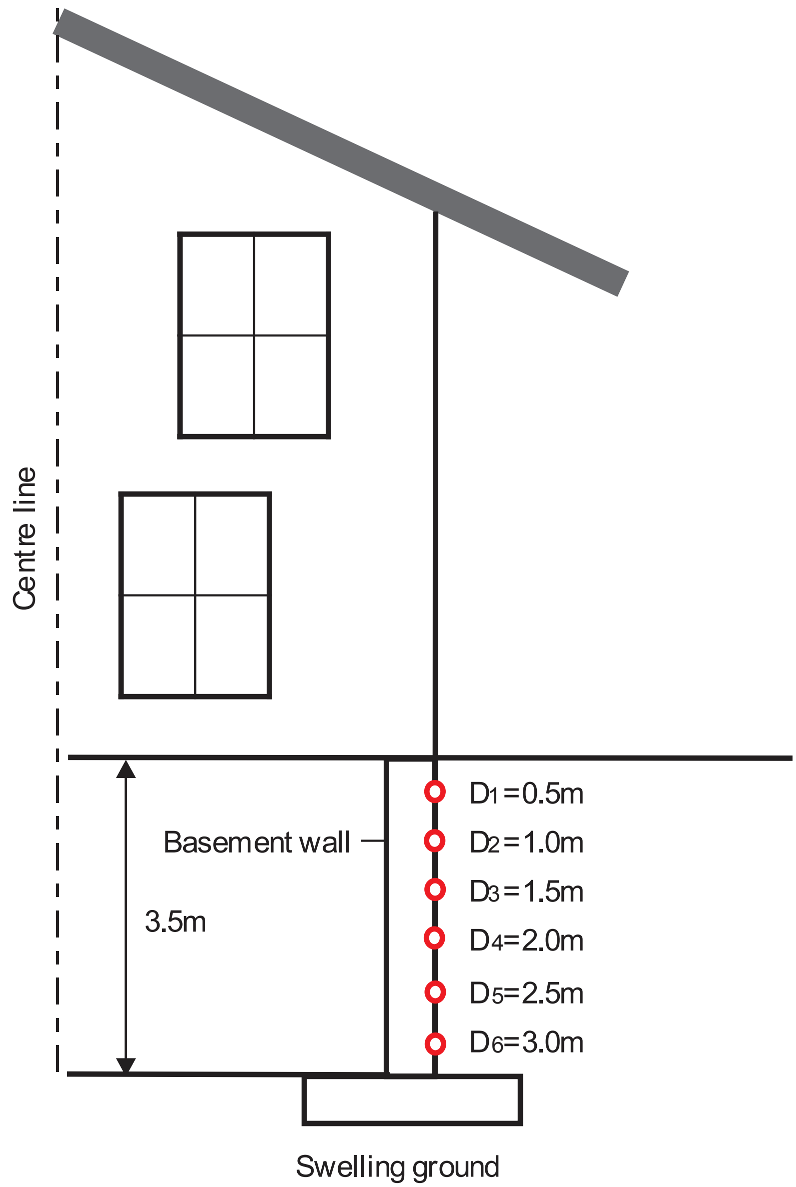

Figure 4.14. Schematic of a basement constructed in swelling ground.

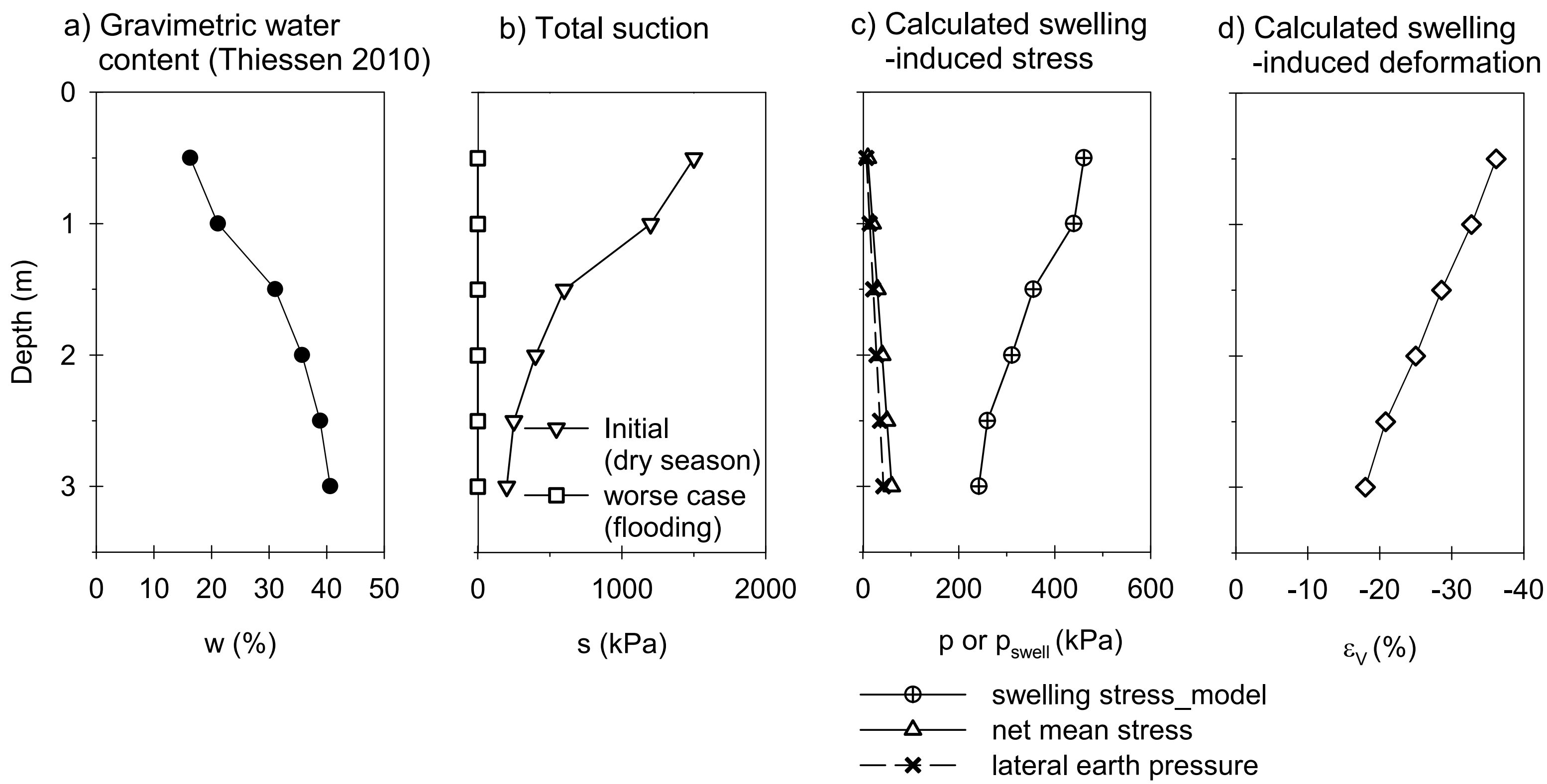

Figure 4.15. SFG model required initial and final inputs of soil states and calculated results: a) Gravimetric water content (Thiessen 2010); b) Total suction; c) Calculated swelling-induced stresses; and d) Calculated swelling-induced deformation.

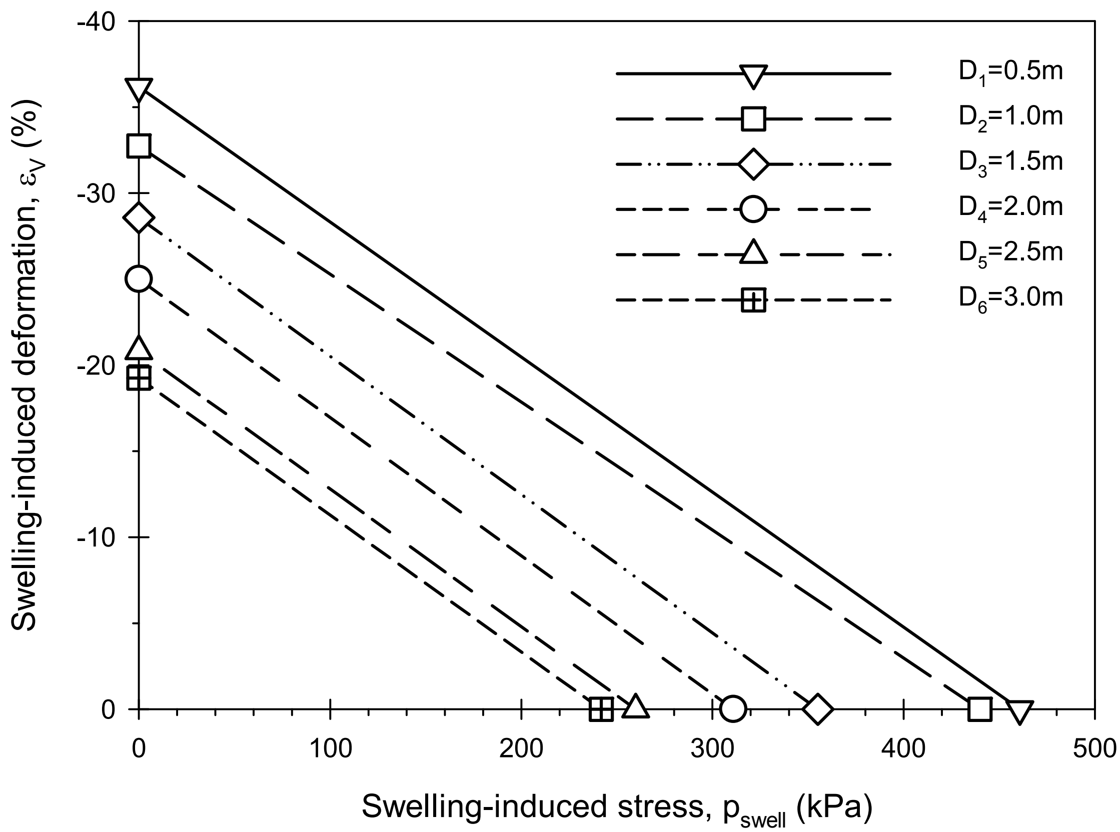

Figure 4.16. Envelope result on SFG model calculated swelling-induced stresses and deformations at each soil depth below ground.

CHAPTER 5: CONCLUSIONS AND RECOMMENDATIONS

5.1 Overview

In this chapter, the conclusions drawn from the research are presented. The research is aimed at better understanding of swelling soil behavior through Swell Equilibrium Limit framework with advanced testing and applying experimental data in a numerical analysis tool. The following presents the summary of the research work.

5.2 Conclusions from the Research

5.2.1 Objective 1

(test swelling behavior under free stress condition and extend the use of SEL framework down to low stress levels.)

A new test apparatus and methodology for measuring swelling deformation under a free stress condition is developed. Swelling soils achieve the highest swelling deformation when the soil is neither subjected any external confining stresses nor restraints on its boundary condition upon wetting. The methodology includes a non-contact measurement using digital image analysis where photographs of swelling specimen are taken progressively during wetting process in a humidity-controlled apparatus.

The image analysis is performed with GeoPIV software. The in-test results allow interpretation of primary and secondary swelling behavior as well as anisotropic swelling. The effect of varying aspect ratios (AR) of specimen is investigated and the influence is noted regarding the initial swelling rate and the time to achieve swelling equilibrium with the environment. The end-of-test caliper measurement is in general agreement with the deformation obtained from digital image correlation. The unconfined swelling test result extends the use of SEL framework down to low stress levels.

5.2.2 Objective 2

(a unifying framework to characterize swelling soils and model swelling behavior in SEL context)

The SEL concept provides a unifying framework to understand and model swelling soil behavior. It allows for a calculation of an upper bound swelling limit depending on the initial state of the soil and the stress-volume paths following wetting. The SEL curve is obtained from two advanced test methods, namely, triaxial swelling test and unconfined swelling test that encompasses a comprehensive scenario of swelling behavior from rigid boundary condition to free swelling without confinement. Two additional recompacted clayey soils were tested for their SEL interpretation, namely, the recompacted Bearpaw clay and recompacted Lake Agassiz clay.

A catalogue of expansive soils is established with four soil materials, namely, bentonite-sand-buffer, recompacted Lake Agassiz clay, recompacted Bearpaw clay and natural Bearpaw shale. The index properties and initial state of the tested soils correlates well with the swelling potential in a SEL context. The swelling potential in decreasing sequence is BSB, recompacted Lake Agassiz clay, recompacted Bearpaw clay and natural Bearpaw shale. The influence of soil history and soil structure is more dominant on the SEL of Bearpaw shale.

The fitting parameters, A and B from SEL plot ($V=A+ B*\ln p$) are correlated with the index properties and initial state of the soils. The developed correlation allowed for a SEL of an expansive soil, namely, Regina clay to be calculated and the calculation agrees well with published data. The unifying SEL framework is capable of characterizing expansive soil behavior in terms of swelling-induced stress and swelling deformation.

5.2.3 Objective 3

(applying experimental data in an unsaturated numerical analysis tool to model swelling soil behavior)

The swelling-induced stresses and swelling deformation given by the SEL curve are important inputs in expansive soils design. The SFG constitutive model is developed from unsaturated soil mechanics theory and it requires two additional input parameters. The two additional input parameters required in SFG model are soil compressibility for swelling and saturation suction (s_{sa}). Other input for the model is the initial state of the soil. The model input parameters are optimized by refinement until the model results match with the experiments. With the optimized model inputs, the SFG model is applied successfully to two expansive clayey soils, namely BSB and recompacted Lake Agassiz clay.

A parametric analysis is performed to examine the sensitivity of the model output to the input parameters. The dominant factor for swelling deformation is soil compressibility but the more influential input in calculating swelling-induced stresses is saturation suction. The simplicity of SFG model has made it an attractive tool for modelling in unsaturated swelling soil behavior.

5.3 Impact of Research

This research work has achieved the objectives set out for the program. Advanced testing apparatus and methodology development allows for more complex swelling soil behavior to be simulated in a laboratory set-up. The varying degree of boundary conditions from free swelling of constant mean stress to confined swelling of constant volume has been successfully simulated in a modified triaxial apparatus. In addition to the capability of stress-volume path control, the new modification allows for relative humidity measurement in the soil specimen. Relative humidity can be correlated to total suction and measurement of the degree of saturation.

A total free stress swelling test methodology is developed successfully to represent an unconfined swelling boundary condition. Non-contact measurement through digital image correlation has been applied to calculate swelling deformation of soil specimen. Unconfined swelling test allows for a SEL curve to be interpreted at low stress level.

The characterization of swelling behavior is successfully interpreted in SEL context. A catalogue of expansive soils which consists of two natural recompacted soils (recompacted Lake Agassiz clay and Bearpaw clay), one natural shale (Bearpaw shale) and one engineered buffer (BSB) is established. The SEL curve of expansive soils is correlated to the soil initial condition and index property. With the established correlation, the SEL of an expansive soil namely, Regina clay could be calculated.

SFG model that requires two input parameters is applied successfully to model experimental data from SEL swelling test. The model calculation and test measurement of swelling-induced stresses and deformation agrees well in comparison.

5.4 Recommendations for Future Work

During the course of the research program, the challenges faced have intrigued some different considerations or emphasis in solving the research questions. The following are some recommendations for future works:

- Install an automated wetting mechanism such as sprinkle device in the unconfined swelling test apparatus. The automated sprinkle system would reduce the required manual work of water spraying. Continuous supply of water access would help prevent unintended wetting-drying cycles.
- Further explore the characteristics of the SEL framework with the variability in testing condition:
    a. Vary stress-volume paths from direct constant mean stress or constant volume in order to examine if SEL curve is stress-volume path dependent (Liu et al. 2014).
    b. Vary targeted initial dry density to 95% of wet or dry side of optimum condition of a Proctor curve (Puppala et al. 2013) to investigate the effect on swelling potential.
    c. Vary initial water content at a constant dry density (Komine and Ogata 1994) to study the effect on SEL curve.
    d. Apply mean stress that exceeds soil swelling pressure as to extend the use of SEL framework in collapsible behavior.
- Perform shear strength tests following triaxial swelling test to examine the effect of swelling boundary condition on the shear strength of post-triaxial swelling specimen. Yield stress and critical state analysis could be employed to have a better understanding of post-SEL strength behavior.
- Perform SEL tests on different type of expansive soils to increase the size of the SEL database.
- Model collapse behavior of swelling soils using the developed numerical tool.
- Formulate SFG model in a finite element method or finite difference package and model soil-environment interactions.

5.5 References

Komine, H. and Ogata, N. 1994. Experimental study on swelling characteristics of compacted bentonite. Canadian Geotechnical Journal 31 (4): 478-90.

Liu, X.F., Buzzi, O.P. and Vaunat, J. 2014. Influence of stress-volume path on swelling behavior of an expansive clay. Paper presented at 6th International Conference on Unsaturated Soils: Research & Applications, Sydney, Australia.

Puppala, A.J., Manosuthikij, T. and Chittoori, B.C.S. 2013. Swell and shrinkage characterizations of unsaturated expansive clays from Texas. Engineering Geology 164 : 187-94.

APPENDIX

APPENDIX A - Summary table for triaxial swelling test

APPENDIX B - Summary table for unconfined swelling test

APPENDIX C - Triaxial swelling test result for recompacted Bearpaw clay

APPENDIX D - Fitting parameters A and B (V=A+B ln p) correlation

APPENDIX E - Photograph and drawing for triaxial swelling test

APPENDIX F - Photograph for unconfined swelling test

APPENDIX G - Measuring instruments calibration sheet

APPENDIX H - Laboratory record for Atterberg Limits, Modified Proctor and Grain size distribution

APPENDIX I - SFG modelling spreadsheet for recompacted Lake Agassiz clay

APPENDIX J - SFG modelling spreadsheet for BSB

APPENDIX K - Published journal papers

APPENDIX L ï Published conference papers

APPENDIX A - SUMMARY TABLE FOR TRIAXIAL SWELLING TEST

Project: PhD thesis on swelling soil behavior

Title: Summary of SEL swelling test

by: blim

															Gs=	2.75					
						Saturation (SEL)															
						Initial - SEL									EOT (SEL)						
	Test #		Cell# 1/Cell#2?	Start Date	End Date	$\rho_d = \frac{G_s \rho_w}{1+e}$ Dry Density	Bulk Density	M_{ini}	WC	e	p	V	Sr		WC	e	Sr	V	p	Pswell	EMDD
						(Mg/m3)	(Mg/m3)	(g)	(%)	(-)	(-)	(-)	(%)		(%)	(-)	(%)	-	kPa	Mpa	Mg/m3
recomp. Bearpaw 1.5, 30%	3	#3_CMS200	#1	16/03/2012	10/05/2012	1.472	1.903	402.4	29.3	0.869	200	1.869	92.9	CMS200	31.9	0.897	97.8	1.897	204	0.304	0.669
	4	#4_CMS400	#1	16/05/2012	28/06/2012	1.460	1.866	401.0	27.8	0.884	400	1.884	86.5	CMS400	31.6	0.865	100.5	1.865	401	0.593	0.684
	7	#7_CMS200	#2	10/07/2012	22/10/2012	1.410	1.858	398.6	31.8	0.951	200	1.951	91.9	*CMS200	33.5	0.954	96.6	1.954	187	0.277	0.635
										1.879	400			*CMS400	31	0.879	97.0	1.879	400		
										1.826	600			*CMS600	29.5	0.826	98.2	1.826	600		
										1.794	800			*CMS800	28.3	0.794	98.0	1.794	800		
	8	#8_CMS400 ->200	#1	27/08/2012	09/11/2012	1.409	1.843	390.4	30.9	0.953	400	1.953	89.2	"CMS200	31.3	0.883	97.5	1.883	400	0.591	0.705
											200			"CMS400	32.3	0.830	107.0	1.830	200		
	10	#10_CV400	#1	19/12/2012	21/01/2013	1.441	1.868	395.0	29.6	0.909	400	1.909	89.7	CV400	30.8	0.829	102.2	1.829	410	0.605	0.706
recompacted L.Ag - 1.60, 20%	14	#14_CV150	#1	18/02/2013	21/02/2013	1.571	1.899	398.9	20.9	0.757	150	1.757	76.3	150	-	-	-	-	-	-	-
	15	#15_CV150r	#1	25/02/2013	29/03/2013	1.568	1.907	398.9	21.6	0.760	150	1.760	78.5	150	29.0	0.762	105.0	1.762	753	1.137	0.692
	16	#16_CMS150	#2	01/03/2013	12/04/2013	1.591	1.917	401.7	20.3	0.735	150	1.735	76.9	150	39.1	0.986	109.0	1.986	143	0.216	0.567
	17	#17_CV300	#1	08/04/2013	07/05/2013	1.602	1.906	400.2	19.0	0.723	300	1.723	72.6	300	26.3	0.702	103.0	1.702	1200	1.814	0.735
	18	#18_CMS300	#2	18/04/2013	18/05/2013	1.578	1.910	399.0	21.1	0.750	300	1.750	77.7	300	32.4	0.877	102.0	1.877	291	0.439	0.622
	19	#19_CMS600	#2	12/06/2013	12/07/2013	1.576	1.881	399.1	19.3	0.751	600	1.751	71.0	600	29.2	0.802	100.7	1.802	606	0.916	0.666

All infiltration tests in the table are completed with 100 kPa water pressure.

APPENDIX B - SUMMARY TABLE FOR UNCONFINED SWELLING TEST

Project: PhD thesis on swelling soil behavior | Date: 15/11/2013

Subject: Summary of Unconfined Swelling Test (Caliper measurement)

by: blim

Summary of Free Swelling Test Data from water content, mass and caliper measurement

		Aspect ratio	ID	Targeted dry density	Initial dimension				Final dimension				Bulk density			Dry density			Water content			Void ratio			Degree of saturation			Total volume change	
				Mg/m3	mm	mm	mm2	mm3	mm	mm	mm2	mm3	Mg/m3			Mg/m3			%			-			%			%	%
		H/dia	-	Targeted	Dia.	Height	Area	Vol	Dia.	Height	Area	Vol	Initial	Final	D	Initial	Final	D	Initial	Final	D	Initial	Final	D	Initial	Final	D	Scaled picture	De/(1+eo)
1	I-B1	0.51	189	1.74	51.3	26.4	2070	54590	62.7	32.1	3083	98821	1.78	1.50	-0.28	1.55	0.87	-0.67	15.0%	71.1%	56.1%	0.78	2.15	1.37	52.8%	91.0%	38.2%	62.6%	76.9%
2	I-B2	0.5	169	1.49	51.2	25.6	2058	52584	59.4	29.6	2767	81985	1.79	1.54	-0.26	1.42	0.90	-0.52	26.7%	70.9%	44.2%	0.94	2.06	1.12	77.8%	94.7%	16.9%	49.8%	57.5%
3	I-B3	0.5	169	1.49	51.3	25.4	2069	52575	55.6	28.1	2427	68231	1.59	1.54	-0.05	1.32	1.00	-0.32	20.2%	54.2%	34.0%	1.08	1.75	0.67	51.4%	85.2%	33.8%	50.4%	32.2%
4	I-B4	0.75	189	1.74	51.2	38.6	2061	79662	60.8	46.5	2905	135016	1.85	1.58	-0.27	1.61	0.96	-0.64	15.0%	63.5%	48.5%	0.71	1.85	1.14	57.9%	94.3%	36.4%	57.5%	66.7%
5	I-B5	1.49	189	1.74	51.4	76.4	2078	158859	57.6	86.4	2606	225138	1.85	1.63	-0.23	1.61	1.14	-0.47	15.0%	42.8%	27.9%	0.71	1.42	0.71	58.3%	83.2%	24.9%	40.8%	41.7%
6	II-B1	0.44	181v	1.57	72.1	31.5	4077	128560	75.1	33.7	4427	149333	1.93	1.84	-0.09	1.57	1.37	-0.21	22.8%	34.7%	11.9%	0.75	1.01	0.26	83.7%	94.3%	10.6%	13.2%	15.0%
7	II-B2	0.48	181v	1.57	71.9	34.5	4063	140032	76.2	37.5	4558	171026	1.92	1.78	-0.15	1.57	1.31	-0.26	22.6%	35.4%	12.8%	0.75	1.09	0.34	82.5%	88.9%	6.3%	15.0%	19.5%
*8	II-B3	0.27	189	1.74	51.4	13.7	2075	28376	61.0	15.7	2918	45786	1.85	1.68	-0.16	1.60	1.01	-0.59	15.6%	66.5%	50.9%	0.72	1.72	1.00	59.5%	106.4%	46.9%	68.8%	58.0%
*9	II-B4	0.75	189	1.74	51.5	38.9	2085	81018	61.3	45.7	2954	134913	2.02	1.66	-0.36	1.75	1.08	-0.67	15.2%	53.8%	38.6%	0.57	1.54	0.97	73.8%	96.0%	22.2%	67.6%	62.1%
*10	II-B5	1.98	189	1.74	51.6	101.9	2088	212698	59.3	117.5	2765	324888	2.00	1.70	-0.31	1.74	1.16	-0.58	15.3%	46.7%	31.4%	0.58	1.38	0.79	72.4%	93.4%	21.0%	50.0%	50.2%
*11	III-B5	0.15	189	1.74	51.2	7.6	2058	15627	61.3	9.7	2952	28554	2.02	1.56	-0.46	1.71	0.97	-0.74	17.8%	61.4%	40.0%	0.61	1.84	1.23	81.0%	91.8%	10.8%	79.4%	76.9%
12	III-B1	0.24	189	1.74	51.2	12.4	2062	25475	56.9	14.4	2545	36540	1.90	1.65	-0.25	1.53	1.07	-0.45	24.7%	53.8%	29.1%	0.80	1.56	0.76	84.8%	94.9%	10.1%	38.2%	42.1%
13	III-B2	0.26	202v	1.67	57.4	15.2	2583	39209	60.9	17.7	2910	51547	2.02	1.75	-0.27	1.67	1.32	-0.35	21.0%	32.5%	11.5%	0.64	1.08	0.44	89.5%	82.6%	-7.0%	31.9%	26.7%
14	III-B3	0.26	189	1.74	51.3	13.3	2065	27515	60.6	17.0	2888	49104	1.79	1.55	-0.23	1.65	0.94	-0.72	7.9%	65.9%	58.0%	0.66	1.93	1.27	32.9%	93.7%	60.8%	70.9%	76.6%
15	III-B4	0.16	202v	1.74	56.2	9.0	2477	22246	59.9	11.5	2816	32412	1.99	1.61	-0.38	1.69	1.18	-0.52	17.5%	36.8%	19.4%	0.62	1.34	0.71	77.0%	75.9%	-1.2%	53.5%	43.8%
16	III-B5	0.15	189	1.74	51.2	7.6	2058	15627	61.3	9.7	2952	28554	2.02	1.56	-0.45	1.71	0.97	-0.74	17.8%	61.4%	43.6%	0.61	1.84	1.23	81.0%	91.8%	10.8%	61.4%	76.9%
17	IV-B1	0.34	164v	1.42	71.3	23.5	3995	93810	76.1	24.6	4551	111950	1.78	1.71	-0.07	1.42	1.21	-0.22	25.2%	41.3%	16.1%	0.93	1.27	0.34	74.5%	89.2%	14.7%	22.0%	17.8%
"19	V-B1 (RH)	0.5	169	1.50	51.0	25.9	2043	52909	57.5	30.1	2597	78161	1.90	1.63	-0.28	1.46	1.00	-0.46	30.0%	61.8%	31.8%	0.88	1.74	0.86	93.8%	97.8%	4.0%	44.7%	45.8%
20	V-B2	0.15	169	1.50	50.8	7.5	2027	15201	58.9	9.3	2725	25340	1.90	1.58	-0.32	1.48	0.92	-0.56	28.3%	72.3%	44.0%	0.86	2.00	1.14	90.4%	99.4%	9.0%	56.5%	61.1%
21	Va-B3	0.15	L.Ag	1.62	51.2	7.8	2059	16018	59.0	9.8	2734	26656	1.86	1.57	-0.29	1.57	0.95	-0.62	18.7%	66.1%	47.4%	0.76	1.91	1.15	67.8%	95.3%	27.5%	51.8%	65.4%
22	Va-B4	0.25	L.Ag	1.62	51.2	13.0	2059	26765	59.4	16.0	2771	44339	1.87	1.59	-0.28	1.58	0.95	-0.63	18.7%	68.5%	49.8%	0.75	1.92	1.17	68.8%	98.4%	29.6%	61.4%	66.9%
23	Va-B5	0.5	L.Ag	1.62	51.3	25.9	2067	53533	59.3	31.8	2762	87827	1.88	1.59	-0.29	1.58	0.95	-0.63	18.7%	67.1%	48.4%	0.74	1.90	1.16	69.5%	97.3%	27.8%	57.9%	66.6%
"24	VI-B1(RH)	0.5	L.Ag	1.62	51.2	26.3	2056	54064	60.8	31.5	2903	91455	1.88	1.54	-0.35	1.56	0.92	-0.64	20.6%	67.3%	46.7%	0.77	2.00	1.24	74.1%	92.7%	18.6%	66.2%	69.9%
25	VI-B2	0.25	L.Ag	1.62	51.2	12.8	2059	26354	59.6	16.4	2790	45754	1.93	1.50	-0.43	1.60	0.93	-0.68	20.4%	62.6%	42.2%	0.72	1.99	1.26	77.9%	87.0%	9.1%	62.5%	73.2%
27	VI-B4	0.15	L.Ag	1.62	51.1	7.8	2051	15997	58.4	11.0	2679	29465	1.95	1.46	-0.48	1.61	0.89	-0.72	20.8%	63.4%	42.6%	0.71	2.09	1.37	80.3%	83.9%	3.6%	50.0%	80.0%
28	VI-B5	0.15	L.Ag	1.62	51.1	7.9	2051	16202	59.6	11.1	2790	30967	1.84	1.45	-0.38	1.57	0.83	-0.74	16.7%	74.8%	58.1%	0.76	2.32	1.57	61.0%	88.9%	27.9%	63.2%	89.1%

* result presented in Unconfined swelling paper (Lim and Siemens 2013)

" result presented in Multiple SELs paper (Chapter 3, blim thesis 2014)

APPENDIX C - TRIAXIAL SWELLING TEST RESULT FOR RECOMPACTED BEARPAW CLAY

recompacted BPaw 169 - SEL Test

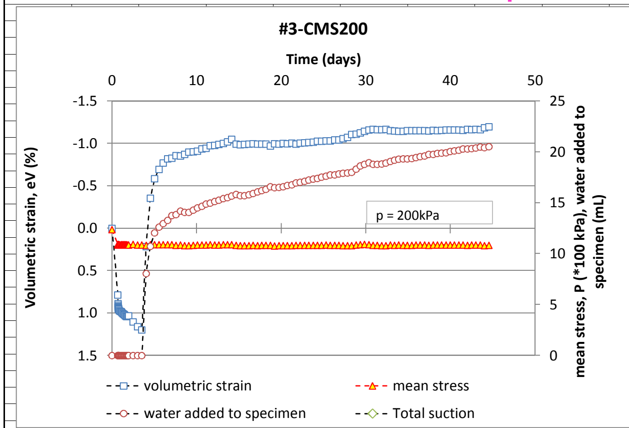

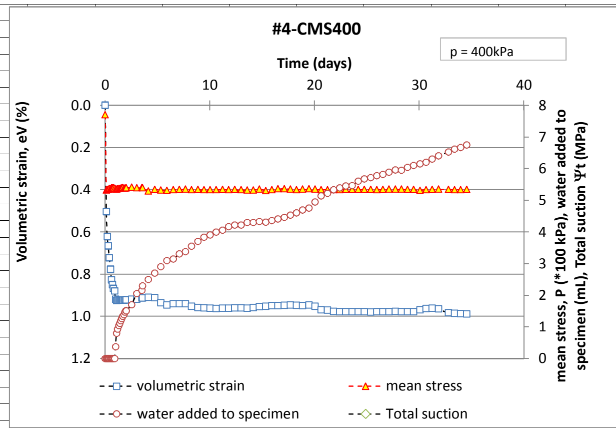

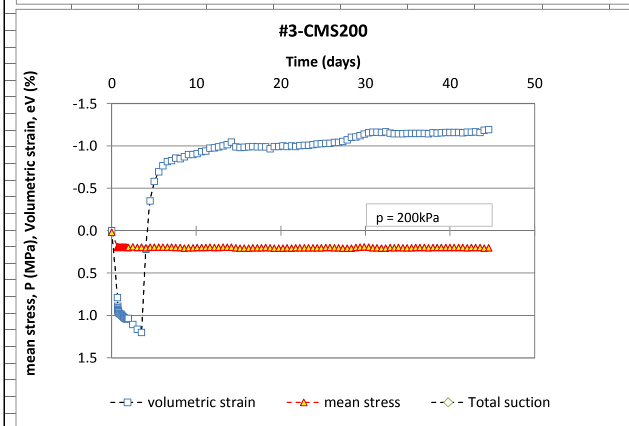

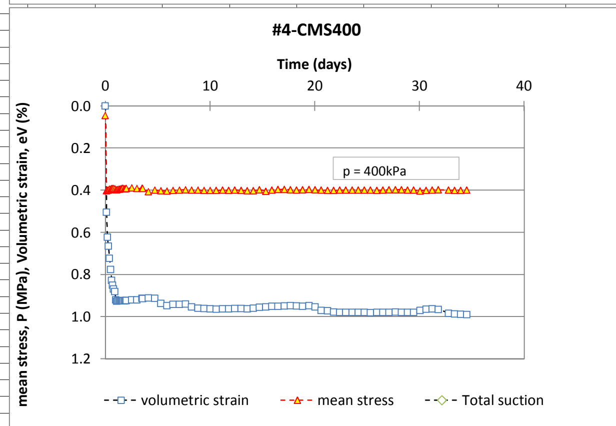

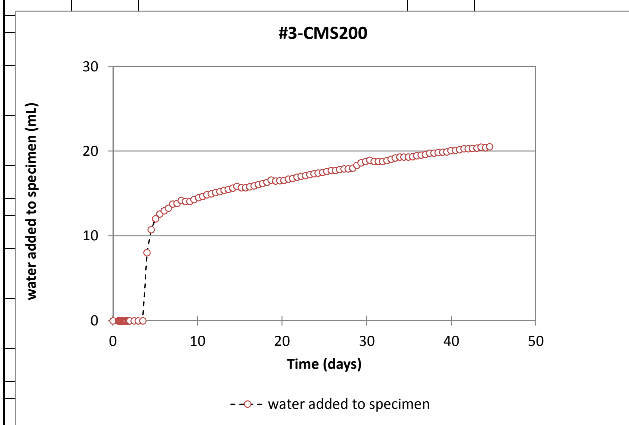

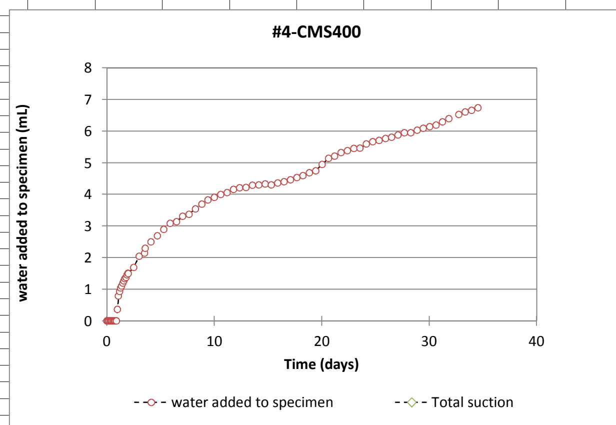

recompacted BPaw 169 - SEL Test

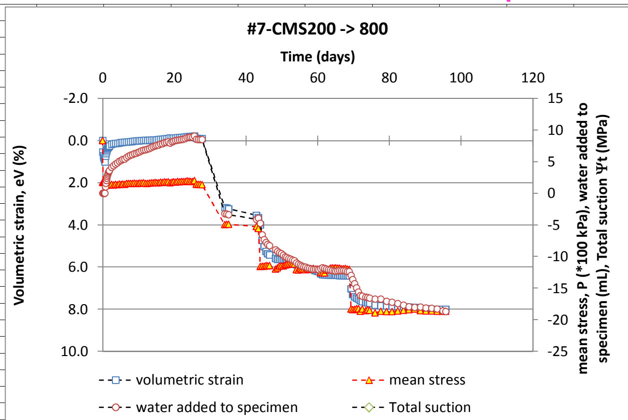

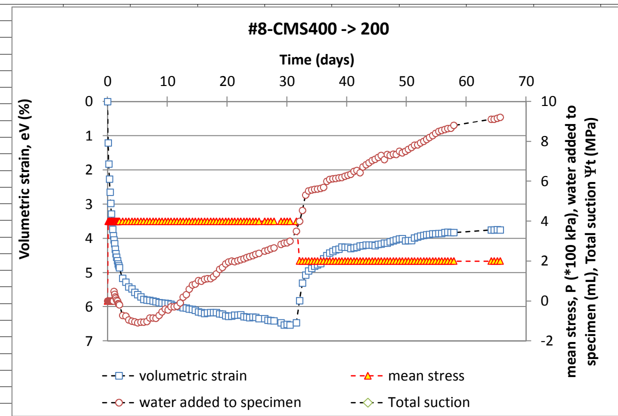

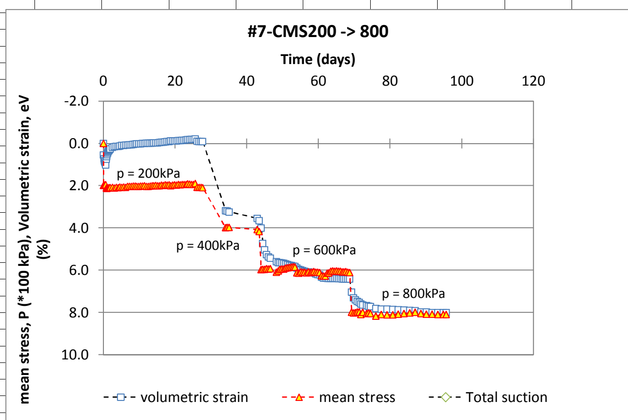

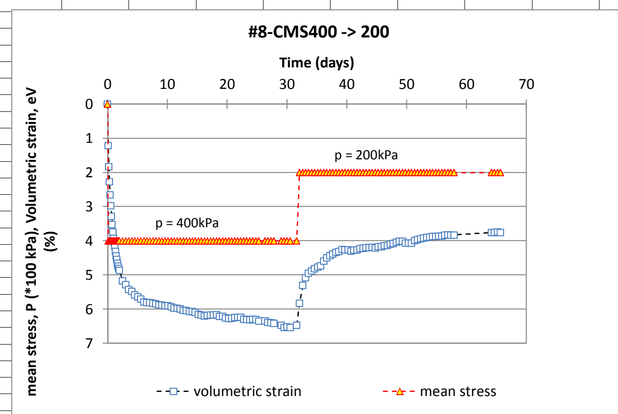

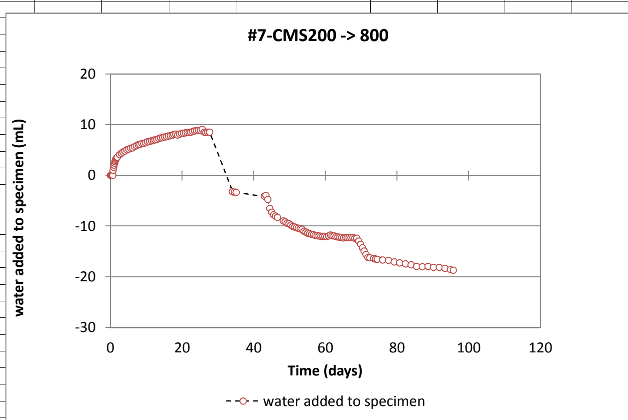

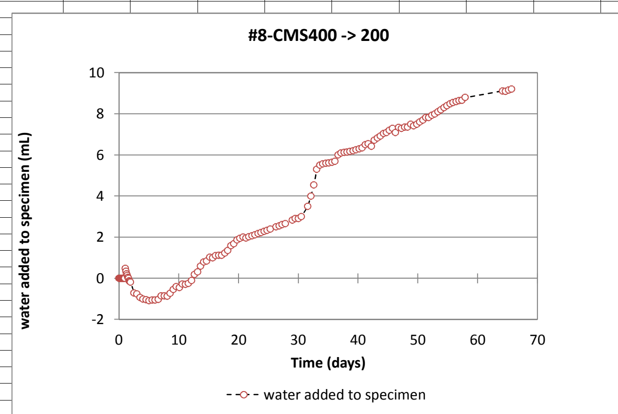

recompacted BPaw 169 - SEL Test

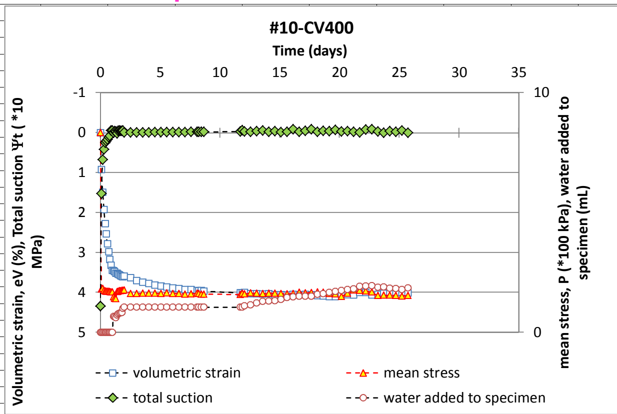

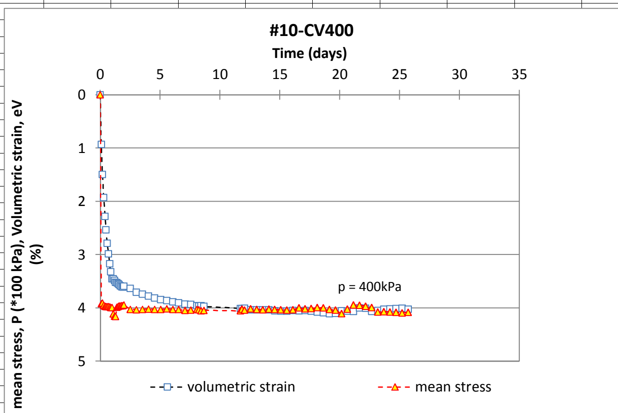

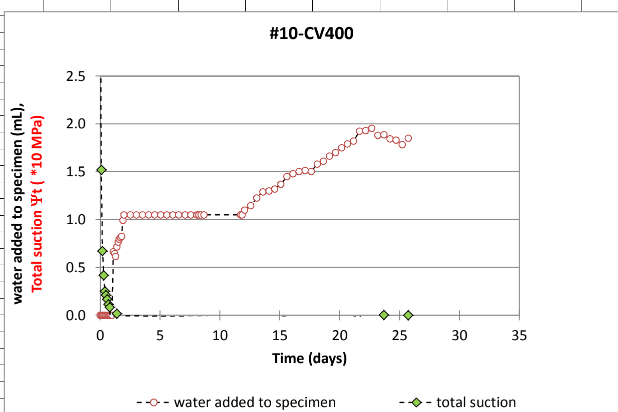

recompacted BPaw 169 - SEL Test

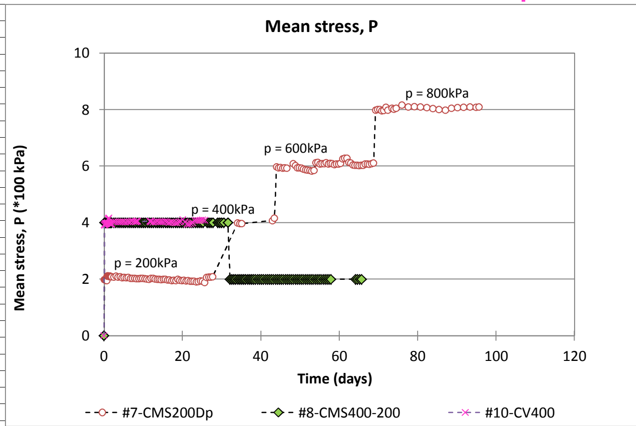

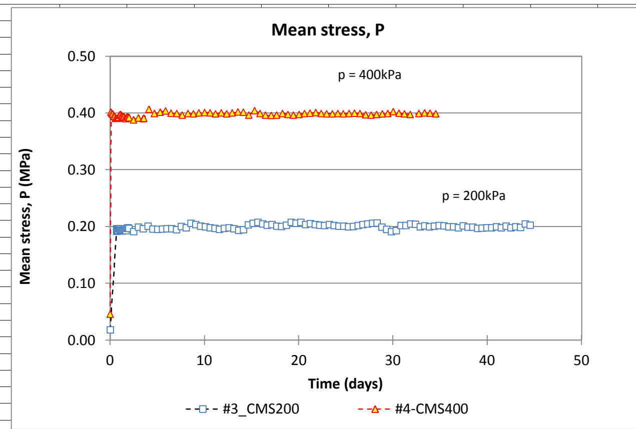

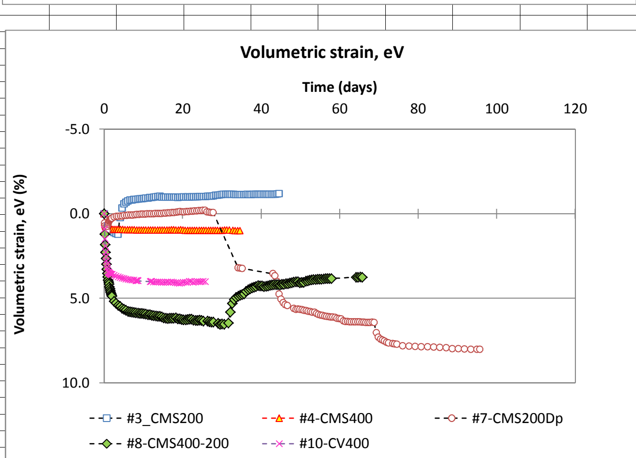

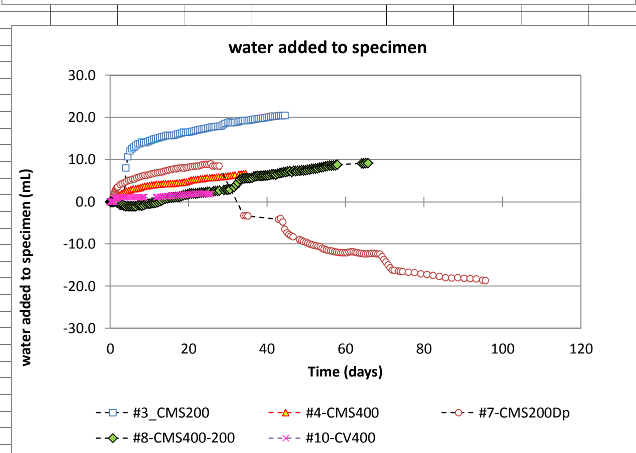

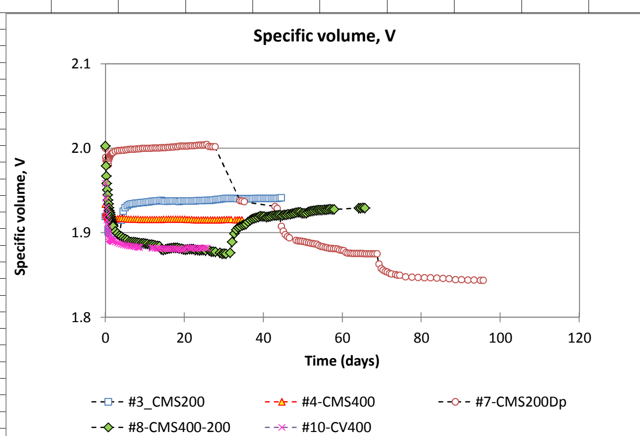

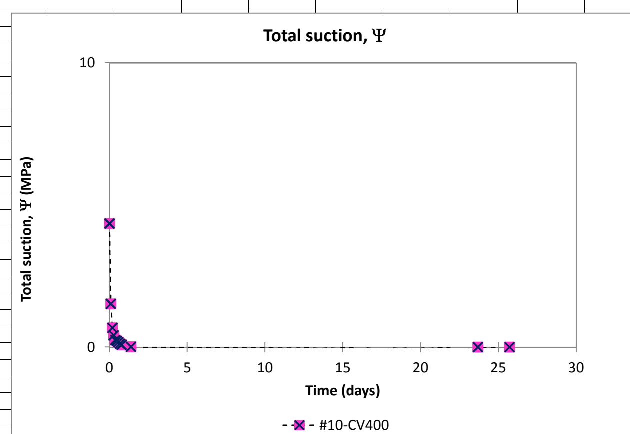

recompacted BPaw 169 - SEL Test

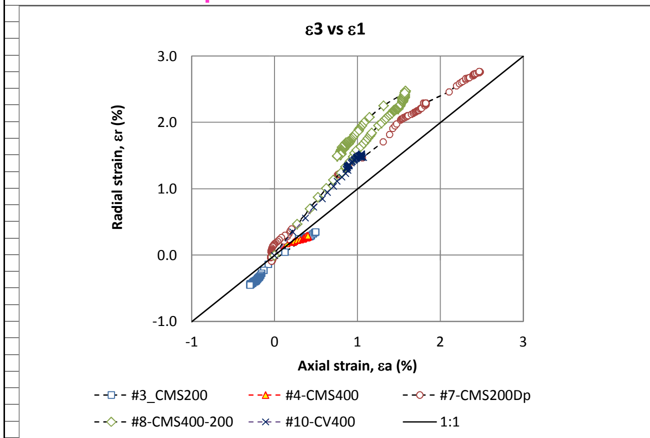

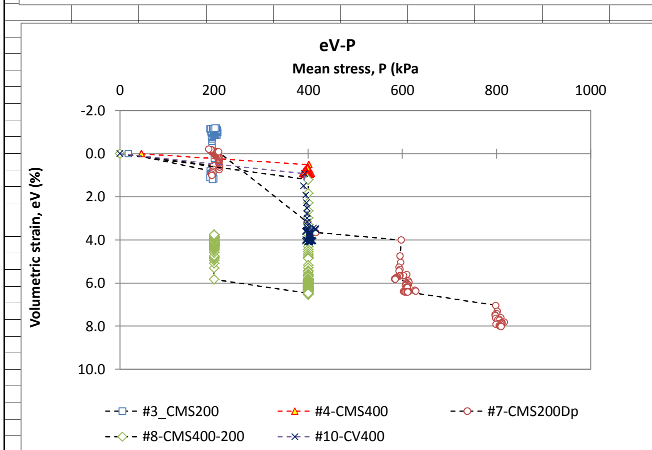

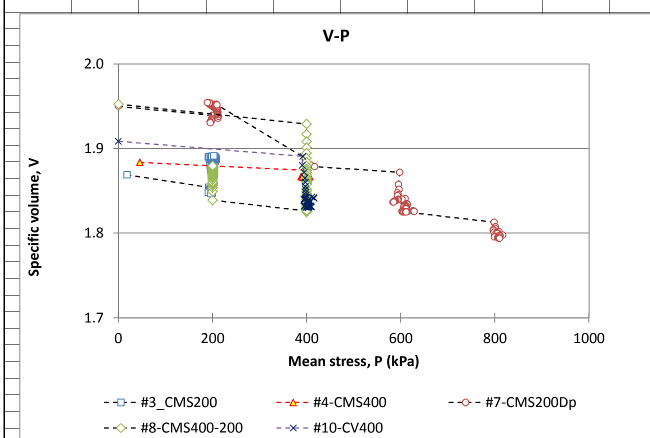

APPENDIX D - FITTING PARAMETERS A AND B (V=A+B LN P) CORRELATION

V=A+Blnp

		EMDD					SEL V-P plot									Eq of V-P		Eq of Pequil vs EMDD	
	Soil Type	clay content, fc	montmorillonite content, fm	fc.fm	fc.fm.γd	Gs	initial wc	LL	PL	PI	PL/LL	PI/LL	A=PI/% clay	LI=(wn-PL)/PI	Vo	Intersect A	Slope of (V-P)	Slope (P-EMDD)	EXP
		%	%	-			%	%	%	-					average	A	B	C	D
Tested soils	[1]Natural Bearpaw	39	72	0.281	0.421	2.75	30.0	145	23	122	0.159	0.841	3.13	0.06	1.833	2.102	-0.04628	1.2540.E-10	31.45
	Recompacted Bearpaw	39	72	0.281	0.408	2.75	30.0	67	26	41	0.385	0.615	1.05	0.11	1.894	2.596	-0.1265	0.0001565	11.73
	Lake Agassiz	75	30	0.225	0.357	2.76	20.0	85	34	51	0.398	0.602	0.68	-0.27	1.742	2.691	-0.1406	0.0004966	12.27
	[2]Bentonite Sand Buffer	50	90	0.450	0.753	2.70	19.4	265	21	244	0.079	0.921	4.88	-0.01	1.615	3.023	-0.2138	0.0076090	4.56
Soil to be predicted	Regina_fredlund	51	77	0.393	0.392	2.83		76	26	50	0.344	0.656	0.97		2.838				
	Hunter Expressway		27			2.56	28.0			50									

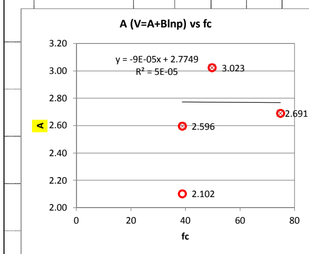

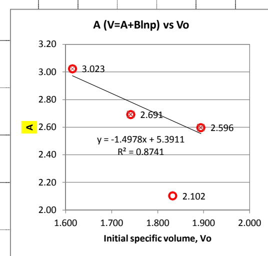

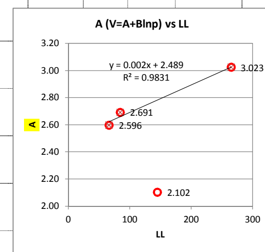

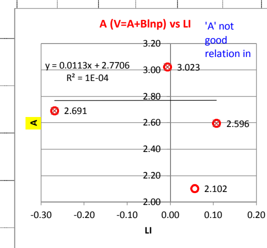

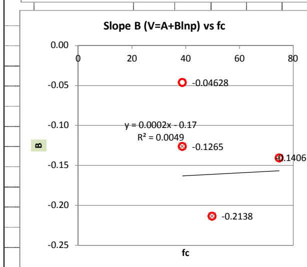

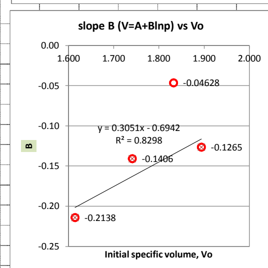

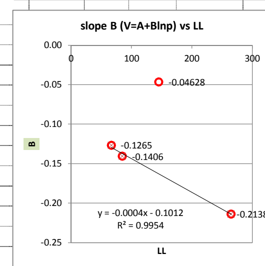

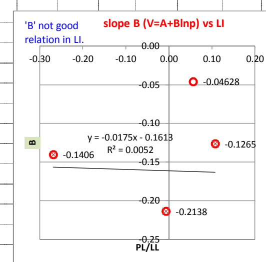

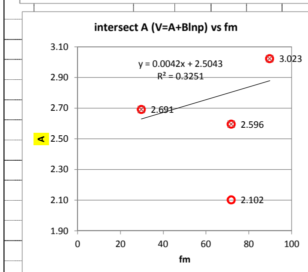

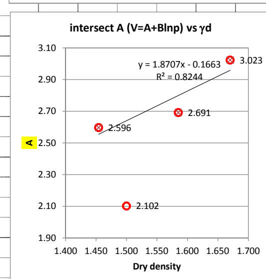

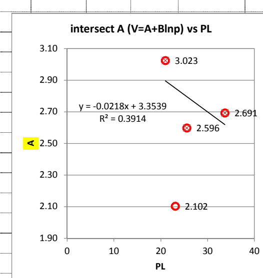

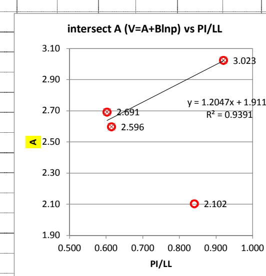

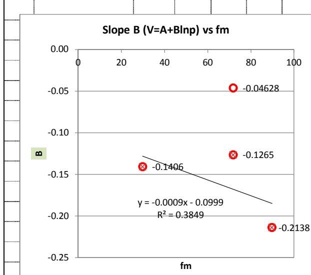

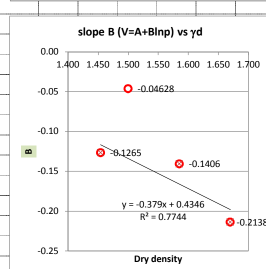

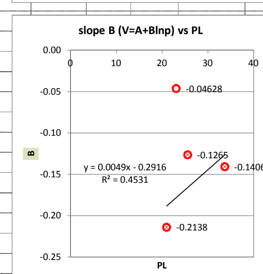

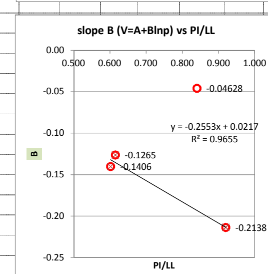

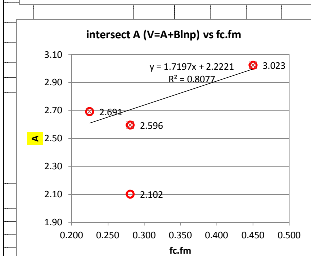

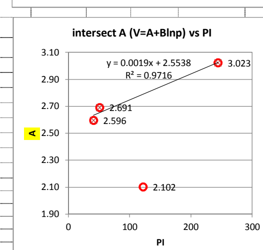

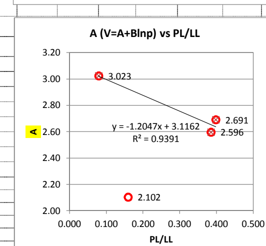

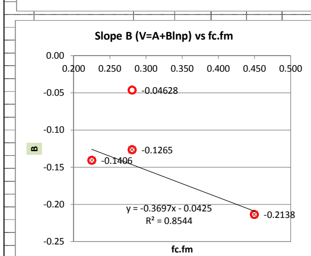

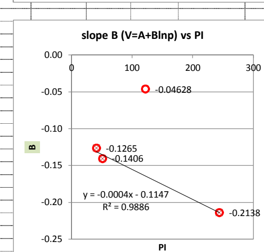

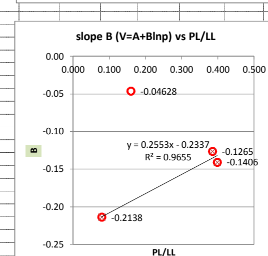

APPENDIX E - PHOTOGRAPH AND DRAWING FOR TRIAXIAL SWELLING TEST

General set-up of triaxial swelling test in the laboratory.

Triaxial specimen wrapped with a layer of filter paper and a layer of non-woven geotextile.

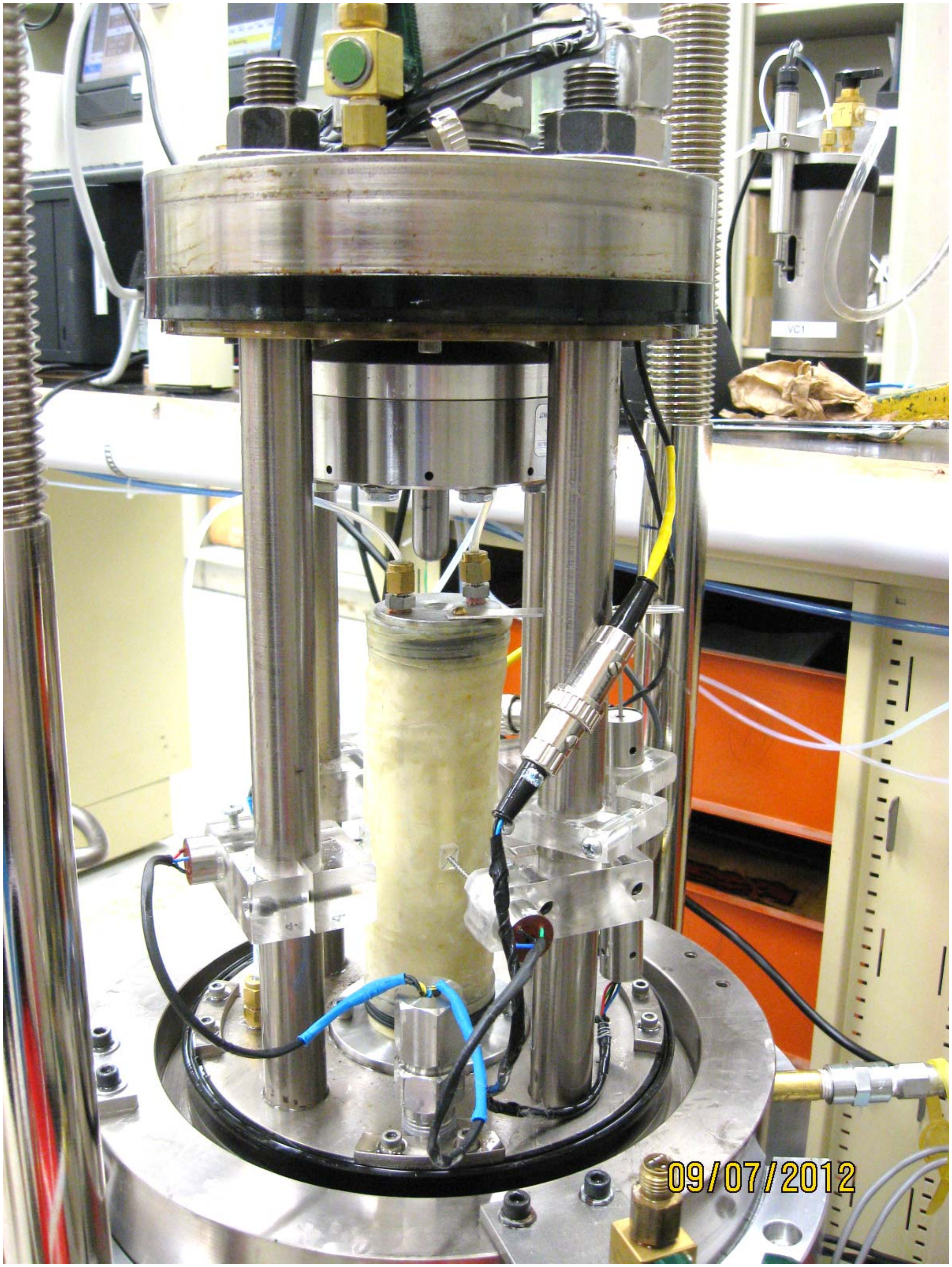

Triaxial specimen following installation in the modified apparatus.

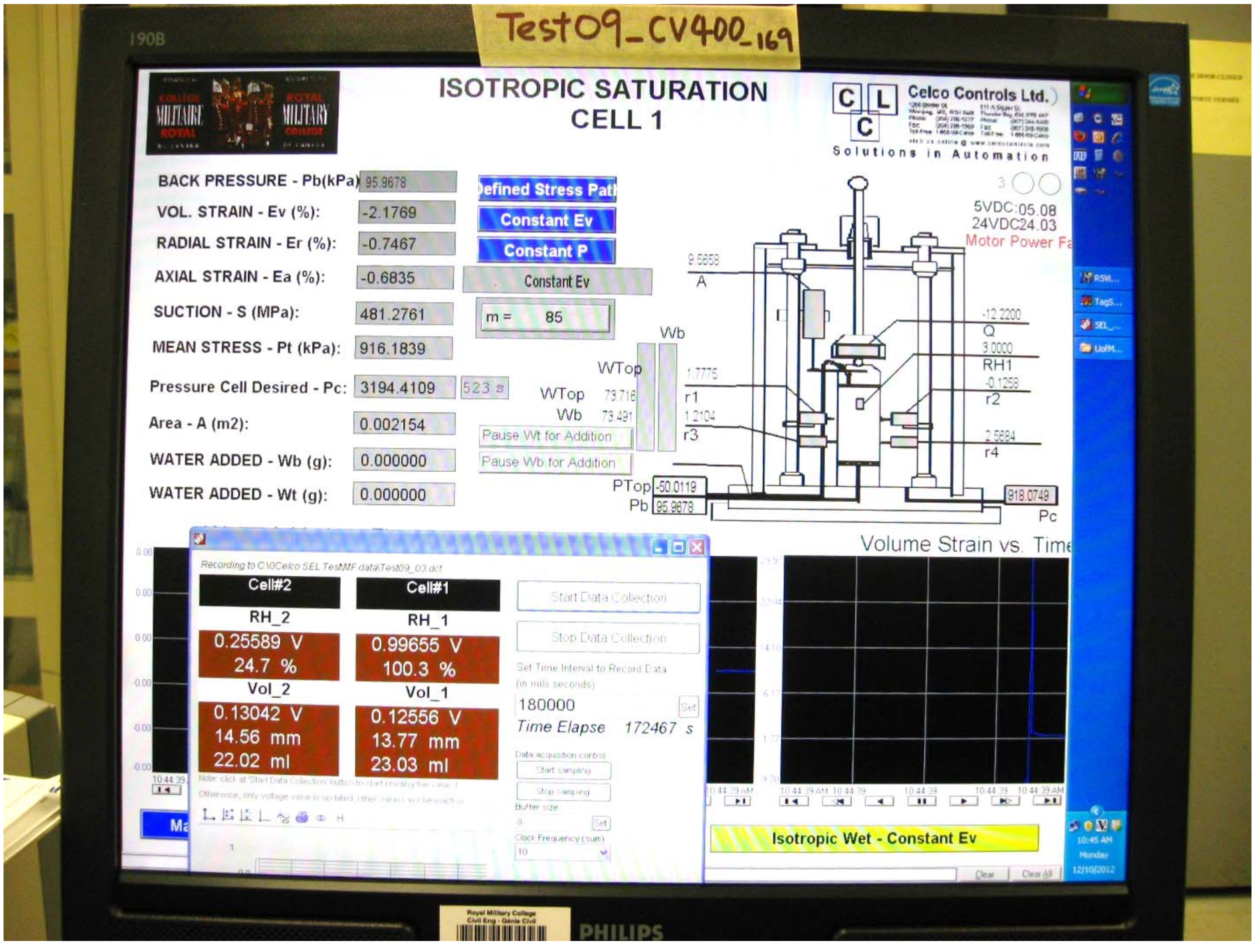

Screenshot of data acquisition and software control at triaxial swelling test.

2” diameter hydraulic compaction tool for specimen tested in unconfined swelling test and triaxial swelling test.

Preparation tools for mixing and compacting triaxial swelling test specimen.

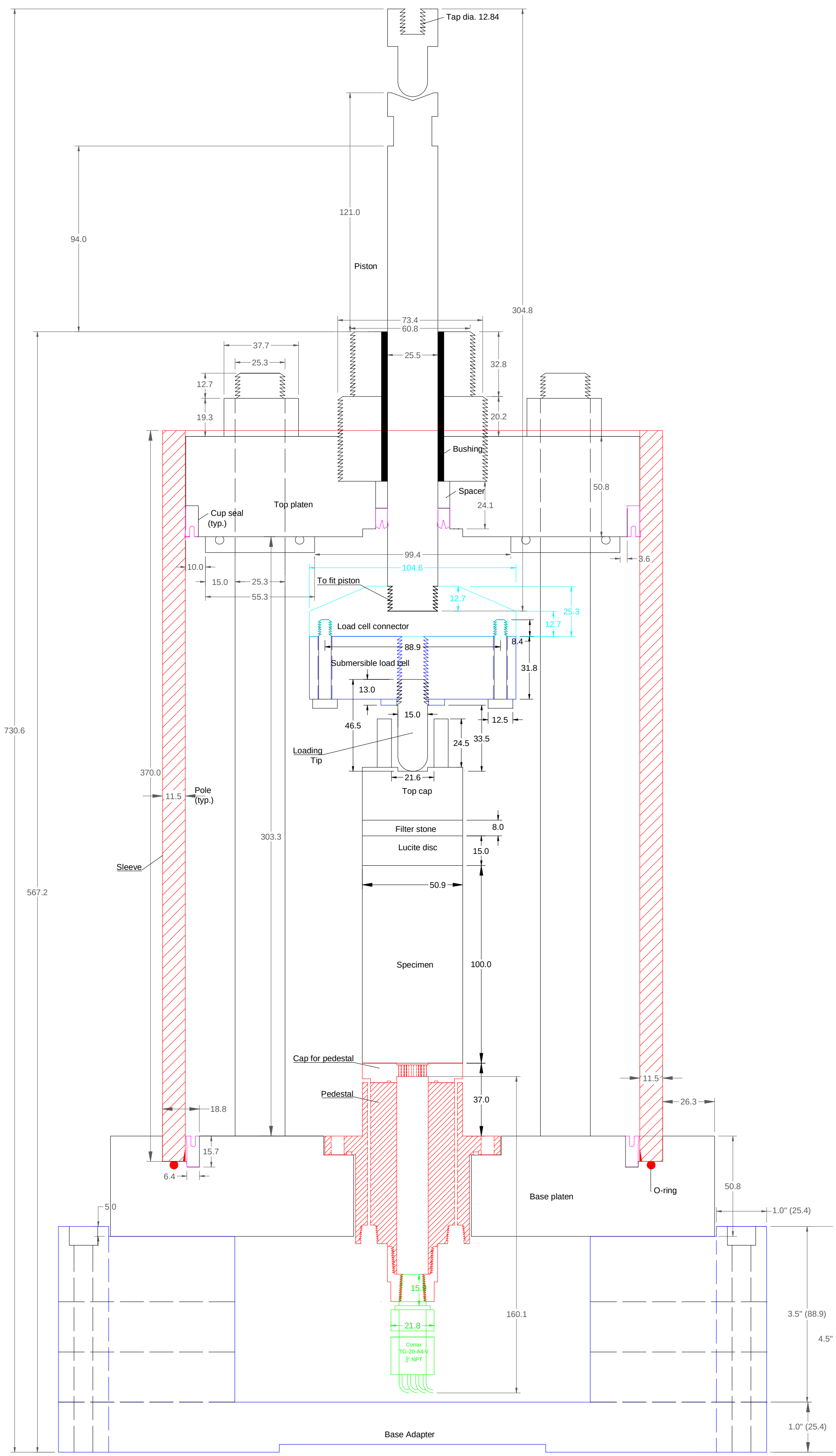

Detail drawing for modified triaxial apparatus (Cell#2).

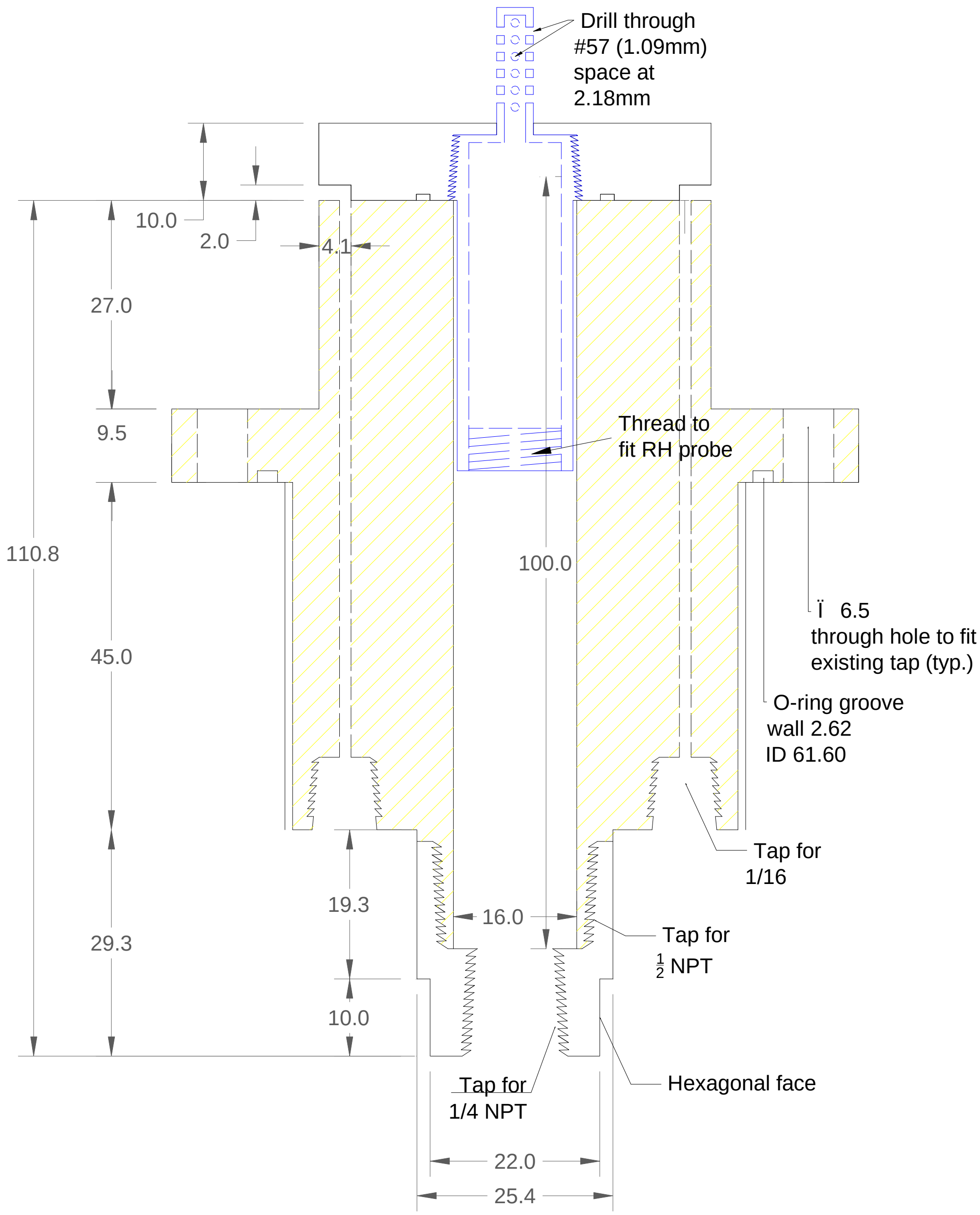

Modification at triaxial pedestal for suction measurement location.

APPENDIX F - PHOTOGRAPH FOR UNCONFINED SWELLING TEST

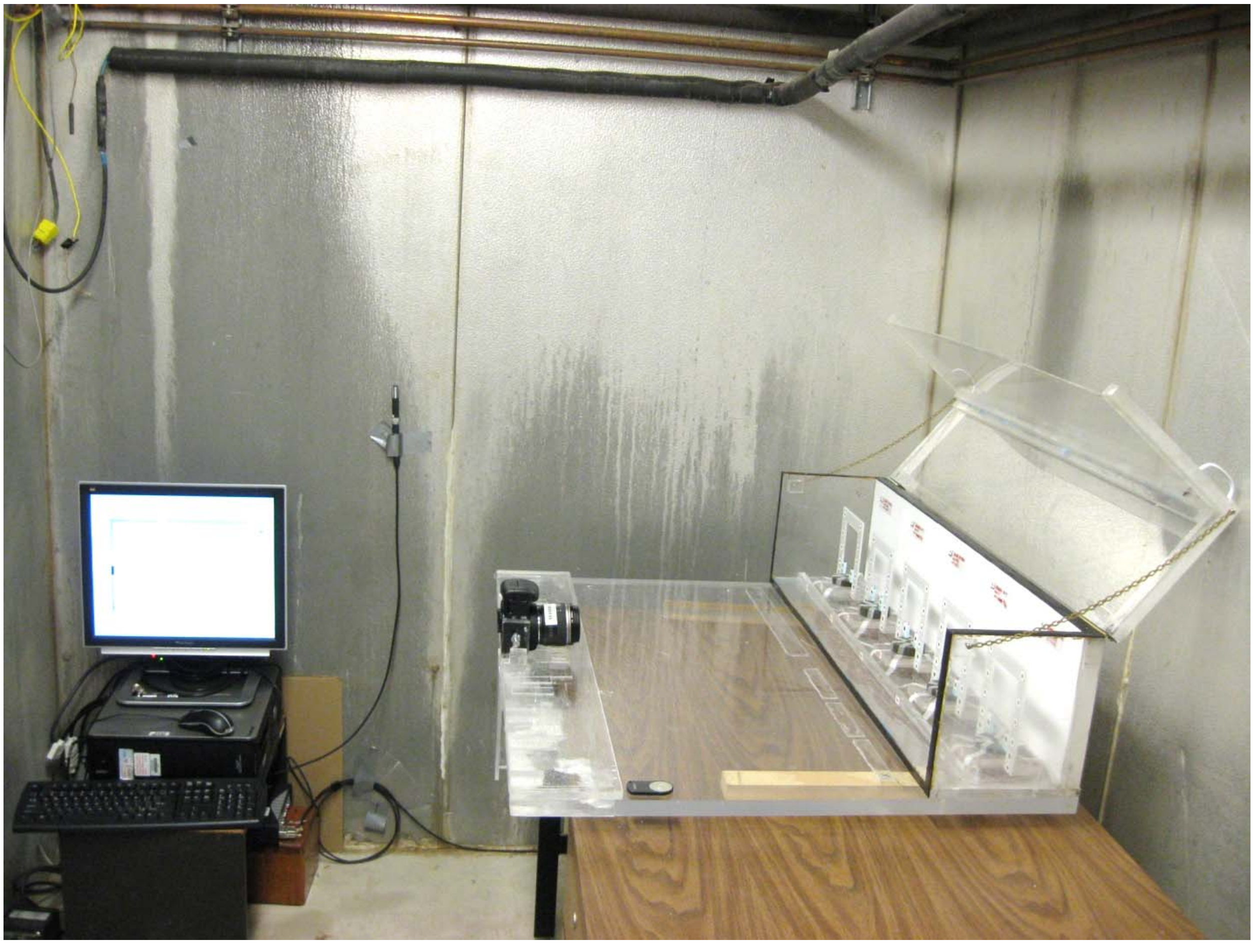

General set-up of unconfined swelling test in laboratory.

Relative humidity measuring probe (Rotronic HygroClip HC2-S) used in unconfined swelling test.

Cutting and measuring tools used in unconfined swelling test.

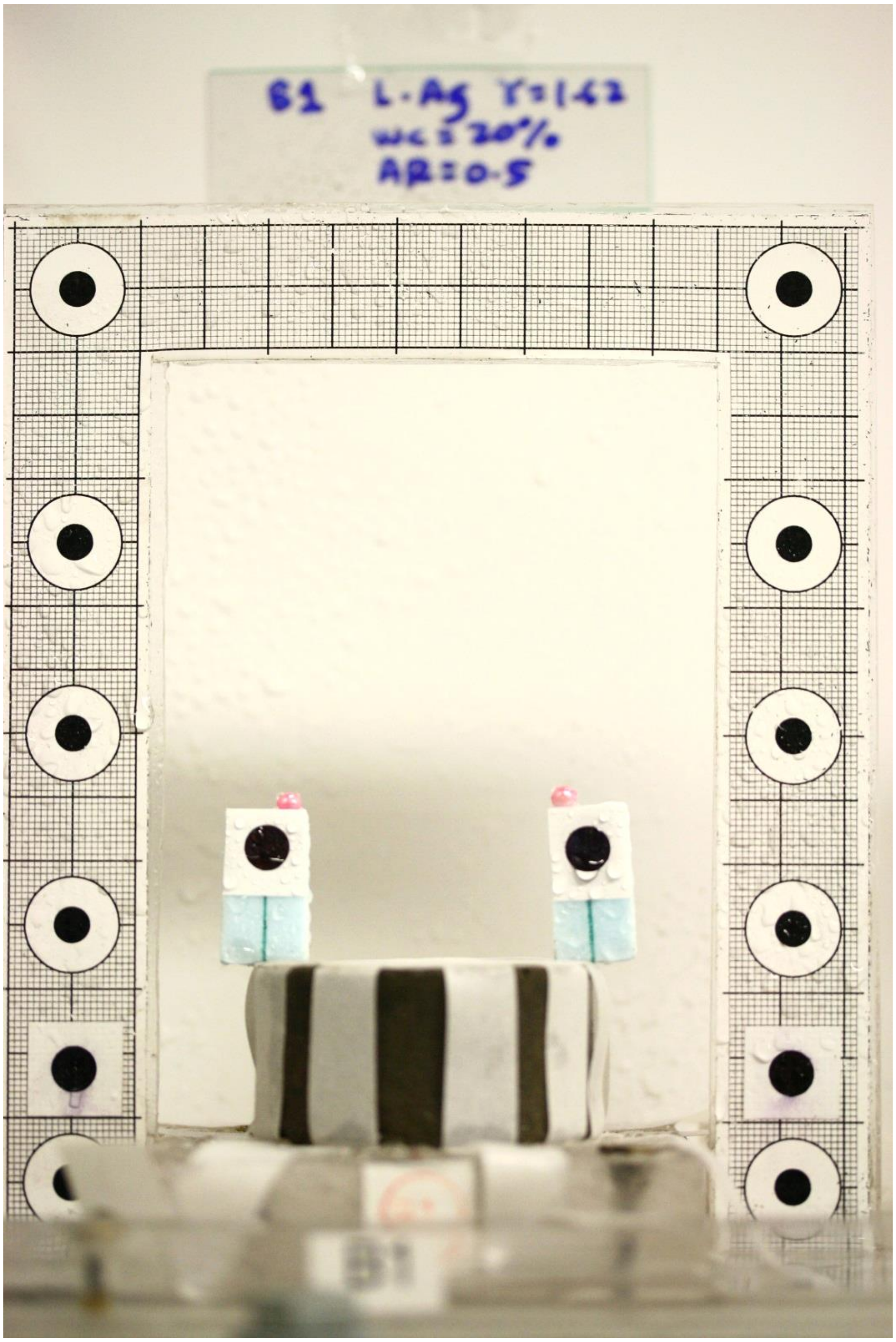

Installation of unconfined swelling test specimen and image markers.

APPENDIX G - MEASURING INSTRUMENTS CALIBRATION SHEET

Project :	Calibration of SEL Triaxial Cell #1 - load cell	
Date created:	19-Jan-11	
by:	blim	
Model:	Futek LCF 450	
S/N:	227779	
Cap:	100,000	lb
Frame :	4.6 kg	
Lever arm ratio :	1:10	
Note:	tightened with donut	

Weight loaded (kg)	Accum. Weight (kg)	Celco reading -	Celco (kg)	Δ (kg)	Calibration
0	0	-2	-2.9	-2.9	
4.6	4.6	-4	1.76	-2.84	
5.6117	10.2117	-5	11.08	0.8683	y=-4.4497x - 11.07
10.0075	20.2192	-7	20.4	0.1808	
9.0673	29.2865	-9	29.72	0.4335	
9.0682	38.3547	-11	34.38	-3.9747	
90.766	129.1207	-30	127.58	-1.5407	
90.746	219.8667	-50	216.12	-3.7467	
100.197	320.0637	-71	318.64	-1.4237	
90.716	410.7797	-91	411.84	1.0603	
90.74	501.5197	-110	500.38	-1.1397	y=-4.66x - 11.61
100.235	601.7547	-132	602.9	1.1453	
90.783	692.5377	-151	691.44	-1.0977	
90.772	783.3097	-171	784.6	1.2903	
90.774	874.0837	-190	873.2	-0.8837	

load < 100kg => y= -4.4497x - 11.07
load > 100kg => y= -4.66x - 11.61

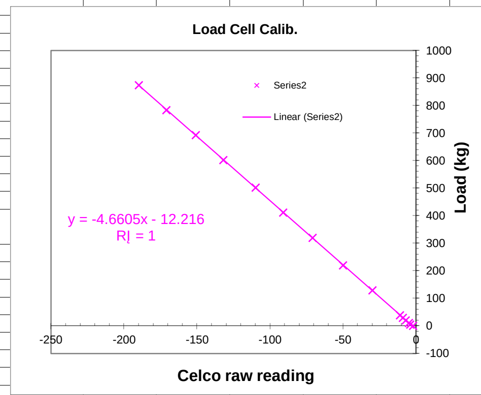

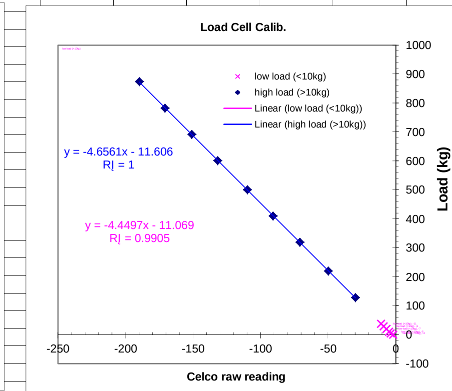

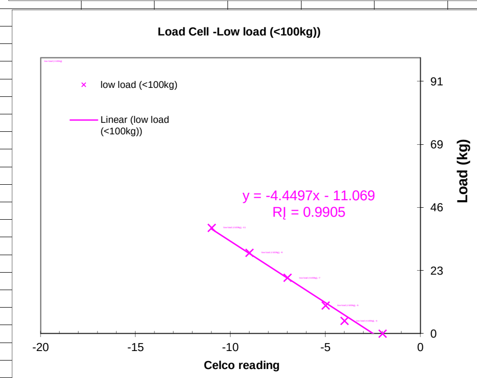

Project :	Calibration of SEL Triaxial Cell #1 - Cell Pressure
Date created:	21/01/2011
by:	blim
Model:	PX 319-3kGI
S/N:	12206 D099
Pressure range:	0-3000 psi

load	
Calibrator	Celco raw reading
kPa	-
30.7	-29772
119.4	-29520
240.6	-29172
407.6	-28699
521.6	-28382
745.8	-27745
800.8	-27590

unload	
Calibrator	Celco raw reading
kPa	-
788.9	-27623
657.2	-27995
497.7	-28445
318.5	-28950
81	-29630
27.9	-29779
8.3	-29838
0	-29860

Calibrator	Celco (measured)	Δ
kPa	kPa	kPa
136.4	134.6	-1.8
380.6	378.4	-2.2
625	624.8	-0.2
790.6	788.9	-1.7

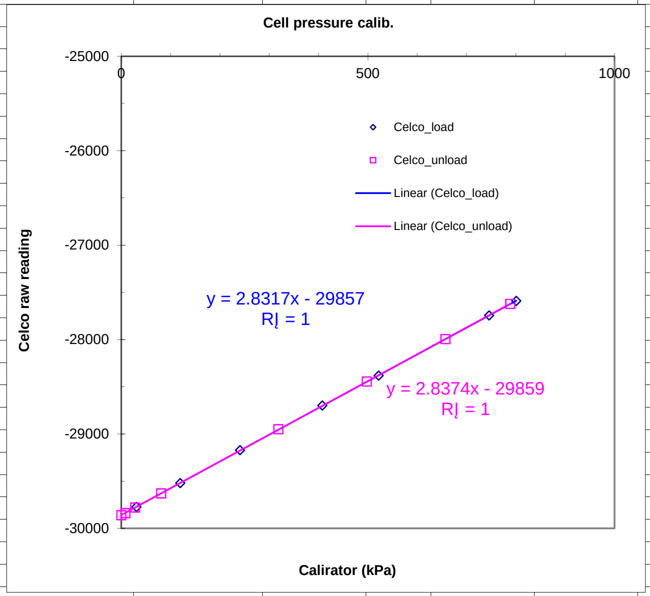

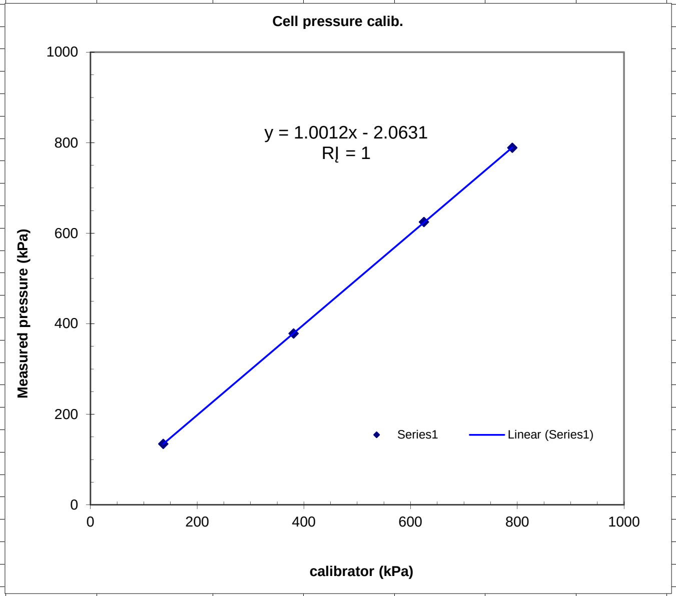

Project :	Calibration of SEL Triaxial Cell #1 - Back Pressure
Date created:	21/01/2011
by:	blim
Model:	PX 319-300GI
S/N:	121806D365
Pressure range:	0-300 psi

Load		unload	
Calibrator reading	Celco raw reading	Calibrator reading	Celco raw reading
kPa	-	kPa	-
0.4	-28967	734.7	-7958
51.3	-27509	692.1	-9164
100.1	-26096	510.3	-14348
193.6	-23421	348.9	-18971
359.2	-18688	180.9	-23767
527.4	-13872	102.3	-26005
635.8	-10782	69.4	-26960
729.3	-8111	34.7	-27964
		18.6	-28427
		0.6	-28963
		0.3	-28964

Calibrated reading

Calibrator reading	calibrated reading	Δ.
kPa	kPa	kPa
0.30	-0.31	-0.61
120.60	120.4	-0.20
267.50	267.8	0.30
451.70	451.9	0.20
573.60	573.3	-0.30
720.50	719.6	-0.90

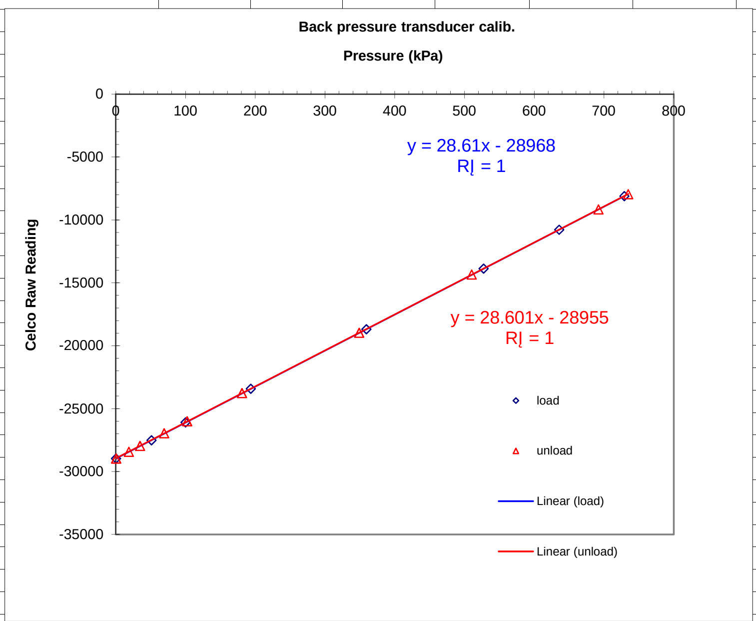

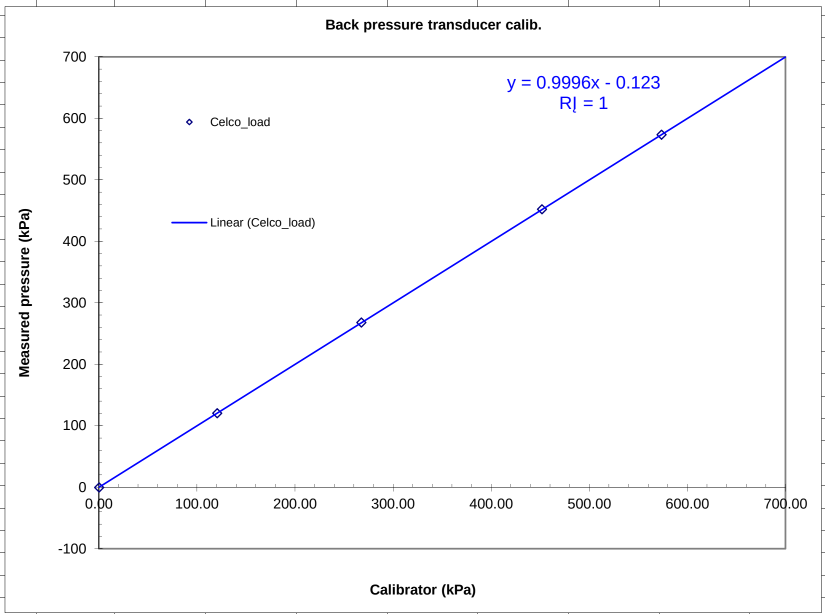

Project :	Calibration of SEL Triaxial Cell#1 Axial LVDT (axial)
Date created:	06-Jul-11
By:	blim
Note:	after LVDT soaked in water while cleaning
	Check LVDT reading with vernier calibrator

Vernier Calibrator

Disp (in)	Disp (mm)	Celco reading (mm)	Corrected Celco reading (mm)	Δ (Celco-Disp) (mm)	% of difference (Δ / Vernier Disp)	Celco raw reading -
0	0.0000	0.4502	0	0.0000	#DIV/0!	-25937
1/40	0.6350	1.0893	0.6391	0.0041	0.65%	-24878
1/20	1.2700	1.7248	1.2746	0.0046	0.36%	-23826
3/40	1.9050	2.3602	1.91	0.0050	0.26%	-22772
1/10	2.5400	2.9969	2.5467	0.0067	0.26%	-21717
1/5	5.0800	5.543	5.0928	0.0128	0.25%	-17498
3/10	7.6200	8.0933	7.6431	0.0231	0.30%	-13273
2/5	10.1600	10.6654	10.2152	0.0552	0.54%	-9011
3/5	15.2400	15.7497	15.2995	0.0595	0.39%	-585
4/5	20.3200	20.749	20.2988	-0.0212	-0.10%	7699
9/10	22.8600	23.2275	22.7773	-0.0827	-0.36%	11806
37/40	23.4950	23.837	23.3868	-0.1082	-0.46%	12817
19/20	24.1300	24.4399	23.9897	-0.1403	-0.58%	13815
39/40	24.7650	25.50307	25.05287	0.2879	1.16%	14795
1	25.4000	25.6052	25.155	-0.2450	-0.96%	15747

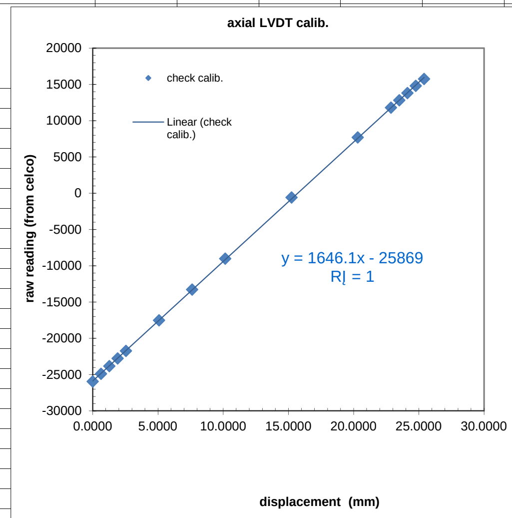

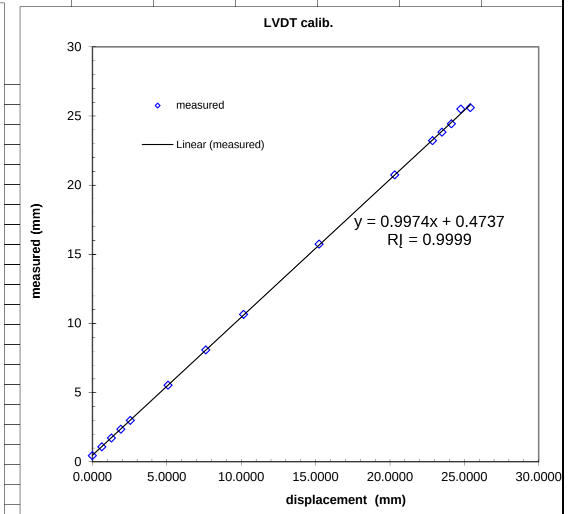

Project :		Calibration of SEL Triaxial Cell #1 Radial LVDT (r_A)			
Date created:		18/1/2011			
by:		blim			
			horizontal		
	calib. block		load1		
	in	mm	raw		
	0	0	-26585	0.0254	mm
	0.05	1.27	-17379		
	0.10	2.54	-8451		
	0.15	3.81	4		
linear until this point	0.20	5.08	7562		
	0.21	5.36	8886		
	0.225	5.72	10679		
	0.237	6.02	11840		
	0.25	6.35	13179		

		horizontal		
Block		Celco	Δ (mm)	
(in)	(mm)	(mm)		
0	0.00	-0.0151	0.0151	0.30%
0.05	1.27	1.3769	-0.1069	-2.10%
0.1	2.54	2.7164	-0.1764	-3.47%
0.2	5.08	5.0869	-0.0069	-0.14%

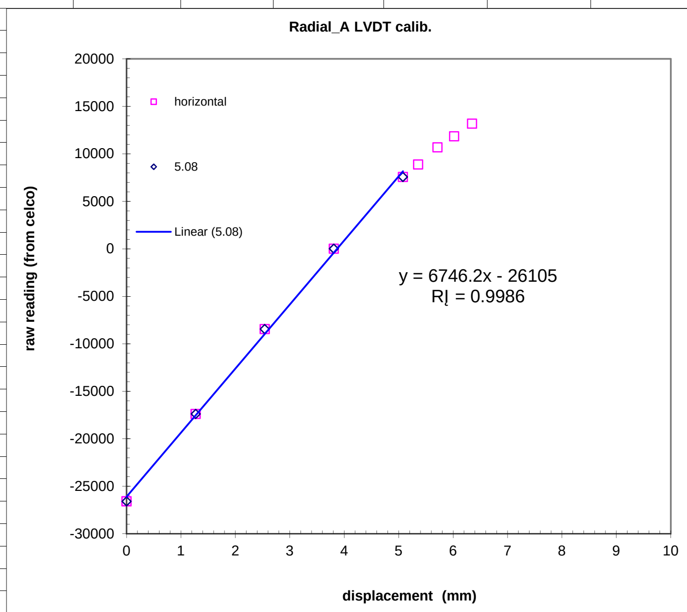

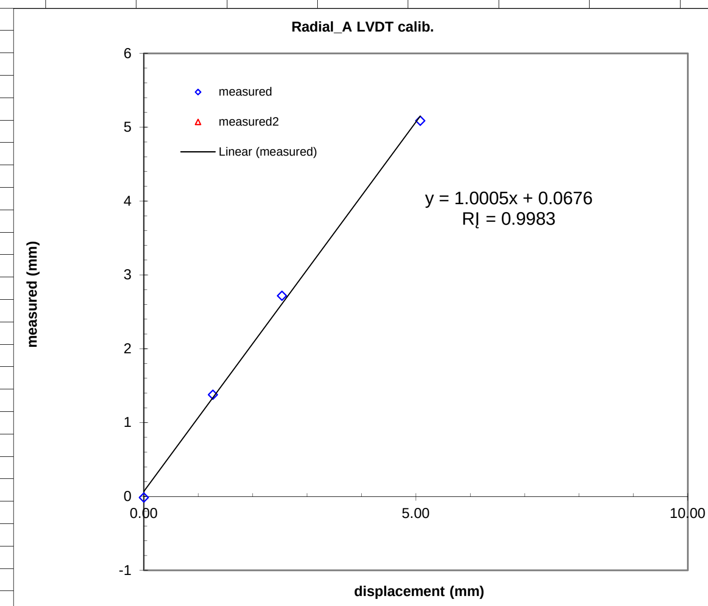

E:\RMC\P2_SEL Testing prep\SEL_cali\Cell#1_cali.xls
r_A

Project :		Calibration of SEL Triaxial Cell #1 Radial LVDT (r_B)								
Date created:		18/1/2011								
by:		blim								
	calib. block					Block		Celco	Δ (mm)	
	in	mm	raw			(in)	(mm)	(mm)		
	0	0	-26572	0.0254	mm	0	0.00	0	0	0.00%
	0.05	1.27	-18024			0.05	1.27	1.3206	-0.0506	-1.00%
	0.10	2.54	-9272			0.1	2.54	2.634	-0.094	-1.85%
	0.15	3.81	-1028			0.2	5.08	5.0561	0.0239	0.47%
	0.20	5.08	6569							
	0.21	5.36	8399							
	0.225	5.72	9979							
	0.237	6.02	10978							
	0.25	6.35	12166							

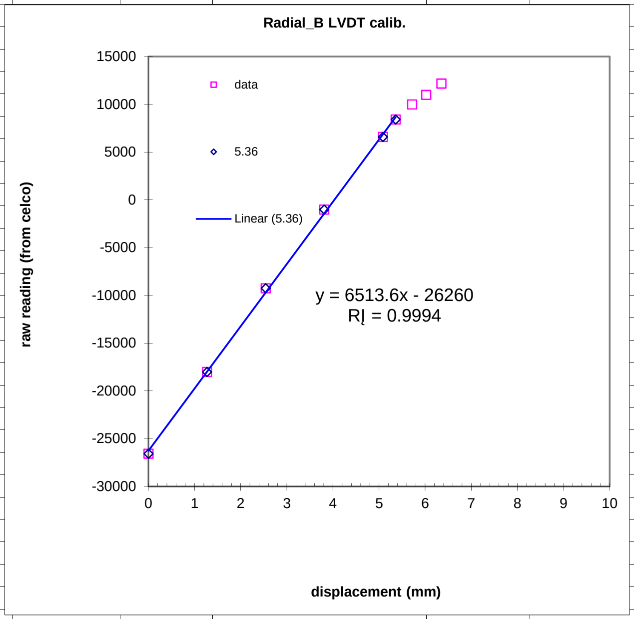

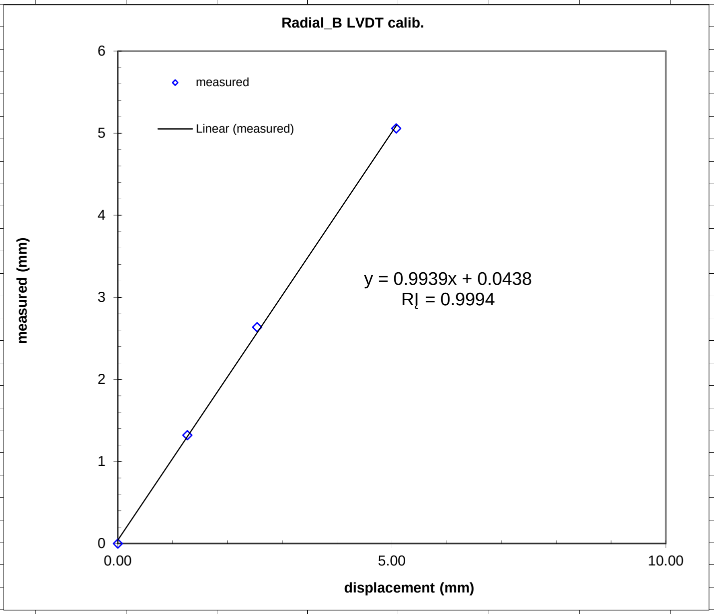

Project :		Calibration of SEL Triaxial Radial Cell #1 LVDT (r_C)									
Date created:		17/1/2011									
by:		blim									
	calib. block						Block		Celco	Δ (mm)	refer to 5.08mm
	in	mm	raw			(in)	(mm)		(mm)		
	0	0	-26916	0.0254	mm	0	0.00		0.0233	-0.0233	-0.46%
	0.05	1.27	-18018			0.05	1.27		1.3287	-0.0587	-1.16%
	0.10	2.54	-8859			0.1	2.54		2.6212	-0.0812	-1.60%
	0.15	3.81	246			0.2	5.08		5.1544	-0.0744	-1.46%
	0.20	5.08	8898								
	0.21	5.36	10593								
	0.225	5.72	12568								
	0.237	6.02	14078								
	0.25	6.35	15518								

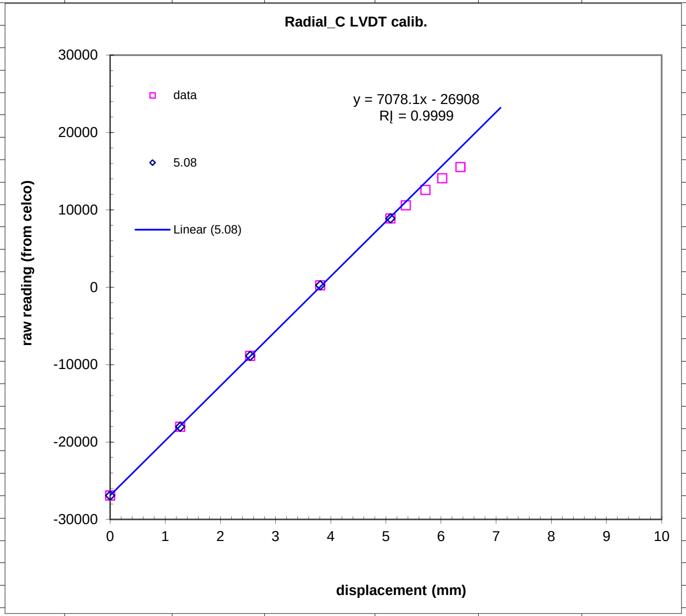

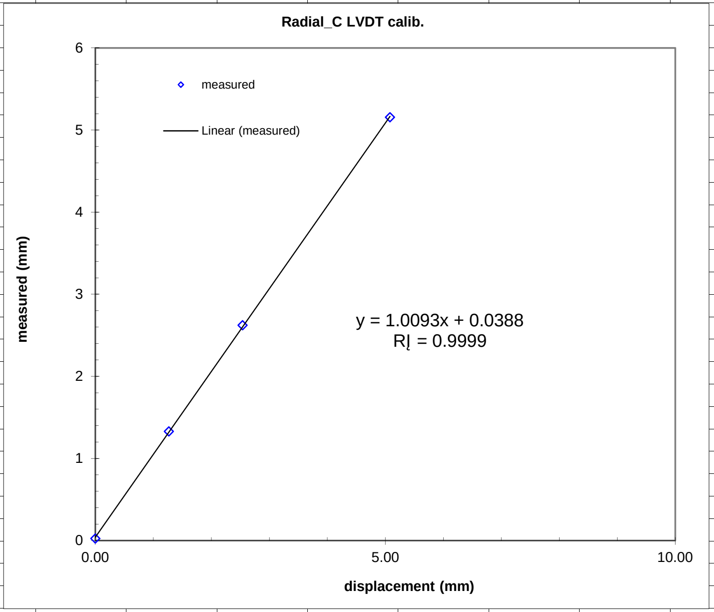

Project :		Calibration of SEL Triaxial Cell #1 Radial LVDT (r_D)								
Date created:		17/1/2011								
by:		blim								
	calib. block			0.5% of working range		Block		Celco	Δ (mm)	
	in	mm	raw			(in)	(mm)	(mm)		
	0	0	-27068	0.0254	mm	0	0.00		0	0.00%
	0.05	1.27	-18303			0.05	1.27		1.27	25.00%
	0.10	2.54	-9485			0.1	2.54		2.54	50.00%
	0.15	3.81	-1101			0.2	5.08		5.08	100.00%
	0.20	5.08	6599							
	0.21	5.36	8070							
	0.225	5.72	9809							
	0.237	6.02	11157							
	0.25	6.35	12435							

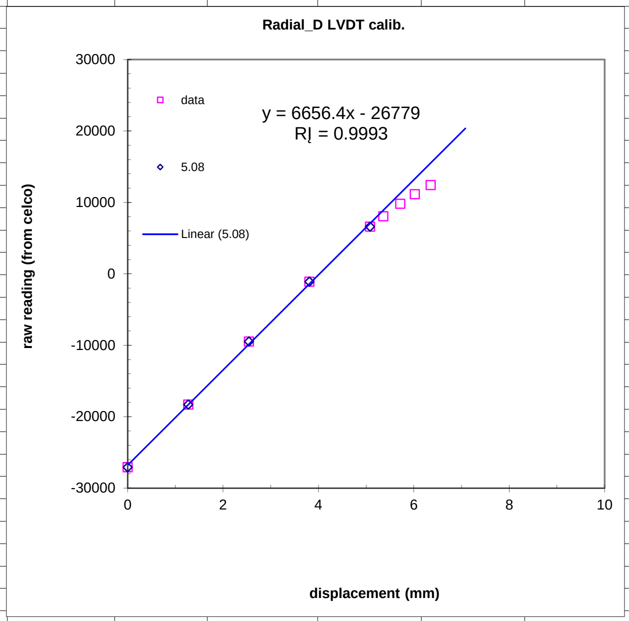

Cell #2

Project :	Calibration of SEL Triaxial - submersible load cell				
by:	blim				
Date:	13-Jul-11				
Load cell Cell #2 calibrated using direct shear laod frame after re-wired. Wire at Conax was broken.					
Direct shear load frame:	HW-25403	Max load :	10kN	(100kg)	
Frame :	4.6	kg			
Load cell model:	LCF450 (L2900)				
S/N:	227778				
Pressure range:	10,000 lbs	(4,535kg)			
Note:	Load cell is attached with load cell adaptor (donut).				
Scaling factor :	4.6	Offset:	-2.563		

	Weight Added (kg)	Accumulated load (kg)	Celco raw reading	Celco (kg)		Δ difference (%)	Note
loading	0	0.000	-1	-7.163	7.163	#DIV/0!	
	4.6	4.600	-2	-11.763	11.763	155.72%	
	5.6329	10.233	-4	-16.363	16.363	59.91%	
	4.9998	15.233	-5	-25.563	25.563	67.82%	
	11.2516	26.484	-7	-34.763	34.763	31.26%	Frame only
	2.814	32.740	-8	-39.363	39.363	20.23%	with lever arm 1:10 ratio
	5.6329	89.069	-20	-94.563	94.563	6.17%	
	4.9998	139.067	-31	-145.16	145.16	4.38%	
	9.0716	229.783	-51	-237.16	237.16	3.21%	
	11.2425	342.208	-75	-347.56	347.56	1.56%	
	22.5351	567.559	-124	-572.96	572.96	0.95%	
	22.4471	792.030	-172	-793.76	793.76	0.22%	
	16.8778	960.808	-208	-959.36	959.36	-0.15%	
unloading	16.8778	792.030	-172	-793.76	793.76	0.22%	with lever arm 1:10 ratio
	22.4471	567.559	-124	-572.96	572.96	0.95%	
	22.5351	342.208	-75	-347.56	347.56	1.56%	
	11.2425	229.783	-51	-237.16	237.16	3.21%	
	9.0716	139.067	-31	-145.16	145.16	4.38%	
	4.9998	89.069	-20	-94.563	94.563	6.17%	
	5.6329	32.740	-8	-43.963	43.963	34.28%	
	2.814	4.600	-2	-11.763	11.763	155.72%	Frame only
	-4.6	0.000	-1	-7.163	7.163	###########	

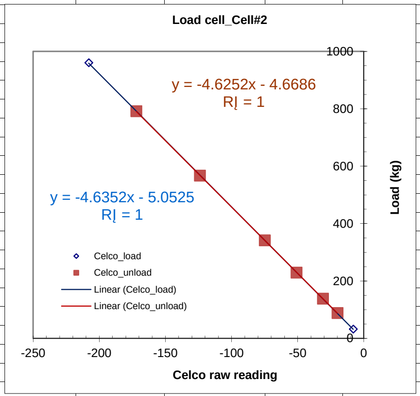

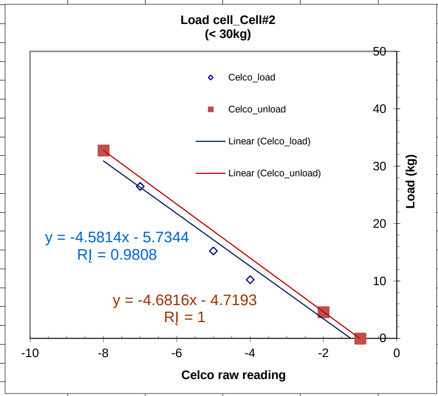

Higher range (>30kg)

	m	C	y=mx +C
loading	-4.6352	-5.0525	
unloading	-4.6252	-4.6686	
	-4.6302	-4.86055	

Lower range: < 30kg

	m	C	y=mx +C
loading	-4.5814	-5.7344	
unloading	-4.6816	-4.7193	
	-4.6315	-5.22685	

Project :	Calibration of SEL Triaxial - Cell Pressure					
by:	blim					
Model:	PX 319-3kGI					
S/N:	122 206 D368					
Pressure range:	0-3000 psi					
Date:	13-May-11					

Cell pressure Cell #2 calibrated using pressure calibrator after re-wired with longer cables.

loading			Unloading		
	Check1			Check2	
Calibrator	Celco readin	Δ	Calibrator	Celco readin	Δ
kPa	kPa	kPa	kPa	kPa	
0.300	-10.091		903.6	891	-12.6
62.600	51.76	10.840	790.7	780	-10.7
170.300	160.809	9.491	619.6	607	-12.6
329.900	318.13	11.770	463.4	454	-9.4
514.000	504.71	9.290	320.4	310	-10.4
767.100	755.6	11.500	162.2	152	-10.2
			87.9	77	-10.9
			49.5	39	-10.5
			13.7	2.8	-10.9
			0.0	-10.5	-10.5

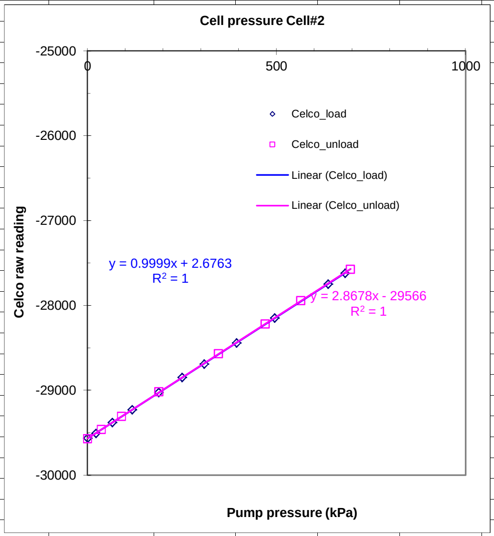

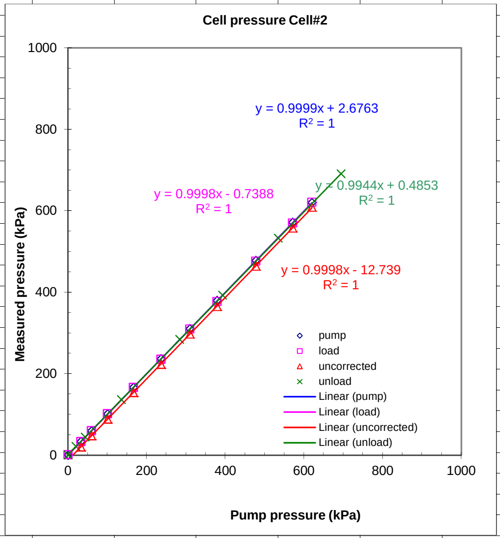

Project :	Calibration of SEL Triaxial - Back Pressure
by:	blim
Model:	PX 319-300GI
S/N:	121 806 D392
Pressure range:	0-300 psi
Date:	13-May-11

Back pressure calibrated using pressure calibrator after re-wired with longer cables.

loading			Unloading		
	Check1			Check2	
Calibrator	Celco readi	Δ	Calibrator	Celco readin	Δ
kPa	kPa	kPa	kPa	kPa	
116.000	116.1		894.8	894.9	0.1
383.700	384.1	-0.400	736.8	736.7	-0.1
659.700	659.9	-0.200	572.3	572.6	0.3
790.600	790.7	-0.100	400.4	400.8	0.4
			204.5	204.8	0.3
			93.4	93.6	0.2
			52.1	52	0.2
			6.0	6.11	0.1

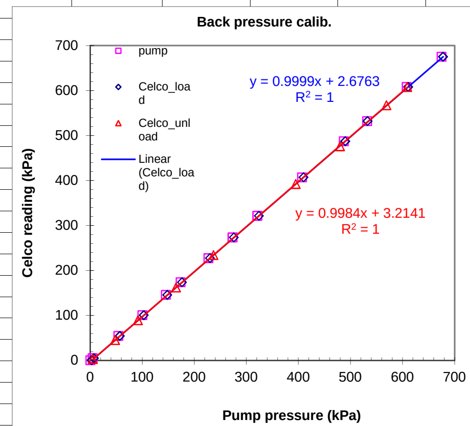

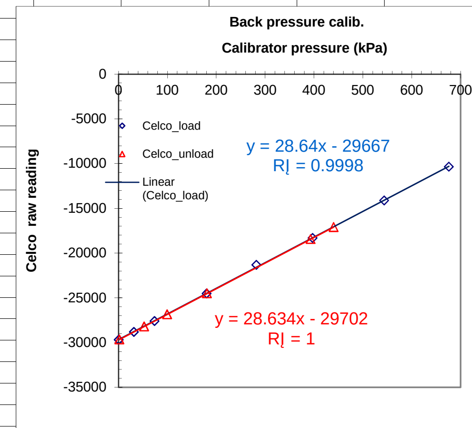

Project :	Calibration of SEL Triaxial Axial LVDT (axial)				
by:	blim				
Axial LVDT					
Model :	0244-0014				
S/N:					
Working range:	+/- 25.4	mm			
Date:	13-May-11				

LVDT axial calibrated using vernier calibrator after re-wired with longer cables.

		Check1		Check2	
Disp (vernier)		Celco reading	Δ	Celco reading	Δ
inch	mm	mm	mm	mm	mm
0	0.000				
1/10	2.540	2.05093	0.489	2.5049	-0.035
1/5	5.080	5.5048	-0.425	5.0529	-0.027
1/2	12.700	12.7492	-0.049	12.751	0.051
7/10	17.780	17.8326	-0.053		
4/5	20.320	20.3731	-0.053		
1	25.4	25.3792	0.021		
1.5/10	3.81			3.7752	-0.035
3/10	7.62			7.6239	0.004

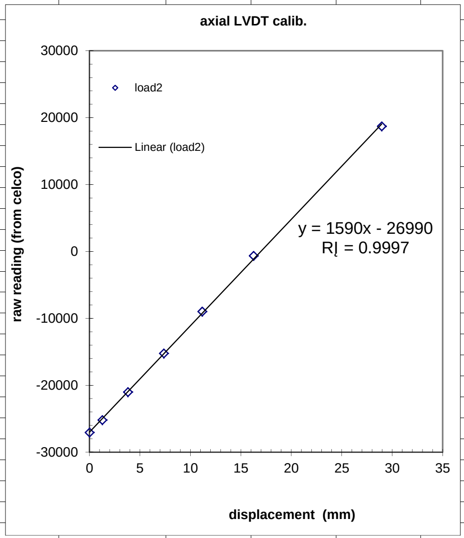

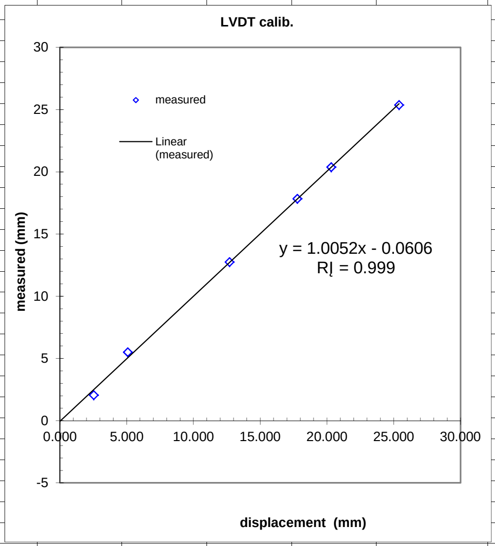

Project :	Calibration of SEL Triaxial Radial LVDT (r_1)
by:	blim
Radial LVDT	
Model :	0241-0007
S/N:	
Working range:	+/- 2.54 mm
Date:	12-May-11

Radial_1 calibrated using vernier calibrator after re-wired with longer cables.

Celco reading		Disp (vernier)	
Volt	mm	inch	mm
-25333	0.24	0	0.000
-20502	0.9079	1/40	0.635
-15733	1.5674	1/20	1.270
-6352	2.8645	1/10	2.540
2929	4.1479	3/20	3.810
7394	4.7653	7/40	4.445
11410	5.3206	1/5	5.080
14774	5.7856	9/40	5.715
7370	4.7621	7/40	4.445
-1731	3.5036	1/8	3.175
-11081	2.2108	3/40	1.905
-20553	0.9009	1/40	0.635

		Check1		Check2	
Disp (vernier)		Celco reading	Δ	Celco read	Δ
inch	mm	mm	mm	mm	mm
0	0.000				
1/40	0.635	0.6612	-0.026	0.6192	-0.016
1/20					
3/40	1.905	1.9411	-0.036	1.9171	0.012
1/8	3.175	3.2045	-0.030	3.1905	0.016
1/5	5.080	5.011	0.069	5.0197	-0.060

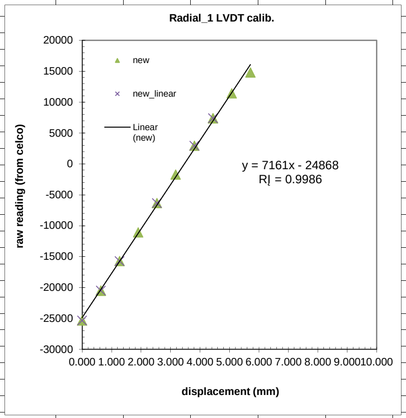

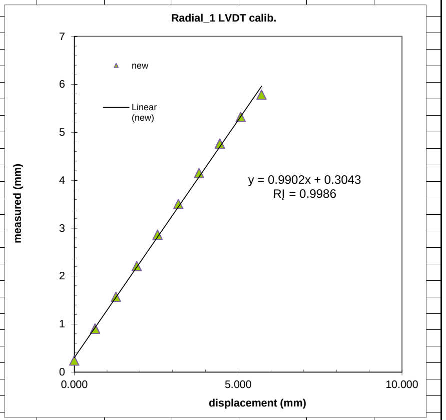

Project :	Calibration of SEL Triaxial Radial LVDT (r_2)					
by:	blim					
Radial LVDT						
Model :	0241-0007					
S/N:						
Working range:	+/- 2.54	mm				
Date:	13-May-11					
Radial_2 calibrated using vernier calibrator after re-wired with longer cables.						

		Check1		Check2	
Disp (vernier)		Celco reading	Δ	Celco reading	Δ
inch	mm	mm	mm	mm	mm
0	0.000				
1/40	0.635	0.6758	-0.041	0.5826	-0.052
3/40	1.905	1.9851	-0.080	1.924	0.019
1/8	3.175	3.2511	-0.076	3.2156	0.041
7/40	4.445			4.4265	-0.018
1/5	5.080	5.0102	0.070		

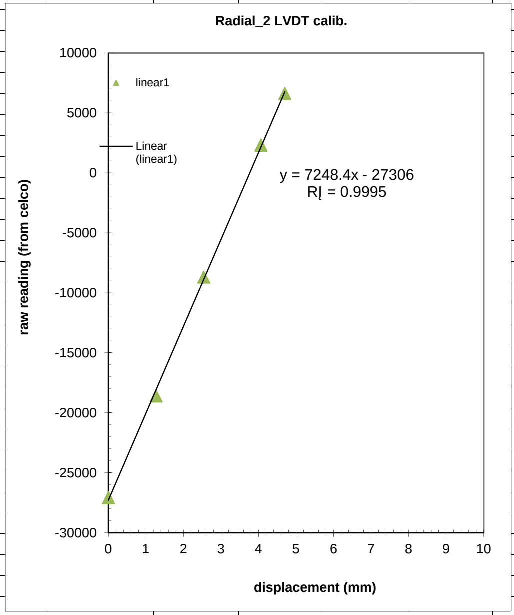

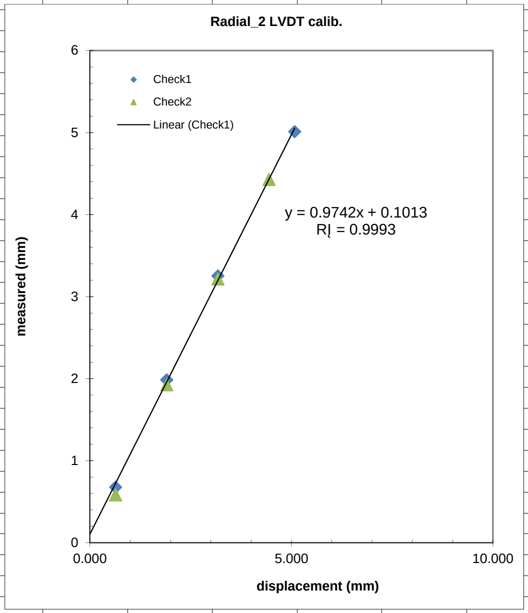

Project :	Calibration of SEL Triaxial Radial LVDT (r_3)				
by:	blim				
Radial LVDT					
Model :	0241-0007				
S/N:					
Working range:	+/- 2.54	mm			
Date:	13-May-11				
Radial_3 calibrated using vernier calibrator after re-wired with longer cables.					

		Check1			
Disp (vernier)		Celco readin	Δ		
inch	mm	mm	mm		
0	0.000				
1/40	0.635	0.6477	-0.013		
3/40	1.905	1.9429	-0.038		
1/8	3.175	3.2044	-0.029		
7/40	4.445	4.439	0.006		
1/5	5.080				

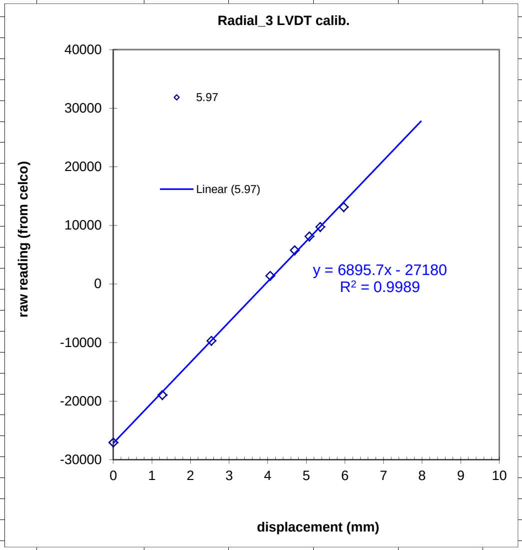

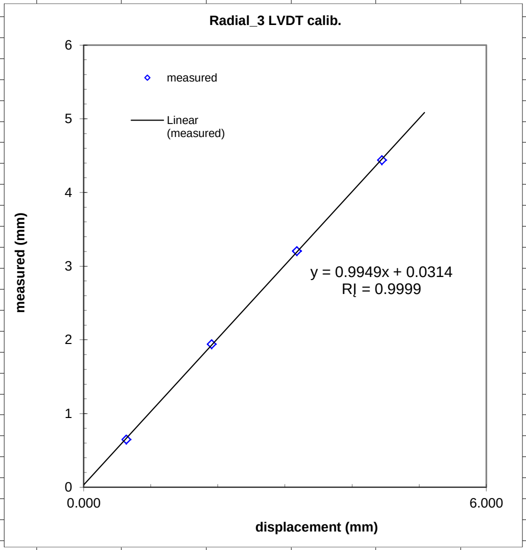

Project :	Calibration of SEL Triaxial Radial LVDT (r_4)	
by:	blim	
Radial LVDT		
Model :	0241-0007	
S/N:		
Working range:	+/- 2.54	mm
Date:	13-May-11	

Radial_4 calibrated using vernier calibrator after re-wired with longer cables.

Disp (vernier)		Check1		Check2	
		Celco readin	Δ	Celco reading	Δ
inch	mm	mm	mm	mm	mm
0	0.000				
1/40	0.635	0.4423	0.193	0.6522	-0.017
3/40	1.905	1.7945	0.111	1.9297	-0.025
1/8	3.175	3.1219	0.053	3.1971	-0.022
7/40	4.445	4.4444	0.001	4.4444	0.001
1/5	5.080	5.0727	0.007	5.014	0.066

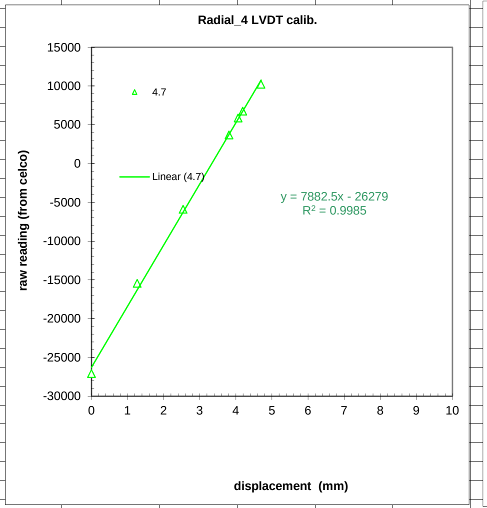

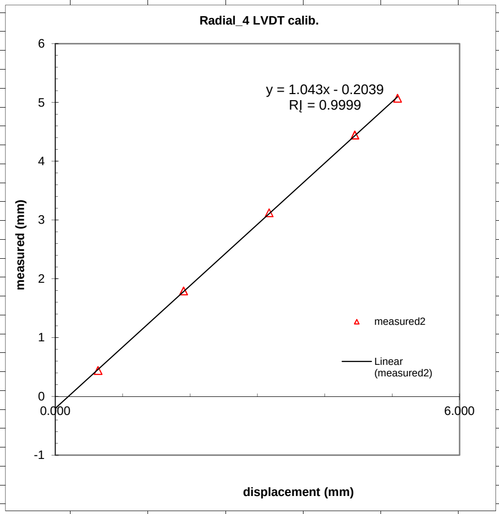

Project:	Volume Change Device used in SEL Cells	Date:	14-Jun-10
Subject:	Sensitivity of voltage reading for I.C. Volume Change Device		
By:	blim		

Device name		Linear Displacement Sensor				Capacity of volume change	50 cc (=ml)
Model		LDS 25					
Serial		11201	11203				
Used in		Cell#1	Cell#2				
Supplier		Hoskin (Jon Matheson)					

		LDS25 (S/N: 11201)			LDS25 (S/N: 11203)	
Max Disp (mm)		25.64	mm		25.71	mm
Non-linearity		0.06	% Full Scale		0.04	% Full Scale
Excitation volts		10	V		10	V
Volts sensitivity		7.58	mV/V		7.57	mV/V
Full scale		0.07580	V		0.07570	V
Volume Change Sensitivity (Δml)	factor	Change in voltage (ΔV)	Change in Disp (Δmm)		Change in voltage (ΔV)	Change in Disp (Δmm)
0.01	5000	0.0000152	0.005128		0.0000151	0.005142
0.05	1000	0.0000758	0.02564		0.0000757	0.02571
0.1	500	0.0001516	0.05128		0.0001514	0.05142
0.15	333.3333	0.0002274	0.07692		0.0002271	0.07713
0.2	250	0.0003032	0.10256		0.0003028	0.10284
0.5	100	0.0007580	0.2564		0.0007570	0.2571
1	50	0.0015160	0.5128		0.0015140	0.5142

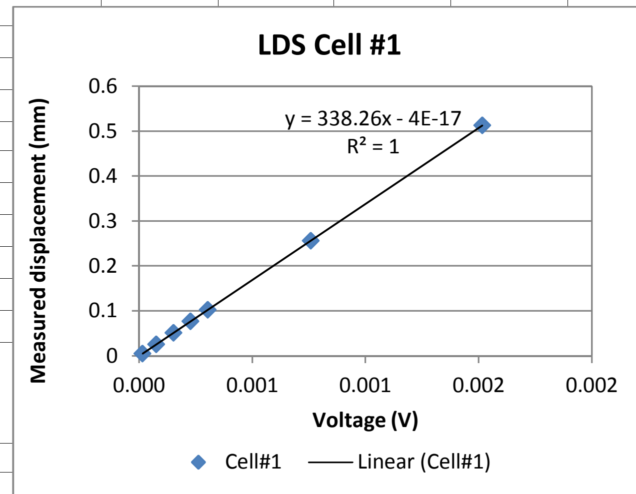

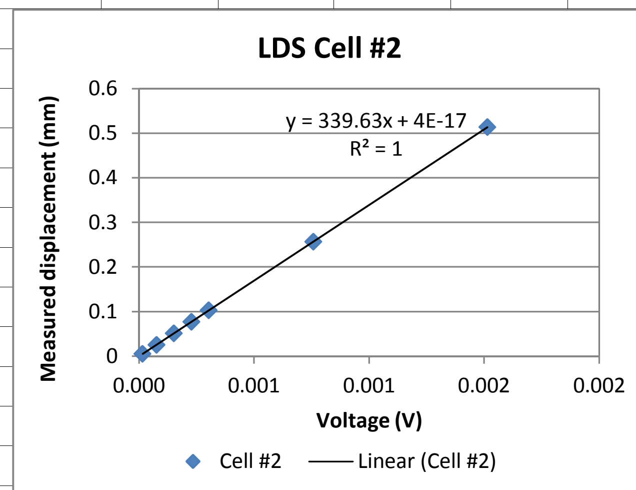

Project:	SEL Tests	Date:	30/11/2011
Subject:	Calibration RH probe (SN:60597340)		
By:	blim		

	Rotronic
Probe	RH2
Model Type	HC2-S
Serial Number	60597340
Software	MF

y=mx + C	From plots :	
	m	C
wetting	101.7	-0.3859
wetting_II	101.55	-0.0065
drying	101.95	-1.2353
average	101.7333333	-0.542566667

Wetting

Date & Time	RH solution	Temp (thermometer)	RH measured (04 Nov '11)	RH measured (30 Nov '11)	Note
	%	oC	V	V	
04/11/2011 9:41	11	22.8	0.1155	0.11306	
04/11/2011 14:03	33	-	0.3272	0.3230	
07/11/2011 9:57	59	-	0.5799	0.5749	
07/11/2011 15:42	85	-	0.8351	0.8350	
	98	-		0.9706	not tested
08/11/2011 10:56	100	-	0.9932		

Drying

Date	RH solution	Temp (thermometer)	RH measured	Note
	%	oC	V	
	100			
08/11/2011 15:59	98	-	0.9743	
09/11/2011 10:42	85	-	0.8421	
09/11/2011 15:48	59	-	0.5943	
10/11/2011 9:15	33	-	0.3374	
10/11/2011 16:13	11	-	0.1179	

Voltage	RH
0.00	-0.542566667
0.20	19.8041
0.40	40.15076667
0.60	60.49743333
0.80	80.8441
1.00	101.1907667

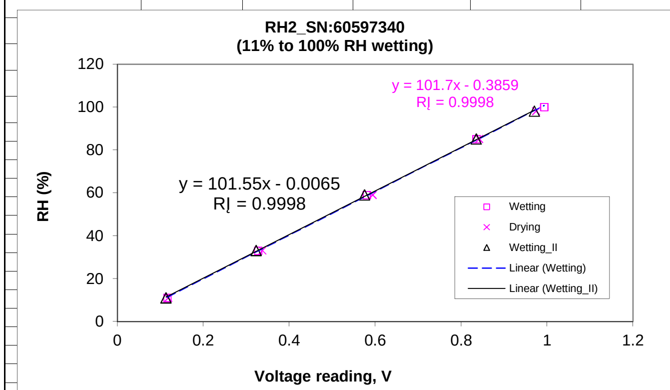

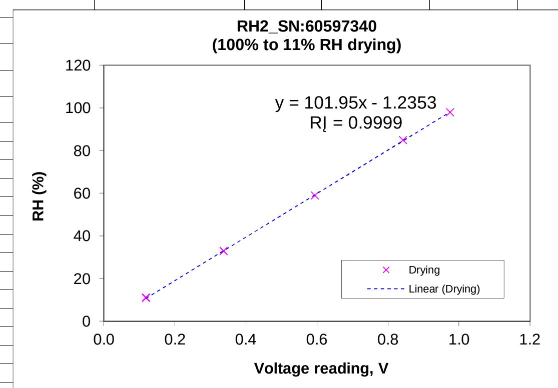

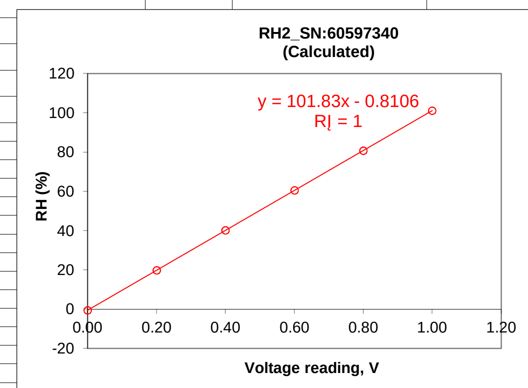

APPENDIX H - LABORATORY RECORD FOR ATTERBERG LIMITS, MODIFIED PROCTOR AND GRAIN SIZE DISTRIBUTION

Project:	Lake Agassiz (Winnipeg) Clay_Modified Proctor	Date:	05/02/2013
Title:	OMC for L.Ag Clay		
by:	blim		

Moisture Content Determination

		1		2		3		4		5	
Specimen ID				L. Agassiz (Winnipeg) Clay							
Date put in oven				07-Feb-13							
Date take out from oven				08-Feb-13							
Oven temperature	oC			105							
Tare ID	-			12	6	25	100	14	61	18	75
Tare mass	g			4.67	8.07	8.11	8.23	4.75	7.89	7.95	4.72
Tare + Moist soil	g			33.35	36.21	25.51	21.11	18.13	25.84	30.18	35.02
Tare + Dry soil	g			25.35	28.34	23.42	19.34	16.03	22.6	25.11	28.36
Moisture content (m.c.)	%	#DIV/0!	#DIV/0!	38.7%	38.8%	13.7%	15.9%	18.6%	22.0%	29.5%	28.2%
Average m.c.	%	20.0		38.8		14.8		20.3		28.9	
Targeted moisture content	%	20		40		15		20		30	

forget to take moisture measurement

Compacted Density Measurement

		1	2	3	4	5
Mold #		5	5	7	7	7
Mold + base	g	4447.7	4449.6	4405.7	4405.5	4405.6
Mold + base + Compacted soil	g	6268.8	5898	6115	6241.6	6228.6
Compacted volume	cm3	944	944	944	944	944
Measured bulk density	Mg/m3	1.9291	1.5343	1.8107	1.9450	1.9311
Measured dry density	Mg/m3	1.6076	1.1058	1.5774	1.6165	1.4986

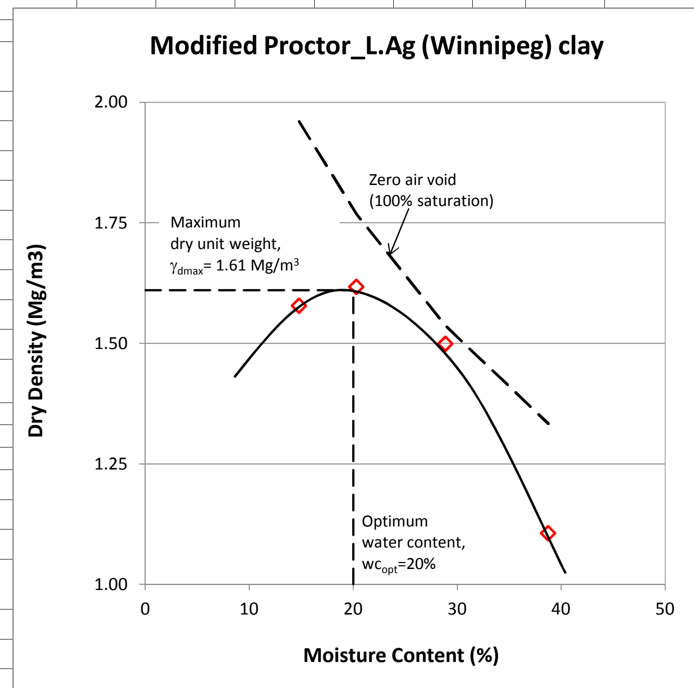

(for plot)

Compacted Moisture Content (%)	Dry Density (Mg/m3)	Zero air void, Sr =1: e	Dry Density (Mg/m3)
38.8	1.106	1.070	1.334
14.8	1.577	0.408	1.960
20.3	1.617	0.561	1.768
28.9	1.499	0.797	1.536

Project:		PhD Research_Bearpaw Shale Swelly Behaviour									
Title:		Modified Proctor Compaction Test on Bearpaw Shale - ID189 (ASTMD1557-09)									
Date:		17-Oct-11									

Moisture Content Determination

		1		2		3		4		5	
Specimen ID		Bearpaw RM06-189		Bearpaw RM06-189		Bearpaw RM06-189		Bearpaw RM06-189		Bearpaw RM06-189	
Date put in oven		14-Oct-11		14-Oct-11		17-Oct-11		17-Oct-11		18-Oct-11	
Date take out from oven		17-Oct-11		17-Oct-11		18-Oct-11		18-Oct-11		19-Oct-11	
Oven temperature	oC	105		105		105		105		105	
Tare ID	-	12	23	57	85	2	19	85	57	12	23
Tare mass	g	4.66	8.11	8.15	8.01	8.53	4.67	8	8.14	4.66	8.11
Tare + Moist soil	g	29.06	32.02	32.29	39.48	31.03	28.62	42.11	40.39	39.53	39.92
Tare + Dry soil	g	24.59	27.43	27.57	33.08	29.73	26.58	37.62	36.18	35.61	36.34
Moisture content (m.c.)	%	22.4%	23.8%	24.3%	25.5%	6.1%	9.3%	15.2%	15.0%	12.7%	12.7%
Average m.c.	%	23.09		24.92		7.72		15.09		12.67	
Targeted moisture content	%	25		30		10		15		12	

Compacted Density Measurement

Mold + base	g	4347.6	4347.6	4346.7	4346.7	4346.9
Mold + base + Compacted soil	g	6231.9	6211.4	6097.7	6241.6	6206.2
Compacted volume	cm3	944	944	944	944	944
Measured bulk density	Mg/m3	1.9961	1.9744	1.8549	2.0073	1.9696
Measured dry density	Mg/m3	1.6216	1.5805	1.7219	1.7442	1.7481

(for plot)

Compacted Moisture Content (%)	Dry Density (Mg/m3)
23.09	1.6216
24.92	1.5805
7.72	1.7219
15.09	1.7442
12.67	1.7481

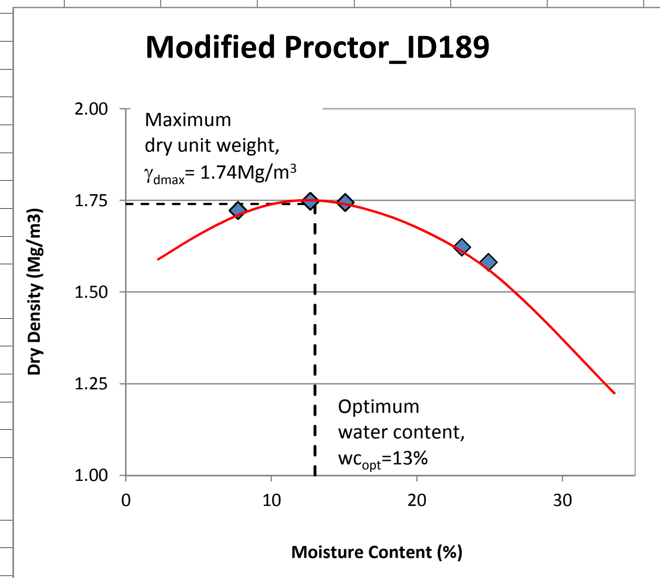

Project:	SEL Triaxial_ Lake Agassiz	Date:	28-May-13
Subject:	Atterberg Limits Measurement		
By:	blim		

Specimen ID :	Lake Agassiz	
Initial density :	1.62	Mg/m3
Initial water content :	20	%

Date put in oven :	27/05/2013 12:30	Oven temperature :	105	oC
Date removed from oven :	28/05/2013 12:30	Oven temperature :	105	oC

Liquid Limit Test

Test No.		1	2	3	4	5	6	7	8
Tare ID		91	78	70	62	15	53	19	68
Tare mass	g	7.97	4.65	8.13	4.72	8.15	7.98	4.68	8.08
Tare + Moist soil	g	13.12	11.38	16.01	13.42	16.28	16.37	13	17
Tare + Dry soil	g	10.96	8.46	12.51	9.46	12.53	12.49	8.91	12.53
Moist soil	g	5.15	6.73	7.88	8.7	8.13	8.39	8.11	8.59
Dry soil	g	2.99	3.81	4.38	4.74	4.38	4.51	4.23	4.45
Water content	%	72.2%	76.6%	79.9%	83.5%	85.6%	86.0%	91.7%	93.0%
Number of blows		113	70		25	21		12	10

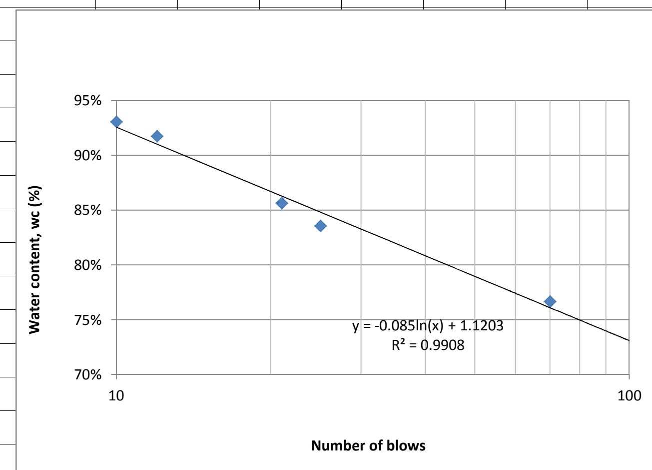

y = -0.085ln(x) + 1.1203

0.846695555

Plastic Limit Test

Test No.		1	2	3
Tare ID		14	Y	Z
Tare mass	g	1.00	1.01	1.01
Tare + Moist soil	g	2.25	2.65	2.5
Tare + Dry soil	g	1.94	2.23	2.13
Moist soil	g	1.25	1.64	1.49
Dry soil	g	0.94	1.22	1.12
Water content	%	33.0%	34.4%	33.0%
Average water content	%		33.7%	

Liquid Limit :	84.7%
Plastic Limit :	33.7%
Plasticity Index :	51.0%
Natural water content:	2.0%
Liquidity Index:	-0.622019

$$PI = LL - PL$$

$$LI = \frac{w_n - PL}{PI}$$

Project:	Bentonite-sand-buffer (BSB)_Greg's thesis material	Date:	06-May-14
Subject:	Atterberg Limits Measurement Casagrande cup		
By:	blim		

Specimen ID :	BSB (50:50 by dry mass)						
Initial density :	-	Mg/m3					
Initial water content :	-	%					
Date put in oven :	05/05/2014 15:30			Oven temperature :	105	oC	
Date removed from oven :	06/05/2014 15:30			Oven temperature :	105	oC	

Liquid Limit Test

Test No.		1	2	3	4	5	6	7	8
Tare ID		93	19	17	39	91	89	24	76
Tare mass	g	8.1	4.7	8.2	8.1	8	8.2	8	8
Tare + Moist soil	g	13.7	15.28	17.24	17.09	17.47	20.05	19	19
Tare + Dry soil	g	9.63	7.5	10.6	10.67	10.64	11.6	11.27	10.85
Moist soil	g	5.6	10.58	9.04	8.99	9.47	11.85	11.39	10.55
Dry soil	g	1.53	2.8	2.4	2.57	2.64	3.4	3.27	2.85
Water content	%	266.0%	277.9%	276.7%	249.8%	258.7%	248.5%	248.3%	270.2%
Number of blows			17	18	60	40	87	51	9

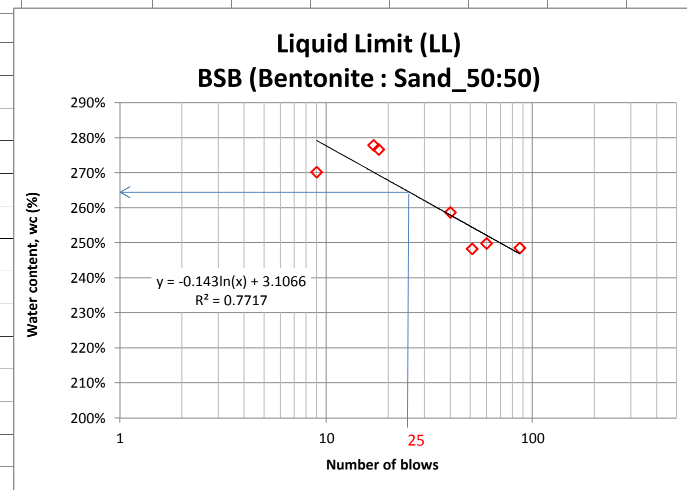

y = -0.143ln(x) + 3.1066

2.646301

Plastic Limit Test

Test No.		1	2	3	4
Tare ID		4	87	88	22
Tare mass	g	8.24	8.03	8.11	7.97
Tare + Moist soil	g	9.68	10.14	10.71	10.83
Tare + Dry soil	g	9.44	9.76	10.18	10.25
Moist soil	g	1.44	2.11	2.6	2.86
Dry soil	g	1.2	1.73	2.07	2.28
Water content	%	20.0%	22.0%	25.6%	25.4%
Average wc (= Plastic Limit)	%	21.0%			

Liquid Limit :	264.6%
Plastic Limit :	21.0%
Plasticity Index :	243.6%
Natural water content:	-
Liquidity Index:	-

$$PI = LL - PL$$

$$LI = \frac{w_n - PL}{PI}$$

Project:	SEL Triaxial_ Bearpaw	Date:	06-Jun-13
Subject:	Atterberg Limits Measurement		
By:	blim		

Specimen ID :	RM06-ID169 recompacted			
Initial density :	1.5 Mg/m3			
Initial water content :	30 %			
Date put in oven :	04/06/2013 12:30	Oven temperature :	105	oC
Date removed from oven :	05/06/2013 12:30	Oven temperature :	105	oC

Liquid Limit Test

Test No.		1	2	3	4	5	6	7	8
Tare ID		78	62	70	15	68	19	91	53
Tare mass	g	4.66	4.72	8.12	8.15	8.08	4.68	7.96	8.08
Tare + Moist soil	g	13.89	13.87	17.72	17.58	17.4	14	18	17
Tare + Dry soil	g	10.5	10.49	13.98	13.79	13.59	10.05	13.58	13.26
Moist soil	g	9.23	9.15	9.6	9.43	9.32	9.15	9.7	9.11
Dry soil	g	5.84	5.77	5.86	5.64	5.51	5.37	5.62	5.18
Water content	%	58.0%	58.6%	63.8%	67.2%	69.1%	70.4%	72.6%	75.9%
Number of blows			140	56	36	23	16		11

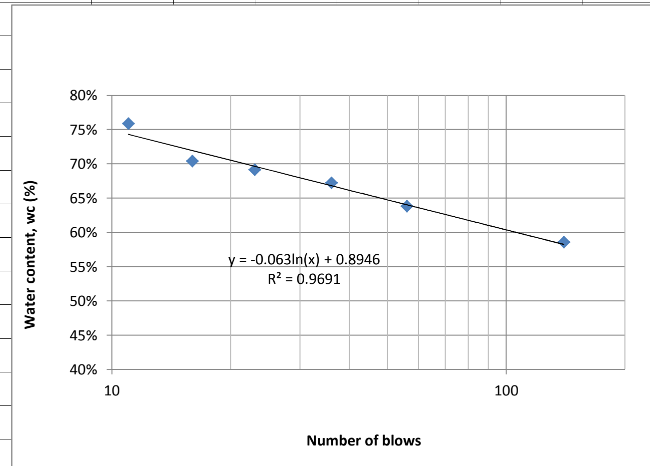

Plastic Limit Test

Test No.		1	2	3
Tare ID		14	Z	Y
Tare mass	g	0.99	1	1.01
Tare + Moist soil	g	2.43	2.17	2.74
Tare + Dry soil	g	2.09	1.89	2.3
Moist soil	g	1.44	1.17	1.73
Dry soil	g	1.1	0.89	1.29
Water content	%	30.9%	31.5%	34.1%
Average water content	%	31.2%		

Liquid Limit :	69.2%
Plastic Limit :	31.2%
Plasticity Index :	38.0%
Natural water content:	15.0%
Liquidity Index:	-0.42596056

y = -0.063ln(x) + 0.8946

0.691810823

$$PI = LL - PL$$

$$LI = \frac{w_n - PL}{PI}$$

E:\RMC\P2_Test result\01_SEL_BPaw\Atterberg limit & Proctor\Atterberg Limits_169.xlsx
ID169

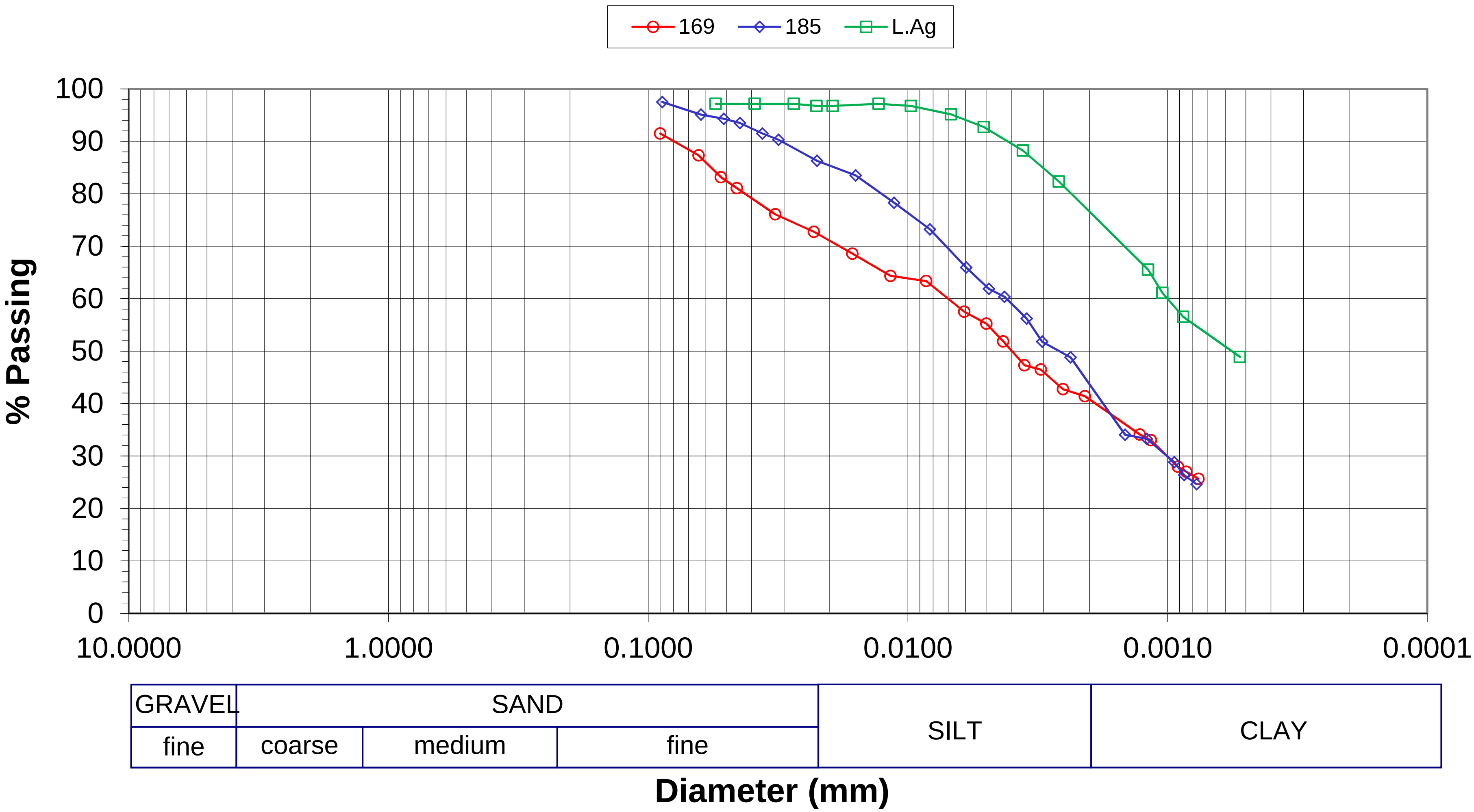

169
185
L.Ag
% Passing
100
90
80
70
60
50
40
30
20
10
0
10.0000
1.0000
0.1000
0.0100
0.0010
0.0001
GRAVEL
SAND
SILT
CLAY
fine
coarse
medium
fine
Diameter (mm)

APPENDIX I - SFG MODELLING SPREADSHEET FOR RECOMPACTED LAKE AGASSIZ CLAY

	SFG model and SEL experimental data- L.Agassiz										
	SFG model input			SEL test data			SFG prediction			% difference	
	p	λvp	ssa	Pswell	V	eV	Pswell	V	eV	Pswell	eV
	Fswell	0.73	140	no data	3.032	-72.8%	635	3.020	-72.1	no data	0.7
b	150	0.28	140	753	1.986	-15.1%	781	2.003	-15.2	28	-0.1
a	150	0.17	215	753	1.986	-15.1%	1064	1.949	-12.1	311	3.1
	300	0.17	215	1198	1.918	-9.9%	1210	1.884	-9.1	12	0.8
20	600	0.17	215	no data	1.803	-5.7%	1501	1.815	-6.4	no data	-0.7

L.Ag_Fswell (parameter input not linked with first test input)

CV Module

λvp	0.73	λvs max	0.73	
κvp	0.009	Ps (CV)=	nodata	#VALUE!
s_{sa}	140		635	
p'=	1	ds=	-150	

s (kPa)	ds	λvs	Cal_Psw ell	dp	p+s	dv from suction change	dv due to mean stress	dv (total)	cal_V_cv
									0.000
7900		0.01303	1.0		7901.0				1.755
7750	-150	0.01328	3.7	2.68	7753.7	-0.00025	-0.00025	0	1.755
7600	-150	0.01354	6.4	2.73	7606.4	-0.00026	-0.00026	0	1.755
7450	-150	0.01381	9.2	2.78	7459.2	-0.00027	-0.00027	0	1.755
7300	-150	0.01410	12.0	2.84	7312.0	-0.00028	-0.00028	0	1.755
7150	-150	0.01439	14.9	2.90	7164.9	-0.00029	-0.00029	0	1.755
7000	-150	0.01470	17.9	2.96	7017.9	-0.00030	-0.0003	0	1.755
6850	-150	0.01502	20.9	3.02	6870.9	-0.00031	-0.00031	0	1.755
6700	-150	0.01536	24.0	3.09	6724.0	-0.00033	-0.00033	0	1.755
6550	-150	0.01571	27.1	3.16	6577.1	-0.00034	-0.00034	0	1.755
6400	-150	0.01608	30.4	3.23	6430.4	-0.00036	-0.00036	0	1.755
6250	-150	0.01647	33.7	3.30	6283.7	-0.00038	-0.00038	0	1.755
6100	-150	0.01687	37.1	3.38	6137.1	-0.00039	-0.00039	0	1.755
5950	-150	0.01730	40.5	3.47	5990.5	-0.00041	-0.00041	0	1.755
5800	-150	0.01774	44.1	3.55	5844.1	-0.00043	-0.00043	0	1.755
5650	-150	0.01821	47.7	3.65	5697.7	-0.00046	-0.00046	0	1.755
5500	-150	0.01871	51.5	3.74	5551.5	-0.00048	-0.00048	0	1.755
5350	-150	0.01924	55.3	3.84	5405.3	-0.00051	-0.00051	0	1.755
5200	-150	0.01979	59.3	3.95	5259.3	-0.00053	-0.00053	0	1.755
5050	-150	0.02038	63.3	4.07	5113.3	-0.00056	-0.00056	0	1.755
4900	-150	0.02100	67.5	4.19	4967.5	-0.00060	-0.0006	0	1.755
4750	-150	0.02166	71.8	4.32	4821.8	-0.00063	-0.00063	0	1.755
4600	-150	0.02237	76.3	4.45	4676.3	-0.00067	-0.00067	0	1.755
4450	-150	0.02313	80.9	4.60	4530.9	-0.00072	-0.00072	0	1.755
4300	-150	0.02393	85.6	4.75	4385.6	-0.00077	-0.00077	0	1.755
4150	-150	0.02480	90.6	4.92	4240.6	-0.00082	-0.00082	0	1.755
4000	-150	0.02573	95.7	5.10	4095.7	-0.00088	-0.00088	0	1.755
3850	-150	0.02673	100.9	5.29	3950.9	-0.00094	-0.00094	0	1.755
3700	-150	0.02781	106.4	5.49	3806.4	-0.00101	-0.00101	0	1.755
3550	-150	0.02899	112.1	5.71	3662.1	-0.00110	-0.0011	0	1.755
3400	-150	0.03026	118.1	5.96	3518.1	-0.00119	-0.00119	0	1.755
3250	-150	0.03166	124.3	6.22	3374.3	-0.00129	-0.00129	0	1.755
3100	-150	0.03319	130.8	6.51	3230.8	-0.00141	-0.00141	0	1.755
2950	-150	0.03488	137.6	6.82	3087.6	-0.00154	-0.00154	0	1.755
2800	-150	0.03675	144.8	7.17	2944.8	-0.00169	-0.00169	0	1.755
2650	-150	0.03883	152.4	7.55	2802.4	-0.00187	-0.00187	0	1.755
2500	-150	0.04116	160.3	7.98	2660.3	-0.00208	-0.00208	0	1.755
2350	-150	0.04378	168.8	8.46	2518.8	-0.00232	-0.00232	0	1.755
2200	-150	0.04677	177.8	9.00	2377.8	-0.00261	-0.00261	0	1.755
2050	-150	0.05019	187.4	9.61	2237.4	-0.00295	-0.00295	0	1.755
1900	-150	0.05415	197.7	10.31	2097.7	-0.00336	-0.00336	0	1.755
1750	-150	0.05878	208.8	11.13	1958.8	-0.00387	-0.00387	0	1.755
1600	-150	0.06429	220.9	12.08	1820.9	-0.00450	-0.0045	0	1.755
1450	-150	0.07094	234.1	13.21	1684.1	-0.00530	-0.0053	0	1.755
1300	-150	0.07912	248.7	14.58	1548.7	-0.00632	-0.00632	0	1.755
1150	-150	0.08943	265.0	16.26	1415.0	-0.00766	-0.00766	0	1.755
1000	-150	0.10283	283.3	18.38	1283.3	-0.00948	-0.00948	0	1.755
850	-150	0.12095	304.5	21.13	1154.5	-0.01202	-0.01202	0	1.755
700	-150	0.14683	329.3	24.85	1029.3	-0.01572	-0.01572	0	1.755
550	-150	0.18681	359.5	30.17	909.5	-0.02140	-0.0214	0	1.755
400	-150	0.25668	397.9	38.38	797.9	-0.03081	-0.03081	0	1.755
250	-150	0.41008	450.6	52.74	700.6	-0.04826	-0.04826	0	1.755
100	-150	0.73000	534.9	84.26	634.9	-0.08780	-0.0878	0	1.755
0	-100	0.73000	634.9	100.00	634.9	-0.11498	-0.11498	0	1.755

CMS module

λvp	0.73	λvs max	0.73	vol_p	-72.1%
κvp	0.009			V_cms_te:	3.032
s_{sa}	140	kPa		EOT_p	3.020
p'=	1	ds=	-150		

s (kPa)	ds	λvs	p	dp	p+s	dv from suction change	dv due to mean stress	dv (total)	cal_V-cms	eV
7900		0.01303	1		7901				1.755	0.0
7750	-150	0.01328	1	0	7751	-0.00025	0	-0.00025	1.755	0.0
7600	-150	0.01354	1	0	7601	-0.00026	0	-0.00026	1.755	0.0
7450	-150	0.01381	1	0	7451	-0.00027	0	-0.00027	1.756	0.0
7300	-150	0.01410	1	0	7301	-0.00028	0	-0.00028	1.756	-0.1
7150	-150	0.01439	1	0	7151	-0.00029	0	-0.00029	1.756	-0.1
7000	-150	0.01470	1	0	7001	-0.00030	0	-0.00030	1.757	-0.1
6850	-150	0.01502	1	0	6851	-0.00032	0	-0.00032	1.757	-0.1
6700	-150	0.01536	1	0	6701	-0.00033	0	-0.00033	1.757	-0.1
6550	-150	0.01571	1	0	6551	-0.00034	0	-0.00034	1.758	-0.1
6400	-150	0.01608	1	0	6401	-0.00036	0	-0.00036	1.758	-0.2
6250	-150	0.01647	1	0	6251	-0.00038	0	-0.00038	1.758	-0.2
6100	-150	0.01687	1	0	6101	-0.00040	0	-0.00040	1.759	-0.2
5950	-150	0.01730	1	0	5951	-0.00041	0	-0.00041	1.759	-0.2
5800	-150	0.01774	1	0	5801	-0.00044	0	-0.00044	1.760	-0.3
5650	-150	0.01821	1	0	5651	-0.00046	0	-0.00046	1.760	-0.3
5500	-150	0.01871	1	0	5501	-0.00048	0	-0.00048	1.760	-0.3
5350	-150	0.01924	1	0	5351	-0.00051	0	-0.00051	1.761	-0.3
5200	-150	0.01979	1	0	5201	-0.00054	0	-0.00054	1.761	-0.4
5050	-150	0.02038	1	0	5051	-0.00057	0	-0.00057	1.762	-0.4
4900	-150	0.02100	1	0	4901	-0.00061	0	-0.00061	1.763	-0.4
4750	-150	0.02166	1	0	4751	-0.00064	0	-0.00064	1.763	-0.5
4600	-150	0.02237	1	0	4601	-0.00068	0	-0.00068	1.764	-0.5
4450	-150	0.02313	1	0	4451	-0.00073	0	-0.00073	1.765	-0.6
4300	-150	0.02393	1	0	4301	-0.00078	0	-0.00078	1.766	-0.6
4150	-150	0.02480	1	0	4151	-0.00083	0	-0.00083	1.766	-0.7
4000	-150	0.02573	1	0	4001	-0.00090	0	-0.00090	1.767	-0.7
3850	-150	0.02673	1	0	3851	-0.00096	0	-0.00096	1.768	-0.8
3700	-150	0.02781	1	0	3701	-0.00104	0	-0.00104	1.769	-0.8
3550	-150	0.02899	1	0	3551	-0.00113	0	-0.00113	1.770	-0.9
3400	-150	0.03026	1	0	3401	-0.00122	0	-0.00122	1.772	-1.0
3250	-150	0.03166	1	0	3251	-0.00133	0	-0.00133	1.773	-1.0
3100	-150	0.03319	1	0	3101	-0.00146	0	-0.00146	1.774	-1.1
2950	-150	0.03488	1	0	2951	-0.00161	0	-0.00161	1.776	-1.2
2800	-150	0.03675	1	0	2801	-0.00177	0	-0.00177	1.778	-1.3
2650	-150	0.03883	1	0	2651	-0.00197	0	-0.00197	1.780	-1.4
2500	-150	0.04116	1	0	2501	-0.00220	0	-0.00220	1.782	-1.5
2350	-150	0.04378	1	0	2351	-0.00247	0	-0.00247	1.784	-1.7
2200	-150	0.04677	1	0	2201	-0.00279	0	-0.00279	1.787	-1.8
2050	-150	0.05019	1	0	2051	-0.00319	0	-0.00319	1.790	-2.0
1900	-150	0.05415	1	0	1901	-0.00367	0	-0.00367	1.794	-2.2
1750	-150	0.05878	1	0	1751	-0.00427	0	-0.00427	1.798	-2.5
1600	-150	0.06429	1	0	1601	-0.00504	0	-0.00504	1.803	-2.8
1450	-150	0.07094	1	0	1451	-0.00602	0	-0.00602	1.809	-3.1
1300	-150	0.07912	1	0	1301	-0.00733	0	-0.00733	1.817	-3.5
1150	-150	0.08943	1	0	1151	-0.00912	0	-0.00912	1.826	-4.0
1000	-150	0.10283	1	0	1001	-0.01165	0	-0.01165	1.837	-4.7
850	-150	0.12095	1	0	851	-0.01541	0	-0.01541	1.853	-5.6
700	-150	0.14683	1	0	701	-0.02132	0	-0.02132	1.874	-6.8
550	-150	0.18681	1	0	551	-0.03142	0	-0.03142	1.906	-8.6
400	-150	0.25668	1	0	401	-0.05085	0	-0.05085	1.956	-11.5
250	-150	0.41008	1	0	251	-0.09602	0	-0.09602	2.053	-17.0
100	-150	0.73000	1	0	101	-0.24507	0	-0.24507	2.298	-30.9
0	-100	0.73000	1	0	1	-0.72277	0	-0.72277	3.020	-72.1

Test_a: 150

These values are linked to other tests. Other cells values would be updated simultaneously.

CV Module

CMS module

λvp	0.17	λvs max	0.17								λvp	0.17	λvs max	0.17						vol_p	-12.1%
κvp	0.009	Ps (CV)=	753	41.3%							κvp	0.009								V_cms_te:	1.986
s_{sa}	215		1064								s_{sa}	215								EOT_p	1.949
p'=	150	ds=	-150						1.739		p'=	150	ds=	-150							
s (kPa)	ds	λvs	Cal_Psw ell	dp	p+s	dv from suction change	dv due to mean stress	dv (total)	cal_V_cv		s (kPa)	ds	λvs	p	dp	p+s	dv from suction change	dv due to mean stress	dv (total)	cal_V-cms	eV
7750		0.00474	150.0		7900.0				1.739		7750		0.00474	150		7900				1.739	0.0
7600	-150	0.00483	154.2	4.18	7754.2	-0.00009	-9E-05	0	1.739		7600	-150	0.00483	150	0	7750	-0.00009	0	-0.00009	1.739	0.0
7450	-150	0.00493	158.4	4.26	7608.4	-0.00009	-9.3E-05	0	1.739		7450	-150	0.00493	150	0	7600	-0.00009	0	-0.00009	1.739	0.0
7300	-150	0.00503	162.8	4.35	7462.8	-0.00010	-9.7E-05	0	1.739		7300	-150	0.00503	150	0	7450	-0.00010	0	-0.00010	1.739	0.0
7150	-150	0.00513	167.2	4.44	7317.2	-0.00010	-0.0001	0	1.739		7150	-150	0.00513	150	0	7300	-0.00010	0	-0.00010	1.739	0.0
7000	-150	0.00524	171.8	4.53	7171.8	-0.00011	-0.00011	0	1.739		7000	-150	0.00524	150	0	7150	-0.00011	0	-0.00011	1.739	0.0
6850	-150	0.00536	176.4	4.63	7026.4	-0.00011	-0.00011	0	1.739		6850	-150	0.00536	150	0	7000	-0.00011	0	-0.00011	1.739	0.0
6700	-150	0.00548	181.1	4.73	6881.1	-0.00011	-0.00011	0	1.739		6700	-150	0.00548	150	0	6850	-0.00011	0	-0.00011	1.739	0.0
6550	-150	0.00561	186.0	4.84	6736.0	-0.00012	-0.00012	0	1.739		6550	-150	0.00561	150	0	6700	-0.00012	0	-0.00012	1.739	0.0
6400	-150	0.00574	190.9	4.95	6590.9	-0.00012	-0.00012	0	1.739		6400	-150	0.00574	150	0	6550	-0.00013	0	-0.00013	1.740	-0.1
6250	-150	0.00587	196.0	5.06	6446.0	-0.00013	-0.00013	0	1.739		6250	-150	0.00587	150	0	6400	-0.00013	0	-0.00013	1.740	-0.1
6100	-150	0.00602	201.1	5.18	6301.1	-0.00014	-0.00014	0	1.739		6100	-150	0.00602	150	0	6250	-0.00014	0	-0.00014	1.740	-0.1
5950	-150	0.00617	206.5	5.31	6156.5	-0.00014	-0.00014	0	1.739		5950	-150	0.00617	150	0	6100	-0.00014	0	-0.00014	1.740	-0.1
5800	-150	0.00633	211.9	5.44	6011.9	-0.00015	-0.00015	0	1.739		5800	-150	0.00633	150	0	5950	-0.00015	0	-0.00015	1.740	-0.1
5650	-150	0.00650	217.5	5.59	5867.5	-0.00016	-0.00016	0	1.739		5650	-150	0.00650	150	0	5800	-0.00016	0	-0.00016	1.740	-0.1
5500	-150	0.00668	223.2	5.73	5723.2	-0.00017	-0.00017	0	1.739		5500	-150	0.00668	150	0	5650	-0.00017	0	-0.00017	1.741	-0.1
5350	-150	0.00686	229.1	5.89	5579.1	-0.00017	-0.00017	0	1.739		5350	-150	0.00686	150	0	5500	-0.00018	0	-0.00018	1.741	-0.1
5200	-150	0.00706	235.2	6.05	5435.2	-0.00018	-0.00018	0	1.739		5200	-150	0.00706	150	0	5350	-0.00019	0	-0.00019	1.741	-0.1
5050	-150	0.00727	241.4	6.23	5291.4	-0.00019	-0.00019	0	1.739		5050	-150	0.00727	150	0	5200	-0.00020	0	-0.00020	1.741	-0.1
4900	-150	0.00749	247.8	6.41	5147.8	-0.00021	-0.00021	0	1.739		4900	-150	0.00749	150	0	5050	-0.00021	0	-0.00021	1.741	-0.2
4750	-150	0.00773	254.4	6.61	5004.4	-0.00022	-0.00022	0	1.739		4750	-150	0.00773	150	0	4900	-0.00022	0	-0.00022	1.742	-0.2
4600	-150	0.00798	261.2	6.82	4861.2	-0.00023	-0.00023	0	1.739		4600	-150	0.00798	150	0	4750	-0.00024	0	-0.00024	1.742	-0.2
4450	-150	0.00825	268.3	7.04	4718.3	-0.00025	-0.00025	0	1.739		4450	-150	0.00825	150	0	4600	-0.00025	0	-0.00025	1.742	-0.2
4300	-150	0.00854	275.6	7.28	4575.6	-0.00026	-0.00026	0	1.739		4300	-150	0.00854	150	0	4450	-0.00027	0	-0.00027	1.742	-0.2
4150	-150	0.00885	283.1	7.53	4433.1	-0.00028	-0.00028	0	1.739		4150	-150	0.00885	150	0	4300	-0.00029	0	-0.00029	1.743	-0.2
4000	-150	0.00918	290.9	7.81	4290.9	-0.00030	-0.0003	0	1.739		4000	-150	0.00918	150	0	4150	-0.00031	0	-0.00031	1.743	-0.2
3850	-150	0.00954	299.0	8.10	4149.0	-0.00032	-0.00032	0	1.739		3850	-150	0.00954	150	0	4000	-0.00033	0	-0.00033	1.743	-0.3
3700	-150	0.00992	307.4	8.41	4007.4	-0.00034	-0.00034	0	1.739		3700	-150	0.00992	150	0	3850	-0.00036	0	-0.00036	1.744	-0.3
3550	-150	0.01034	316.2	8.75	3866.2	-0.00037	-0.00037	0	1.739		3550	-150	0.01034	150	0	3700	-0.00039	0	-0.00039	1.744	-0.3
3400	-150	0.01080	325.3	9.12	3725.3	-0.00040	-0.0004	0	1.739		3400	-150	0.01080	150	0	3550	-0.00042	0	-0.00042	1.744	-0.3
3250	-150	0.01129	334.8	9.53	3584.8	-0.00043	-0.00043	0	1.739		3250	-150	0.01129	150	0	3400	-0.00046	0	-0.00046	1.745	-0.4
3100	-150	0.01184	344.8	9.97	3444.8	-0.00047	-0.00047	0	1.739		3100	-150	0.01184	150	0	3250	-0.00050	0	-0.00050	1.745	-0.4
2950	-150	0.01244	355.2	10.45	3305.2	-0.00052	-0.00052	0	1.739		2950	-150	0.01244	150	0	3100	-0.00055	0	-0.00055	1.746	-0.4
2800	-150	0.01311	366.2	10.98	3166.2	-0.00056	-0.00056	0	1.739		2800	-150	0.01311	150	0	2950	-0.00060	0	-0.00060	1.746	-0.4
2650	-150	0.01385	377.8	11.57	3027.8	-0.00062	-0.00062	0	1.739		2650	-150	0.01385	150	0	2800	-0.00067	0	-0.00067	1.747	-0.5
2500	-150	0.01468	390.0	12.22	2890.0	-0.00069	-0.00069	0	1.739		2500	-150	0.01468	150	0	2650	-0.00074	0	-0.00074	1.748	-0.5
2350	-150	0.01562	402.9	12.95	2752.9	-0.00076	-0.00076	0	1.739		2350	-150	0.01562	150	0	2500	-0.00083	0	-0.00083	1.749	-0.6
2200	-150	0.01668	416.7	13.78	2616.7	-0.00085	-0.00085	0	1.739		2200	-150	0.01668	150	0	2350	-0.00094	0	-0.00094	1.750	-0.6
2050	-150	0.01790	431.5	14.72	2481.5	-0.00096	-0.00096	0	1.739		2050	-150	0.01790	150	0	2200	-0.00106	0	-0.00106	1.751	-0.7
1900	-150	0.01932	447.2	15.80	2347.2	-0.00108	-0.00108	0	1.739		1900	-150	0.01932	150	0	2050	-0.00122	0	-0.00122	1.752	-0.8
1750	-150	0.02097	464.3	17.04	2214.3	-0.00123	-0.00123	0	1.739		1750	-150	0.02097	150	0	1900	-0.00141	0	-0.00141	1.753	-0.8
1600	-150	0.02294	482.8	18.50	2082.8	-0.00142	-0.00142	0	1.739		1600	-150	0.02294	150	0	1750	-0.00166	0	-0.00166	1.755	-0.9
1450	-150	0.02531	503.0	20.24	1953.0	-0.00165	-0.00165	0	1.739		1450	-150	0.02531	150	0	1600	-0.00197	0	-0.00197	1.757	-1.1
1300	-150	0.02822	525.4	22.33	1825.4	-0.00194	-0.00194	0	1.739		1300	-150	0.02822	150	0	1450	-0.00237	0	-0.00237	1.759	-1.2
1150	-150	0.03190	550.3	24.90	1700.3	-0.00232	-0.00232	0	1.739		1150	-150	0.03190	150	0	1300	-0.00292	0	-0.00292	1.762	-1.4
1000	-150	0.03668	578.4	28.15	1578.4	-0.00281	-0.00281	0	1.739		1000	-150	0.03668	150	0	1150	-0.00368	0	-0.00368	1.766	-1.6
850	-150	0.04315	610.8	32.37	1460.8	-0.00349	-0.00349	0	1.739		850	-150	0.04315	150	0	1000	-0.00478	0	-0.00478	1.771	-1.8
700	-150	0.05238	648.9	38.07	1348.9	-0.00443	-0.00443	0	1.739		700	-150	0.05238	150	0	850	-0.00647	0	-0.00647	1.777	-2.2
550	-150	0.06664	695.1	46.22	1245.1	-0.00583	-0.00583	0	1.739		550	-150	0.06664	150	0	700	-0.00924	0	-0.00924	1.786	-2.7
400	-150	0.09157	753.9	58.80	1153.9	-0.00803	-0.00803	0	1.739		400	-150	0.09157	150	0	550	-0.01428	0	-0.01428	1.801	-3.6
250	-150	0.14629	834.7	80.80	1084.7	-0.01190	-0.0119	0	1.739		250	-150	0.14629	150	0	400	-0.02497	0	-0.02497	1.826	-5.0
100	-150	0.17000	963.8	129.08	1063.8	-0.02023	-0.02023	0	1.739		100	-150	0.17000	150	0	250	-0.05486	0	-0.05486	1.881	-8.2
0	-100	0.17000	1063.8	100.00	1063.8	-0.01598	-0.01598	0	1.739		0	-100	0.17000	150	0	150	-0.06800	0	-0.06800	1.949	-12.1

Test_b: 150_b => different lvp from other tests																					
CV Module											**CMS module**										
λvp	0.28	λvs max	0.28								λvp	0.28	λvs max	0.28						vol_p	-15.2%
κvp	0.009	Ps (CV)=	753	3.7%							κvp	0.009								V_cms_te:	1.986
s_{sa}	140		781								s_{sa}	140								EOT_p	2.003
p'=	150	ds=	-150			-0.13300			0.000		p'=	150	ds=	-150			-0.26455				
s (kPa)	ds	λvs	Cal_Pswell	dp	p+s	dv from suction change	dv due to mean stress	dv (total)	cal_V_cv		s (kPa)	ds	λvs	p	dp	p+s	dv from suction change	dv due to mean stress	dv (total)	cal_V-cms	eV
7750		0.00509	150.0		7900.0				1.739		7750		0.00509	150		7900				1.739	0.0
7600	-150	0.00519	152.7	2.73	7752.7	-0.00010	-9.7E-05	0.00000	1.739		7600	-150	0.00519	150	0	7750	-0.00010	0	-0.00010	1.739	0.0
7450	-150	0.00530	155.5	2.78	7605.5	-0.00010	-0.0001	0.00000	1.739		7450	-150	0.00530	150	0	7600	-0.00010	0	-0.00010	1.739	0.0
7300	-150	0.00541	158.3	2.84	7458.3	-0.00010	-0.0001	0.00000	1.739		7300	-150	0.00541	150	0	7450	-0.00010	0	-0.00010	1.739	0.0
7150	-150	0.00552	161.2	2.90	7311.2	-0.00011	-0.00011	0.00000	1.739		7150	-150	0.00552	150	0	7300	-0.00011	0	-0.00011	1.739	0.0
7000	-150	0.00564	164.2	2.96	7164.2	-0.00011	-0.00011	0.00000	1.739		7000	-150	0.00564	150	0	7150	-0.00011	0	-0.00011	1.739	0.0
6850	-150	0.00576	167.2	3.02	7017.2	-0.00012	-0.00012	0.00000	1.739		6850	-150	0.00576	150	0	7000	-0.00012	0	-0.00012	1.739	0.0
6700	-150	0.00589	170.3	3.09	6870.3	-0.00012	-0.00012	0.00000	1.739		6700	-150	0.00589	150	0	6850	-0.00012	0	-0.00012	1.739	0.0
6550	-150	0.00603	173.5	3.16	6723.5	-0.00013	-0.00013	0.00000	1.739		6550	-150	0.00603	150	0	6700	-0.00013	0	-0.00013	1.740	-0.1
6400	-150	0.00617	176.7	3.23	6576.7	-0.00013	-0.00013	0.00000	1.739		6400	-150	0.00617	150	0	6550	-0.00013	0	-0.00013	1.740	-0.1
6250	-150	0.00632	180.0	3.30	6430.0	-0.00014	-0.00014	0.00000	1.739		6250	-150	0.00632	150	0	6400	-0.00014	0	-0.00014	1.740	-0.1
6100	-150	0.00647	183.4	3.38	6283.4	-0.00015	-0.00015	0.00000	1.739		6100	-150	0.00647	150	0	6250	-0.00015	0	-0.00015	1.740	-0.1
5950	-150	0.00663	186.9	3.47	6136.9	-0.00015	-0.00015	0.00000	1.739		5950	-150	0.00663	150	0	6100	-0.00016	0	-0.00016	1.740	-0.1
5800	-150	0.00681	190.4	3.55	5990.4	-0.00016	-0.00016	0.00000	1.739		5800	-150	0.00681	150	0	5950	-0.00016	0	-0.00016	1.740	-0.1
5650	-150	0.00699	194.1	3.65	5844.1	-0.00017	-0.00017	0.00000	1.739		5650	-150	0.00699	150	0	5800	-0.00017	0	-0.00017	1.740	-0.1
5500	-150	0.00718	197.8	3.74	5697.8	-0.00018	-0.00018	0.00000	1.739		5500	-150	0.00718	150	0	5650	-0.00018	0	-0.00018	1.741	-0.1
5350	-150	0.00738	201.6	3.84	5551.6	-0.00019	-0.00019	0.00000	1.739		5350	-150	0.00738	150	0	5500	-0.00019	0	-0.00019	1.741	-0.1
5200	-150	0.00759	205.6	3.95	5405.6	-0.00020	-0.0002	0.00000	1.739		5200	-150	0.00759	150	0	5350	-0.00020	0	-0.00020	1.741	-0.1
5050	-150	0.00782	209.7	4.07	5259.7	-0.00021	-0.00021	0.00000	1.739		5050	-150	0.00782	150	0	5200	-0.00021	0	-0.00021	1.741	-0.1
4900	-150	0.00806	213.8	4.19	5113.8	-0.00022	-0.00022	0.00000	1.739		4900	-150	0.00806	150	0	5050	-0.00023	0	-0.00023	1.741	-0.2
4750	-150	0.00831	218.2	4.32	4968.2	-0.00024	-0.00024	0.00000	1.739		4750	-150	0.00831	150	0	4900	-0.00024	0	-0.00024	1.742	-0.2
4600	-150	0.00858	222.6	4.45	4822.6	-0.00025	-0.00025	0.00000	1.739		4600	-150	0.00858	150	0	4750	-0.00025	0	-0.00025	1.742	-0.2
4450	-150	0.00887	227.2	4.60	4677.2	-0.00027	-0.00027	0.00000	1.739		4450	-150	0.00887	150	0	4600	-0.00027	0	-0.00027	1.742	-0.2
4300	-150	0.00918	232.0	4.75	4532.0	-0.00028	-0.00028	0.00000	1.739		4300	-150	0.00918	150	0	4450	-0.00029	0	-0.00029	1.743	-0.2
4150	-150	0.00951	236.9	4.92	4386.9	-0.00030	-0.0003	0.00000	1.739		4150	-150	0.00951	150	0	4300	-0.00031	0	-0.00031	1.743	-0.2
4000	-150	0.00987	242.0	5.10	4242.0	-0.00033	-0.00033	0.00000	1.739		4000	-150	0.00987	150	0	4150	-0.00033	0	-0.00033	1.743	-0.3
3850	-150	0.01025	247.3	5.29	4097.3	-0.00035	-0.00035	0.00000	1.739		3850	-150	0.01025	150	0	4000	-0.00036	0	-0.00036	1.744	-0.3
3700	-150	0.01067	252.8	5.49	3952.8	-0.00038	-0.00038	0.00000	1.739		3700	-150	0.01067	150	0	3850	-0.00038	0	-0.00038	1.744	-0.3
3550	-150	0.01112	258.5	5.71	3808.5	-0.00040	-0.0004	0.00000	1.739		3550	-150	0.01112	150	0	3700	-0.00042	0	-0.00042	1.744	-0.3
3400	-150	0.01161	264.4	5.96	3664.4	-0.00044	-0.00044	0.00000	1.739		3400	-150	0.01161	150	0	3550	-0.00045	0	-0.00045	1.745	-0.4
3250	-150	0.01214	270.6	6.22	3520.6	-0.00048	-0.00048	0.00000	1.739		3250	-150	0.01214	150	0	3400	-0.00049	0	-0.00049	1.745	-0.4
3100	-150	0.01273	277.1	6.51	3377.1	-0.00052	-0.00052	0.00000	1.739		3100	-150	0.01273	150	0	3250	-0.00054	0	-0.00054	1.746	-0.4
2950	-150	0.01338	284.0	6.82	3234.0	-0.00057	-0.00057	0.00000	1.739		2950	-150	0.01338	150	0	3100	-0.00059	0	-0.00059	1.746	-0.4
2800	-150	0.01409	291.1	7.17	3091.1	-0.00062	-0.00062	0.00000	1.739		2800	-150	0.01409	150	0	2950	-0.00065	0	-0.00065	1.747	-0.5
2650	-150	0.01489	298.7	7.55	2948.7	-0.00068	-0.00068	0.00000	1.739		2650	-150	0.01489	150	0	2800	-0.00072	0	-0.00072	1.748	-0.5
2500	-150	0.01579	306.7	7.98	2806.7	-0.00076	-0.00076	0.00000	1.739		2500	-150	0.01579	150	0	2650	-0.00080	0	-0.00080	1.749	-0.6
2350	-150	0.01679	315.1	8.46	2665.1	-0.00084	-0.00084	0.00000	1.739		2350	-150	0.01679	150	0	2500	-0.00089	0	-0.00089	1.749	-0.6
2200	-150	0.01794	324.1	9.00	2524.1	-0.00095	-0.00095	0.00000	1.739		2200	-150	0.01794	150	0	2350	-0.00101	0	-0.00101	1.750	-0.7
2050	-150	0.01925	333.7	9.61	2383.7	-0.00107	-0.00107	0.00000	1.739		2050	-150	0.01925	150	0	2200	-0.00114	0	-0.00114	1.752	-0.7
1900	-150	0.02077	344.0	10.31	2244.0	-0.00121	-0.00121	0.00000	1.739		1900	-150	0.02077	150	0	2050	-0.00131	0	-0.00131	1.753	-0.8
1750	-150	0.02255	355.2	11.13	2105.2	-0.00139	-0.00139	0.00000	1.739		1750	-150	0.02255	150	0	1900	-0.00152	0	-0.00152	1.754	-0.9
1600	-150	0.02466	367.2	12.08	1967.2	-0.00161	-0.00161	0.00000	1.739		1600	-150	0.02466	150	0	1750	-0.00178	0	-0.00178	1.756	-1.0
1450	-150	0.02721	380.5	13.21	1830.5	-0.00188	-0.00188	0.00000	1.739		1450	-150	0.02721	150	0	1600	-0.00211	0	-0.00211	1.758	-1.1
1300	-150	0.03035	395.0	14.58	1695.0	-0.00223	-0.00223	0.00000	1.739		1300	-150	0.03035	150	0	1450	-0.00255	0	-0.00255	1.761	-1.3
1150	-150	0.03430	411.3	16.26	1561.3	-0.00269	-0.00269	0.00000	1.739		1150	-150	0.03430	150	0	1300	-0.00314	0	-0.00314	1.764	-1.5
1000	-150	0.03944	429.7	18.38	1429.7	-0.00330	-0.0033	0.00000	1.739		1000	-150	0.03944	150	0	1150	-0.00396	0	-0.00396	1.768	-1.7
850	-150	0.04639	450.8	21.13	1300.8	-0.00414	-0.00414	0.00000	1.739		850	-150	0.04639	150	0	1000	-0.00514	0	-0.00514	1.773	-2.0
700	-150	0.05632	475.6	24.85	1175.6	-0.00535	-0.00535	0.00000	1.739		700	-150	0.05632	150	0	850	-0.00696	0	-0.00696	1.780	-2.4
550	-150	0.07165	505.8	30.17	1055.8	-0.00719	-0.00719	0.00000	1.739		550	-150	0.07165	150	0	700	-0.00994	0	-0.00994	1.790	-3.0
400	-150	0.09845	544.2	38.38	944.2	-0.01018	-0.01018	0.00000	1.739		400	-150	0.09845	150	0	550	-0.01535	0	-0.01535	1.805	-3.8
250	-150	0.15729	596.9	52.74	846.9	-0.01564	-0.01564	0.00000	1.739		250	-150	0.15729	150	0	400	-0.02685	0	-0.02685	1.832	-5.4
100	-150	0.28000	681.2	84.26	781.2	-0.02786	-0.02786	0.00000	1.739		100	-150	0.28000	150	0	250	-0.05898	0	-0.05898	1.891	-8.8
0	-100	0.28000	781.2	100.00	781.2	-0.03584	-0.03584	0.00000	1.739		0	-100	0.28000	150	0	150	-0.11200	0	-0.11200	2.003	-15.2

Test: 300

CV Module

λvp	0.17	λvs max	0.17						
κvp	0.009	Ps (CV)=	1198	1.0%					
s_{sa}	215		1209.6						
p'=	300	ds=	-150						1.727
s (kPa)	ds	λvs	Cal_Pswell	dp	p+s	dv from suction change	dv due to mean stress	dv (total)	cal_V_cv
7600		0.00483	300.0		7900.0				1.7270
7450	-150	0.00493	304.3	4.26	7754.3	-0.00009	-9.2E-05	0	1.727
7300	-150	0.00503	308.6	4.35	7608.6	-0.00010	-9.5E-05	0	1.727
7150	-150	0.00513	313.0	4.44	7463.0	-0.00010	-9.9E-05	0	1.727
7000	-150	0.00524	317.6	4.53	7317.6	-0.00010	-0.0001	0	1.727
6850	-150	0.00536	322.2	4.63	7172.2	-0.00011	-0.00011	0	1.727
6700	-150	0.00548	326.9	4.73	7026.9	-0.00011	-0.00011	0	1.727
6550	-150	0.00561	331.8	4.84	6881.8	-0.00012	-0.00012	0	1.727
6400	-150	0.00574	336.7	4.95	6736.7	-0.00012	-0.00012	0	1.727
6250	-150	0.00587	341.8	5.06	6591.8	-0.00013	-0.00013	0	1.727
6100	-150	0.00602	347.0	5.18	6447.0	-0.00013	-0.00013	0	1.727
5950	-150	0.00617	352.3	5.31	6302.3	-0.00014	-0.00014	0	1.727
5800	-150	0.00633	357.7	5.44	6157.7	-0.00015	-0.00015	0	1.727
5650	-150	0.00650	363.3	5.59	6013.3	-0.00015	-0.00015	0	1.727
5500	-150	0.00668	369.0	5.73	5869.0	-0.00016	-0.00016	0	1.727
5350	-150	0.00686	374.9	5.89	5724.9	-0.00017	-0.00017	0	1.727
5200	-150	0.00706	381.0	6.05	5581.0	-0.00018	-0.00018	0	1.727
5050	-150	0.00727	387.2	6.23	5437.2	-0.00019	-0.00019	0	1.727
4900	-150	0.00749	393.6	6.41	5293.6	-0.00020	-0.0002	0	1.727
4750	-150	0.00773	400.2	6.61	5150.2	-0.00021	-0.00021	0	1.727
4600	-150	0.00798	407.1	6.82	5007.1	-0.00023	-0.00023	0	1.727
4450	-150	0.00825	414.1	7.04	4864.1	-0.00024	-0.00024	0	1.727
4300	-150	0.00854	421.4	7.28	4721.4	-0.00025	-0.00025	0	1.727
4150	-150	0.00885	428.9	7.53	4578.9	-0.00027	-0.00027	0	1.727
4000	-150	0.00918	436.7	7.81	4436.7	-0.00029	-0.00029	0	1.727
3850	-150	0.00954	444.8	8.10	4294.8	-0.00031	-0.00031	0	1.727
3700	-150	0.00992	453.2	8.41	4153.2	-0.00033	-0.00033	0	1.727
3550	-150	0.01034	462.0	8.75	4012.0	-0.00036	-0.00036	0	1.727
3400	-150	0.01080	471.1	9.12	3871.1	-0.00039	-0.00039	0	1.727
3250	-150	0.01129	480.6	9.53	3730.6	-0.00042	-0.00042	0	1.727
3100	-150	0.01184	490.6	9.97	3590.6	-0.00045	-0.00045	0	1.727
2950	-150	0.01244	501.0	10.45	3451.0	-0.00049	-0.00049	0	1.727
2800	-150	0.01311	512.0	10.98	3312.0	-0.00054	-0.00054	0	1.727
2650	-150	0.01385	523.6	11.57	3173.6	-0.00059	-0.00059	0	1.727
2500	-150	0.01468	535.8	12.22	3035.8	-0.00065	-0.00065	0	1.727
2350	-150	0.01562	548.8	12.95	2898.8	-0.00073	-0.00073	0	1.727
2200	-150	0.01668	562.6	13.78	2762.6	-0.00081	-0.00081	0	1.727
2050	-150	0.01790	577.3	14.72	2627.3	-0.00091	-0.00091	0	1.727
1900	-150	0.01932	593.1	15.80	2493.1	-0.00102	-0.00102	0	1.727
1750	-150	0.02097	610.1	17.04	2360.1	-0.00116	-0.00116	0	1.727
1600	-150	0.02294	628.6	18.50	2228.6	-0.00133	-0.00133	0	1.727
1450	-150	0.02531	648.9	20.24	2098.9	-0.00154	-0.00154	0	1.727
1300	-150	0.02822	671.2	22.33	1971.2	-0.00181	-0.00181	0	1.727
1150	-150	0.03190	696.1	24.90	1846.1	-0.00215	-0.00215	0	1.727
1000	-150	0.03668	724.2	28.15	1724.2	-0.00259	-0.00259	0	1.727
850	-150	0.04315	756.6	32.37	1606.6	-0.00319	-0.00319	0	1.727
700	-150	0.05238	794.7	38.07	1494.7	-0.00403	-0.00403	0	1.727
550	-150	0.06664	840.9	46.22	1390.9	-0.00526	-0.00526	0	1.727
400	-150	0.09157	899.7	58.80	1299.7	-0.00719	-0.00719	0	1.727
250	-150	0.14629	980.5	80.80	1230.5	-0.01057	-0.01057	0	1.727
100	-150	0.17000	1109.6	129.08	1209.6	-0.01783	-0.01783	0	1.727
0	-100	0.17000	1209.6	100.00	1209.6	-0.01405	-0.01405	0	1.727

CMS module

λvp	0.17	λvs max	0.17						vol_p	-9.1%
κvp	0.009								V_cms_te:	1.918
s_{sa}	215								EOT_p	1.884
p'=	300	ds=	-150							
s (kPa)	ds	λvs	p	dp	p+s	dv from suction change	dv due to mean stress	dv (total)	cal_V-cms	eV
7600		0.00483	300		7900				1.7270	0.0
7450	-150	0.00493	300	0	7750	-0.00009	0	-0.00009	1.727	0.0
7300	-150	0.00503	300	0	7600	-0.00010	0	-0.00010	1.727	0.0
7150	-150	0.00513	300	0	7450	-0.00010	0	-0.00010	1.727	0.0
7000	-150	0.00524	300	0	7300	-0.00010	0	-0.00010	1.727	0.0
6850	-150	0.00536	300	0	7150	-0.00011	0	-0.00011	1.727	0.0
6700	-150	0.00548	300	0	7000	-0.00011	0	-0.00011	1.728	0.0
6550	-150	0.00561	300	0	6850	-0.00012	0	-0.00012	1.728	0.0
6400	-150	0.00574	300	0	6700	-0.00012	0	-0.00012	1.728	0.0
6250	-150	0.00587	300	0	6550	-0.00013	0	-0.00013	1.728	-0.1
6100	-150	0.00602	300	0	6400	-0.00013	0	-0.00013	1.728	-0.1
5950	-150	0.00617	300	0	6250	-0.00014	0	-0.00014	1.728	-0.1
5800	-150	0.00633	300	0	6100	-0.00015	0	-0.00015	1.728	-0.1
5650	-150	0.00650	300	0	5950	-0.00016	0	-0.00016	1.729	-0.1
5500	-150	0.00668	300	0	5800	-0.00016	0	-0.00016	1.729	-0.1
5350	-150	0.00686	300	0	5650	-0.00017	0	-0.00017	1.729	-0.1
5200	-150	0.00706	300	0	5500	-0.00018	0	-0.00018	1.729	-0.1
5050	-150	0.00727	300	0	5350	-0.00019	0	-0.00019	1.729	-0.1
4900	-150	0.00749	300	0	5200	-0.00020	0	-0.00020	1.729	-0.1
4750	-150	0.00773	300	0	5050	-0.00022	0	-0.00022	1.730	-0.2
4600	-150	0.00798	300	0	4900	-0.00023	0	-0.00023	1.730	-0.2
4450	-150	0.00825	300	0	4750	-0.00024	0	-0.00024	1.730	-0.2
4300	-150	0.00854	300	0	4600	-0.00026	0	-0.00026	1.730	-0.2
4150	-150	0.00885	300	0	4450	-0.00028	0	-0.00028	1.731	-0.2
4000	-150	0.00918	300	0	4300	-0.00030	0	-0.00030	1.731	-0.2
3850	-150	0.00954	300	0	4150	-0.00032	0	-0.00032	1.731	-0.3
3700	-150	0.00992	300	0	4000	-0.00034	0	-0.00034	1.732	-0.3
3550	-150	0.01034	300	0	3850	-0.00037	0	-0.00037	1.732	-0.3
3400	-150	0.01080	300	0	3700	-0.00040	0	-0.00040	1.732	-0.3
3250	-150	0.01129	300	0	3550	-0.00044	0	-0.00044	1.733	-0.3
3100	-150	0.01184	300	0	3400	-0.00048	0	-0.00048	1.733	-0.4
2950	-150	0.01244	300	0	3250	-0.00052	0	-0.00052	1.734	-0.4
2800	-150	0.01311	300	0	3100	-0.00057	0	-0.00057	1.734	-0.4
2650	-150	0.01385	300	0	2950	-0.00063	0	-0.00063	1.735	-0.5
2500	-150	0.01468	300	0	2800	-0.00070	0	-0.00070	1.736	-0.5
2350	-150	0.01562	300	0	2650	-0.00079	0	-0.00079	1.737	-0.6
2200	-150	0.01668	300	0	2500	-0.00088	0	-0.00088	1.737	-0.6
2050	-150	0.01790	300	0	2350	-0.00100	0	-0.00100	1.738	-0.7
1900	-150	0.01932	300	0	2200	-0.00114	0	-0.00114	1.740	-0.7
1750	-150	0.02097	300	0	2050	-0.00132	0	-0.00132	1.741	-0.8
1600	-150	0.02294	300	0	1900	-0.00153	0	-0.00153	1.742	-0.9
1450	-150	0.02531	300	0	1750	-0.00181	0	-0.00181	1.744	-1.0
1300	-150	0.02822	300	0	1600	-0.00217	0	-0.00217	1.746	-1.1
1150	-150	0.03190	300	0	1450	-0.00265	0	-0.00265	1.749	-1.3
1000	-150	0.03668	300	0	1300	-0.00330	0	-0.00330	1.752	-1.5
850	-150	0.04315	300	0	1150	-0.00423	0	-0.00423	1.757	-1.7
700	-150	0.05238	300	0	1000	-0.00563	0	-0.00563	1.762	-2.0
550	-150	0.06664	300	0	850	-0.00786	0	-0.00786	1.770	-2.5
400	-150	0.09157	300	0	700	-0.01176	0	-0.01176	1.782	-3.2
250	-150	0.14629	300	0	550	-0.01962	0	-0.01962	1.801	-4.3
100	-150	0.17000	300	0	400	-0.03990	0	-0.03990	1.841	-6.6
0	-100	0.17000	300	0	300	-0.04250	0	-0.04250	1.884	-9.1

Test: 600									
CV Module									
λvp	0.17	λvs max	0.17						
κvp	0.009	Ps (CV)=	no test dat	#VALUE!					
S_{sa}	215		1501						
p'=	600	ds=	-150						1.706
s (kPa)	ds	λvs	Cal_Psw ell	dp	p+s	dv from suction change	dv due to mean stress	dv (total)	cal_V_cv
7300		0.00503	600.0		7900.0				1.706
7150	-150	0.00513	604.4	4.44	7754.4	-0.00010	-9.5E-05	0	1.706
7000	-150	0.00524	609.0	4.53	7609.0	-0.00010	-9.9E-05	0	1.706
6850	-150	0.00536	613.6	4.63	7463.6	-0.00010	-0.0001	0	1.706
6700	-150	0.00548	618.3	4.73	7318.3	-0.00011	-0.00011	0	1.706
6550	-150	0.00561	623.2	4.84	7173.2	-0.00011	-0.00011	0	1.706
6400	-150	0.00574	628.1	4.95	7028.1	-0.00012	-0.00012	0	1.706
6250	-150	0.00587	633.2	5.06	6883.2	-0.00012	-0.00012	0	1.706
6100	-150	0.00602	638.4	5.18	6738.4	-0.00013	-0.00013	0	1.706
5950	-150	0.00617	643.7	5.31	6593.7	-0.00013	-0.00013	0	1.706
5800	-150	0.00633	649.1	5.44	6449.1	-0.00014	-0.00014	0	1.706
5650	-150	0.00650	654.7	5.59	6304.7	-0.00015	-0.00015	0	1.706
5500	-150	0.00668	660.4	5.73	6160.4	-0.00015	-0.00015	0	1.706
5350	-150	0.00686	666.3	5.89	6016.3	-0.00016	-0.00016	0	1.706
5200	-150	0.00706	672.4	6.05	5872.4	-0.00017	-0.00017	0	1.706
5050	-150	0.00727	678.6	6.23	5728.6	-0.00018	-0.00018	0	1.706
4900	-150	0.00749	685.0	6.41	5585.0	-0.00019	-0.00019	0	1.706
4750	-150	0.00773	691.6	6.61	5441.6	-0.00020	-0.0002	0	1.706
4600	-150	0.00798	698.4	6.82	5298.4	-0.00021	-0.00021	0	1.706
4450	-150	0.00825	705.5	7.04	5155.5	-0.00023	-0.00023	0	1.706
4300	-150	0.00854	712.8	7.28	5012.8	-0.00024	-0.00024	0	1.706
4150	-150	0.00885	720.3	7.53	4870.3	-0.00026	-0.00026	0	1.706
4000	-150	0.00918	728.1	7.81	4728.1	-0.00027	-0.00027	0	1.706
3850	-150	0.00954	736.2	8.10	4586.2	-0.00029	-0.00029	0	1.706
3700	-150	0.00992	744.6	8.41	4444.6	-0.00031	-0.00031	0	1.706
3550	-150	0.01034	753.4	8.75	4303.4	-0.00033	-0.00033	0	1.706
3400	-150	0.01080	762.5	9.12	4162.5	-0.00036	-0.00036	0	1.706
3250	-150	0.01129	772.0	9.53	4022.0	-0.00039	-0.00039	0	1.706
3100	-150	0.01184	782.0	9.97	3882.0	-0.00042	-0.00042	0	1.706
2950	-150	0.01244	792.4	10.45	3742.4	-0.00046	-0.00046	0	1.706
2800	-150	0.01311	803.4	10.98	3603.4	-0.00050	-0.0005	0	1.706
2650	-150	0.01385	815.0	11.57	3465.0	-0.00055	-0.00055	0	1.706
2500	-150	0.01468	827.2	12.22	3327.2	-0.00060	-0.0006	0	1.706
2350	-150	0.01562	840.2	12.95	3190.2	-0.00066	-0.00066	0	1.706
2200	-150	0.01668	853.9	13.78	3053.9	-0.00073	-0.00073	0	1.706
2050	-150	0.01790	868.7	14.72	2918.7	-0.00082	-0.00082	0	1.706
1900	-150	0.01932	884.5	15.80	2784.5	-0.00092	-0.00092	0	1.706
1750	-150	0.02097	901.5	17.04	2651.5	-0.00104	-0.00104	0	1.706
1600	-150	0.02294	920.0	18.50	2520.0	-0.00119	-0.00119	0	1.706
1450	-150	0.02531	940.2	20.24	2390.2	-0.00137	-0.00137	0	1.706
1300	-150	0.02822	962.6	22.33	2262.6	-0.00159	-0.00159	0	1.706
1150	-150	0.03190	987.5	24.90	2137.5	-0.00187	-0.00187	0	1.706
1000	-150	0.03668	1015.6	28.15	2015.6	-0.00224	-0.00224	0	1.706
850	-150	0.04315	1048.0	32.37	1898.0	-0.00273	-0.00273	0	1.706
700	-150	0.05238	1086.1	38.07	1786.1	-0.00341	-0.00341	0	1.706
550	-150	0.06664	1132.3	46.22	1682.3	-0.00440	-0.0044	0	1.706
400	-150	0.09157	1191.1	58.80	1591.1	-0.00594	-0.00594	0	1.706
250	-150	0.14629	1271.9	80.80	1521.9	-0.00863	-0.00863	0	1.706
100	-150	0.17000	1401.0	129.08	1501.0	-0.01442	-0.01442	0	1.706
0	-100	0.17000	1501.0	100.00	1501.0	-0.01133	-0.01133	0	1.706

CMS module										
λvp	0.17	λvs max	0.17						vol_p	6.4%
κvp	0.009								V_cms_te	1.803
S_{sa}	215								EOT_p	1.815
p'=	600	ds=	-150							
s (kPa)	ds	λvs	p	dp	p+s	dv from suction change	dv due to mean stress	dv (total)	cal_V-cms	eV
7300		0.00503	600		7900				1.706	0.0
7150	-150	0.00513	600	0	7750	-0.00010	0	-0.00010	1.706	0.0
7000	-150	0.00524	600	0	7600	-0.00010	0	-0.00010	1.706	0.0
6850	-150	0.00536	600	0	7450	-0.00010	0	-0.00010	1.706	0.0
6700	-150	0.00548	600	0	7300	-0.00011	0	-0.00011	1.706	0.0
6550	-150	0.00561	600	0	7150	-0.00011	0	-0.00011	1.707	0.0
6400	-150	0.00574	600	0	7000	-0.00012	0	-0.00012	1.707	0.0
6250	-150	0.00587	600	0	6850	-0.00012	0	-0.00012	1.707	0.0
6100	-150	0.00602	600	0	6700	-0.00013	0	-0.00013	1.707	-0.1
5950	-150	0.00617	600	0	6550	-0.00013	0	-0.00013	1.707	-0.1
5800	-150	0.00633	600	0	6400	-0.00014	0	-0.00014	1.707	-0.1
5650	-150	0.00650	600	0	6250	-0.00015	0	-0.00015	1.707	-0.1
5500	-150	0.00668	600	0	6100	-0.00016	0	-0.00016	1.707	-0.1
5350	-150	0.00686	600	0	5950	-0.00016	0	-0.00016	1.708	-0.1
5200	-150	0.00706	600	0	5800	-0.00017	0	-0.00017	1.708	-0.1
5050	-150	0.00727	600	0	5650	-0.00018	0	-0.00018	1.708	-0.1
4900	-150	0.00749	600	0	5500	-0.00019	0	-0.00019	1.708	-0.1
4750	-150	0.00773	600	0	5350	-0.00020	0	-0.00020	1.708	-0.1
4600	-150	0.00798	600	0	5200	-0.00022	0	-0.00022	1.709	-0.2
4450	-150	0.00825	600	0	5050	-0.00023	0	-0.00023	1.709	-0.2
4300	-150	0.00854	600	0	4900	-0.00025	0	-0.00025	1.709	-0.2
4150	-150	0.00885	600	0	4750	-0.00026	0	-0.00026	1.709	-0.2
4000	-150	0.00918	600	0	4600	-0.00028	0	-0.00028	1.710	-0.2
3850	-150	0.00954	600	0	4450	-0.00030	0	-0.00030	1.710	-0.2
3700	-150	0.00992	600	0	4300	-0.00032	0	-0.00032	1.710	-0.2
3550	-150	0.01034	600	0	4150	-0.00035	0	-0.00035	1.711	-0.3
3400	-150	0.01080	600	0	4000	-0.00037	0	-0.00037	1.711	-0.3
3250	-150	0.01129	600	0	3850	-0.00040	0	-0.00040	1.711	-0.3
3100	-150	0.01184	600	0	3700	-0.00044	0	-0.00044	1.712	-0.3
2950	-150	0.01244	600	0	3550	-0.00048	0	-0.00048	1.712	-0.4
2800	-150	0.01311	600	0	3400	-0.00053	0	-0.00053	1.713	-0.4
2650	-150	0.01385	600	0	3250	-0.00058	0	-0.00058	1.713	-0.4
2500	-150	0.01468	600	0	3100	-0.00064	0	-0.00064	1.714	-0.5
2350	-150	0.01562	600	0	2950	-0.00071	0	-0.00071	1.715	-0.5
2200	-150	0.01668	600	0	2800	-0.00079	0	-0.00079	1.716	-0.6
2050	-150	0.01790	600	0	2650	-0.00089	0	-0.00089	1.716	-0.6
1900	-150	0.01932	600	0	2500	-0.00101	0	-0.00101	1.717	-0.7
1750	-150	0.02097	600	0	2350	-0.00116	0	-0.00116	1.719	-0.7
1600	-150	0.02294	600	0	2200	-0.00134	0	-0.00134	1.720	-0.8
1450	-150	0.02531	600	0	2050	-0.00156	0	-0.00156	1.722	-0.9
1300	-150	0.02822	600	0	1900	-0.00185	0	-0.00185	1.723	-1.0
1150	-150	0.03190	600	0	1750	-0.00223	0	-0.00223	1.726	-1.1
1000	-150	0.03668	600	0	1600	-0.00273	0	-0.00273	1.728	-1.3
850	-150	0.04315	600	0	1450	-0.00344	0	-0.00344	1.732	-1.5
700	-150	0.05238	600	0	1300	-0.00446	0	-0.00446	1.736	-1.8
550	-150	0.06664	600	0	1150	-0.00604	0	-0.00604	1.742	-2.1
400	-150	0.09157	600	0	1000	-0.00869	0	-0.00869	1.751	-2.6
250	-150	0.14629	600	0	850	-0.01374	0	-0.01374	1.765	-3.4
100	-150	0.17000	600	0	700	-0.02582	0	-0.02582	1.791	-5.0
0	-100	0.17000	600	0	600	-0.02429	0	-0.02429	1.815	-6.4

SFG modelling for a basement constructed in Lake Agassiz clay (Figure 4.14)

Pathak, Y.P. 2009

degree 17.5 0.305

k0 0.70

Note:
Initial suction uses Thiessen 2010 water content (Fig 3.12) => SWCC L.Ag gets suction data
EOT suction ends at '0' kPa for all tests.
Slide 26 (PPT) Basement wall application in L.Ag

P	σh	Vini	Depth (m)	p	λvp	ssa	Sini	Seot	WC	Pswell	V	eV	soil
10	7	1.752	0.5	10	0.28	140	1500	0	16.3	461		-36.2%	1
20	14	1.751	1.0	20	0.28	140	1200	0	21.1	440		-32.7%	2
30	21	1.750	1.5	30	0.28	140	600	0	31.1	355		-28.6%	3
40	28	1.749	2.0	40	0.28	140	400	0	35.7	311		-25.0%	4
50	35	1.749	2.5	50	0.28	140	250	0	38.9	260		-20.8%	5
60	42	1.748	3.0	60	0.28	140	200	0	40.6	242		-18.0%	6

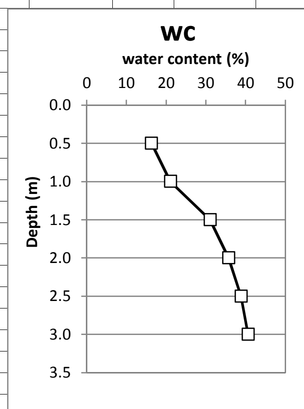

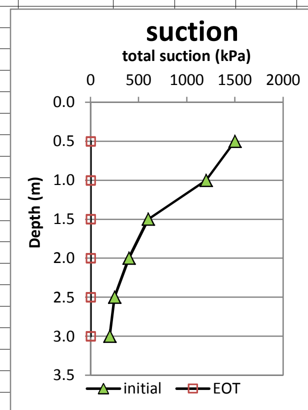

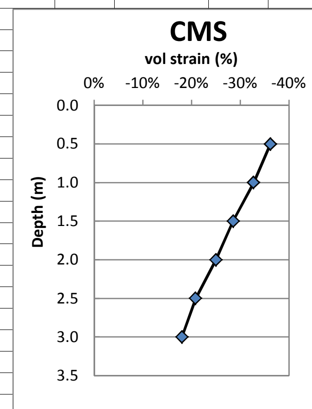

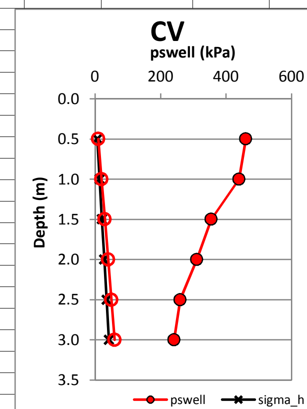

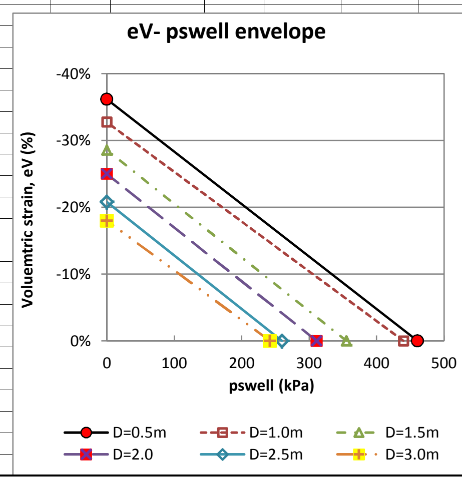

E:\RMC\blim thesis\0Thesis comment\SFG_L.Ag_slide 26.xlsx
opt

26/10/2014

Soil_1 Depth = 0.5 m

CV Module

λvp	0.28	λvs max	0.28	
κvp	0.009	Ps (CV)=	nodata	#VALUE!
s_{sa}	140		461	
p'=	10	ds=	-50	

s (kPa)	ds	λvs	Cal_Pswell	dp	p+s	dv from suction change	dv due to mean stress	dv (total)	cal_V_cv
									#REF!
1500		0.02630	10.0		1510.0			1.752	0.000
1450	-50	0.02721	14.7	4.70	1464.7	-0.00087	-0.00087	0	0.000
1400	-50	0.02818	19.6	4.86	1419.6	-0.00093	-0.00093	0	0.000
1350	-50	0.02922	24.6	5.03	1374.6	-0.00099	-0.00099	0	0.000
1300	-50	0.03035	29.8	5.22	1329.8	-0.00106	-0.00106	0	0.000
1250	-50	0.03156	35.2	5.42	1285.2	-0.00114	-0.00114	0	0.000
1200	-50	0.03287	40.9	5.64	1240.9	-0.00123	-0.00123	0	0.000
1150	-50	0.03430	46.7	5.87	1196.7	-0.00132	-0.00132	0	0.000
1100	-50	0.03586	52.9	6.13	1152.9	-0.00143	-0.00143	0	0.000
1050	-50	0.03756	59.3	6.40	1109.3	-0.00156	-0.00156	0	0.000
1000	-50	0.03944	66.0	6.71	1066.0	-0.00169	-0.00169	0	0.000
950	-50	0.04151	73.0	7.04	1023.0	-0.00185	-0.00185	0	0.000
900	-50	0.04382	80.4	7.41	980.4	-0.00203	-0.00203	0	0.000
850	-50	0.04639	88.2	7.82	938.2	-0.00223	-0.00223	0	0.000
800	-50	0.04929	96.5	8.28	896.5	-0.00247	-0.00247	0	0.000
750	-50	0.05257	105.3	8.80	855.3	-0.00275	-0.00275	0	0.000
700	-50	0.05632	114.7	9.39	814.7	-0.00307	-0.00307	0	0.000
650	-50	0.06065	124.8	10.06	774.8	-0.00346	-0.00346	0	0.000
600	-50	0.06569	135.6	10.83	735.6	-0.00391	-0.00391	0	0.000
550	-50	0.07165	147.3	11.73	697.3	-0.00447	-0.00447	0	0.000
500	-50	0.07880	160.1	12.79	660.1	-0.00514	-0.00514	0	0.000
450	-50	0.08754	174.2	14.07	624.2	-0.00597	-0.00597	0	0.000
400	-50	0.09845	189.8	15.63	589.8	-0.00701	-0.00701	0	0.000
350	-50	0.11248	207.4	17.58	557.4	-0.00835	-0.00835	0	0.000
300	-50	0.13116	227.5	20.09	527.5	-0.01009	-0.01009	0	0.000
250	-50	0.15729	250.9	23.42	500.9	-0.01243	-0.01243	0	0.000
200	-50	0.19642	279.0	28.09	479.0	-0.01570	-0.0157	0	0.000
150	-50	0.26146	314.1	35.07	464.1	-0.02050	-0.0205	0	0.000
100	-50	0.28000	360.8	46.69	460.8	-0.02817	-0.02817	0	0.000
50	-50	0.28000	410.8	50.00	460.8	-0.03038	-0.03038	0	0.000
0	-50	0.28000	460.8	50.00	460.8	-0.03038	-0.03038	0	0.000

CMS module

λvp	0.28	λvs max	0.28	vol_p	-36.2%
κvp	0.009			V_cms_tes	3.032
s_{sa}	140	kPa		EOT_p	2.386
p'=	10	ds=	-50		

s (kPa)	ds	λvs	p	dp	p+s	dv from suction change	dv due to mean stress	dv (total)	cal_V-cms	eV
1500		0.02630	10		1510				1.752	0.0
1450	-50	0.02721	10	0	1460	-0.00087	0	-0.00087	1.753	0.0
1400	-50	0.02818	10	0	1410	-0.00093	0	-0.00093	1.754	-0.1
1350	-50	0.02922	10	0	1360	-0.00100	0	-0.00100	1.755	-0.2
1300	-50	0.03035	10	0	1310	-0.00107	0	-0.00107	1.756	-0.2
1250	-50	0.03156	10	0	1260	-0.00116	0	-0.00116	1.757	-0.3
1200	-50	0.03287	10	0	1210	-0.00125	0	-0.00125	1.758	-0.4
1150	-50	0.03430	10	0	1160	-0.00136	0	-0.00136	1.760	-0.4
1100	-50	0.03586	10	0	1110	-0.00148	0	-0.00148	1.761	-0.5
1050	-50	0.03756	10	0	1060	-0.00162	0	-0.00162	1.763	-0.6
1000	-50	0.03944	10	0	1010	-0.00177	0	-0.00177	1.765	-0.7
950	-50	0.04151	10	0	960	-0.00195	0	-0.00195	1.766	-0.8
900	-50	0.04382	10	0	910	-0.00216	0	-0.00216	1.769	-0.9
850	-50	0.04639	10	0	860	-0.00241	0	-0.00241	1.771	-1.1
800	-50	0.04929	10	0	810	-0.00270	0	-0.00270	1.774	-1.2
750	-50	0.05257	10	0	760	-0.00304	0	-0.00304	1.777	-1.4
700	-50	0.05632	10	0	710	-0.00346	0	-0.00346	1.780	-1.6
650	-50	0.06065	10	0	660	-0.00397	0	-0.00397	1.784	-1.8
600	-50	0.06569	10	0	610	-0.00459	0	-0.00459	1.789	-2.1
550	-50	0.07165	10	0	560	-0.00538	0	-0.00538	1.794	-2.4
500	-50	0.07880	10	0	510	-0.00640	0	-0.00640	1.801	-2.8
450	-50	0.08754	10	0	460	-0.00773	0	-0.00773	1.808	-3.2
400	-50	0.09845	10	0	410	-0.00952	0	-0.00952	1.818	-3.8
350	-50	0.11248	10	0	360	-0.01201	0	-0.01201	1.830	-4.4
300	-50	0.13116	10	0	310	-0.01562	0	-0.01562	1.845	-5.3
250	-50	0.15729	10	0	260	-0.02116	0	-0.02116	1.867	-6.5
200	-50	0.19642	10	0	210	-0.03025	0	-0.03025	1.897	-8.3
150	-50	0.26146	10	0	160	-0.04677	0	-0.04677	1.944	-10.9
100	-50	0.28000	10	0	110	-0.08171	0	-0.08171	2.025	-15.6
50	-50	0.28000	10	0	60	-0.12727	0	-0.12727	2.153	-22.9
0	-50	0.28000	10	0	10	-0.23333	0	-0.23333	2.386	-36.2

Soil_2 Depth = 1 m

CV Module

λvp	0.28	λvs max	0.28	
κvp	0.009	Ps (CV)=	nodata	#VALUE!
s_{sa}	140		440	
p'=	20	ds=	-50	

s (kPa)	ds	λvs	Cal_Pswell	dp	p+s	dv from suction change	dv due to mean stress	dv (total)	cal_V_cv
									#REF!
1200		0.03287	20.0		1220.0			1.751	0.000
1150	-50	0.03430	25.9	5.87	1175.9	-0.00135	-0.00135	0	0.000
1100	-50	0.03586	32.0	6.13	1132.0	-0.00146	-0.00146	0	0.000
1050	-50	0.03756	38.4	6.40	1088.4	-0.00158	-0.00158	0	0.000
1000	-50	0.03944	45.1	6.71	1045.1	-0.00173	-0.00173	0	0.000
950	-50	0.04151	52.1	7.04	1002.1	-0.00189	-0.00189	0	0.000
900	-50	0.04382	59.6	7.41	959.6	-0.00207	-0.00207	0	0.000
850	-50	0.04639	67.4	7.82	917.4	-0.00228	-0.00228	0	0.000
800	-50	0.04929	75.7	8.28	875.7	-0.00253	-0.00253	0	0.000
750	-50	0.05257	84.5	8.80	834.5	-0.00281	-0.00281	0	0.000
700	-50	0.05632	93.9	9.39	793.9	-0.00315	-0.00315	0	0.000
650	-50	0.06065	103.9	10.06	753.9	-0.00355	-0.00355	0	0.000
600	-50	0.06569	114.7	10.83	714.7	-0.00402	-0.00402	0	0.000
550	-50	0.07165	126.5	11.73	676.5	-0.00460	-0.00460	0	0.000
500	-50	0.07880	139.3	12.79	639.3	-0.00530	-0.00530	0	0.000
450	-50	0.08754	153.3	14.07	603.3	-0.00616	-0.00616	0	0.000
400	-50	0.09845	169.0	15.63	569.0	-0.00725	-0.00725	0	0.000
350	-50	0.11248	186.6	17.58	536.6	-0.00865	-0.00865	0	0.000
300	-50	0.13116	206.6	20.09	506.6	-0.01048	-0.01048	0	0.000
250	-50	0.15729	230.1	23.42	480.1	-0.01294	-0.01294	0	0.000
200	-50	0.19642	258.2	28.09	458.2	-0.01638	-0.01638	0	0.000
150	-50	0.26146	293.2	35.07	443.2	-0.02144	-0.02144	0	0.000
100	-50	0.28000	339.9	46.69	439.9	-0.02949	-0.02949	0	0.000
50	-50	0.28000	389.9	50.00	439.9	-0.03182	-0.03182	0	0.000
0	-50	0.28000	439.9	50.00	439.9	-0.03182	-0.03182	0	0.000

CMS module

λvp	0.28	λvs max	0.28	vol_p	-32.7%
κvp	0.009			V_cms_te	3.032
s_{sa}	140	kPa		EOT_p	2.324
p'=	20	ds=	-50		

s (kPa)	ds	λvs	p	dp	p+s	dv from suction change	dv due to mean stress	dv (total)	cal_V-cms	eV
1200		0.03287	20		1220				1.751	0.0
1150	-50	0.03430	20	0	1170	-0.00135	0	-0.00135	1.752	-0.1
1100	-50	0.03586	20	0	1120	-0.00147	0	-0.00147	1.754	-0.2
1050	-50	0.03756	20	0	1070	-0.00160	0	-0.00160	1.755	-0.3
1000	-50	0.03944	20	0	1020	-0.00176	0	-0.00176	1.757	-0.4
950	-50	0.04151	20	0	970	-0.00193	0	-0.00193	1.759	-0.5
900	-50	0.04382	20	0	920	-0.00214	0	-0.00214	1.761	-0.6
850	-50	0.04639	20	0	870	-0.00238	0	-0.00238	1.764	-0.7
800	-50	0.04929	20	0	820	-0.00267	0	-0.00267	1.766	-0.9
750	-50	0.05257	20	0	770	-0.00301	0	-0.00301	1.769	-1.0
700	-50	0.05632	20	0	720	-0.00341	0	-0.00341	1.773	-1.2
650	-50	0.06065	20	0	670	-0.00391	0	-0.00391	1.777	-1.5
600	-50	0.06569	20	0	620	-0.00453	0	-0.00453	1.781	-1.7
550	-50	0.07165	20	0	570	-0.00530	0	-0.00530	1.786	-2.0
500	-50	0.07880	20	0	520	-0.00629	0	-0.00629	1.793	-2.4
450	-50	0.08754	20	0	470	-0.00758	0	-0.00758	1.800	-2.8
400	-50	0.09845	20	0	420	-0.00931	0	-0.00931	1.810	-3.3
350	-50	0.11248	20	0	370	-0.01172	0	-0.01172	1.821	-4.0
300	-50	0.13116	20	0	320	-0.01520	0	-0.01520	1.837	-4.9
250	-50	0.15729	20	0	270	-0.02049	0	-0.02049	1.857	-6.1
200	-50	0.19642	20	0	220	-0.02913	0	-0.02913	1.886	-7.7
150	-50	0.26146	20	0	170	-0.04464	0	-0.04464	1.931	-10.3
100	-50	0.28000	20	0	120	-0.07690	0	-0.07690	2.008	-14.7
50	-50	0.28000	20	0	70	-0.11667	0	-0.11667	2.124	-21.3
0	-50	0.28000	20	0	20	-0.20000	0	-0.20000	2.324	-32.7

Soil_3 Depth = 1.5 m

CV Module

λvp	0.28	λvs max	0.28						
κvp	0.009	Ps (CV)=	nodata	#VALUE!					
s_{sa}	140		355						
p'=	30	ds=	-50						#REF!
s (kPa)	ds	λvs	Cal_Pswell	dp	p+s	dv from suction change	dv due to mean stress	dv (total)	cal_V_cv
600		0.06569	30.0		630.0			1.750	-0.151
550	-50	0.07165	41.7	11.73	591.7	-0.00521	-0.00521	0	-0.151
500	-50	0.07880	54.5	12.79	554.5	-0.00605	-0.00605	0	-0.151
450	-50	0.08754	68.6	14.07	518.6	-0.00711	-0.00711	0	-0.151
400	-50	0.09845	84.2	15.63	484.2	-0.00844	-0.00844	0	-0.151
350	-50	0.11248	101.8	17.58	451.8	-0.01017	-0.01017	0	-0.151
300	-50	0.13116	121.9	20.09	421.9	-0.01245	-0.01245	0	-0.151
250	-50	0.15729	145.3	23.42	395.3	-0.01554	-0.01554	0	-0.151
200	-50	0.19642	173.4	28.09	373.4	-0.01989	-0.01989	0	-0.151
150	-50	0.26146	208.5	35.07	358.5	-0.02630	-0.02630	0	-0.151
100	-50	0.28000	255.2	46.69	355.2	-0.03647	-0.03647	0	-0.151
50	-50	0.28000	305.2	50.00	355.2	-0.03942	-0.03942	0	-0.151
0	-50	0.28000	355.2	50.00	355.2	-0.03942	-0.03942	0	-0.151

CMS module

λvp	0.28	λvs max	0.28						vol_p	-28.6%
κvp	0.009								V_cms_tes	3.032
s_{sa}	140	kPa							EOT_p	2.250
p'=	30	ds=	-50							
s (kPa)	ds	λvs	p	dp	p+s	dv from suction change	dv due to mean stress	dv (total)	cal_V-cms	eV
600		0.06569	30		630				1.750	0.0
550	-50	0.07165	30	0	580	-0.00521	0	-0.00521	1.755	-0.3
500	-50	0.07880	30	0	530	-0.00618	0	-0.00618	1.762	-0.7
450	-50	0.08754	30	0	480	-0.00743	0	-0.00743	1.769	-1.1
400	-50	0.09845	30	0	430	-0.00912	0	-0.00912	1.778	-1.6
350	-50	0.11248	30	0	380	-0.01145	0	-0.01145	1.790	-2.3
300	-50	0.13116	30	0	330	-0.01480	0	-0.01480	1.804	-3.1
250	-50	0.15729	30	0	280	-0.01987	0	-0.01987	1.824	-4.2
200	-50	0.19642	30	0	230	-0.02809	0	-0.02809	1.852	-5.8
150	-50	0.26146	30	0	180	-0.04270	0	-0.04270	1.895	-8.3
100	-50	0.28000	30	0	130	-0.07263	0	-0.07263	1.968	-12.4
50	-50	0.28000	30	0	80	-0.10769	0	-0.10769	2.075	-18.6
0	-50	0.28000	30	0	30	-0.17500	0	-0.17500	2.250	-28.6

Soil_4 Depth = 2.0 m

CV Module

λvp	0.28	λvs max	0.28						
κvp	0.009	Ps (CV)=	nodata	#VALUE!					
s_{sa}	140		311						
p'=	40	ds=	-50						#REF!
s (kPa)	ds	λvs	Cal_Pswell	dp	p+s	dv from suction change	dv due to mean stress	dv (total)	cal_V_cv
400		0.09845	40.0		440.0			1.749	-0.156
350	-50	0.11248	57.6	17.58	407.6	-0.01119	-0.01119	0	-0.156
300	-50	0.13116	77.7	20.09	377.7	-0.01380	-0.01380	0	-0.156
250	-50	0.15729	101.1	23.42	351.1	-0.01736	-0.01736	0	-0.156
200	-50	0.19642	129.2	28.09	329.2	-0.02240	-0.02240	0	-0.156
150	-50	0.26146	164.3	35.07	314.3	-0.02983	-0.02983	0	-0.156
100	-50	0.28000	210.9	46.69	310.9	-0.04160	-0.04160	0	-0.156
50	-50	0.28000	260.9	50.00	310.9	-0.04502	-0.04502	0	-0.156
0	-50	0.28000	310.9	50.00	310.9	-0.04502	-0.04502	0	-0.156

CMS module

λvp	0.28	λvs max	0.28						vol_p	-25.0%
κvp	0.009								V_cms_tes	3.032
s_{sa}	140	kPa							EOT_p	2.187
p'=	40	ds=	-50							
s (kPa)	ds	λvs	p	dp	p+s	dv from suction change	dv due to mean stress	dv (total)	cal_V-cms	eV
400		0.09845	40		440				1.749	0.0
350	-50	0.11248	40	0	390	-0.01119	0	-0.01119	1.761	-0.6
300	-50	0.13116	40	0	340	-0.01442	0	-0.01442	1.775	-1.5
250	-50	0.15729	40	0	290	-0.01929	0	-0.01929	1.794	-2.6
200	-50	0.19642	40	0	240	-0.02712	0	-0.02712	1.821	-4.1
150	-50	0.26146	40	0	190	-0.04092	0	-0.04092	1.862	-6.5
100	-50	0.28000	40	0	140	-0.06880	0	-0.06880	1.931	-10.4
50	-50	0.28000	40	0	90	-0.10000	0	-0.10000	2.031	-16.1
0	-50	0.28000	40	0	40	-0.15556	0	-0.15556	2.187	-25.0

Soil_5 Depth = 2.5 m

CV Module

λvp	0.28	λvs max	0.28	
κvp	0.009	Ps (CV)=	nodata	#VALUE!
s_{sa}	140		260	
p'=	50	ds=	-50	

s (kPa)	ds	λvs	Cal_Pswell	dp	p+s	dv from suction change	dv due to mean stress	dv (total)	cal_V_cv
									#REF!
250		0.15729	50.0		300.0			1.749	-0.166
200	-50	0.19642	78.1	28.09	278.1	-0.02622	-0.02622	0	-0.166
150	-50	0.26146	113.2	35.07	263.2	-0.03532	-0.03532	0	-0.166
100	-50	0.28000	159.9	46.69	259.9	-0.04968	-0.04968	0	-0.166
50	-50	0.28000	209.9	50.00	259.9	-0.05388	-0.05388	0	-0.166
0	-50	0.28000	259.9	50.00	259.9	-0.05388	-0.05388	0	-0.166

CMS module

λvp	0.28	λvs max	0.28	vol_p	-20.8%
κvp	0.009			V_cms_tes	3.032
s_{sa}	140	kPa		EOT_p	2.113
p'=	50	ds=	-50		

s (kPa)	ds	λvs	p	dp	p+s	dv from suction change	dv due to mean stress	dv (total)	cal_V-cms	eV
250		0.15729	50		300				1.749	0.0
200	-50	0.19642	50	0	250	-0.02622	0	-0.02622	1.775	-1.5
150	-50	0.26146	50	0	200	-0.03928	0	-0.03928	1.814	-3.7
100	-50	0.28000	50	0	150	-0.06536	0	-0.06536	1.879	-7.5
50	-50	0.28000	50	0	100	-0.09333	0	-0.09333	1.973	-12.8
0	-50	0.28000	50	0	50	-0.14000	0	-0.14000	2.113	-20.8

Soil_6 Depth = 3.0 m

CV Module

λvp	0.28	λvs max	0.28						
κvp	0.009	Ps (CV)=	nodata	#VALUE!					
s_{sa}	140		242						
p'=	60	ds=	-50						#REF!
s (kPa)	ds	λvs	Cal_Pswell	dp	p+s	dv from suction change	dv due to mean stress	dv (total)	cal_V_cv
200		0.19642	60.0		260.0			1.748	-0.409
150	-50	0.26146	95.1	35.07	245.1	-0.03777	-0.03777	0	-0.409
100	-50	0.28000	141.8	46.69	241.8	-0.05334	-0.05334	0	-0.409
50	-50	0.28000	191.8	50.00	241.8	-0.05791	-0.05791	0	-0.409
0	-50	0.28000	241.8	50.00	241.8	-0.05791	-0.05791	0	-0.409

CMS module

λvp	0.28	λvs max	0.28						vol_p	-18.0%
κvp	0.009								V_cms_tes	3.032
s_{sa}	140	kPa							EOT_p	2.063
p'=	60	ds=	-50							
s (kPa)	ds	λvs	p	dp	p+s	dv from suction change	dv due to mean stress	dv (total)	cal_V-cms	eV
200		0.19642	60		260				1.748	0.0
150	-50	0.26146	60	0	210	-0.03777	0	-0.03777	1.786	-2.2
100	-50	0.28000	60	0	160	-0.06225	0	-0.06225	1.848	-5.7
50	-50	0.28000	60	0	110	-0.08750	0	-0.08750	1.935	-10.7
0	-50	0.28000	60	0	60	-0.12727	0	-0.12727	2.063	-18.0

APPENDIX J - SFG MODELLING SPREADSHEET FOR BSB

	SFG model and SEL experimental data- BSB										
	SFG model input			SEL test data			SFG prediction			Δ difference	
	p	λvp	ssa	Pswell	V	eV	Pswell	V	eV	Pswell, kPa	ev, %
b	250	0.55	320	915	1.8856	-17.3%	917	1.862	-17.4%	2	-0.1%
a	250	0.21	245	915	1.886	-17.3%	761	1.666	-5.1%	-154	12.2%
	500	0.21	245	980	1.621	-5.1%	993	1.599	-4.2%	13	0.9%
	1000	0.21	245	1440	1.538	-2.5%	1450	1.552	-3.1%	10	-0.5%
	1500	0.21	245	1905	1.476	-0.9%	1899	1.488	-2.3%	-6	-1.4%

Test_a: 250_a

CV Module

λvp	0.21	λvs max	0.21						
κvp	0.009	Ps (CV)=	915	-16.8%					
s_{sa}	245		761						
p'=	250	ds=	-50						1.585
s (kPa)	ds	λvs	Cal_Pswell	dp	p+s	dv from suction change	dv due to mean stress	dv (total)	cal_V_cv
3377		0.01529	250.0		3627.2				1.585
3327	-50	0.01552	253.6	3.64	3580.8	-0.00021	-0.00021	0	1.585
3277	-50	0.01576	257.3	3.70	3534.5	-0.00022	-0.00022	0	1.585
3227	-50	0.01600	261.1	3.75	3488.3	-0.00022	-0.00022	0	1.585
3177	-50	0.01625	264.9	3.81	3442.1	-0.00023	-0.00023	0	1.585
3127	-50	0.01651	268.8	3.87	3396.0	-0.00024	-0.00024	0	1.585
3077	-50	0.01678	272.7	3.93	3349.9	-0.00024	-0.00024	0	1.585
3027	-50	0.01706	276.7	4.00	3303.9	-0.00025	-0.00025	0	1.585
2977	-50	0.01735	280.8	4.06	3258.0	-0.00026	-0.00026	0	1.585
2927	-50	0.01764	284.9	4.13	3212.1	-0.00027	-0.00027	0	1.585
2877	-50	0.01795	289.1	4.20	3166.3	-0.00027	-0.00027	0	1.585
2827	-50	0.01827	293.4	4.27	3120.6	-0.00028	-0.00028	0	1.585
2777	-50	0.01859	297.7	4.35	3074.9	-0.00029	-0.00029	0	1.585
2727	-50	0.01894	302.1	4.43	3029.3	-0.00030	-0.0003	0	1.585
2677	-50	0.01929	306.6	4.51	2983.8	-0.00031	-0.00031	0	1.585
2627	-50	0.01966	311.2	4.59	2938.4	-0.00032	-0.00032	0	1.585
2577	-50	0.02004	315.9	4.68	2893.1	-0.00033	-0.00033	0	1.585
2527	-50	0.02043	320.7	4.77	2847.9	-0.00035	-0.00035	0	1.585
2477	-50	0.02085	325.6	4.87	2802.8	-0.00036	-0.00036	0	1.585
2427	-50	0.02128	330.5	4.96	2757.7	-0.00037	-0.00037	0	1.585
2377	-50	0.02172	335.6	5.07	2712.8	-0.00039	-0.00039	0	1.585
2327	-50	0.02219	340.8	5.17	2668.0	-0.00040	-0.0004	0	1.585
2277	-50	0.02268	346.0	5.28	2623.2	-0.00042	-0.00042	0	1.585
2227	-50	0.02318	351.4	5.40	2578.6	-0.00043	-0.00043	0	1.585
2177	-50	0.02372	357.0	5.52	2534.2	-0.00045	-0.00045	0	1.585
2127	-50	0.02427	362.6	5.65	2489.8	-0.00047	-0.00047	0	1.585
2077	-50	0.02486	368.4	5.78	2445.6	-0.00049	-0.00049	0	1.585
2027	-50	0.02547	374.3	5.92	2401.5	-0.00051	-0.00051	0	1.585
1977	-50	0.02611	380.4	6.06	2357.6	-0.00053	-0.00053	0	1.585
1927	-50	0.02679	386.6	6.22	2313.8	-0.00055	-0.00055	0	1.585
1877	-50	0.02751	393.0	6.38	2270.2	-0.00058	-0.00058	0	1.585
1827	-50	0.02826	399.5	6.55	2226.7	-0.00061	-0.00061	0	1.585
1777	-50	0.02905	406.2	6.73	2183.4	-0.00063	-0.00063	0	1.585
1727	-50	0.02989	413.2	6.92	2140.4	-0.00067	-0.00067	0	1.585
1677	-50	0.03078	420.3	7.12	2097.5	-0.00070	-0.0007	0	1.585
1627	-50	0.03173	427.6	7.33	2054.8	-0.00073	-0.00073	0	1.585
1577	-50	0.03273	435.2	7.55	2012.4	-0.00077	-0.00077	0	1.585
1527	-50	0.03380	443.0	7.79	1970.2	-0.00081	-0.00081	0	1.585
1477	-50	0.03495	451.0	8.05	1928.2	-0.00086	-0.00086	0	1.585
1427	-50	0.03617	459.3	8.32	1886.5	-0.00091	-0.00091	0	1.585
1377	-50	0.03748	467.9	8.61	1845.1	-0.00096	-0.00096	0	1.585
1327	-50	0.03889	476.9	8.92	1804.1	-0.00102	-0.00102	0	1.585
1277	-50	0.04042	486.1	9.26	1763.3	-0.00108	-0.00108	0	1.585
1227	-50	0.04206	495.7	9.62	1722.9	-0.00115	-0.00115	0	1.585
1177	-50	0.04385	505.8	10.01	1683.0	-0.00122	-0.00122	0	1.585
1127	-50	0.04579	516.2	10.44	1643.4	-0.00130	-0.0013	0	1.585
1077	-50	0.04791	527.1	10.90	1604.3	-0.00139	-0.00139	0	1.585
1027	-50	0.05024	538.5	11.41	1565.7	-0.00149	-0.00149	0	1.585
977	-50	0.05281	550.5	11.96	1527.7	-0.00160	-0.0016	0	1.585
927	-50	0.05566	563.0	12.57	1490.2	-0.00173	-0.00173	0	1.585
877	-50	0.05882	576.3	13.25	1453.5	-0.00187	-0.00187	0	1.585
827	-50	0.06238	590.3	14.01	1417.5	-0.00202	-0.00202	0	1.585
777	-50	0.06638	605.2	14.85	1382.4	-0.00220	-0.0022	0	1.585
727	-50	0.07094	621.0	15.81	1348.2	-0.00240	-0.0024	0	1.585
677	-50	0.07617	637.9	16.89	1315.1	-0.00263	-0.00263	0	1.585
627	-50	0.08223	656.0	18.14	1283.2	-0.00290	-0.0029	0	1.585
577	-50	0.08935	675.6	19.58	1252.8	-0.00320	-0.0032	0	1.585
527	-50	0.09780	696.8	21.27	1224.0	-0.00357	-0.00357	0	1.585
477	-50	0.10803	720.1	23.29	1197.3	-0.00400	-0.004	0	1.585
427	-50	0.12064	745.8	25.72	1173.0	-0.00451	-0.00451	0	1.585
400	-27	0.12876	761.4	15.51	1161.6	-0.00278	-0.00278	0	1.585

CMS module

λvp	0.21	λvs max	0.21						vol_p	-5.1%
κvp	0.009								V_cms_te:	1.886
s_{sa}	245								EOT_p	1.666
p'=	250	ds=	-50							
s (kPa)	ds	λvs	p	dp	p+s	dv from suction change	dv due to mean stress	dv (total)	cal_V-cms	eV
3377		0.01529	250		3627.2				1.585	0.0
3327	-50	0.01552	250	0	3577	-0.00021	0	-0.00021	1.586	0.0
3277	-50	0.01576	250	0	3527.2	-0.00022	0	-0.00022	1.586	0.0
3227	-50	0.01600	250	0	3477.2	-0.00022	0	-0.00022	1.586	0.0
3177	-50	0.01625	250	0	3427.2	-0.00023	0	-0.00023	1.586	-0.1
3127	-50	0.01651	250	0	3377.2	-0.00024	0	-0.00024	1.587	-0.1
3077	-50	0.01678	250	0	3327.2	-0.00024	0	-0.00024	1.587	-0.1
3027	-50	0.01706	250	0	3277.2	-0.00025	0	-0.00025	1.587	-0.1
2977	-50	0.01735	250	0	3227.2	-0.00026	0	-0.00026	1.587	-0.1
2927	-50	0.01764	250	0	3177.2	-0.00027	0	-0.00027	1.588	-0.1
2877	-50	0.01795	250	0	3127.2	-0.00028	0	-0.00028	1.588	-0.2
2827	-50	0.01827	250	0	3077.2	-0.00029	0	-0.00029	1.588	-0.2
2777	-50	0.01859	250	0	3027.2	-0.00030	0	-0.00030	1.588	-0.2
2727	-50	0.01894	250	0	2977.2	-0.00031	0	-0.00031	1.589	-0.2
2677	-50	0.01929	250	0	2927.2	-0.00032	0	-0.00032	1.589	-0.2
2627	-50	0.01966	250	0	2877.2	-0.00033	0	-0.00033	1.589	-0.2
2577	-50	0.02004	250	0	2827.2	-0.00034	0	-0.00034	1.590	-0.3
2527	-50	0.02043	250	0	2777.2	-0.00035	0	-0.00035	1.590	-0.3
2477	-50	0.02085	250	0	2727.2	-0.00037	0	-0.00037	1.590	-0.3
2427	-50	0.02128	250	0	2677.2	-0.00038	0	-0.00038	1.591	-0.3
2377	-50	0.02172	250	0	2627.2	-0.00040	0	-0.00040	1.591	-0.4
2327	-50	0.02219	250	0	2577.2	-0.00041	0	-0.00041	1.592	-0.4
2277	-50	0.02268	250	0	2527.2	-0.00043	0	-0.00043	1.592	-0.4
2227	-50	0.02318	250	0	2477.2	-0.00045	0	-0.00045	1.592	-0.4
2177	-50	0.02372	250	0	2427.2	-0.00047	0	-0.00047	1.593	-0.5
2127	-50	0.02427	250	0	2377.2	-0.00049	0	-0.00049	1.593	-0.5
2077	-50	0.02486	250	0	2327.2	-0.00051	0	-0.00051	1.594	-0.5
2027	-50	0.02547	250	0	2277.2	-0.00053	0	-0.00053	1.594	-0.6
1977	-50	0.02611	250	0	2227.2	-0.00056	0	-0.00056	1.595	-0.6
1927	-50	0.02679	250	0	2177.2	-0.00059	0	-0.00059	1.596	-0.6
1877	-50	0.02751	250	0	2127.2	-0.00062	0	-0.00062	1.596	-0.7
1827	-50	0.02826	250	0	2077.2	-0.00065	0	-0.00065	1.597	-0.7
1777	-50	0.02905	250	0	2027.2	-0.00068	0	-0.00068	1.598	-0.8
1727	-50	0.02989	250	0	1977.2	-0.00072	0	-0.00072	1.598	-0.8
1677	-50	0.03078	250	0	1927.2	-0.00076	0	-0.00076	1.599	-0.9
1627	-50	0.03173	250	0	1877.2	-0.00080	0	-0.00080	1.600	-0.9
1577	-50	0.03273	250	0	1827.2	-0.00085	0	-0.00085	1.601	-1.0
1527	-50	0.03380	250	0	1777.2	-0.00090	0	-0.00090	1.602	-1.0
1477	-50	0.03495	250	0	1727.2	-0.00095	0	-0.00095	1.603	-1.1
1427	-50	0.03617	250	0	1677.2	-0.00101	0	-0.00101	1.604	-1.1
1377	-50	0.03748	250	0	1627.2	-0.00108	0	-0.00108	1.605	-1.2
1327	-50	0.03889	250	0	1577.2	-0.00115	0	-0.00115	1.606	-1.3
1277	-50	0.04042	250	0	1527.2	-0.00123	0	-0.00123	1.607	-1.4
1227	-50	0.04206	250	0	1477.2	-0.00132	0	-0.00132	1.608	-1.4
1177	-50	0.04385	250	0	1427.2	-0.00142	0	-0.00142	1.610	-1.5
1127	-50	0.04579	250	0	1377.2	-0.00154	0	-0.00154	1.611	-1.6
1077	-50	0.04791	250	0	1327.2	-0.00166	0	-0.00166	1.613	-1.7
1027	-50	0.05024	250	0	1277.2	-0.00181	0	-0.00181	1.615	-1.9
977	-50	0.05281	250	0	1227.2	-0.00197	0	-0.00197	1.617	-2.0
927	-50	0.05566	250	0	1177.2	-0.00215	0	-0.00215	1.619	-2.1
877	-50	0.05882	250	0	1127.2	-0.00236	0	-0.00236	1.621	-2.3
827	-50	0.06238	250	0	1077.2	-0.00261	0	-0.00261	1.624	-2.4
777	-50	0.06638	250	0	1027.2	-0.00290	0	-0.00290	1.627	-2.6
727	-50	0.07094	250	0	977.2	-0.00323	0	-0.00323	1.630	-2.8
677	-50	0.07617	250	0	927.2	-0.00363	0	-0.00363	1.634	-3.0
627	-50	0.08223	250	0	877.2	-0.00411	0	-0.00411	1.638	-3.3
577	-50	0.08935	250	0	827.2	-0.00469	0	-0.00469	1.642	-3.6
527	-50	0.09780	250	0	777.2	-0.00540	0	-0.00540	1.648	-3.9
477	-50	0.10803	250	0	727.2	-0.00629	0	-0.00629	1.654	-4.3
427	-50	0.12064	250	0	677.2	-0.00743	0	-0.00743	1.662	-4.8
400	-27	0.12876	250	0	650.2	-0.00481	0	-0.00481	1.666	-5.1

Test_b: 250_b => different lvp from other tests

CV Module

λvp	0.55	λvs max	0.55						
κvp	0.009	Ps (CV)=	915	0.2%					
s_{sa}	320		917						
p'=	250	ds=	-50			-0.20020			1.585
s (kPa)	ds	λvs	Cal_Psw ell	dp	p+s	dv from suction change	dv due to mean stress	dv (total)	cal_V_cv
3377		0.05226	250.0		3627.2				1.585
3327	-50	0.05305	254.8	4.75	3582.0	-0.00072	-0.00072	0.00000	1.585
3277	-50	0.05386	259.6	4.82	3536.8	-0.00074	-0.00074	0	1.585
3227	-50	0.05469	264.5	4.90	3491.7	-0.00076	-0.00076	0	1.585
3177	-50	0.05555	269.4	4.97	3446.6	-0.00078	-0.00078	0	1.585
3127	-50	0.05644	274.5	5.05	3401.7	-0.00081	-0.00081	0	1.585
3077	-50	0.05735	279.6	5.13	3356.8	-0.00083	-0.00083	0	1.585
3027	-50	0.05830	284.8	5.21	3312.0	-0.00085	-0.00085	0	1.585
2977	-50	0.05928	290.1	5.30	3267.3	-0.00088	-0.00088	0	1.585
2927	-50	0.06029	295.5	5.39	3222.7	-0.00091	-0.00091	0	1.585
2877	-50	0.06134	301.0	5.48	3178.2	-0.00094	-0.00094	0	1.585
2827	-50	0.06242	306.6	5.58	3133.8	-0.00097	-0.00097	0	1.585
2777	-50	0.06355	312.3	5.67	3089.5	-0.00100	-0.001	0	1.585
2727	-50	0.06471	318.0	5.78	3045.2	-0.00103	-0.00103	0	1.585
2677	-50	0.06592	323.9	5.88	3001.1	-0.00106	-0.00106	0	1.585
2627	-50	0.06718	329.9	5.99	2957.1	-0.00110	-0.0011	0	1.585
2577	-50	0.06848	336.0	6.11	2913.2	-0.00114	-0.00114	0	1.585
2527	-50	0.06983	342.2	6.23	2869.4	-0.00118	-0.00118	0	1.585
2477	-50	0.07124	348.6	6.35	2825.8	-0.00122	-0.00122	0	1.585
2427	-50	0.07271	355.1	6.48	2782.3	-0.00126	-0.00126	0	1.585
2377	-50	0.07424	361.7	6.61	2738.9	-0.00131	-0.00131	0	1.585
2327	-50	0.07583	368.4	6.75	2695.6	-0.00136	-0.00136	0	1.585
2277	-50	0.07750	375.3	6.89	2652.5	-0.00141	-0.00141	0	1.585
2227	-50	0.07923	382.4	7.05	2609.6	-0.00146	-0.00146	0	1.585
2177	-50	0.08105	389.6	7.20	2566.8	-0.00152	-0.00152	0	1.585
2127	-50	0.08296	396.9	7.37	2524.1	-0.00158	-0.00158	0	1.585
2077	-50	0.08495	404.5	7.54	2481.7	-0.00164	-0.00164	0	1.585
2027	-50	0.08705	412.2	7.72	2439.4	-0.00171	-0.00171	0	1.585
1977	-50	0.08925	420.1	7.91	2397.3	-0.00178	-0.00178	0	1.585
1927	-50	0.09156	428.2	8.11	2355.4	-0.00186	-0.00186	0	1.585
1877	-50	0.09400	436.6	8.32	2313.8	-0.00194	-0.00194	0	1.585
1827	-50	0.09657	445.1	8.55	2272.3	-0.00203	-0.00203	0	1.585
1777	-50	0.09929	453.9	8.78	2231.1	-0.00212	-0.00212	0	1.585
1727	-50	0.10216	462.9	9.03	2190.1	-0.00223	-0.00223	0	1.585
1677	-50	0.10520	472.2	9.29	2149.4	-0.00233	-0.00233	0	1.585
1627	-50	0.10843	481.8	9.56	2109.0	-0.00245	-0.00245	0	1.585
1577	-50	0.11187	491.6	9.86	2068.8	-0.00257	-0.00257	0	1.585
1527	-50	0.11553	501.8	10.17	2029.0	-0.00270	-0.0027	0	1.585
1477	-50	0.11944	512.3	10.50	1989.5	-0.00285	-0.00285	0	1.585
1427	-50	0.12362	523.1	10.86	1950.3	-0.00300	-0.003	0	1.585
1377	-50	0.12810	534.4	11.24	1911.6	-0.00317	-0.00317	0	1.585
1327	-50	0.13292	546.0	11.65	1873.2	-0.00335	-0.00335	0	1.585
1277	-50	0.13812	558.1	12.08	1835.3	-0.00355	-0.00355	0	1.585
1227	-50	0.14375	570.7	12.56	1797.9	-0.00376	-0.00376	0	1.585
1177	-50	0.14985	583.7	13.07	1760.9	-0.00400	-0.004	0	1.585
1127	-50	0.15649	597.4	13.62	1724.6	-0.00425	-0.00425	0	1.585
1077	-50	0.16375	611.6	14.23	1688.8	-0.00454	-0.00454	0	1.585
1027	-50	0.17171	626.5	14.89	1653.7	-0.00485	-0.00485	0	1.585
977	-50	0.18048	642.1	15.61	1619.3	-0.00519	-0.00519	0	1.585
927	-50	0.19021	658.5	16.41	1585.7	-0.00557	-0.00557	0	1.585
877	-50	0.20104	675.8	17.29	1553.0	-0.00600	-0.006	0	1.585
827	-50	0.21317	694.1	18.28	1521.3	-0.00647	-0.00647	0	1.585
777	-50	0.22687	713.4	19.38	1490.6	-0.00701	-0.00701	0	1.585
727	-50	0.24245	734.1	20.62	1461.3	-0.00761	-0.00761	0	1.585
677	-50	0.26032	756.1	22.04	1433.3	-0.00830	-0.0083	0	1.585
627	-50	0.28104	779.8	23.67	1407.0	-0.00908	-0.00908	0	1.585
577	-50	0.30534	805.3	25.55	1382.5	-0.00999	-0.00999	0	1.585
527	-50	0.33425	833.1	27.76	1360.3	-0.01104	-0.01104	0	1.585
477	-50	0.36920	863.5	30.39	1340.7	-0.01229	-0.01229	0	1.585
427	-50	0.41231	897.0	33.56	1324.2	-0.01377	-0.01377	0	1.585
400	-27	0.44005	917.3	20.24	1317.5	-0.00841	-0.00841	0	1.585

CMS module

λvp	0.55	λvs max	0.55						vol_p	-17.4%
κvp	0.009								V_cms_te:	1.886
s_{sa}	320								EOT_p	1.862
p'=	250	ds=	-50			-0.27664				
s (kPa)	ds	λvs	p	dp	p+s	dv from suction change	dv due to mean stress	dv (total)	cal_V-cms	eV
3377		0.05226	250		3627.2				1.585	0.0
3327	-50	0.05305	250	0	3577	-0.00072	0	-0.00072	1.586	0.0
3277	-50	0.05386	250	0	3527.2	-0.00074	0	-0.00074	1.587	-0.1
3227	-50	0.05469	250	0	3477.2	-0.00076	0	-0.00076	1.588	-0.1
3177	-50	0.05555	250	0	3427.2	-0.00079	0	-0.00079	1.588	-0.2
3127	-50	0.05644	250	0	3377.2	-0.00081	0	-0.00081	1.589	-0.2
3077	-50	0.05735	250	0	3327.2	-0.00084	0	-0.00084	1.590	-0.3
3027	-50	0.05830	250	0	3277.2	-0.00086	0	-0.00086	1.591	-0.3
2977	-50	0.05928	250	0	3227.2	-0.00089	0	-0.00089	1.592	-0.4
2927	-50	0.06029	250	0	3177.2	-0.00092	0	-0.00092	1.593	-0.5
2877	-50	0.06134	250	0	3127.2	-0.00095	0	-0.00095	1.594	-0.5
2827	-50	0.06242	250	0	3077.2	-0.00098	0	-0.00098	1.595	-0.6
2777	-50	0.06355	250	0	3027.2	-0.00101	0	-0.00101	1.596	-0.6
2727	-50	0.06471	250	0	2977.2	-0.00105	0	-0.00105	1.597	-0.7
2677	-50	0.06592	250	0	2927.2	-0.00109	0	-0.00109	1.598	-0.8
2627	-50	0.06718	250	0	2877.2	-0.00113	0	-0.00113	1.599	-0.9
2577	-50	0.06848	250	0	2827.2	-0.00117	0	-0.00117	1.600	-0.9
2527	-50	0.06983	250	0	2777.2	-0.00121	0	-0.00121	1.601	-1.0
2477	-50	0.07124	250	0	2727.2	-0.00126	0	-0.00126	1.603	-1.1
2427	-50	0.07271	250	0	2677.2	-0.00131	0	-0.00131	1.604	-1.2
2377	-50	0.07424	250	0	2627.2	-0.00136	0	-0.00136	1.605	-1.3
2327	-50	0.07583	250	0	2577.2	-0.00141	0	-0.00141	1.607	-1.3
2277	-50	0.07750	250	0	2527.2	-0.00147	0	-0.00147	1.608	-1.4
2227	-50	0.07923	250	0	2477.2	-0.00153	0	-0.00153	1.610	-1.5
2177	-50	0.08105	250	0	2427.2	-0.00160	0	-0.00160	1.611	-1.6
2127	-50	0.08296	250	0	2377.2	-0.00167	0	-0.00167	1.613	-1.7
2077	-50	0.08495	250	0	2327.2	-0.00174	0	-0.00174	1.615	-1.8
2027	-50	0.08705	250	0	2277.2	-0.00183	0	-0.00183	1.616	-2.0
1977	-50	0.08925	250	0	2227.2	-0.00191	0	-0.00191	1.618	-2.1
1927	-50	0.09156	250	0	2177.2	-0.00200	0	-0.00200	1.620	-2.2
1877	-50	0.09400	250	0	2127.2	-0.00210	0	-0.00210	1.623	-2.3
1827	-50	0.09657	250	0	2077.2	-0.00221	0	-0.00221	1.625	-2.5
1777	-50	0.09929	250	0	2027.2	-0.00232	0	-0.00232	1.627	-2.6
1727	-50	0.10216	250	0	1977.2	-0.00245	0	-0.00245	1.629	-2.8
1677	-50	0.10520	250	0	1927.2	-0.00258	0	-0.00258	1.632	-2.9
1627	-50	0.10843	250	0	1877.2	-0.00273	0	-0.00273	1.635	-3.1
1577	-50	0.11187	250	0	1827.2	-0.00289	0	-0.00289	1.638	-3.3
1527	-50	0.11553	250	0	1777.2	-0.00306	0	-0.00306	1.641	-3.5
1477	-50	0.11944	250	0	1727.2	-0.00325	0	-0.00325	1.644	-3.7
1427	-50	0.12362	250	0	1677.2	-0.00346	0	-0.00346	1.647	-3.9
1377	-50	0.12810	250	0	1627.2	-0.00369	0	-0.00369	1.651	-4.1
1327	-50	0.13292	250	0	1577.2	-0.00394	0	-0.00394	1.655	-4.4
1277	-50	0.13812	250	0	1527.2	-0.00421	0	-0.00421	1.659	-4.7
1227	-50	0.14375	250	0	1477.2	-0.00452	0	-0.00452	1.664	-4.9
1177	-50	0.14985	250	0	1427.2	-0.00487	0	-0.00487	1.669	-5.3
1127	-50	0.15649	250	0	1377.2	-0.00525	0	-0.00525	1.674	-5.6
1077	-50	0.16375	250	0	1327.2	-0.00568	0	-0.00568	1.680	-5.9
1027	-50	0.17171	250	0	1277.2	-0.00617	0	-0.00617	1.686	-6.3
977	-50	0.18048	250	0	1227.2	-0.00672	0	-0.00672	1.693	-6.8
927	-50	0.19021	250	0	1177.2	-0.00735	0	-0.00735	1.700	-7.2
877	-50	0.20104	250	0	1127.2	-0.00808	0	-0.00808	1.708	-7.7
827	-50	0.21317	250	0	1077.2	-0.00892	0	-0.00892	1.717	-8.3
777	-50	0.22687	250	0	1027.2	-0.00989	0	-0.00989	1.727	-8.9
727	-50	0.24245	250	0	977.2	-0.01104	0	-0.01104	1.738	-9.6
677	-50	0.26032	250	0	927.2	-0.01241	0	-0.01241	1.750	-10.4
627	-50	0.28104	250	0	877.2	-0.01404	0	-0.01404	1.764	-11.3
577	-50	0.30534	250	0	827.2	-0.01602	0	-0.01602	1.780	-12.3
527	-50	0.33425	250	0	777.2	-0.01846	0	-0.01846	1.799	-13.5
477	-50	0.36920	250	0	727.2	-0.02150	0	-0.02150	1.820	-14.8
427	-50	0.41231	250	0	677.2	-0.02538	0	-0.02538	1.846	-16.4
400	-27	0.44005	250	0	650.2	-0.01644	0	-0.01644	1.862	-17.4

Test: 500																					
CV Module											**CMS module**										
λvp	0.21	λvs max	0.21								λvp	0.21	λvs max	0.21						vol_p	-4.2%
κvp	0.009	Ps (CV)=	980	1.3%							κvp	0.009								V_cms_te	1.621
s_{sa}	245		992.6								s_{sa}	245								EOT_p	1.599
p'=	500	ds=	-50						1.534		p'=	500	ds=	-50							
s (kPa)	ds	λvs	Cal_Psw ell	dp	p+s	dv from suction change	dv due to mean stress	dv (total)	cal_V_cv		s (kPa)	ds	λvs	p	dp	p+s	dv from suction change	dv due to mean stress	dv (total)	cal_V-cms	eV
3127		0.01651	500.0		3627.2				1.5340		3127		0.01651	500		3627.2				1.5340	0.0
3077	-50	0.01678	503.9	3.93	3581.1	-0.00023	-0.00023	0	1.534		3077	-50	0.01678	500	0	3577	-0.00023	0	-0.00023	1.534	0.0
3027	-50	0.01706	507.9	4.00	3535.1	-0.00023	-0.00023	0	1.534		3027	-50	0.01706	500	0	3527.2	-0.00023	0	-0.00023	1.534	0.0
2977	-50	0.01735	512.0	4.06	3489.2	-0.00024	-0.00024	0	1.534		2977	-50	0.01735	500	0	3477.2	-0.00024	0	-0.00024	1.535	0.0
2927	-50	0.01764	516.1	4.13	3443.3	-0.00025	-0.00025	0	1.534		2927	-50	0.01764	500	0	3427.2	-0.00025	0	-0.00025	1.535	-0.1
2877	-50	0.01795	520.3	4.20	3397.5	-0.00026	-0.00026	0	1.534		2877	-50	0.01795	500	0	3377.2	-0.00026	0	-0.00026	1.535	-0.1
2827	-50	0.01827	524.6	4.27	3351.8	-0.00026	-0.00026	0	1.534		2827	-50	0.01827	500	0	3327.2	-0.00027	0	-0.00027	1.536	-0.1
2777	-50	0.01859	528.9	4.35	3306.1	-0.00027	-0.00027	0	1.534		2777	-50	0.01859	500	0	3277.2	-0.00027	0	-0.00027	1.536	-0.1
2727	-50	0.01894	533.4	4.43	3260.6	-0.00028	-0.00028	0	1.534		2727	-50	0.01894	500	0	3227.2	-0.00028	0	-0.00028	1.536	-0.1
2677	-50	0.01929	537.9	4.51	3215.1	-0.00029	-0.00029	0	1.534		2677	-50	0.01929	500	0	3177.2	-0.00029	0	-0.00029	1.536	-0.2
2627	-50	0.01966	542.5	4.59	3169.7	-0.00030	-0.0003	0	1.534		2627	-50	0.01966	500	0	3127.2	-0.00030	0	-0.00030	1.537	-0.2
2577	-50	0.02004	547.2	4.68	3124.4	-0.00031	-0.00031	0	1.534		2577	-50	0.02004	500	0	3077.2	-0.00031	0	-0.00031	1.537	-0.2
2527	-50	0.02043	551.9	4.77	3079.1	-0.00032	-0.00032	0	1.534		2527	-50	0.02043	500	0	3027.2	-0.00033	0	-0.00033	1.537	-0.2
2477	-50	0.02085	556.8	4.87	3034.0	-0.00033	-0.00033	0	1.534		2477	-50	0.02085	500	0	2977.2	-0.00034	0	-0.00034	1.538	-0.2
2427	-50	0.02128	561.8	4.96	2989.0	-0.00034	-0.00034	0	1.534		2427	-50	0.02128	500	0	2927.2	-0.00035	0	-0.00035	1.538	-0.3
2377	-50	0.02172	566.8	5.07	2944.0	-0.00036	-0.00036	0	1.534		2377	-50	0.02172	500	0	2877.2	-0.00036	0	-0.00036	1.538	-0.3
2327	-50	0.02219	572.0	5.17	2899.2	-0.00037	-0.00037	0	1.534		2327	-50	0.02219	500	0	2827.2	-0.00038	0	-0.00038	1.539	-0.3
2277	-50	0.02268	577.3	5.28	2854.5	-0.00038	-0.00038	0	1.534		2277	-50	0.02268	500	0	2777.2	-0.00039	0	-0.00039	1.539	-0.3
2227	-50	0.02318	582.7	5.40	2809.9	-0.00040	-0.0004	0	1.534		2227	-50	0.02318	500	0	2727.2	-0.00041	0	-0.00041	1.540	-0.4
2177	-50	0.02372	588.2	5.52	2765.4	-0.00041	-0.00041	0	1.534		2177	-50	0.02372	500	0	2677.2	-0.00043	0	-0.00043	1.540	-0.4
2127	-50	0.02427	593.8	5.65	2721.0	-0.00043	-0.00043	0	1.534		2127	-50	0.02427	500	0	2627.2	-0.00044	0	-0.00044	1.540	-0.4
2077	-50	0.02486	599.6	5.78	2676.8	-0.00045	-0.00045	0	1.534		2077	-50	0.02486	500	0	2577.2	-0.00046	0	-0.00046	1.541	-0.4
2027	-50	0.02547	605.5	5.92	2632.7	-0.00046	-0.00046	0	1.534		2027	-50	0.02547	500	0	2527.2	-0.00048	0	-0.00048	1.541	-0.5
1977	-50	0.02611	611.6	6.06	2588.8	-0.00048	-0.00048	0	1.534		1977	-50	0.02611	500	0	2477.2	-0.00050	0	-0.00050	1.542	-0.5
1927	-50	0.02679	617.8	6.22	2545.0	-0.00050	-0.0005	0	1.534		1927	-50	0.02679	500	0	2427.2	-0.00053	0	-0.00053	1.542	-0.5
1877	-50	0.02751	624.2	6.38	2501.4	-0.00053	-0.00053	0	1.534		1877	-50	0.02751	500	0	2377.2	-0.00055	0	-0.00055	1.543	-0.6
1827	-50	0.02826	630.7	6.55	2457.9	-0.00055	-0.00055	0	1.534		1827	-50	0.02826	500	0	2327.2	-0.00058	0	-0.00058	1.543	-0.6
1777	-50	0.02905	637.5	6.73	2414.7	-0.00057	-0.00057	0	1.534		1777	-50	0.02905	500	0	2277.2	-0.00061	0	-0.00061	1.544	-0.7
1727	-50	0.02989	644.4	6.92	2371.6	-0.00060	-0.0006	0	1.534		1727	-50	0.02989	500	0	2227.2	-0.00064	0	-0.00064	1.545	-0.7
1677	-50	0.03078	651.5	7.12	2328.7	-0.00063	-0.00063	0	1.534		1677	-50	0.03078	500	0	2177.2	-0.00067	0	-0.00067	1.545	-0.7
1627	-50	0.03173	658.8	7.33	2286.0	-0.00066	-0.00066	0	1.534		1627	-50	0.03173	500	0	2127.2	-0.00071	0	-0.00071	1.546	-0.8
1577	-50	0.03273	666.4	7.55	2243.6	-0.00069	-0.00069	0	1.534		1577	-50	0.03273	500	0	2077.2	-0.00075	0	-0.00075	1.547	-0.8
1527	-50	0.03380	674.2	7.79	2201.4	-0.00073	-0.00073	0	1.534		1527	-50	0.03380	500	0	2027.2	-0.00079	0	-0.00079	1.548	-0.9
1477	-50	0.03495	682.2	8.05	2159.4	-0.00077	-0.00077	0	1.534		1477	-50	0.03495	500	0	1977.2	-0.00083	0	-0.00083	1.548	-0.9
1427	-50	0.03617	690.6	8.32	2117.8	-0.00081	-0.00081	0	1.534		1427	-50	0.03617	500	0	1927.2	-0.00088	0	-0.00088	1.549	-1.0
1377	-50	0.03748	699.2	8.61	2076.4	-0.00085	-0.00085	0	1.534		1377	-50	0.03748	500	0	1877.2	-0.00094	0	-0.00094	1.550	-1.1
1327	-50	0.03889	708.1	8.92	2035.3	-0.00090	-0.0009	0	1.534		1327	-50	0.03889	500	0	1827.2	-0.00100	0	-0.00100	1.551	-1.1
1277	-50	0.04042	717.4	9.26	1994.6	-0.00096	-0.00096	0	1.534		1277	-50	0.04042	500	0	1777.2	-0.00106	0	-0.00106	1.552	-1.2
1227	-50	0.04206	727.0	9.62	1954.2	-0.00101	-0.00101	0	1.534		1227	-50	0.04206	500	0	1727.2	-0.00114	0	-0.00114	1.554	-1.3
1177	-50	0.04385	737.0	10.01	1914.2	-0.00108	-0.00108	0	1.534		1177	-50	0.04385	500	0	1677.2	-0.00122	0	-0.00122	1.555	-1.3
1127	-50	0.04579	747.4	10.44	1874.6	-0.00115	-0.00115	0	1.534		1127	-50	0.04579	500	0	1627.2	-0.00131	0	-0.00131	1.556	-1.4
1077	-50	0.04791	758.3	10.90	1835.5	-0.00122	-0.00122	0	1.534		1077	-50	0.04791	500	0	1577.2	-0.00141	0	-0.00141	1.557	-1.5
1027	-50	0.05024	769.7	11.41	1796.9	-0.00131	-0.00131	0	1.534		1027	-50	0.05024	500	0	1527.2	-0.00152	0	-0.00152	1.559	-1.6
977	-50	0.05281	781.7	11.96	1758.9	-0.00140	-0.0014	0	1.534		977	-50	0.05281	500	0	1477.2	-0.00164	0	-0.00164	1.561	-1.7
927	-50	0.05566	794.3	12.57	1721.5	-0.00150	-0.0015	0	1.534		927	-50	0.05566	500	0	1427.2	-0.00179	0	-0.00179	1.562	-1.8
877	-50	0.05882	807.5	13.25	1684.7	-0.00162	-0.00162	0	1.534		877	-50	0.05882	500	0	1377.2	-0.00195	0	-0.00195	1.564	-2.0
827	-50	0.06238	821.5	14.01	1648.7	-0.00175	-0.00175	0	1.534		827	-50	0.06238	500	0	1327.2	-0.00214	0	-0.00214	1.566	-2.1
777	-50	0.06638	836.4	14.85	1613.6	-0.00189	-0.00189	0	1.534		777	-50	0.06638	500	0	1277.2	-0.00235	0	-0.00235	1.569	-2.3
727	-50	0.07094	852.2	15.81	1579.4	-0.00206	-0.00206	0	1.534		727	-50	0.07094	500	0	1227.2	-0.00260	0	-0.00260	1.571	-2.4
677	-50	0.07617	869.1	16.89	1546.3	-0.00225	-0.00225	0	1.534		677	-50	0.07617	500	0	1177.2	-0.00289	0	-0.00289	1.574	-2.6
627	-50	0.08223	887.2	18.14	1514.4	-0.00246	-0.00246	0	1.534		627	-50	0.08223	500	0	1127.2	-0.00324	0	-0.00324	1.578	-2.8
577	-50	0.08935	906.8	19.58	1484.0	-0.00272	-0.00272	0	1.534		577	-50	0.08935	500	0	1077.2	-0.00365	0	-0.00365	1.581	-3.1
527	-50	0.09780	928.1	21.27	1455.3	-0.00301	-0.00301	0	1.534		527	-50	0.09780	500	0	1027.2	-0.00415	0	-0.00415	1.585	-3.3
477	-50	0.10803	951.4	23.29	1428.6	-0.00336	-0.00336	0	1.534		477	-50	0.10803	500	0	977.2	-0.00476	0	-0.00476	1.590	-3.7
427	-50	0.12064	977.1	25.72	1404.3	-0.00378	-0.00378	0	1.534		427	-50	0.12064	500	0	927.2	-0.00553	0	-0.00553	1.596	-4.0
400	-27	0.12883	992.6	15.51	1392.6	-0.00232	-0.00232	0	1.534		400	-27	0.12883	500	0	900	-0.00351	0	-0.00351	1.599	-4.2

Test: 1000

CV Module

λvp	0.21	λvs max	0.21						
κvp	0.009	Ps (CV)=	1440	0.7%					
s_{sa}	245		1450						
p'=	1000	ds=	-50						1.506
s (kPa)	ds	λvs	Cal_Pswell	dp	p+s	dv from suction change	dv due to mean stress	dv (total)	cal_V_cv
2627		0.01966	1000.0		3627.2				1.506
2577	-50	0.02004	1004.7	4.68	3581.9	-0.00027	-0.00027	0	1.506
2527	-50	0.02043	1009.5	4.77	3536.7	-0.00028	-0.00028	0	1.506
2477	-50	0.02085	1014.3	4.87	3491.5	-0.00029	-0.00029	0	1.506
2427	-50	0.02128	1019.3	4.96	3446.5	-0.00030	-0.0003	0	1.506
2377	-50	0.02172	1024.3	5.07	3401.5	-0.00031	-0.00031	0	1.506
2327	-50	0.02219	1029.5	5.17	3356.7	-0.00032	-0.00032	0	1.506
2277	-50	0.02268	1034.8	5.28	3312.0	-0.00033	-0.00033	0	1.506
2227	-50	0.02318	1040.2	5.40	3267.4	-0.00034	-0.00034	0	1.506
2177	-50	0.02372	1045.7	5.52	3222.9	-0.00035	-0.00035	0	1.506
2127	-50	0.02427	1051.4	5.65	3178.6	-0.00037	-0.00037	0	1.506
2077	-50	0.02486	1057.1	5.78	3134.3	-0.00038	-0.00038	0	1.506
2027	-50	0.02547	1063.1	5.92	3090.3	-0.00040	-0.0004	0	1.506
1977	-50	0.02611	1069.1	6.06	3046.3	-0.00041	-0.00041	0	1.506
1927	-50	0.02679	1075.3	6.22	3002.5	-0.00043	-0.00043	0	1.506
1877	-50	0.02751	1081.7	6.38	2958.9	-0.00045	-0.00045	0	1.506
1827	-50	0.02826	1088.3	6.55	2915.5	-0.00046	-0.00046	0	1.506
1777	-50	0.02905	1095.0	6.73	2872.2	-0.00048	-0.00048	0	1.506
1727	-50	0.02989	1101.9	6.92	2829.1	-0.00051	-0.00051	0	1.506
1677	-50	0.03078	1109.0	7.12	2786.2	-0.00053	-0.00053	0	1.506
1627	-50	0.03173	1116.4	7.33	2743.6	-0.00055	-0.00055	0	1.506
1577	-50	0.03273	1123.9	7.55	2701.1	-0.00058	-0.00058	0	1.506
1527	-50	0.03380	1131.7	7.79	2658.9	-0.00061	-0.00061	0	1.506
1477	-50	0.03495	1139.8	8.05	2617.0	-0.00064	-0.00064	0	1.506
1427	-50	0.03617	1148.1	8.32	2575.3	-0.00067	-0.00067	0	1.506
1377	-50	0.03748	1156.7	8.61	2533.9	-0.00070	-0.0007	0	1.506
1327	-50	0.03889	1165.6	8.92	2492.8	-0.00074	-0.00074	0	1.506
1277	-50	0.04042	1174.9	9.26	2452.1	-0.00078	-0.00078	0	1.506
1227	-50	0.04206	1184.5	9.62	2411.7	-0.00082	-0.00082	0	1.506
1177	-50	0.04385	1194.5	10.01	2371.7	-0.00087	-0.00087	0	1.506
1127	-50	0.04579	1205.0	10.44	2332.2	-0.00092	-0.00092	0	1.506
1077	-50	0.04791	1215.9	10.90	2293.1	-0.00098	-0.00098	0	1.506
1027	-50	0.05024	1227.3	11.41	2254.5	-0.00104	-0.00104	0	1.506
977	-50	0.05281	1239.2	11.96	2216.4	-0.00111	-0.00111	0	1.506
927	-50	0.05566	1251.8	12.57	2179.0	-0.00119	-0.00119	0	1.506
877	-50	0.05882	1265.1	13.25	2142.3	-0.00128	-0.00128	0	1.506
827	-50	0.06238	1279.1	14.01	2106.3	-0.00137	-0.00137	0	1.506
777	-50	0.06638	1293.9	14.85	2071.1	-0.00148	-0.00148	0	1.506
727	-50	0.07094	1309.7	15.81	2036.9	-0.00160	-0.0016	0	1.506
677	-50	0.07617	1326.6	16.89	2003.8	-0.00174	-0.00174	0	1.506
627	-50	0.08223	1344.7	18.14	1971.9	-0.00190	-0.0019	0	1.506
577	-50	0.08935	1364.3	19.58	1941.5	-0.00209	-0.00209	0	1.506
527	-50	0.09780	1385.6	21.27	1912.8	-0.00230	-0.0023	0	1.506
477	-50	0.10803	1408.9	23.29	1886.1	-0.00256	-0.00256	0	1.506
427	-50	0.12064	1434.6	25.72	1861.8	-0.00286	-0.00286	0	1.506
400	-27	0.12876	1450.1	15.51	1850.3	-0.00175	-0.00175	0	1.506

CMS module

λvp	0.21	λvs max	0.21						vol_p	-3.1%
κvp	0.009								V_cms_te:	1.538
s_{sa}	245								EOT_p	1.552
p'=	1000	ds=	-50							
s (kPa)	ds	λvs	p	dp	p+s	dv from suction change	dv due to mean stress	dv (total)	cal_V-cms	eV
2627		0.01966	1000		3627.2				1.506	0.0
2577	-50	0.02004	1000	0	3577	-0.00027	0	-0.00027	1.506	0.0
2527	-50	0.02043	1000	0	3527.2	-0.00028	0	-0.00028	1.506	0.0
2477	-50	0.02085	1000	0	3477.2	-0.00029	0	-0.00029	1.507	-0.1
2427	-50	0.02128	1000	0	3427.2	-0.00030	0	-0.00030	1.507	-0.1
2377	-50	0.02172	1000	0	3377.2	-0.00031	0	-0.00031	1.507	-0.1
2327	-50	0.02219	1000	0	3327.2	-0.00032	0	-0.00032	1.508	-0.1
2277	-50	0.02268	1000	0	3277.2	-0.00033	0	-0.00033	1.508	-0.1
2227	-50	0.02318	1000	0	3227.2	-0.00035	0	-0.00035	1.508	-0.2
2177	-50	0.02372	1000	0	3177.2	-0.00036	0	-0.00036	1.509	-0.2
2127	-50	0.02427	1000	0	3127.2	-0.00037	0	-0.00037	1.509	-0.2
2077	-50	0.02486	1000	0	3077.2	-0.00039	0	-0.00039	1.509	-0.2
2027	-50	0.02547	1000	0	3027.2	-0.00040	0	-0.00040	1.510	-0.3
1977	-50	0.02611	1000	0	2977.2	-0.00042	0	-0.00042	1.510	-0.3
1927	-50	0.02679	1000	0	2927.2	-0.00044	0	-0.00044	1.511	-0.3
1877	-50	0.02751	1000	0	2877.2	-0.00046	0	-0.00046	1.511	-0.4
1827	-50	0.02826	1000	0	2827.2	-0.00048	0	-0.00048	1.512	-0.4
1777	-50	0.02905	1000	0	2777.2	-0.00050	0	-0.00050	1.512	-0.4
1727	-50	0.02989	1000	0	2727.2	-0.00052	0	-0.00052	1.513	-0.5
1677	-50	0.03078	1000	0	2677.2	-0.00055	0	-0.00055	1.513	-0.5
1627	-50	0.03173	1000	0	2627.2	-0.00057	0	-0.00057	1.514	-0.5
1577	-50	0.03273	1000	0	2577.2	-0.00060	0	-0.00060	1.514	-0.6
1527	-50	0.03380	1000	0	2527.2	-0.00064	0	-0.00064	1.515	-0.6
1477	-50	0.03495	1000	0	2477.2	-0.00067	0	-0.00067	1.516	-0.7
1427	-50	0.03617	1000	0	2427.2	-0.00071	0	-0.00071	1.516	-0.7
1377	-50	0.03748	1000	0	2377.2	-0.00075	0	-0.00075	1.517	-0.7
1327	-50	0.03889	1000	0	2327.2	-0.00079	0	-0.00079	1.518	-0.8
1277	-50	0.04042	1000	0	2277.2	-0.00084	0	-0.00084	1.519	-0.9
1227	-50	0.04206	1000	0	2227.2	-0.00089	0	-0.00089	1.520	-0.9
1177	-50	0.04385	1000	0	2177.2	-0.00094	0	-0.00094	1.521	-1.0
1127	-50	0.04579	1000	0	2127.2	-0.00101	0	-0.00101	1.522	-1.0
1077	-50	0.04791	1000	0	2077.2	-0.00108	0	-0.00108	1.523	-1.1
1027	-50	0.05024	1000	0	2027.2	-0.00115	0	-0.00115	1.524	-1.2
977	-50	0.05281	1000	0	1977.2	-0.00124	0	-0.00124	1.525	-1.3
927	-50	0.05566	1000	0	1927.2	-0.00134	0	-0.00134	1.526	-1.4
877	-50	0.05882	1000	0	1877.2	-0.00144	0	-0.00144	1.528	-1.5
827	-50	0.06238	1000	0	1827.2	-0.00157	0	-0.00157	1.529	-1.6
777	-50	0.06638	1000	0	1777.2	-0.00171	0	-0.00171	1.531	-1.7
727	-50	0.07094	1000	0	1727.2	-0.00187	0	-0.00187	1.533	-1.8
677	-50	0.07617	1000	0	1677.2	-0.00205	0	-0.00205	1.535	-1.9
627	-50	0.08223	1000	0	1627.2	-0.00227	0	-0.00227	1.537	-2.1
577	-50	0.08935	1000	0	1577.2	-0.00253	0	-0.00253	1.540	-2.3
527	-50	0.09780	1000	0	1527.2	-0.00283	0	-0.00283	1.543	-2.4
477	-50	0.10803	1000	0	1477.2	-0.00320	0	-0.00320	1.546	-2.7
427	-50	0.12064	1000	0	1427.2	-0.00366	0	-0.00366	1.549	-2.9
400	-27	0.12876	1000	0	1400.2	-0.00228	0	-0.00228	1.552	-3.1

Test: 1500																					
CV Module											**CMS module**										
λvp	0.21	λvs max	0.21								λvp	0.21	λvs max	0.21						vol_p	-2.3%
κvp	0.009	Ps (CV)=	1905	-0.3%							κvp	0.009								V_cms_te:	1.476
s_{sa}	245		1899								s_{sa}	245	kPa							EOT_p	1.488
p'=	1500	ds=	-50						1.454		p'=	1500	ds=	-50							
s (kPa)	ds	λvs	Cal_Psw ell	dp	p+s	dv from suction change	dv due to mean stress	dv (total)	cal_V_cv		s (kPa)	ds	λvs	p	dp	p+s	dv from suction change	dv due to mean stress	dv (total)	cal_V-cms	eV
2127		0.02427	1500.0		3627.2				1.454		2127		0.02427	1500		3627.2				1.454	0.0
2077	-50	0.02486	1505.8	5.78	3583.0	-0.00033	-0.00033	0	1.454		2077	-50	0.02486	1500	0	3577	-0.00033	0	-0.00033	1.455	0.0
2027	-50	0.02547	1511.7	5.92	3538.9	-0.00035	-0.00035	0	1.454		2027	-50	0.02547	1500	0	3527.2	-0.00035	0	-0.00035	1.455	0.0
1977	-50	0.02611	1517.8	6.06	3495.0	-0.00036	-0.00036	0	1.454		1977	-50	0.02611	1500	0	3477.2	-0.00036	0	-0.00036	1.455	-0.1
1927	-50	0.02679	1524.0	6.22	3451.2	-0.00037	-0.00037	0	1.454		1927	-50	0.02679	1500	0	3427.2	-0.00038	0	-0.00038	1.456	-0.1
1877	-50	0.02751	1530.4	6.38	3407.6	-0.00039	-0.00039	0	1.454		1877	-50	0.02751	1500	0	3377.2	-0.00039	0	-0.00039	1.456	-0.1
1827	-50	0.02826	1536.9	6.55	3364.1	-0.00040	-0.0004	0	1.454		1827	-50	0.02826	1500	0	3327.2	-0.00041	0	-0.00041	1.456	-0.2
1777	-50	0.02905	1543.6	6.73	3320.8	-0.00042	-0.00042	0	1.454		1777	-50	0.02905	1500	0	3277.2	-0.00042	0	-0.00042	1.457	-0.2
1727	-50	0.02989	1550.6	6.92	3277.8	-0.00044	-0.00044	0	1.454		1727	-50	0.02989	1500	0	3227.2	-0.00044	0	-0.00044	1.457	-0.2
1677	-50	0.03078	1557.7	7.12	3234.9	-0.00046	-0.00046	0	1.454		1677	-50	0.03078	1500	0	3177.2	-0.00046	0	-0.00046	1.458	-0.2
1627	-50	0.03173	1565.0	7.33	3192.2	-0.00048	-0.00048	0	1.454		1627	-50	0.03173	1500	0	3127.2	-0.00048	0	-0.00048	1.458	-0.3
1577	-50	0.03273	1572.6	7.55	3149.8	-0.00050	-0.0005	0	1.454		1577	-50	0.03273	1500	0	3077.2	-0.00051	0	-0.00051	1.459	-0.3
1527	-50	0.03380	1580.3	7.79	3107.5	-0.00052	-0.00052	0	1.454		1527	-50	0.03380	1500	0	3027.2	-0.00053	0	-0.00053	1.459	-0.3
1477	-50	0.03495	1588.4	8.05	3065.6	-0.00054	-0.00054	0	1.454		1477	-50	0.03495	1500	0	2977.2	-0.00056	0	-0.00056	1.460	-0.4
1427	-50	0.03617	1596.7	8.32	3023.9	-0.00057	-0.00057	0	1.454		1427	-50	0.03617	1500	0	2927.2	-0.00059	0	-0.00059	1.460	-0.4
1377	-50	0.03748	1605.3	8.61	2982.5	-0.00060	-0.0006	0	1.454		1377	-50	0.03748	1500	0	2877.2	-0.00062	0	-0.00062	1.461	-0.5
1327	-50	0.03889	1614.3	8.92	2941.5	-0.00063	-0.00063	0	1.454		1327	-50	0.03889	1500	0	2827.2	-0.00065	0	-0.00065	1.462	-0.5
1277	-50	0.04042	1623.5	9.26	2900.7	-0.00066	-0.00066	0	1.454		1277	-50	0.04042	1500	0	2777.2	-0.00069	0	-0.00069	1.462	-0.6
1227	-50	0.04206	1633.1	9.62	2860.3	-0.00070	-0.0007	0	1.454		1227	-50	0.04206	1500	0	2727.2	-0.00073	0	-0.00073	1.463	-0.6
1177	-50	0.04385	1643.2	10.01	2820.4	-0.00074	-0.00074	0	1.454		1177	-50	0.04385	1500	0	2677.2	-0.00077	0	-0.00077	1.464	-0.7
1127	-50	0.04579	1653.6	10.44	2780.8	-0.00078	-0.00078	0	1.454		1127	-50	0.04579	1500	0	2627.2	-0.00082	0	-0.00082	1.465	-0.7
1077	-50	0.04791	1664.5	10.90	2741.7	-0.00082	-0.00082	0	1.454		1077	-50	0.04791	1500	0	2577.2	-0.00087	0	-0.00087	1.466	-0.8
1027	-50	0.05024	1675.9	11.41	2703.1	-0.00087	-0.00087	0	1.454		1027	-50	0.05024	1500	0	2527.2	-0.00093	0	-0.00093	1.466	-0.8
977	-50	0.05281	1687.9	11.96	2665.1	-0.00093	-0.00093	0	1.454		977	-50	0.05281	1500	0	2477.2	-0.00099	0	-0.00099	1.467	-0.9
927	-50	0.05566	1700.4	12.57	2627.6	-0.00099	-0.00099	0	1.454		927	-50	0.05566	1500	0	2427.2	-0.00107	0	-0.00107	1.469	-1.0
877	-50	0.05882	1713.7	13.25	2590.9	-0.00106	-0.00106	0	1.454		877	-50	0.05882	1500	0	2377.2	-0.00115	0	-0.00115	1.470	-1.1
827	-50	0.06238	1727.7	14.01	2554.9	-0.00114	-0.00114	0	1.454		827	-50	0.06238	1500	0	2327.2	-0.00124	0	-0.00124	1.471	-1.2
777	-50	0.06638	1742.5	14.85	2519.7	-0.00122	-0.00122	0	1.454		777	-50	0.06638	1500	0	2277.2	-0.00134	0	-0.00134	1.472	-1.2
727	-50	0.07094	1758.4	15.81	2485.6	-0.00132	-0.00132	0	1.454		727	-50	0.07094	1500	0	2227.2	-0.00146	0	-0.00146	1.474	-1.3
677	-50	0.07617	1775.2	16.89	2452.4	-0.00143	-0.00143	0	1.454		677	-50	0.07617	1500	0	2177.2	-0.00159	0	-0.00159	1.475	-1.5
627	-50	0.08223	1793.4	18.14	2420.6	-0.00155	-0.00155	0	1.454		627	-50	0.08223	1500	0	2127.2	-0.00175	0	-0.00175	1.477	-1.6
577	-50	0.08935	1813.0	19.58	2390.2	-0.00170	-0.0017	0	1.454		577	-50	0.08935	1500	0	2077.2	-0.00193	0	-0.00193	1.479	-1.7
527	-50	0.09780	1834.2	21.27	2361.4	-0.00187	-0.00187	0	1.454		527	-50	0.09780	1500	0	2027.2	-0.00215	0	-0.00215	1.481	-1.9
477	-50	0.10803	1857.5	23.29	2334.7	-0.00207	-0.00207	0	1.454		477	-50	0.10803	1500	0	1977.2	-0.00241	0	-0.00241	1.484	-2.0
427	-50	0.12064	1883.2	25.72	2310.4	-0.00231	-0.00231	0	1.454		427	-50	0.12064	1500	0	1927.2	-0.00273	0	-0.00273	1.486	-2.2
400	-27	0.12876	1898.8	15.51	2299.0	-0.00141	-0.00141	0	1.454		400	-27	0.12876	1500	0	1900.2	-0.00169	0	-0.00169	1.488	-2.3

APPENDIX K - PUBLISHED JOURNAL PAPERS

Lim, B.F. and Siemens, G.A. 2013. An unconfined swelling test for clayey soils that incorporates digital image correlation. Geotechnical Testing Journal 36 (6): 1-11.

Siddiqua, S., Siemens, G., Blatz, J., Man, A. and Lim, B.F. 2014. Influence of pore fluid chemistry on the mechanical properties of clay-based materials. Geotechnical and Geological Engineering 32 (4): 1029-42.

Geotechnical Testing Journal, Vol. 36, No. 6, 2013
Available online at www.astm.org
doi:10.1520/GTJ20120220

B. F. Lim[1] *and G. A. Siemens*[2]

An Unconfined Swelling Test for Clayey Soils That Incorporates Digital Image Correlation

REFERENCE: Lim, B. F. and Siemens, G. A., "An Unconfined Swelling Test for Clayey Soils That Incorporates Digital Image Correlation," *Geotechnical Testing Journal*, Vol. 36, No. 6, 2013, pp. 1–11, doi:10.1520/GTJ20120220. ISSN 0149-6115.

ABSTRACT: A new laboratory test apparatus and methodology have been developed for characterizing the swelling potential of expansive soil under free stress conditions. Soil specimens are given access to water under true free swell conditions, and the maximum swelling potential is determined experimentally. Real-time deformation measurements and interpretation are obtained through digital image correlation using GeoPIV. The capabilities of the new test are illustrated using a remolded natural swelling soil. Both primary and secondary swelling behavior were observed during testing. The effect of the aspect ratio was assessed, and it was found that smaller specimens achieved equivalent swelling strains with significantly shorter test durations. The non-contact deformation results agree with the end-of-test hand measurements. The non-contact method also provides additional valuable information regarding the time-dependent swell behavior and evaluation of the end-of-test criterion. The results are interpreted using the Swell Equilibrium Limit, which is a unifying framework for the analysis and prediction of swelling soil deformations under defined initial and boundary conditions.

KEYWORDS: unconfined swelling, free swell, digital image analysis, wetting, primary and secondary swelling curves, swelling rate, aspect ratio, Swell Equilibrium Limit

Introduction

The characterization of swelling potential is of critical importance in the analysis and design of infrastructure founded in swelling soil. The behavior of expansive soil is complicated by excessive volume changes during swelling and the development of swelling-induced stresses when expansion is restrained. Damage to infrastructure founded in swelling soil due to excessive deformation is measured in billions of dollars every year. The swelling ability of soil also provides self-healing qualities, which can also be utilized in waste isolation applications. Design optimization requires accurate predictions of swelling potential and swelling pressures.

Traditionally, the swelling potential and swelling pressures are measured using an oedometer apparatus as shown schematically in Fig. 1(*a*) (ASTM D4546-96). Specimens are subjected to wetting under free swell or constant volume conditions. The test results provide the maximum vertical swelling strain or vertical swelling pressure. Recently the standard test was revised (ASTM D4546-08), and it now calls for the application of constant vertical stress conditions followed by wetting. Several tests are completed at increasing vertical stresses until the stress that inhibits swelling is determined. The test method imposes laterally constrained conditions on the swelling behavior, but these conditions rarely persist in the field. Numerous researchers and practitioners have successfully used these, or similar, test methods to characterize expansive soils (Baille et al. 2010; Cerato et al. 2009; DiMaio et al. 2004; Dixon et al. 2002; Imbert and Villar 2006; Ito and Azam 2010; Kodikara 2012; Komine and Ogata 1994; Lee et al. 2012; Nagaraj et al. 2009; Peng and Horn 2007; Powell et al. 2012a, 2012b, 2013; Rao et al. 2004; Rao and Tripathy 2003; Singhal et al. 2011). Micro-porosity effects on the behavior of swelling materials have also been examined (Vallejo 2011; Siemens et al. 2007). Vallejo (2011) studied the influence of pore microgeometry on the slaking of shales and concluded that smoother and smaller pores have a reduced resistance to slaking.

Rojas et al. (2011) reported a test methodology and apparatus for measuring wetting and drying water-retention curves using the vapor equilibrium technique, and they also included digital image analysis to measure deformations. Compacted bentonite specimens were subjected to constant relative humidity environments, and the specimens either shrank or swelled in response to the imposed suction level. Soil images were captured during the test with a digital single-lens reflex (SLR) camera, and strains were interpreted using commercial photo-editing software. Their result confirms the effectiveness of the vapor equilibrium method for applying wetting and drying conditions and non-contact measurement techniques to measure soil strains.

Siemens and Blatz (2009) reported a unifying framework for the behavior of swelling soils. Termed the Swell Equilibrium

Manuscript received November 26, 2012; accepted for publication June 24, 2013; published online September 9, 2013.

[1]Ph.D. Candidate, GeoEngineering Centre at Queen's-RMC, Dept. of Civil Engineering, Royal Military College of Canada, Kingston, ON, Canada, K7K 7H5, e-mail: Bee.Fong.Lim@rmc.ca

[2]Associate Professor, GeoEngineering Centre at Queen's-RMC, Dept. of Civil Engineering, Royal Military College of Canada, Kingston, ON, Canada, K7K 7H5 (Corresponding author), e-mail: Greg.Siemens@rmc.ca

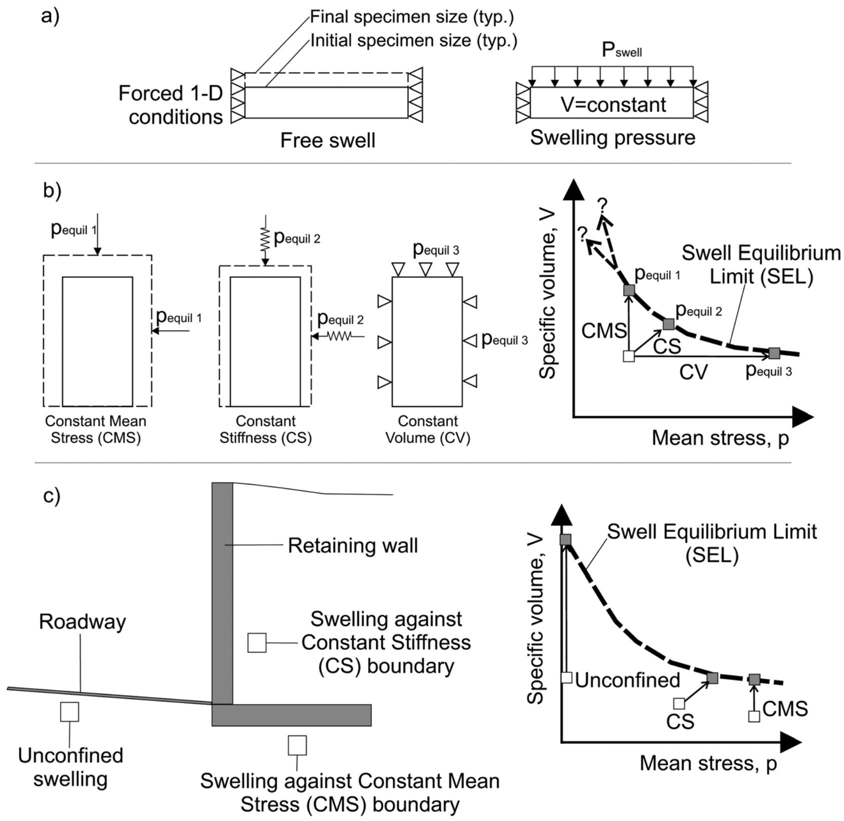

FIG. 1—*(a) Traditional swelling tests: free swell and swelling pressure tests. (b) Triaxial swelling tests: boundary conditions during swell tests and Swell Equilibrium Limit (SEL) schematic. (c) Practical application of SEL: unconfined swelling under a roadway, swelling under foundation (constant mean stress), and swelling against a retaining wall (idealized as constant stiffness).*

Limit, the framework can be used to predict swelling-induced pressures and swelling strains based on the initial conditions and the boundary conditions during swelling. The soil is characterized, as illustrated in Fig. 1(*b*), with constant mean stress, constant stiffness, or constant volume boundary conditions imposed during triaxial swelling tests (Siemens and Blatz 2007). The end points of the swell tests are then connected to form the Swell Equilibrium Limit. The Swell Equilibrium Limit was developed for a highly swelling engineered barrier with 50 % bentonite (Siemens and Blatz 2009) and later was applied to a natural soil (Powell et al. 2013). The Swell Equilibrium Limit framework works well at stress conditions found in many applications and may have several uses within a single engineering application.

Figure 1(*c*) displays a retaining wall system that provides multiple boundary conditions to the surrounding swelling soil. Below the cantilever wall, the swelling soil is under a constant mean stress boundary imposed by the constant vertical stress from the overlying soil and concrete. Under wetting conditions, the soil underneath the wall footing swells along a vertical stress path in a specific volume–mean stress (V-p) space. Adjacent to the retaining wall, the soil swells against the wall, which leads to displacement. This complex soil–structure interaction has been idealized as a constant stiffness boundary, which is a spring-like boundary condition. In V-p space, the stress path plots along a sloped line, with the slope angle being a function of the wall stiffness. The other bounding boundary condition would be a perfectly stiff wall that would plot as a horizontal stress path in V-p space (not shown).

Few studies have focused on swelling soil behavior at low stresses. The Swell Equilibrium Limit framework has been characterized using triaxial swelling tests, but its use at nominal stress levels has not been investigated. Continuing with the retaining-wall example [Fig. 1(*c*)], the soil underneath the road in front of the retaining wall will swell against a pseudo-unconfined condition at a shallow depth. In this location, free swell conditions persist; however, one-dimensional conditions do not. Given the significant non-linearity in the Swell Equilibrium Limit [Figs. 1(*b*) and 1(*c*)], accurate prediction of the potential vertical deformations at these low stresses is very difficult. This motivated us to develop a new test apparatus and methodology for characterizing the swelling potential at nominal stresses under true free swell boundary conditions.

Herein we propose an unconfined swelling test for measuring the maximum swelling potential for direct water access. The swell measurements obtained from the unconfined swelling test allow the Swell Equilibrium Limit framework to be applied at low stresses where significant non-linearity is expected [Figs. 1(*b*) and 1(*c*)]. The soil specimen is given free access to water and allowed to deform without any restraining boundary condition upon swelling. The test method uses digital image correlation or particle image velocimetry (GeoPIV) (White et al. 2003), which has been used in many geotechnical applications to measure soil deformations. Test results are presented to verify the apparatus and methodology, and then preliminary interpretation is provided in the Swell Equilibrium Limit framework.

Test Apparatus

The unconfined test apparatus provides water uptake and a high-humidity environment to soil specimens to enable measurement of their unrestrained swelling potential. A photograph of an overall view of the unconfined swelling test setup is shown in Fig. 2(*a*). Plan and cross-section drawings are included in Figs. 2(*b*) and 2(*c*). The configuration allows for five unconfined swelling tests to be completed simultaneously. The apparatus is constructed from 25.4-mm-thick Perspex and includes a sealed box that is 1.00 m wide, 0.24 m tall, and 0.20 m deep. The box is designed with a removable cover to allow digital images to be captured without obstruction and to allow water to be applied during the test. A rubber seal is placed around the edge of the removable cover, and vacuum grease is applied to ensure that the box is sealed during the swelling tests. Soil specimens are given direct access to water via spraying and wicking action from filter paper strips dipped into the reservoir. At the beginning of the test, six 10-mm-wide wicking strips are secured radially around the soil specimens with the ends placed in the water reservoir. The reservoir also maintains a high humidity level in the airspace within the box.

The process for making manual measurements of specimen height and diameter during the test is difficult because of the size of the specimens and the size constraints within the box. Unconfined swelling test durations can range from a few weeks to a few months depending on the size of the specimen. Thus a non-contact displacement measurement technique is incorporated into the apparatus. Digital images of the soil specimens are recorded using a digital SLR camera. Figure 3 illustrates typical deformations that are recorded during an unconfined swelling test. The camera is attached to a custom mount, and the mount is placed into a slot to position the camera in front of a soil specimen [see Figs. 2(*a*), 2(*b*), and 2(*c*) for camera, mount, and slot locations]. Soil deformations during the unconfined swelling test are measured by interpreting digital images using GeoPIV (White et al. 2003). A rigid frame with black circular targets is positioned around each pedestal. The locations of the targets are measured in a local coordinate system. The software uses the targets on the frame to correct digital images for small differences in the location of the camera and as reference locations to calculate soil deformations within a local coordinate system. Targets are also secured to the top of the soil specimen along its center plane. Soil specimen targets are used to track soil deformations during the unconfined swelling test.

The choice of a suitable digital camera and lens was made during the design stage. Of the possible suitable combinations, a Canon EOS Digital Rebel XTi with an EFS60mm f/2.8 Macro USM Lens was selected to record digital images of the soil specimens. The camera has a CCD that is 14.8 mm by 22.2 mm in size with an image resolution of 2592 pixels by 3888 pixels. The focal length of the macro lens is 60 mm. The camera is located 0.69 m in front of the center plane of each soil specimen, giving an average resolution of 0.04 mm/pixel. The camera is relocated from one slot to another slot to take images of soil specimens at each location. To prevent undesired movement while recording a digital image, a remote control with a self-timer setting of 2 s is used.

Test Methodology and Analysis

Unconfined swelling tests may be performed on natural or remolded specimens. A series of tests was carried out in the same or similar configuration to assess the repeatability of the testing method. According to the test method, test specimens are prepared and their initial mass, dimensions, and water content are recorded. Six 10-mm-wide wicking strips are installed along the side of the specimen. Figure 3 displays the wicking strips and illustrates typical deformations recorded during an unconfined swelling test. Two GeoPIV targets are pinned diametrically on the top surface of the specimen for image analysis. The soil specimen, with the wicking strips and targets, is then placed on a pedestal inside the sealed box. The specimen is located in such a way that the specimen targets face the camera and are in the same plane as the frame of the GeoPIV targets. Once the compacted soil specimen is placed on the pedestal, an initial photograph is recorded and the legs of the wicking strips are submerged in the water reservoir. To maintain the specimens in a pseudo-submerged state, de-ionized water is sprayed at the specimens on a daily basis. The water is sprayed all around each specimen until the wicking strips and soil specimen are visibly wet. The cover of the humidity box normally remains closed to prevent the loss of humidity through evaporation. The cover is opened only when an image is to be captured or when the specimens are sprayed. Periodically, digital images are taken of the soil specimen, which also requires opening of the sealed box. Between spraying events, the wicking strips effectively retain moisture in the soil specimen. In our tests, a relative humidity probe within the box airspace confirmed that the relative humidity was greater than 99 %.

Unconfined swelling tests continue until the specimen equilibrates with the moist environment. Progressive swelling of compacted specimen 189_AR = 0.15 at elapsed times of 1 day, 1.8 days, and 9.7 days is shown in Fig. 3. The dashed box in the figure indicates the original size of the soil specimen prior to wetting. Significant swelling deformations can be observed in this series of images. At the end of the test, the final dimensions, mass, and moisture contents of swelled specimens are measured. The spatial distribution of the moisture content is measured by dividing specimens vertically using a knife and then radially using two circular cutting rings with diameters of 36.4 mm and 13.6 mm. The soil specimen is divided to the outermost diameter, middle diameter, and core section. This division allows for the moisture content distribution to be measured radially across the specimen.

Deformation Analysis

Soil deformation is measured using a non-contact method employing the image-based software GeoPIV (White et al. 2003), which allows for real-time measurements. The software calculates soil deformation over a series of digital images by searching for characteristic patches of pixels in consecutive digital images and calculating the displacement. Vertical and horizontal displacements are inferred from the measured movement of GeoPIV targets installed on diametrically opposite sides of the top of specimens (Fig. 3). A secondary option is to select a patch of pixels at the

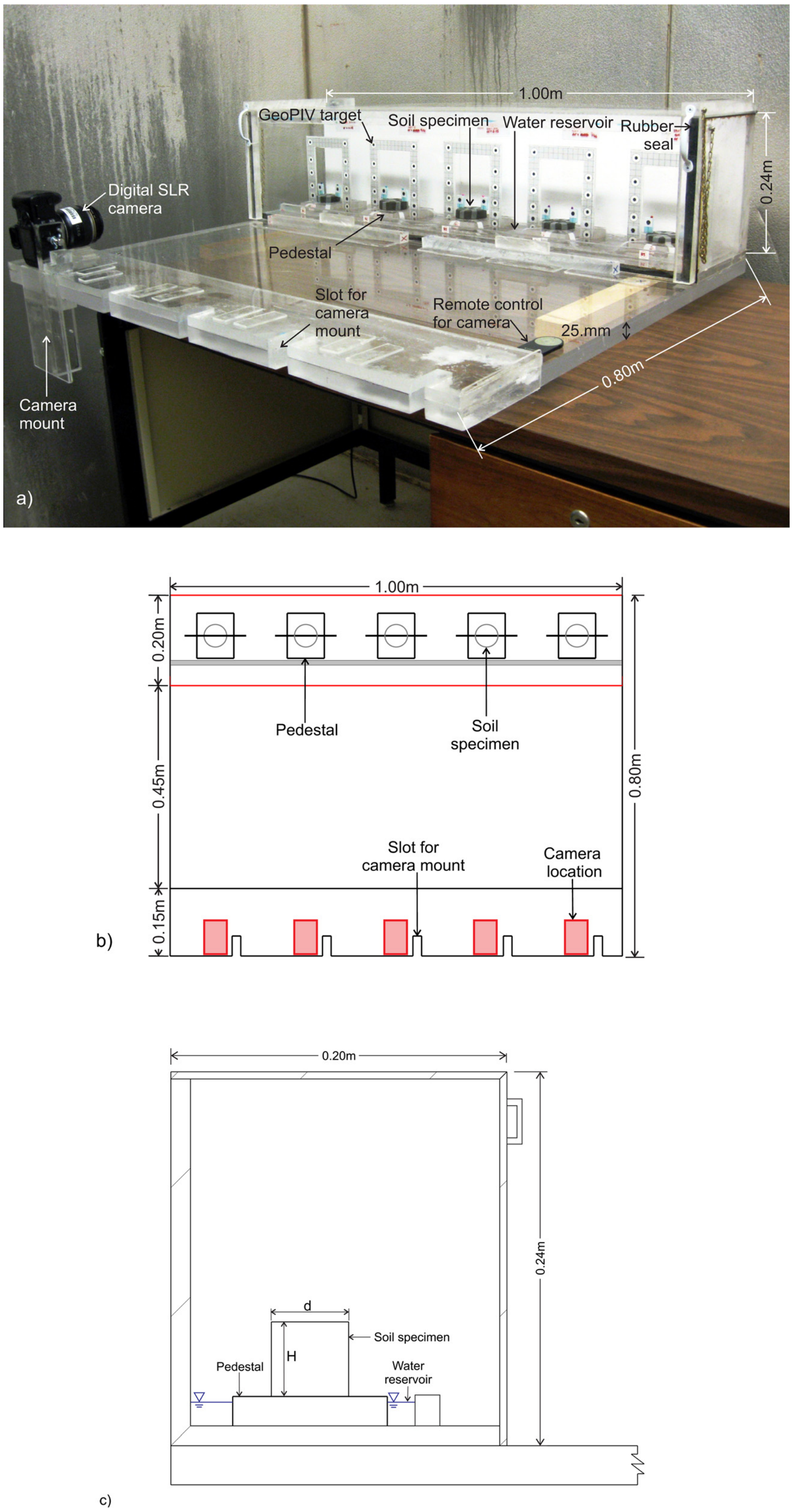

FIG. 2—*Unconfined swelling test apparatus: (a) photograph; (b) plan view drawing; and (c) side view.*

intersection between the bottom of the target holder and the edge of the specimen, as illustrated in Fig. 3(*a*). From the vertical and horizontal displacement measurements at the top edges of the specimen, axial strain and radial strain are calculated to determine the volume strain of the specimen during the test. The results obtained from the GeoPIV analysis are then compared with the caliper measurements taken at the end of the test. Strain analysis of soil deformation in the test uses the following equations:

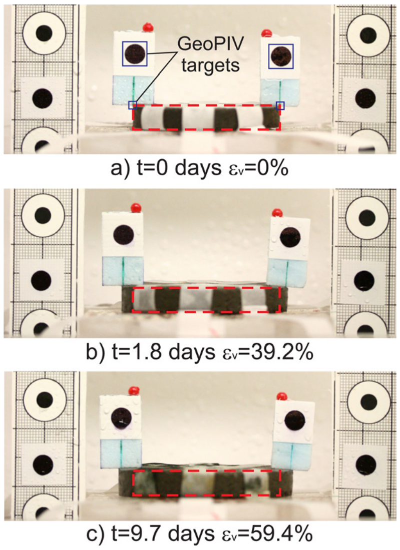

FIG. 3—*Progressive swelling of specimen 189_AR = 0.15.*

$$\varepsilon_a = \frac{\Delta H}{H_0} \tag{1}$$

$$\varepsilon_r = \frac{\Delta r}{r_0} = \frac{\Delta d}{d_0} \tag{2}$$

$$\varepsilon_v = \frac{\Delta V}{V_0} \tag{3}$$

where:

ε_a = axial strain,
ΔH = change in height,
H_0 = initial height,
ε_r = radial strain,
Δr = change in radius,
r_0 = initial radius,
Δd = change in diameter,
d_0 = initial diameter,
ε_v = volumetric strain,
ΔV = change in volume, and
V_0 = initial volume.

In geotechnical analysis, small strains are normally assumed; however, this assumption is invalid in the analysis of unconfined swelling tests because of the large deformations. Therefore, the volume strain is calculated from axial and radial strains as (Ehrgott 1971)

$$\frac{\Delta V}{V_0} = \varepsilon_a + 2\varepsilon_r - 2\varepsilon_r\varepsilon_a + \varepsilon_r^2\ (\varepsilon_a - 1) \tag{4}$$

Results and Interpretation

The material used to verify the capabilities of the unconfined swelling test was Bearpaw clay-shale, which was obtained from Southern Saskatchewan (Powell et al. 2012a, 2012b, 2013). Bearpaw is classified as high-plasticity clay with liquid and plastic limits ranging from 99 % to 145 % and 22 % to 29 %, respectively, and is composed of 39 % clay. The profile consists of high-plasticity soil from depths of 30 to 90 m, and remolded specimens from sample 189 were used for the testing program. Remolded specimens were prepared from dried and pulverized soil that was mixed to a target water content using the method described by Siemens (2006). The moistened soil was double-bagged and stored in a refrigerator for 48 h to allow for moisture equilibrium and a confirmatory measurement of the moisture content. The soil was removed and compacted into 50-mm-diameter specimens in lifts. Initial testing focused on optimizing the aspect ratio while holding the diameter constant. The aspect ratio (AR) is defined as

$$\text{AR} = \frac{\text{Height}}{\text{Diameter}} \tag{5}$$

Unconfined Swelling Test Results

An unconfined swelling test on specimen 189_AR = 0.15 is presented as a typical test to display the capabilities of the unconfined swelling test apparatus and methodology. The specimen was compacted to a target initial state of modified Proctor optimum, which was determined to have a gravimetric water content of 15 % and a dry density of 1.74 Mg/m^3. Table 1 highlights the initial conditions of the test specimens. Following preparation, the specimen was installed and given access to water. The swell results in terms of axial, radial, and volumetric strain versus time, plotted on both linear and logarithmic axes, are shown in Figs. 4(*a*) and 4(*b*), respectively. The specimen swelled at a high initial rate, and then the swell rate decreased after a few days. The volumetric strains of the soil specimen were 60 % and 61 % after 14 and 21 days, respectively (Fig. 4). The specimen expanded more radially than axially, and both expansions equilibrated with the moisture conditions at similar times. When the same data are re-plotted on a semi-log scale [Fig. 4(*b*)], the result resembles an unloading curve of a consolidation plot. Peng and Horn (2007) investigated the anisotropic behavior of some organic and inorganic soils that underwent shrinkage and swelling processes. They found that a typical swelling curve consists of two distinctive parts, the virgin swelling and the residual swelling curves. The virgin swelling curve contributes more than 80 % of the total soil volume expansion. The semi-log plot [Fig. 4(*b*)] also shows two distinctive swelling slopes, a primary swelling slope and a secondary swelling slope. The secondary swelling slope represents a decreasing rate of volume change over time. The primary swells at a gradient of 80 %/cycle and decreases to 9 %/cycle along the secondary swelling [Fig. 4(*b*)]. The intersection of the two curves indicates the end of primary swelling. For specimen 189_AR = 0.15, the end of primary swelling occurred at $t = 2.5$ d, which is very efficient for this type of test. Overall, primary swelling contributes more than 80 % of the total swelling strains (volumetric strain at $t = 2.5$ is 54 %, and final total swell is 63 %), which is consistent with results from Peng and Horn (2007). After four days, the specimen swelled at a log-linear rate for the remainder of the test. The test was completed after 27 days.

TABLE 1—*Initial conditions for unconfined swelling tests.*

Test ID	Target Aspect Ratio H/d	Height H, mm	Diameter d, mm	Bulk Density γ, Mg/m^3	Dry Density γ_d, Mg/m^3	Water Content w, %	Void Ratio e	Specific Volume V	Degree of Saturation S_r, %
189_AR=0.15	0.15	7.6	51.2	2.02	1.71	17.8	0.61	1.61	81.0
189_AR=0.25	0.25	13.7	51.4	1.85	1.60	15.6	0.72	1.72	59.5
189_AR=0.75	0.75	38.9	51.5	2.02	1.75	15.2	0.57	1.57	73.8
189_AR=2.0	2.0	101.9	51.6	2.00	1.74	15.3	0.58	1.58	72.4

Test results for four specimens, which varied in their target ARs (AR = 0.15, 0.25, 0.75, and 2.0), are presented in Fig. 5 on linear and logarithmic time scales. The four specimens had identical initial dry densities of 1.7 Mg/m^3, except for the specimen with AR = 0.25, which had a density of 1.6 Mg/m^3. The varying ARs enabled an interpretation of the dimensional effect on swelling behavior. The test results show similar trends with high initial swelling rates that decreased over time. The specimens with smaller ARs (0.15, 0.25, and 0.75) reached equilibrium in less than 20 days and achieved similar overall swelling magnitudes. The initial rate of swelling is related to the AR of a specimen; the smaller the AR, the higher the rate of swelling. The specimen with AR = 2.0 had a significantly lower initial swelling rate and, based on Fig. 5(*a*), achieved a significantly lower swelling magnitude at the end of the test.

Re-plotting the time-dependent swell data on a semi-log plot [Fig. 5(*b*)] shows similar results for the specimens with lower ARs and different behavior for the larger AR (AR = 2.0). The three lower AR specimens showed distinctive primary and secondary swelling curves with progressively increasing equilibration times ranging from 2.5 days for AR = 0.15 to 19 days for AR = 0.75. Even after almost 70 days of testing, a secondary swelling curve was not evident in the AR = 2.0 specimen. If the primary swelling curve is projected to the equilibrium strains for the smaller specimens, the end of primary swelling may arrive at between 120 and 250 days. A swelling test of this length is not feasible for normal site characterizations.

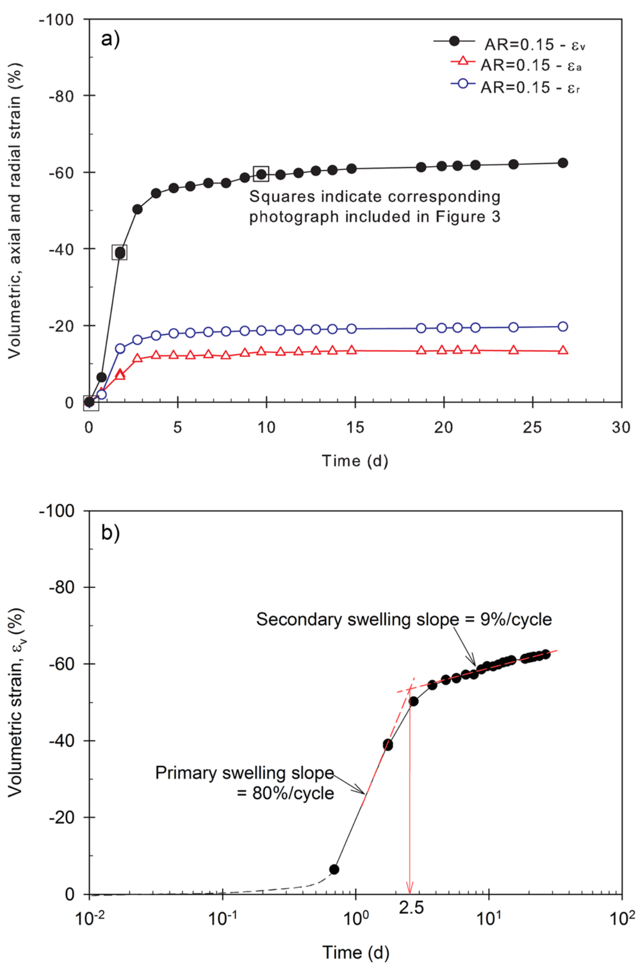

FIG. 4—*Volumetric, axial, and radial strain versus time for 189_AR = 0.15 upon wetting plotted versus time on (a) a linear scale and (b) a logarithmic scale.*

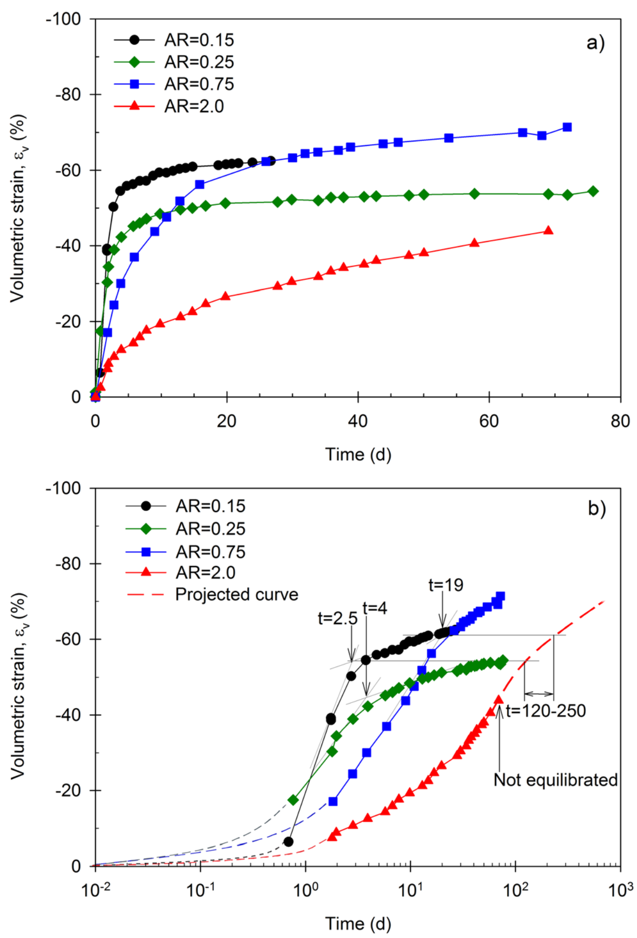

FIG. 5—*Volumetric strain versus time for varied aspect ratios plotted on (a) a linear scale and (b) a logarithmic scale.*

TABLE 2—*Swelling rate for unconfined swelling.*

Test ID	Target Aspect Ratio *H*/*d*	Surface Area/Volume, m^2/m^3	Time to End of Primary Swelling, d	Primary Swelling Slope, %/cycle	Secondary Swelling Slope, %/cycle	Initial Swelling Rate, %/d
189_AR=0.15	0.15	0.34	2.5	−80	−9	0.227
189_AR=0.25	0.25	0.22	4	−35	−7	0.147
189_AR=0.75	0.75	0.13	19	−39	−20	0.081
189_AR=2.0	2.0	0.10	120–250[a]	−37	—	0.045

[a]Projected.

The time required in order to achieve the end of primary swelling is directly related to the AR and the associated drainage length of the specimen. Unconfined swelling test results are summarized in Table 2 in terms of the duration needed to reach the end of primary swelling, primary swelling slope, secondary swelling slope, and initial swelling rate. Smaller ARs are associated with higher surface-area-to-volume ratios. Holding the initial diameter constant and increasing the height from 7.6 mm (AR = 0.15) to 101.9 mm (AR = 2.0) resulted in a 100-fold increase in the time to the end of primary swelling. The specimens that arrived at the end of primary swelling showed consistent swell magnitudes relative to their initial conditions. Thus, reducing the size decreases the overall testing time without having a significant effect on the final results.

The use of image analysis allows the measurement of axial and radial deformations that can be used to study potential anisotropic swelling behavior. Axial and radial strains are plotted against time in Fig. 4(*a*), and further data are presented in Fig. 6, which shows radial strain versus axial strain. Also plotted in Fig. 6 are triaxial swelling results from constant mean stress swelling tests, performed at 200 kPa and 400 kPa mean stress, on Bearpaw clay (Powell et al. 2013). The unconfined swelling test results initiate at the origin and plot into the lower left quadrant. The four swelling tests show internal variability in terms of the relative anisotropy; however, broadly speaking, swelling occurs along the 1:1 line. Figure 6(*b*) shows a close-up view of the higher stress swelling data. During swelling, the deformations occur along similar slopes in the higher stress tests, indicating that the swell properties are consistent with what is observed in the unconfined swelling tests.

End-of-test Measurements

The end-of-test measurements display the consistency of the results, as well as the benefits of using smaller test specimens. The end-of-test volume strain is plotted in Fig. 7 and summarized in Table 3 versus the AR. The GeoPIV and caliper end-of-test measurements are in good agreement, as plotted in Fig. 7. The difference between the caliper measurement and GeoPIV analysis is within ±2 mm, as presented in Table 3. The effect of the discrepancy was analyzed, and it contributes to a difference in volumetric strain of +3 % to −11 % depending on the original size of the specimens. Caliper measurements are generally different, as the soil specimen will have become very soft by the end of the test. Extreme care is needed when taking caliper measurements on the softened soil. The average swelling deformation from the caliper measurement and GeoPIV analysis is around 70 %. This deformation is considered as the maximum volumetric strain upon wetting. The two types of volume measurements show general agreement with similar end-of-test volume strains and changes in height and diameter.

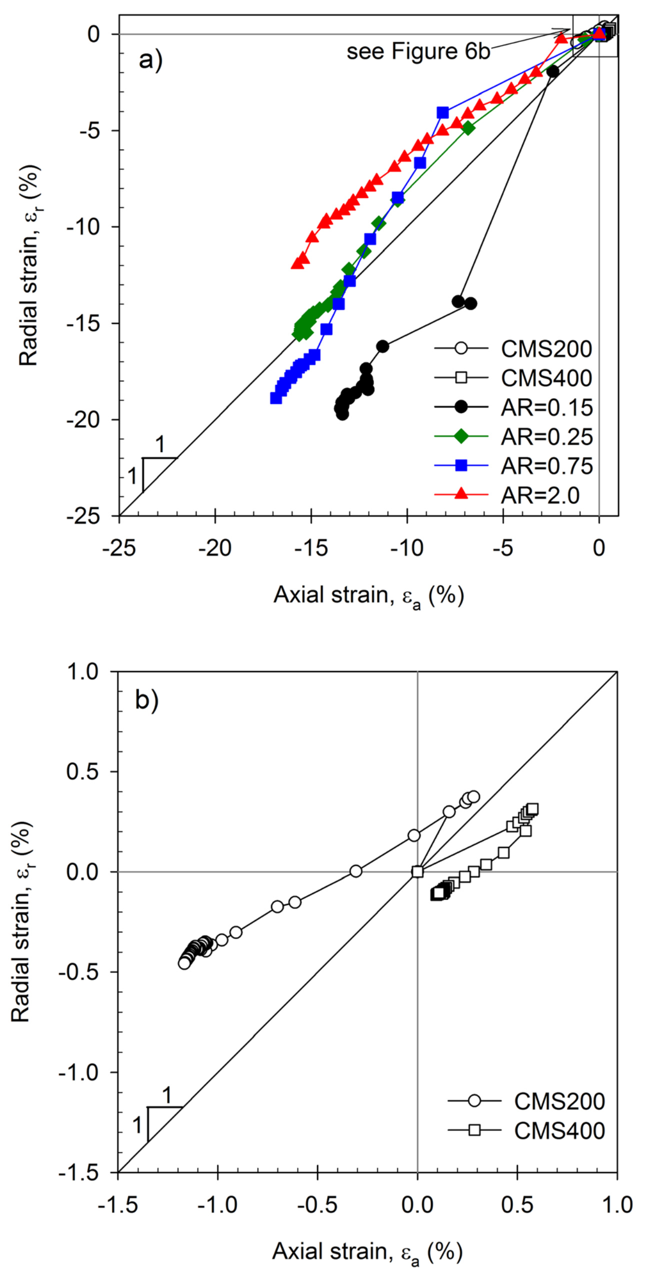

FIG. 6—*Radial strain versus axial strain upon swelling highlighting the similarity to triaxial swelling tests in part (b).*

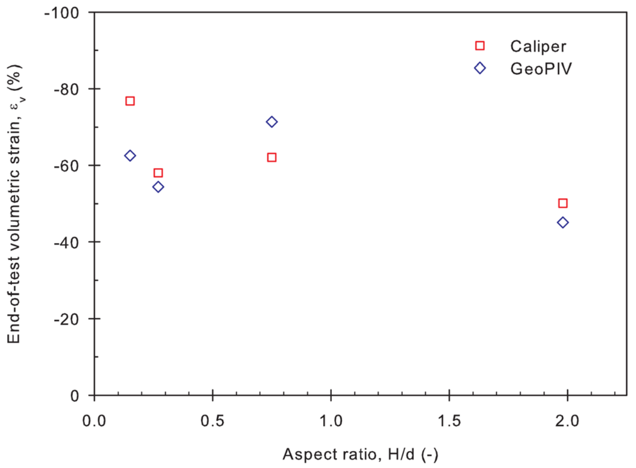

FIG. 7—*End-of-test volumetric strain versus aspect ratio (H/d) for caliper and GeoPIV methods.*

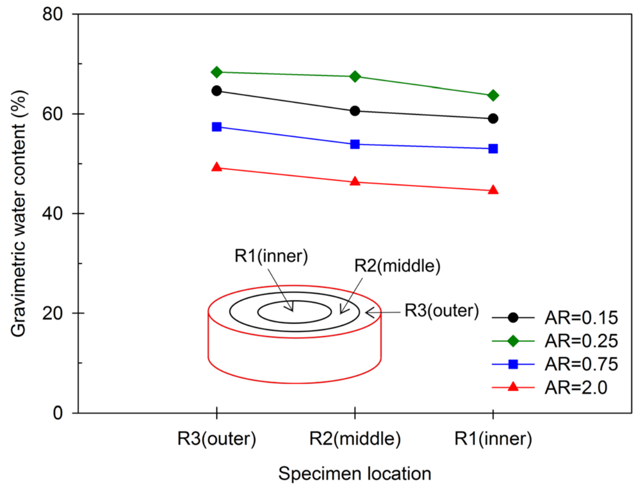

FIG. 8—*Spatial distribution of end-of-test moisture content.*

TABLE 3—*Comparison of caliper and GeoPIV measurements for unconfined swelling tests.*

		Caliper		GeoPIV		Difference Between Caliper and GeoPIV		
Test ID	Target Aspect Ratio *H*/*d*	Height *H*, mm	Diameter *d*, mm	Height *H*, mm	Diameter *d*, mm	Height *H*, mm	Diameter *d*, mm	ΔEnd-of-Test Volumetric Strain, %
189_AR=0.15	0.15	9.7	61.3	8.7	61.3	−1.0	0.0	−11
189_AR=0.25	0.25	15.7	60.9	15.8	59.4	0.1	−1.5	−4
189_AR=0.75	0.75	45.7	61.3	46.4	61.3	0.7	0.0	3
189_AR=2.0	2.0	117.5	59.3	117.4	57.3	−0.1	−2.0	−5

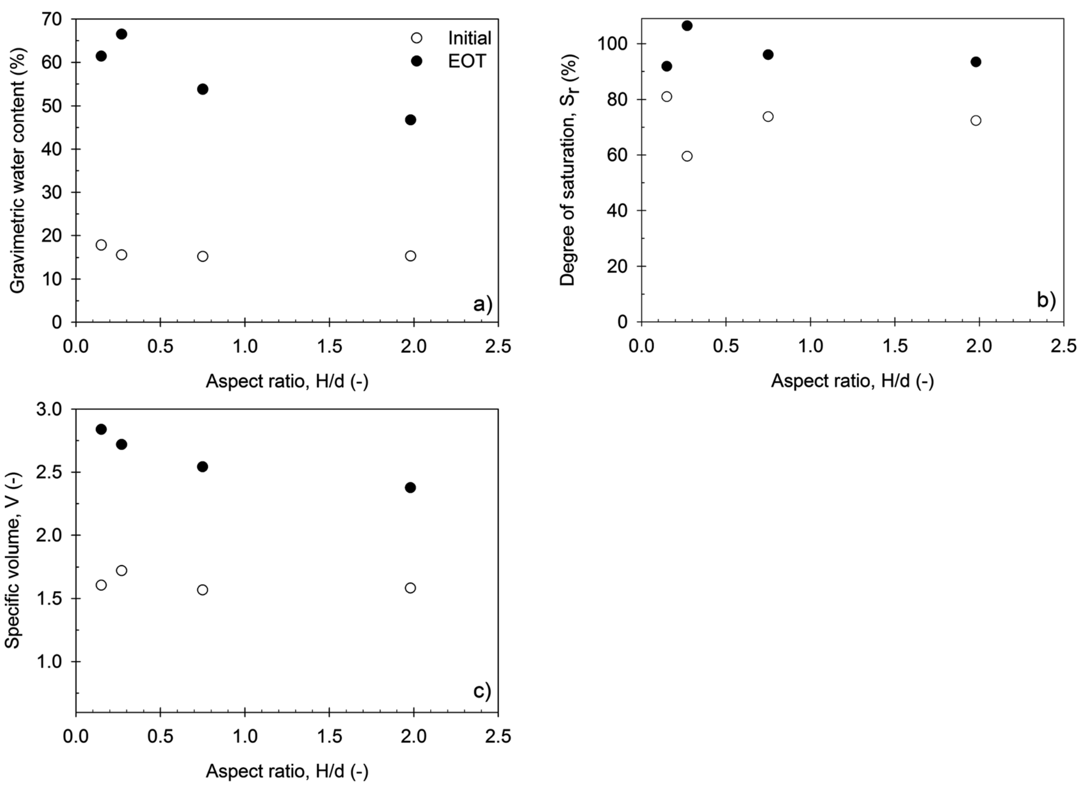

FIG. 9—*Initial and end-of-test (EOT) (a) gravimetric water content, (b) degree of saturation, and (c) specific volume versus aspect ratio (H/d).*

TABLE 4—*End-of-test results for unconfined swelling.*

Test ID	Height H, mm	Diameter d, mm	Bulk Density γ, Mg/m^3	Dry Density γ_d, Mg/m^3	Water Content w, %	Void Ratio e	Specific Volume V	Degree of Saturation S_r, %	Volumetric Strain ε_v, %
189_AR=0.15	9.7	61.3	1.56	0.97	61.4	1.84	2.84	91.8	−62.5
189_AR=0.25	15.7	60.9	1.68	1.01	66.5	1.72	2.72	106.4	−54.4
189_AR=0.75	45.7	61.3	1.66	1.08	53.8	1.54	2.54	96.0	−71.4
189_AR=2.0	117.5	59.3	1.70	1.16	46.7	1.38	2.38	93.4	−45.1

After the unconfined swelling tests are complete, the spatial distribution of the moisture content is measured radially. The gravimetric water content is measured at three different radial locations (R1, R2, and R3, moving from the center to the perimeter of the specimen) using cutters with diameters of 36.4 mm and 13.6 mm. The results in Fig. 8 show that the water content decreased toward the inner core of the specimen. The water content at the outer area of the specimen was the highest relative to the other two locations. The outer area of the soil specimen has the most direct access to water; water needs to permeate a longer path through the soil particles toward the core of the specimen.

Summaries of the end-of-test measurements are plotted in Fig. 9 and listed in Table 4. Figure 9(*a*) demonstrates the results for the gravimetric water content of the specimens at the beginning and the end of swelling tests. The target initial compacted state was optimum water content and dry density. By the end of the test, the water content had increased to a range of 46 % to 67 %. The final degree of saturation reached more than 90 % [refer to Fig. 9(*b*)], which indicates high saturation, especially considering that there was no external confining stress or back pressure applied to the specimens. The initial and the end-of-test specific volumes are plotted in Fig. 9(*c*). The soil specimens had relatively homogeneous compaction because the initial specific volume was in the range of 1.57 to 1.61, except in the specimen with AR = 0.25, which had a slightly larger void ($V = 1.72$) and a slightly lower initial dry density ($\gamma_d = 1.60$ Mg/m^3).

In order to demonstrate that the specimens had achieved a satisfactory degree of saturation by the end of the test, data are presented in a plot of dry density versus gravimetric water content. In Fig. 10, the initial compacted soil specimens are close to the optimum point. By the end of the test, the soil specimens had reached the line above $S_r = 90$ %, which indicates a high degree of saturation. The extent to which the soil swelled from its compacted state demonstrates the high swelling potential of the Bearpaw clay-shale.

The Swell Equilibrium Limit of Compacted Bearpaw Soil

The Swell Equilibrium Limit is a unifying concept used to analyze and predict maximum swelling potential which may be realized as expansion or swelling induced pressure. Powell et al. (2013) reported a Swell Equilibrium Limit for natural Bearpaw, which is

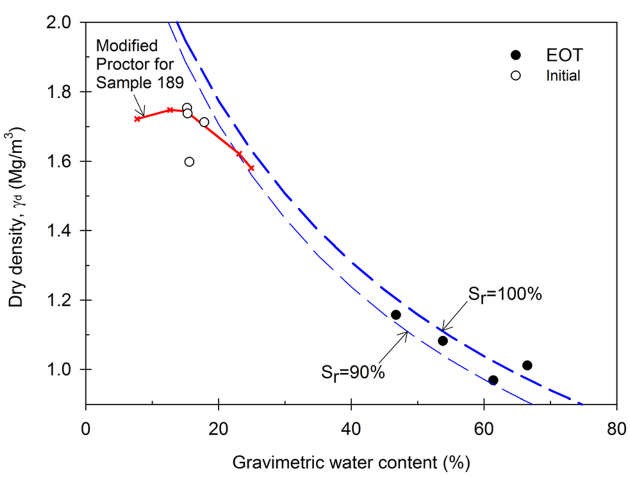

FIG. 10—*Initial and end-of-test (EOT) dry density versus water content and modified Proctor results for sample 189.*

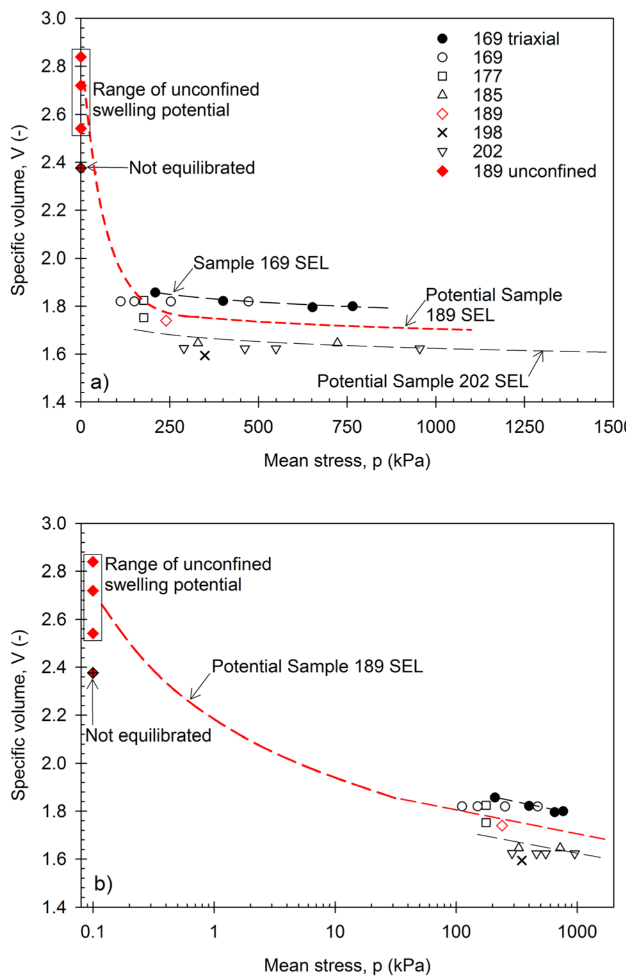

FIG. 11—*Swell equilibrium limit from unconfined swelling, triaxial swelling, and oedometer swelling pressure tests.*

presented in Fig. 11 along with the unconfined swell data from the current study. Powell et al. (2013) reported triaxial swelling and oedometer swelling pressure test results and showed the influence of sample depth on the Swell Equilibrium Limit. The data from the unconfined swelling tests are plotted along the *y*-axis in the linear scale and at 0.1 kPa (arbitrary value) in the semi-log plot [Fig. 11(*b*)]. There is noted variation in the final specific volume values for the unconfined swelling tests; however, this is in line with the variation noted by Beddoe et al. (2011) in swelling tests on geosynthetic clay liners performed at 2-kPa vertical stress. A Swell Equilibrium Limit for sample 189 is interpreted from the oedometer tests and unconfined swelling tests. With the low-stress data points, the upper-bound limit of swelling potential in this framework is measured experimentally. The data points at very low stress represent the worst-case scenario in which a soil would expand to its full potential at low confining stress.

Conclusions

An unconfined swelling test apparatus and methodology are presented for measuring the maximum swelling deformation of a soil under true free stress conditions. The methodology includes a non-contact method using digital image analysis to measure deformations. The in-test results indicate that primary and secondary swelling behavior and anisotropic swelling can be measured using the employed non-contact deformation method. The soil swelling deformation calculated with GeoPIV analysis is also in general agreement with end-of-test measurements. The effect of the AR on the swelling behavior is noted regarding the initial swelling rate and the time needed to reach equilibrium with the applied wetting conditions. The end-of-test measurements indicate consistent behavior for the specimens tested and that a high degree of saturation was achieved during the test. The maximum swelling deformation for Bearpaw soil is in the range of 60 % to 70 % volumetric strain under unconfined swelling conditions. The results are interpreted in the Swell Equilibrium Limit framework to allow analysis and prediction of swelling soil deformations. This extends the use of the Swell Equilibrium Limit framework down to nominal stress levels.

References

ASTM D4546-96: Standard Test Methods for One-Dimensional Swell or Settlement Potential of Cohesive Soils, *Annual Book of ASTM Standards*, ASTM International, West Conshohocken, PA, 1996.

ASTM D4546-08: Standard Test Methods for One-Dimensional Swell or Collapse of Cohesive Soils, *Annual Book of ASTM Standards*, ASTM International, West Conshohocken, PA, 2008.

Baille, W., Tripathy, S., and Schanz, T., 2010, "Swelling Pressures and One-Dimensional Compressibility Behaviour of Bentonite at Large Pressures," *Appl. Clay Sci.*, Vol. 48, pp. 324–333.

Beddoe, R. A., Take, W. A., and Rowe, R. K., 2011, "Water-Retention Behavior of Geosynthetic Clay Liners," *J. Geotech. Geoenviron. Eng.*, Vol. 137(11), pp. 1028–1038.

Cerato, A. B., Miller, G. A., and Hajjat, J. A., 2009, "Influence of Clod-size and Structure on Wetting-Induced Volume Change of Compacted Soil," *J. Geotech. Geoenviron. Eng.*, Vol. 135(11), pp. 1620–1628.

DiMaio, C., Santoli, L., and Schiavone, P., 2004, "Volume Change Behaviour of Clays: The Influence of Mineral Composition, Pore Fluid Composition and Stress State," *Mech. Mater.*, Vol. 36, pp. 435–451.

Dixon, D. A., Chandler, N. A., and Baumgartner, P., 2002, "The Influence of Groundwater Salinity and Influences on the Performance of Potential Backfill Materials," *Proc. 6th International Workshop on Design and Construction of Final Repositories*, Brussels, Belgium, March 11–13, 2002.

Ehrgott, J. Q., 1971, "Calculation of Stress and Strain From Triaxial Test Data on Undrained Soil Specimens," *Paper S-71-9*, U. S. Army Engineer Waterways Experiment Station, Vicksburg, MS; Unclassified.

Imbert, C. and Villar, M. V., 2006, "Hydro-Mechanical Response of a Bentonite Pellets/Powder Mixture upon Infiltration," *Appl. Clay Sci.*, Vol. 32, pp. 197–209.

Ito, M. and Azam, S., 2010, "Determination of Swelling and Shrinkage Properties of Undisturbed Expansive Soils," *Geotech. Geologic. Eng.*, Vol. 28, pp. 413–422.

Kodikara, J., 2012, "New Framework for Volumetric Constitutive Behavior of Compacted Unsaturated Soils," *Can. Geotech. J.*, Vol. 49, pp. 1227–1243.

Komine, H. and Ogata, N., 1994, "Experimental Study on Swelling Characteristics of Compacted Bentonite," *Can. Geotech. J.*, Vol. 31(4), pp. 478–490.

Lee, J. O., Lim, J. G., Kang, I. M., and Kwon, S., 2012, "Swelling Pressures of Compacted Ca-Bentonite," *Eng. Geol.*, Vols. 129–130, pp. 20–26.

Nagaraj, H. B., Munnas, M. M., and Sridharan, A., 2009, "Critical Evaluation of Determining Swelling Pressure by Swell-Load Method and Constant Volume Method," *Geotech. Test. J.*, Vol. 32(4), pp. 1–10.

Peng, X. and Horn, R., 2007, "Anisotropic Shrinkage and Swelling of Some Organic and Inorganic Soils," *Eur. J. Soil Sci.*, Vol. 58, pp. 98–107.

Powell, J. S., Siemens, G., Take, W. A., and Remenda, V., 2012a, "Influence of Specimen Geometry on Sample Disturbance Observed in Oedometric Testing of Clay Shales," *Geotech. Test. J.*, Vol. 35(5), pp. 771–783.

Powell, J. S., Siemens, G. A., Take, W. A., and Remenda, V. H., 2013, "Characterizing the Swell Potential of Bearpaw Shale," *Eng. Geol.*, Vol. 158, pp. 89–97.

Powell, J. S., Take, W. A., Siemens, G. A., and Remenda, V. H., 2012b, "Time Dependent Behavior of the Bearpaw Shale in Oedometric Loading and Unloading," *Can. Geotech. J.*, Vol. 49(4), pp. 427–441.

Rao, A. S., Phanilumar, B. R., and Sharma, R. S., 2004, "Prediction of Swelling Characteristics of Remolded and Compacted Expansive Soils Using Free Swell Index," *Q. J. Eng. Geol. Hydrogeol.*, Vol. 37, pp. 217–226.

Rao, K. S. S. and Tripathy, S., 2003, "Effect of Aging on Swelling and Swell-Shrink Behavior of a Compacted Expansive Soil," *Geotech. Test. J.*, Vol. 26(1), pp. 1–11.

Rojas, J. C., Gallipoli, D., and Wheeler, S. J., 2010, "Image Analysis of Strains in Soils Subjected to Wetting and Drying," *Geotech. Test. J.*, Vol. 35(1), pp. 1–14.

Siemens, G. A., 2006, "The Influence of Boundary Conditions on the Hydraulic-Mechanical Behaviour of an Unsaturated Swelling Soil," Ph.D. thesis, Department of Civil Engineering, University of Manitoba, Winnipeg, MB.

Siemens, G. and Blatz, J. A., 2007, "Triaxial Apparatus for Applying Liquid Infiltration With Controlled Boundary Conditions and Internal Suction Measurement," *J. Geotech. Geoenviron. Eng.*, Vol. 133(6), pp. 748–752.

Siemens, G. A. and Blatz, J. A., 2009, "Evaluation of the Influence of Boundary Confinement on the Behaviour of Unsaturated Swelling Clay Soils," *Can. Geotech. J.*, Vol. 46, pp. 339–356.

Siemens, G. A., Blatz, J. A., and Ruth, D. G., 2007, "A Capillary Tube Model for Transient Two-Phase Flow through Swelling Soil," *Can. Geotech. J.*, Vol. 44(12), pp. 1446–1461.

Singhal, S., Houston, S. L., and Houston, W. N., 2011, "Effects of Testing Procedures on the Laboratory Determination of Swell Pressure of Expansive Soils," *Geotech. Test. J.*, Vol. 34(5), pp. 1–13.

Vallejo, L. E., 2011, "Mechanics of the Slaking of Shales," *Geomechanics and Engineering*, Vol. 3(3), pp. 219–231.

White, D. J., Take, W. A., and Bolton, M. D., 2003, "Soil Deformation Measurement Using Particle Image Velocimetry (PIV) and Photogrammetry," *Géotechnique*, Vol. 53(7), pp. 619–631.

Geotech Geol Eng (2014) 32:1029–1042
DOI 10.1007/s10706-014-9778-z

ORIGINAL PAPER

Influence of Pore Fluid Chemistry on the Mechanical Properties of Clay-Based Materials

Sumi Siddiqua · Greg Siemens · James Blatz · Alex Man · Bee Fong Lim

Received: 5 December 2013 / Accepted: 16 May 2014 / Published online: 27 May 2014

Abstract The producers of nuclear waste, within all countries exploring options, including Canada, have determined the long-term solution to be a deep geological repository. In the Canadian concept, within the deep geologic repository a number of clay-based barriers will separate the containers from the surrounding geosphere. Following placement the surrounding groundwater will infiltrate into the repository. In order to analyze the performance of the repository under very complex conditions, accurate material properties are required. The chemistry of the host rock is an important aspect as the behaviour of clay-based barrier materials could be affected by the saturating saline groundwater. This paper investigates the saturated mechanical behaviour of light backfill (composed of 50 % silica sand and 50 % Na-bentonite clay) and dense backfill (composed of 70 % crushed granite, 25 % glacial lake clay and 5 % Na-bentonite clay) and the quantifying the effect of pore fluid chemistry on the strength and compressibility behaviour of the materials. The results indicate that light backfill behaviour is strongly influenced by its pore fluid chemistry while dense backfill shows limited effects. The material parameters of light backfill and dense backfill are interpreted for input into numerical simulations. These results and interpretation enrich the understanding of the mechanical response of light and dense backfill, two components of the sealing system of the Canadian deep geologic repository.

Keywords Used nuclear fuel storage · Engineered barriers · Triaxial · Pore fluid chemistry · Mechanical properties · Bentonite

S. Siddiqua (✉)
School of Engineering, UBC Okanagan Campus, EME, 3333 University Way, Kelowna, BC V1V 1V7, Canada
e-mail: sumi.siddiqua@ubc.ca

G. Siemens · B. F. Lim
GeoEngineering Centre at Queen's-RMC, Department of Civil Engineering, Royal Military College of Canada, Kingston, ON, Canada

J. Blatz
Civil Engineering Department, University of Manitoba, Winnipeg, MB, Canada

A. Man
Golder Associates, Winnipeg, MB, Canada

1 Introduction

A number of countries are currently considering proposed solutions for long-term storage of spent nuclear fuel (for example, Pusch 2001; Thomas et al. 2003; Romero et al. 2005; Johannesson et al. 2007; Villar et al. 2008; Gens et al. 2009; Tang et al. 2011). The Canadian repository concept for disposal of radioactive and chemical wastes is a multi-component sealing system (Fig. 1) placed deep underground (>500 m) in either crystalline or low permeability sedimentary rock (NWMO 2005). A number of

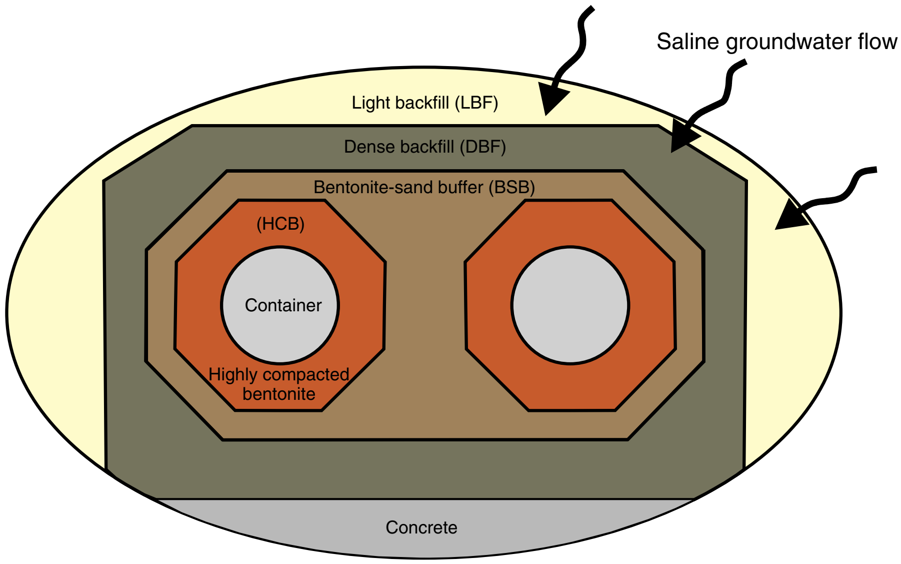

Fig. 1 Cross-section of the in-room emplacement concept for the Canadian deep geologic repository system (modified from Gierszewski et al. 2004)

engineered barrier materials will be placed between the waste containers and the local geosphere that are designed for specific requirements of the repository. The overall design requirements for the barrier materials are to support the waste containers, transfer thermal energy from the initially hot containers to the cooler end of the repository and cease movement of radionuclides from the repository to surrounding environment.

The sealing system components are designed to function under a wide range of environmental conditions, which are time-dependent. The repository and surrounding host rock will undergo thermal, hydraulic, mechanical, chemical and biological processes until the system reaches a state of equilibrium. Initially the waste containers are at an elevated temperature (up to 100 °C); the barriers will transfer the thermal energy to the local environment while at the same time moisture will move away from the containers following the thermal gradient. Local groundwater will begin to infiltrate into the repository. Groundwater in the Canadian Shield, one of the potential host locations, has total dissolved solids (TDS) concentration ranging from 8 to >100 g/L (Pearson 1985). A second potential host location is in sedimentary formations within Southern Ontario. Mazurek (2004) reported TDS between 191 and 325 g/L at depths greater than 300 m in groundwater from southwestern Ontario as well as the Michigan Basin. The coupled processes that involve in reaching equilibrium at the repository environment can be influenced by the chemistry of the groundwater of the proposed location of host rock.

One of the first studies considering the sensitivity of the physical properties of clay to pore fluid chemistry was reported in Winterkorn and Moorman (1941). Other early investigations on the influence of pore fluid chemistry focused mainly on the peak strength of clay materials (Skempton and Northey 1952; Rosenqvist 1953; Bjerrum 1954; Matsuo 1957; Moum and Rosenqvist 1961; Warkentin and Yong 1962). Later focus was given to study the effect of pore fluid chemistry on residual strength (Kenny 1967; Ramiah et al. 1970; Steward and Cripps 1983; Moore 1991, 1992; Di Maio and Fenelli 1994; Di Maio 1996; Anson and Hawkins 1998). The knowledge gained from these studies suggests that pore fluid chemistry has significant impacts on the strength of clay-based materials. However, little is known about the stress–strain behaviour of clayey materials with respect to effective stress. A recent study by Man and Graham (2010) presented the impact of pore fluid chemistry on stress–strain and yielding behaviour of highly plastic Lake Agassiz clay from the Red River valley in southern Manitoba.

In the Canadian concept for a spent nuclear fuel repository, the most widely studied sealing material is bentonite–sand buffer including saturated (Sun 1986; Saadat 1989; Oswell 1991; Yin 1990) as well as unsaturated experiments (Blatz 2000; Wan 1996; Tang 1999; Tang et al. 2002; Blatz and Graham 2003; Blatz et al. 2007; Siemens and Blatz 2009). Bentonite–sand buffer has the same overall composition as light backfill but with higher dry density ($\rho_d = 1.65$ Mg/m^3 compared with $\rho_d = 1.24$ Mg/m^3 for light backfill). These studies indicate that saturated bentonite–sand buffer generally behaves as similar to a normally consolidated plastic clay. Although no experiments were performed to investigate the stress–strain behaviour of bentonite–sand buffer under changes of pore fluid chemistry.

Quantifying the effect of elevated saline concentration on the mechanical properties of two of the clay-based barrier materials that are proposed in the Canadian repository concept is the objective of this paper. There is limited experimental data available for light backfill and dense backfill (Siddiqua et al. 2011a, b), which have been identified as a constraint for attempts to model the behaviour of sealing materials in potential repository settings (Priyanto et al. 2008). The influence of pore water chemistry on the saturated mechanical properties of two clay-based barriers (light backfill and dense backfill) is reported. The first material, light backfill, is composed of equal parts bentonite and sand with dry density 1.24 Mg/m^3 and sand while the second material is made up of a combination of crushed rock (70 %), natural swelling clay (25 %) and bentonite clay (5 %) compacted to a dry density of 2.12 Mg/m^3. Two pore fluids were tested including distilled water (Siddiqua et al. 2011b) and a $CaCl_2$ solution at >225 g/L (227 g/L for light backfill and 250 g/L for dense backfill). The effect of pore water chemistry was found to be different for the two materials based on their bentonite content.

2 Materials and Methods

2.1 Material Properties

Light backfill and dense backfill were the two clay-based materials studied in the experimental program. Light backfill is a 50:50 mixture by dry weight of silica sand and Na-bentonite clay. Within the repository the target initial dry density for light backfill is 1.24 ± 0.02 Mg/m^3 and water content of 15 ± 0.2 %, which gives an initial degree of saturation of approximately 33 %. The second material of the experimental program is dense backfill, composed of 70 % crushed granite, 25 % glacial lake clay and 5 % Na-bentonite clay by dry weight. The glacial lake clay is composed of 95–99 % clay-sized fraction (Man and Graham 2010). The initial target dry density for dense backfill within the repository is 2.12 ± 0.02 Mg/m^3 and water content of 8.5 ± 0.2 %, which results in a degree of saturation of approximately 80 %. Table 1 summarizes the preconsolidation pressure, swelling pressure, and hydraulic conductivity of light backfill and dense backfill for the pore fluids tested.

The bentonite component of materials is commercially mined Wyoming Bentonite. The Wyoming Bentonite was purchased from Bentonite Corporation of Wyoming under the trade name Standard-Western Bentonite (200 mesh). As received in the laboratory the sodium (Na) bentonite is in powder form following processing. It is composed of 75 % montmorillonite with the remaining being quartz and feldspars. The other clay component is the glacial lake clay, which is dominated by illite and also contains quantities of other minerals such as quartz, feldspar, dolomite and pyroxene.

Table 1 Material properties of light backfill and dense backfill (Siddiqua et al. 2011a)

Material	Pore fluid	Preconsolidation pressure (kPa)	Swelling pressure (kPa)	Hydraulic conductivity (m/s)
Light backfill	DW	100–150	120	10^{-12}–10^{-13}
Light backfill	227 g/L	45	28	10^{-11}–10^{-12}
Dense backfill	DW	180–300	250	10^{-11}–10^{-12}
Dense backfill	250 g/L	450	78	10^{-10}–10^{-11}

2.2 Triaxial Specimen Preparation

Triaxial specimen preparation followed standard testing procedures developed for clay-based barriers (Siemens and Blatz 2007, 2009; Siddiqua et al. 2011b). Prior to mixing light backfill with the desired pore fluid, the material was placed in oven for 48 h at 100 ± 5 °C to ensure consistent initial moisture content and dry density following compaction. The material was then removed and sealed in a mixing bowl to allow thermal equilibrium within the laboratory environment and at the same time preventing the adsorption of moisture from the atmosphere. A premeasured mass of de-aired distilled water or chemical solution was sprayed on the desired amount of dry sample and gently mixed to ensure uniform distribution. For specimens mixed with a chemical solution the mass of dissolved salts was taken into account in moisture content calculations. After mixing, the material was compacted to form 50 mm diameter by 100 mm tall cylindrical specimens. A strain-based criterion was employed for specimen compaction to ensure consistent dry density across the test specimen. The material was statically compacted in five 20 mm lifts and remaining material was used for confirmatory water content measurement. After compaction the specimen was installed in a triaxial cell.

The material composition of dense backfill demands a different technique for specimen preparation compared with light backfill. Specimens were prepared by separating the finer components (clay) from the granular ones (crushed rock) using a 2.38 mm sieve. After separation, the finer components were pulverized in order to break down the clay clumps and ensure even moisture conditions and remixed with granular portion and placed in oven at 100 ± 5 °C for 48 h. Periodically, during completion of the test matrix, grain-size analysis was performed to confirm that the composition of the dense backfill specimens was consistent. The remaining steps were similar to light backfill specimen preparation however the size of the dense backfill triaxial specimens were 102 mm in diameter and 250 mm in height.

Two types of pore fluid were selected for the triaxial tests to represent the range of potential field pore fluid salinities, distilled water and $CaCl_2$ solution. Light backfill specimens were saturated with 227 g/L $CaCl_2$ solution and dense backfill specimens were saturated with 250 g/L $CaCl_2$ solution.

2.3 Triaxial Tests

The test matrix for triaxial tests is presented in Table 2. Triaxial specimens were subjected to consolidated drained testing (CID) or consolidated undrained testing with pore water pressure measurement (CIU) in general accordance with ASTM D4767 (2004). The initial moisture content, dry density and effective montmorillonite dry density (EMDD) are also listed in Table 2. EMDD is defined as the mass of montmorillonite divided by the sum of the volume of montmorillonite and void space. Following compaction specimens were installed in the triaxial cell and immediately subjected to their target mean effective stress levels. The saturation and consolidation procedures of triaxial specimens were developed after several trials. It is important to note that due to a low hydraulic conductivity of light backfill (Table 1), 12–14 months were required to achieve full saturation. Saturation of all specimens was verified via B tests. Once a B test value greater than 0.95 was achieved, the specimen was considered to be saturated. Saturation data and observed B test values for LBF_1007 were plotted in Fig. 2 for example to show the extended time period (>1 year) required to achieve the target degree of saturation. Measurements were taken during the saturation phase to record the volume of liquid uptake by the specimens. After achieving the target degree of saturation, specimens were sheared at a constant displacement rate of 0.0021 mm/min. During the shearing phase, measurements of axial load, axial strain, cell pressure and back pressure were recorded. Drainage of the specimen was prevented in CIU tests with measurement of pore water pressure taken near the base of the triaxial cell. Volume change was measured during the shearing of the specimens in CID tests using burettes connected to the specimen drainage lines. After removal, numerous height and diameter measurements were taken as well as wax density tests in some cases to establish the end-of-test dry density and void ratio.

3 Test Results and Analysis

3.1 Stress–Strain Behaviour

Triaxial test results for light backfill specimens saturated with distilled water and 227 g/L $CaCl_2$

Table 2 Test matrix and measured properties of light backfill and dense backfill

Material (test type)	Specimen ID	Pore fluid	Effective stress (kPa)	Initial moisture content (%)	Initial dry density (mg/m^3)	Initial EMDD (mg/m^3)	Initial void ratio (−)	Void ratio before shearing (−)
Light backfill (CIU)	GS-LB15	DW	400	15.3	1.19	0.643	1.293	1.540
	GS-LB09	DW	800	15.6	1.21	0.661	1.247	1.360
	GS-LB10	DW	900	13.0	1.24	0.679	1.205	1.249
	JB-LB17	DW	1,200	17.0	1.18	0.635	1.317	1.343
	LBF_1004	227 g/L $CaCl_2$	400	14.0	1.28	0.707	1.104	0.630
	LBF_1008	227 g/L $CaCl_2$	800	13.2	1.28	0.710	1.096	0.536
	LBF_1010	227 g/L $CaCl_2$	1,200	13.4	1.28	0.713	1.111	0.572
Light backfill (CID)	GS-LB11	DW	400	15.5	1.25	0.692	1.174	1.569
	GS-LB14	DW	800	15.5	1.23	0.677	1.209	1.429
	GS-LB12	DW	1,200 (1)	15.0	1.23	0.678	1.206	1.142
	JB-LB16	DW	1,200 (2)	15.4	1.20	0.656	1.509	1.324
	LBF_1009	227 g/L $CaCl_2$	400	11.7	1.30	0.726	1.085	0.653
	LBF_1006	227 g/L $CaCl_2$	800	14.3	1.26	0.699	1.120	0.544
	LBF_1007	227 g/L $CaCl_2$	1,200	14.3	1.27	0.705	1.276	0.522
Dense backfill (CIU)	GS-DBF19	DW	400	6.6	2.12	0.451	0.273	0.230
	JB-DB16	DW	800	6.4	2.10	0.432	0.311	0.197
	GS-DBF17	DW	900	6.8	2.15	0.477	0.257	0.231
	SS-DBF02	250 g/L $CaCl_2$	800	8.0	2.13	0.458	0.269	0.177
Dense backfill (CID)	JB-DBF15	DW	400	6.2	2.10	0.438	0.306	0.241
	GS-DB18	DW	800	6.8	2.12	0.454	0.271	0.212
	JB-DBF13	DW	1,200	5.5	2.15	0.476	0.281	0.161
	SS-DBF01	250 g/L $CaCl_2$	400	9.4	2.03	0.382	0.328	0.258
	SS-DBF03	250 g/L $CaCl_2$	800	6.8	2.17	0.505	0.243	0.170
	SS-DBF04	250 g/L $CaCl_2$	1,200	7.4	2.11	0.439	0.282	0.199

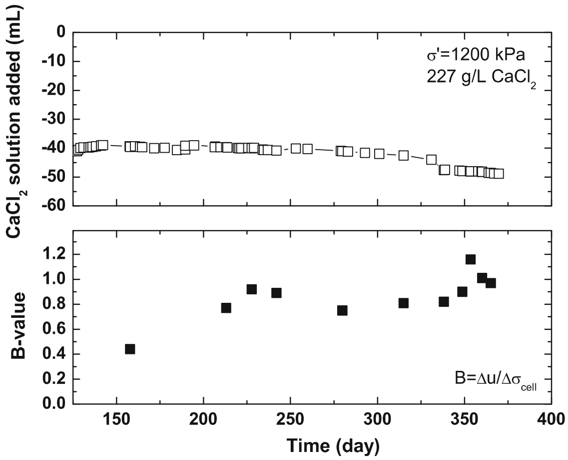

Fig. 2 Saturation and B test data for light backfill specimen LBF_1007 saturated with 227 g/L $CaCl_2$

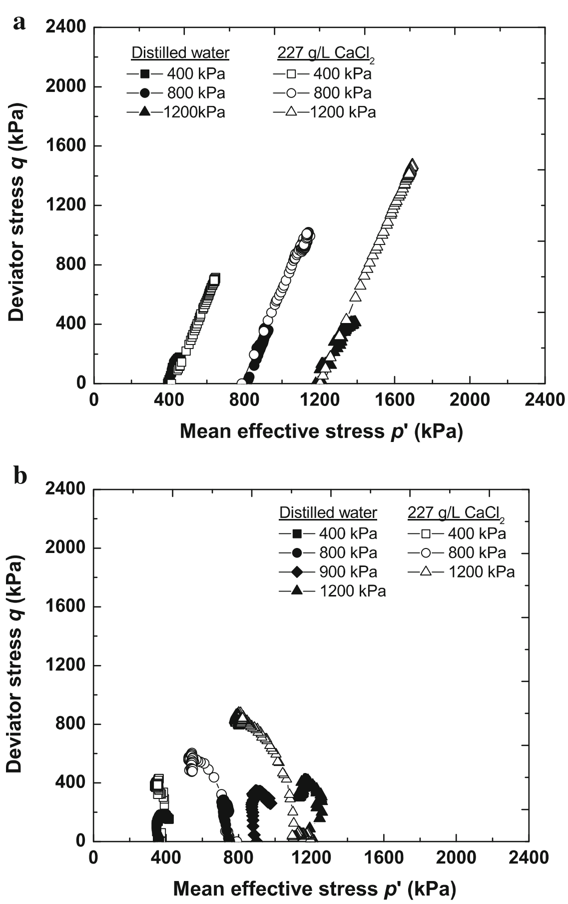

Fig. 3 **a** Stress paths for CID triaxial tests on light backfill. **b** Stress paths for CIU triaxial tests on light backfill

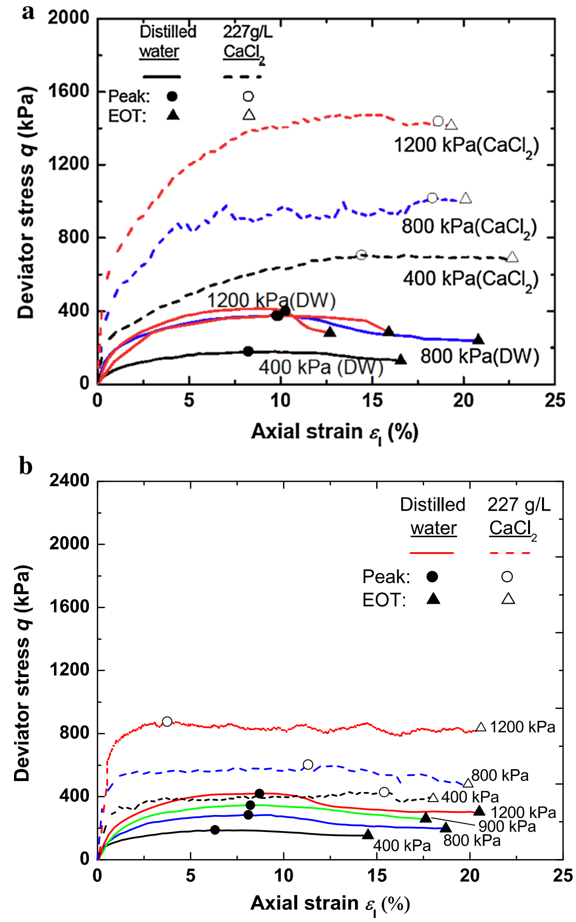

Fig. 4 **a** Stress–strain curves for CID triaxial tests on light backfill. **b** Stress–strain curves for CIU triaxial tests on light backfill

solution are plotted in Figs. 3 and 4. Triaxial shearing was completed using one of two stress paths, which were drained (CID) or undrained (CIU). Figure 3a, b displays the data (grouped by test type) in deviator stress (q) versus mean effective stress (p') and Fig. 4a, b displays the same tests as deviator stress versus axial strain (ε_l). The CID tests display a clear $q{:}p' = 3{:}1$ relationship (Fig. 3a) for both saline pore fluid and distilled water specimens. Based on the preconsolidation pressure (Table 1) all tests specimens are normally consolidated. Comparing the tests in terms of the pore fluids, the $CaCl_2$ specimens show an increase in initial stiffness as well as the peak and post-peak stress clearly displaying the effect of pore fluid chemistry within the experimental conditions. In the distilled water specimens for both CID and CIU strain-

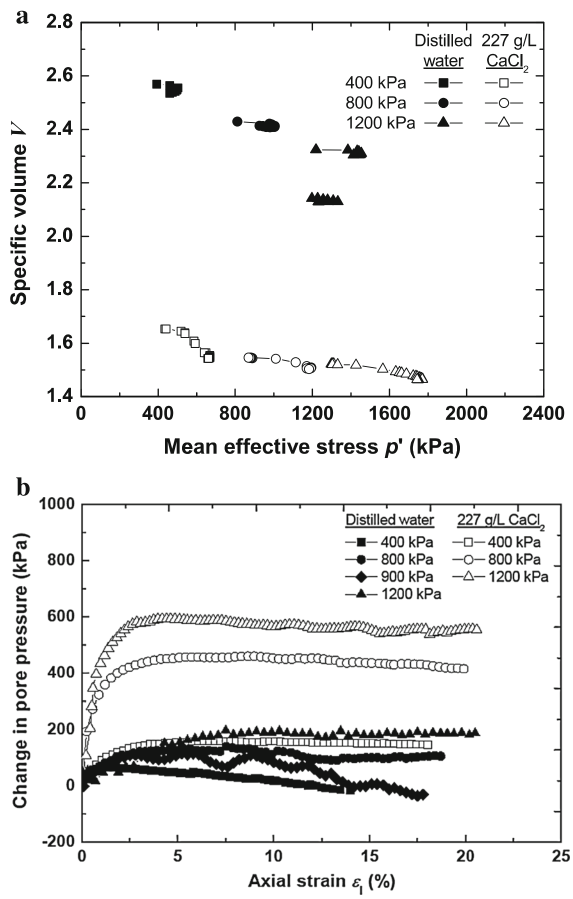

Fig. 5 **a** Relationship between specific volume and mean effective stress, p′, during CID shearing for light backfill specimens saturated with distilled water and 227 g/L $CaCl_2$. **b** Pore pressure–axial strain relationship for CIU triaxial tests on light backfill

softening of the material is observed with additional straining beyond peak (for axial strain >10 %). The strain-softening behaviour of the material is clearer in Fig. 4a, b. Little strain-softening is observed for the specimens saturated with chemical solution for both CID and CIU tests.

The stress–volume paths for the CID tests are plotted in Fig. 5a in specific volume–mean effective stress space (V–p′). All test specimens had equivalent initial target dry density before installation in the triaxial cell. The only difference between the tests is the pore water chemistry. At the end of the saturation phase and during the shearing phase, the specimens saturated with saline solution had significantly lower specific volume (and associated dry density) than their distilled water counterparts (also listed in Table 1). The difference in specific volume ranges from $\Delta V = 0.916$ at 400 kPa to $\Delta V = 0.802$ at 1,200 kPa at the beginning of the shearing phase. In terms of CIU tests, the pore pressure and axial strain relationship are presented in Fig. 5b.

Whilst the light backfill test results displayed a significant effect of pore fluid chemistry, the dense backfill showed very little impact. The results plotted in Figs. 6 and 7 present dense backfill specimens saturated using distilled water and 250 g/L $CaCl_2$ solution. For the effective stresses applied (400–1,200 kPa) and the preconsolidation pressure (180–300 kPa for distilled and 450 kPa for $CaCl_2$ solution), the specimens are either normally consolidated or slightly overconsolidated. The stress paths in CID and CIU tests are presented in Fig. 6a, b respectively. The CID tests follow a clear 3:1 stress path in q:p′ space (Fig. 6a). Both distilled water and $CaCl_2$ saturated specimens exhibited broadly similar stress-path behaviour with a similar peak strength magnitude. The stress–strain relationship plotted in Fig. 7a, b for dense backfill specimens generally displayed ductile behaviour with increasing strength to a peak value and little strain-softening. Broadly the stress–strain curves are similar with the initial stiffness of the distilled water specimens being somewhat greater than their $CaCl_2$ counterparts. Although the distilled water specimens show an increase in stiffness with increasing effective stress, the $CaCl_2$ specimens' stress–strain curves overlap with each other over the range of 400–1,200 kPa effective stress (Fig. 7a). Comparing the larger-strain behaviour, the tests with $CaCl_2$ pore fluid show that the peak is attained at higher strain than the distilled water tests at same effective stress level. Gradual strain-softening above 10 % axial strain is noted for CID tests performed at 800 and 1,200 kPa for both distilled water and $CaCl_2$ saturated specimens. The CIU test results (Fig. 7b) display ductile behaviour with strength increasing to a peak value which is maintained for the remainder of the test.

The stress–volume paths of the CID tests are plotted in Fig. 8a in specific volume–mean effective stress space (V–p′). Similar values of specific volume are noted for both specimens saturated with distilled water and 250 g/L $CaCl_2$. The results indicate little influence of the pore water chemistry on the equilibrium specific volume following saturation ($\Delta V < 0.042$). During shearing the bulk stiffness of dense backfill also shows

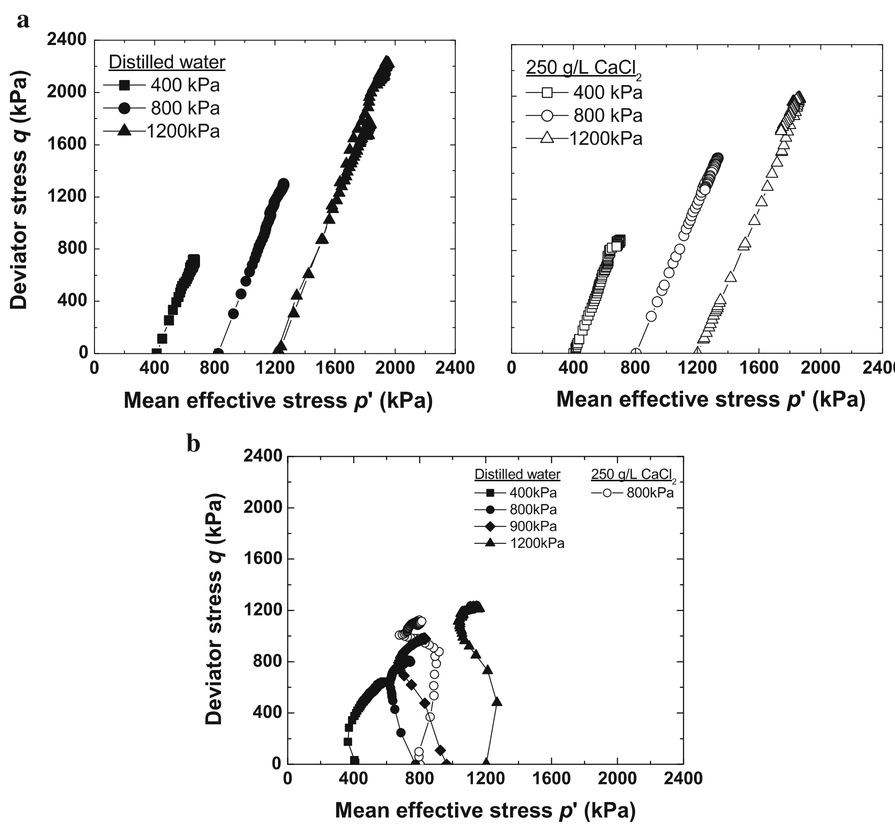

Fig. 6 **a** Stress paths fort CID triaxial tests on dense backfill. **b** Stress paths for CIU triaxial tests on dense backfill

insignificant influence of pore fluid chemistry with similar stiffness noted. Also, Fig. 8b presents the pore pressure changes with respect to axial strain for CIU tests.

Tests results have indicated that deformation patterns and failure mechanisms in light backfill and dense backfill are a function of pore water chemistry. Moreover, differences in material behaviour are also observed in light backfill depending on the type of pore fluid. Photographs of typical failure modes are shown in Fig. 9 of a 1,200 kPa distilled water CID test (Fig. 9a) and a 1,200 kPa $CaCl_2$ CIU test (Fig. 9b). The stress–strain behaviour indicated strain-softening for the distilled water specimen (Fig. 4a) and ductile behaviour for the $CaCl_2$ test (Fig. 4b). The failure modes of specimens agree with the observed behaviour with a well-defined shear plane apparent in the distilled water and ductile failure mode for the $CaCl_2$ specimen. Although the strain-softening occurred in the distilled water test, it occurs at axial strains greater than 10 %, which indicates an intermediate brittle nature of the material. The second material, dense backfill, showed consistent failure modes for the tests completed. A barrel shaped failure was observed for the material tested with both distilled water and $CaCl_2$ solution consistent with the stress–strain and stress paths followed.

3.2 Yield States

While examining soil behaviour in an elastic–plastic framework, it is helpful to normalize deviator stress and mean effective stress with respect to the preconsolidation pressure (Graham et al. 1983, 1989, 1990; Blatz et al. 2007). The range of stresses applied in the tests (400–1,200 kPa) is greater than the preconsolidation pressure for the material (Table 1). Therefore, the specimens are normally consolidated and the results are presented in p′–q space normalized with respect to the maximum isotropic stress applied for individual tests in Figs. 10 and 11. Also plotted are the normalized yield envelopes for light backfill and dense backfill. The shapes are similar to earlier findings by Oswell (1991) for anisotropic behaviour of bentonite–

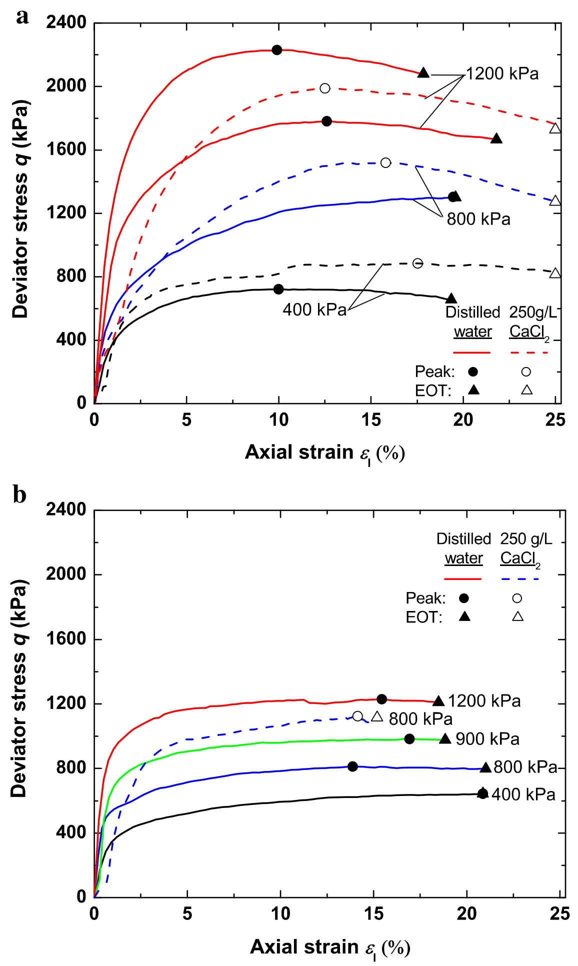

Fig. 7 **a** Stress–strain curves for CID triaxial tests on dense backfill. **b** Typical stress–strain curves for CIU triaxial tests on dense backfill

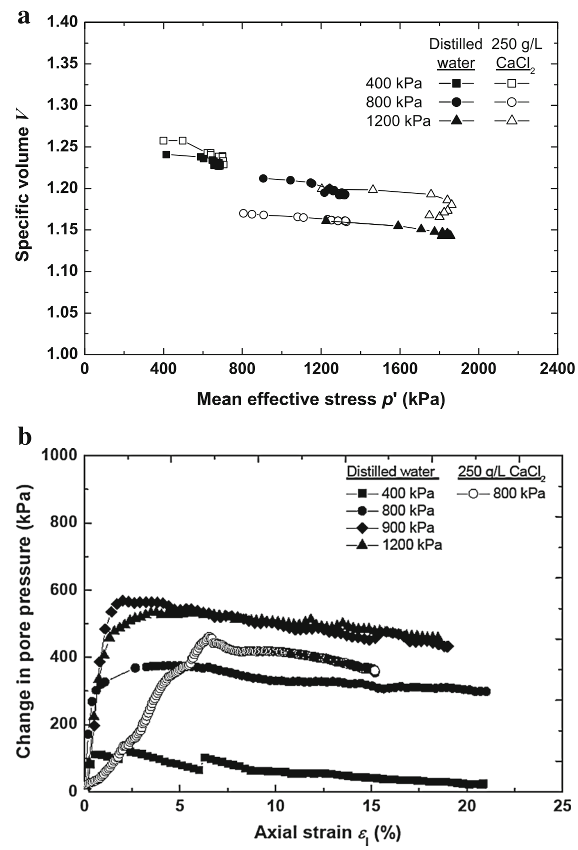

Fig. 8 **a** Relationship between specific volume, V, and mean effective stress, p′, during CID shearing for dense backfill specimens saturated with distilled water and 250 g/L $CaCl_2$. **b** Pore pressure–axial strain relationship for CIU triaxial tests on dense backfill

sand buffer. Oswell (1991) found that a single anisotropic yield locus could be used to describe the yield state of high density ($\gamma_d = 1.67$ Mg/m^3) and low density ($\gamma_d = 1.50$ Mg/m^3) bentonite–sand buffer.

The yield locus for light backfill specimens tested with distilled water indicates a narrow range of normalized yield stresses (Fig. 10). This corresponds to the fact that the material is relatively soft at its as-compacted state and behaves elastically for a small range of stresses. Beyond this range the material shows plastic hardening. Comparing the effect of pore fluid shows the yield envelope expands when the material tested is prepared and saturated with 227 g/L of $CaCl_2$. Given the significantly lower specific volume for light backfill saturated with saline pore fluid (Fig. 5; Table 2) an increase in yield state is anticipated. Conversely the yield locus for dense backfill specimens is independent on the type of pore fluid. As plotted in Fig. 11, both distilled water and chemical solution saturated specimens reach similar normalized yield stresses.

3.3 Strength Parameters

Shear strength of light backfill indicates an influence of pore water chemistry while dense backfill shows no detectable difference. Peak and post-peak strength parameters have been defined using the shearing data and are plotted in Fig. 12 for light backfill and Fig. 13 for dense backfill. Table 3 provides a summary of strength parameters for light backfill and dense backfill include slope M (peak or critical state) in p′–q space and the corresponding Mohr–Coulomb angle

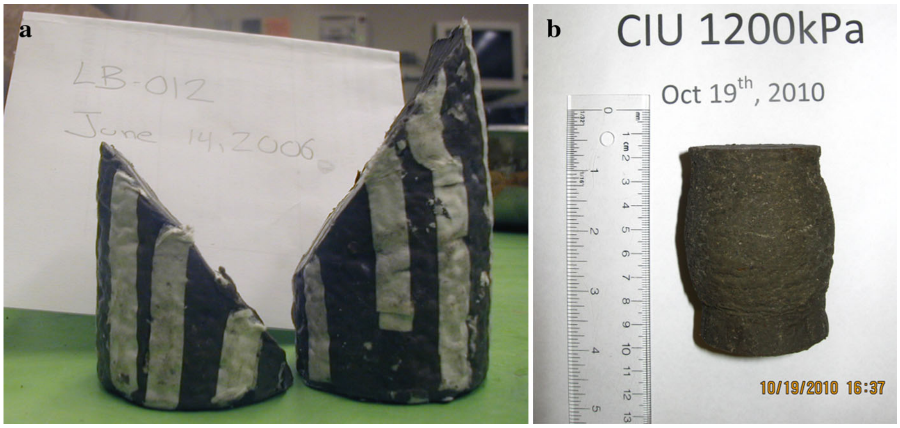

Fig. 9 Typical failure modes for light backfill specimens. **a** Light backfill distilled water CID specimen tested at 1,200 kPa illustrating typical shear-plane failure mode. **b** Light backfill $CaCl_2$ CIU specimen tested at 1,200 kPa illustrating typical ductile failure mode

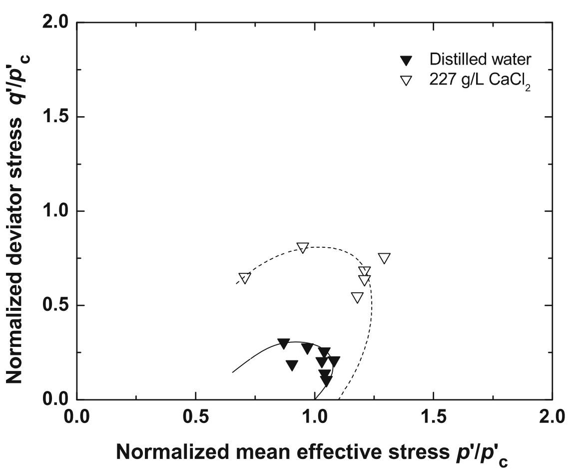

Fig. 10 Yielding states in normalized p'–q space for light backfill

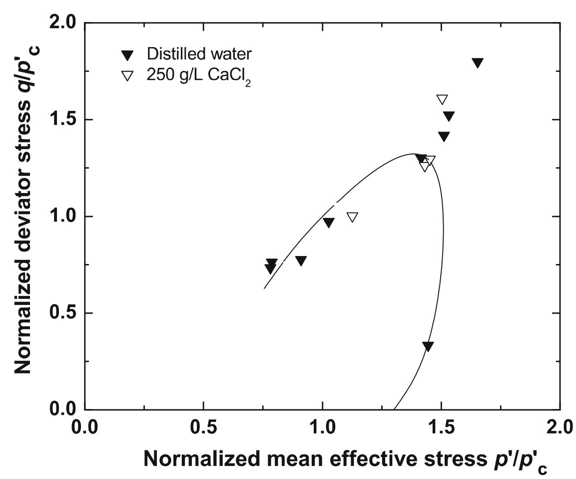

Fig. 11 Yielding states in normalized p'–q space for dense backfill

of friction. The slope $M_{peak} = 0.4$ for distilled water saturated light backfill specimens and increases to $M_{peak} = 0.96$ for specimens saturated with 227 g/L $CaCl_2$ solution. This corresponds to Mohr–Coulomb angle of friction $\phi'_{peak} = 11°$ for distilled water and $\phi'_{peak} = 24°$ for the $CaCl_2$ solution. This data yield a slope $M_{cs} = 0.37$ for distilled water saturated light backfill specimens and $M_{cs} = 0.9$ for light backfill specimens saturated with $CaCl_2$ solution. The Mohr–Coulomb angle of friction at critical state for distilled water becomes $\phi'_{cs} = 10°$ and for the $CaCl_2$ solution increases to $\phi'_{cs} = 22°$. These results suggest that the slope M and corresponding angle of friction increase directly with pore fluid chemistry.

A similar approach is adopted to define the strength parameters for dense backfill (Fig. 13). The slope, M at peak (M_{peak}) and post peak, i.e. at critical state (M_{cs}) is 1.1, which yields to a Mohr–Coulomb angle of friction $\phi' = 28°$ (Table 3). Most importantly, altering the pore fluid chemistry did not show any detectable impact on the material's strength.

3.4 Material Stiffness

Material stiffness was compared between the distilled water and $CaCl_2$ solution specimens to investigate the effect of pore fluid chemistry. Young's modulus (E) was calculated from q–ε_l behaviour obtained from

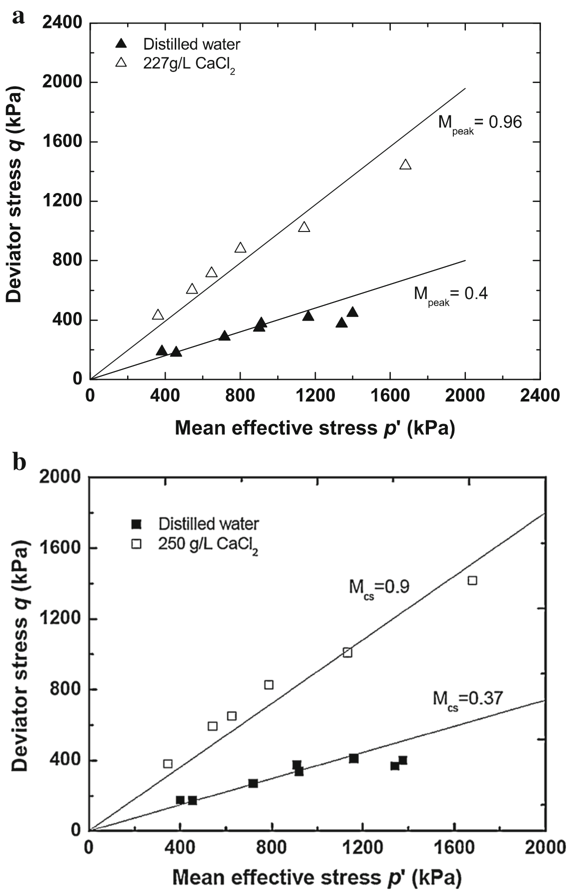

Fig. 12 **a** Peak strengths in $p'–q$ space for light backfill. **b** Post peak strengths in $p'–q$ space for light backfill

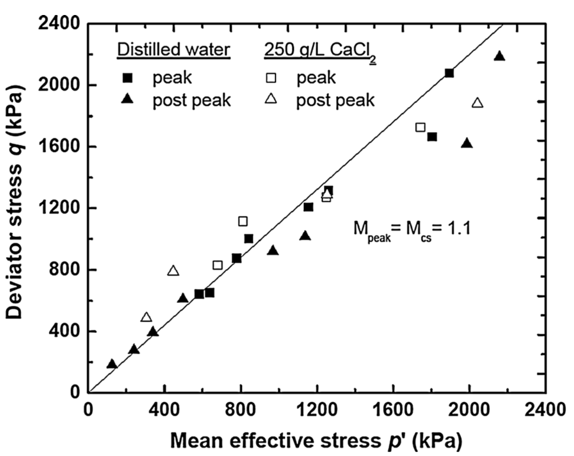

Fig. 13 Peak and post peak strengths in $p'–q$ space for dense backfill

Table 3 Summary of strength parameters for light and dense backfill

Material	Pore fluid	Peak state (p'–q space)		Post peak state	
		M_{peak}	ϕ'_{peak} (°)	M_{peak}	ϕ'_{cs} (°)
Light backfill	DW	0.40	11	0.37	10
Light backfill	227 g/L $CaCl_2$	0.96	24	0.90	22
Dense backfill	DW	1.1	28	1.1	28
Dense backfill	250 g/L $CaCl_2$	1.1	28	1.1	28

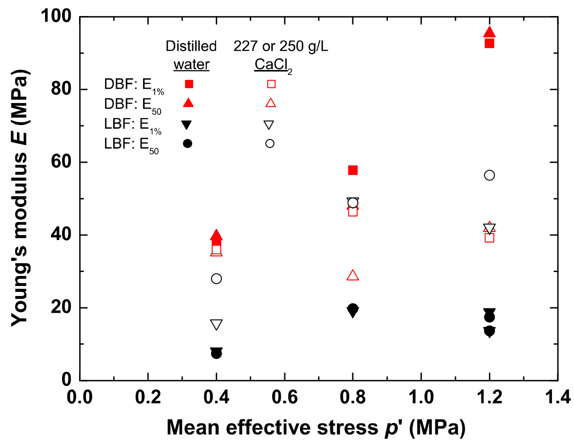

Fig. 14 Young's modulus (E_1 % and E_{50}) for light backfill and dense backfill at varying isotropic consolidation pressure grouped by pore fluid chemistry

CID tests (Figs. 4a, 7a) and CIU tests respectively (Figs. 4b, 7b). Figure 14 presents data for Young's modulus as a function of mean effective stress. Results were grouped according to the material type and pore fluid chemistry. E_1 % was interpreted by selecting deviator stress at axial strain of 1 % and calculating the secant modulus. E_{50} was calculated by selecting axial strain at 50 % of maximum deviator stress and calculating the secant modulus.

Stiffness of light backfill generally increases with effective stress for both pore fluids as expected. The effect of pore fluid chemistry significantly impacted the stiffness parameters of light backfill. The values for the $CaCl_2$ tests (open black symbols in Fig. 14) are greater than distilled water ones (closed black symbols) tested at the same isotropic consolidation pressure.

Dense backfill stiffness for distilled water specimens increases with mean effective stress. Young's modulus for 250 g/L $CaCl_2$ (open red symbols in Fig. 14) was similar to distilled water at 400 kPa, however, little influence of confining stress was noted. At 1,200 kPa the stiffness of distilled water specimens is more than double the 250 g/L $CaCl_2$ counterparts.

4 Interpretation

4.1 Light Backfill

The pore water chemistry has a notable influence on the mechanical behaviour of saturated light backfill. The material is composed of 50 % Na-bentonite as well as an elevated EMDD and, therefore, mechanical properties were anticipated to be strongly influenced by the pore water chemistry. The triaxial test results indicate that increasing the saline content of the pore fluid from zero to 227 g/L of $CaCl_2$ increases the shear strength (Figs. 3, 4, 12; Table 3), normalized yield envelope (Fig. 10) and stiffness (Fig. 14) properties of light backfill. Light backfill also has a tighter structure when prepared and saturated with high salinity pore fluid as indicated by a lower specific volume (Fig. 5; Table 2). The cations within the pore fluid reduce the diffusive double layer thickness resulting in a more stable structure (Barbour and Yang 1993). This reduction in specific volume is associated with a tighter micro-structure of light backfill saturated with a chemical solution. The term open micro-structure is used to explain particle spacing with more edge-to-edge or edge-to-face contacts of the particles. The tighter spacing reduces the specific volume and the additional particle contacts increase the friction angle. Therefore, the expansion of elastic region and the reduction in specific volume for these specimens can be a result of osmotically induced consolidation (Barbour and Yang 1993).

Within the scope of the experiments, these results clearly indicate that the change of pore fluid chemistry can influence the overall mechanical behaviour of light backfill material. This behaviour of the material can be explained by the diffuse double layer (DDL) concept (Mitchell 1993) and the effective stress concept described by Graham et al. (1992). The effective stress in clay can be written as follow (Graham et al. 1992):

$$\{\sigma'\} = \{\sigma^*\} + \{|R - A|\} \tag{1}$$

where σ' is the effective stress, σ^* is the stress transferred between physical contacts of particles, $|R–A|$ is net long-range repulsive stress. Effective stress is a combination of two components; the stress (σ^*) which is transferred between particles due to physical contacts including friction and cementation bonds and net long-range repulsive stress denoted by $|R–A|$ in the equation. The thicker DDL result in higher repulsive forces for a given particle spacing (Yong et al. 1992) and an attractive force will exist between particles as a reason of van der Waals forces. These two forces can be integrated over a number of particles from a unit section of the material to obtain the long-range repulsive stress. Repulsion is governed by pore fluid chemistry, which plays significantly in volume changes, shear strength and hydraulic conductivity of active clay, such as bentonite (Graham 2006). In other words an increase in pore fluid salinity results in decrease in DDL thickness (Yong et al. 1992; Mitchell 1993), which causes the effective stress due to inter particle contacts (σ^*) to dominate over net long-range repulsive stress.

Results of peak and critical-state parameters for light backfill clearly agreed with the above statements. Both peak and critical-state lines are observed to shift upwards indicating an increase of the slope M in p′–q space for the specimens saturated with chemical solution. Increases in the yield envelope and stiffness of light backfill were also noted.

4.2 Dense Backfill

Results from dense backfill testing indicated limited influence of pore water chemistry on the mechanical behaviour. Although compacted to a high dry density, dense backfill is composed of just 5 % Na-bentonite and 25 % glacial clay, which results in a lower EMDD. Material properties for dense backfill prepared and saturated with distilled water were consistent with saline pore fluid for shear strength (Figs. 6, 7, 13; Table 3) and yielding (Fig. 11). The only exception was in the stiffness parameters (Fig. 14), which indicated dense backfill with distilled water was relatively stiffer compared with the saline pore fluid. Overall the results indicated that the crushed granite component (70 %) and high density has a stronger influence on the saturated mechanical behaviour rather than the clay components.

5 Summary

Countries around the world are considering solutions to the challenge of long-term storing of used nuclear fuel. In the Canadian context, a deep geologic repository is a proposed solution, which involves surrounding waste containers with a number of engineered barriers within a stable geologic formation. Within the repository setting, the thermal energy stored in the containers will start to dissipate and the surrounding groundwater will infiltrate into the repository. Salinity of the groundwater within proposed geologic units is significantly high and, therefore, the effect of pore fluid chemistry on the behaviour of barrier materials is of interest to the performance of the repository.

Laboratory experiments on two proposed barrier materials, light backfill and dense backfill, were performed to examine the effect of pore fluid chemistry on the mechanical behaviour of the materials. Within the context of the experiments, light backfill showed a notable effect of the pore fluid chemistry, which included increased shear strength, stiffness and yield behaviour. This change in behaviour is consistent with a clay-dominated material with variable microstructure due to changes to the salinity of the pore fluid. The other sealing material considered, dense backfill, is composed mainly of crushed granite with a smaller percentage of active clays. Therefore material properties are not primarily dominated by the pore fluid chemistry. Dense backfill did not show any detectable sensitivity to the pore fluid chemistry on the shear strength and yielding behaviour with limited effects on the stiffness. The material properties are now available to be used in analysis of the proposed repository.

References

Anson RWW, Hawkins AB (1998) The effect of calcium ions in pore water on the residual shear strength of kaolinite and sodium montmorillonite. Géotechnique 48(6):787–800

ASTM (2004) Standard test method for consolidated undrained triaxial compression test for cohesive soils. ASTM standard D4767-04. American Society for Testing and Materials (ASTM), West Conshohocken, PA

Barbour SL, Yang N (1993) A review of the influence of clay–brine interactions on the geotechnical properties of Ca-montmorillonitic clayey soils from western Canada. Can Geotech J 30:920–934

Bjerrum L (1954) Geotechnical properties of Norwegian marine clays. Géotechnique 4:49–69

Blatz JA (2000) Elastic–plastic modeling of unsaturated high plastic clay using results from a new triaxial test with controlled suction. Ph.D. thesis, Department of Civil Engineering. The University of Manitoba, Winnipeg, MB

Blatz JA, Graham J (2003) Elastic plastic modelling of unsaturated high-plastic clay using results from a new triaxial test with controlled suction. Géotechnique 53(1):113–122

Blatz JA, Anderson D, Siemens GA (2007) Evaluation of elastic–plastic model parameters for two unsaturated compacted bentonite mixtures. Can Geotech J 44:436–446

Di Maio C (1996) Exposure of bentonite to salt solution: osmotic and mechanical effects. Géotechnique 46:695–707

Di Maio C, Fenelli GB (1994) Residual strength of kaolin and bentonite: the influence of their constituent pore fluid. Géotechnique 44(2):217–226

Gens A, Sánchez M, Do L, Guimarães N, Alonso EE, Lloret A, Olivella S, Villar MV, Huertas F (2009) A full-scale in situ heating test for high-level nuclear waste disposal: observations, analysis and interpretation. Géotechnique 59(4): 377–399

Gierszewski P, Avis J, Calder A, D'Andrea A, Garisto F, Kitson C et al (2004) Third case study-post closure safety assessment. Ontario Power Generation, Toronto, Ontario Nuclear Waste Management Division Report 06819-REP-01200-10109-R00

Graham J (2006) The 2003 R.M. Hardy lecture: soil parameters for numerical analysis in clay. Can Geotech J 43:187–209

Graham J, Noonan ML, Lew KV (1983) Yield states and stress–strain relationships in a natural plastic clay. Can Geotech J 20:502–516

Graham J, Saadat F, Gray MN, Dixon DA, Zhang QY (1989) Strength and volume change behaviour of a sand–bentonite mixture. Can Geotech J 26:292–305

Graham J, Saadat F, Gray MN (1990) High-pressure triaxial testing on the Canadian reference buffer material. Eng Geol 28:391–403

Graham J, Oswell JM, Gray MN (1992) The effective stress concept in saturated sand–clay buffer. Can Geotech J 29:1033–1043

Johannesson L-E, Börgesson L, Goudarzi R, Sandén T, Gunnarsson D, Svemar C (2007) Prototype repository: a full scale experiment at Äspö HRL. Phys Chem Earth 32: 58–76

Kenny TC (1967) The influence of mineral composition on the residual strength of natural soils. In: Proceedings of the geotechnical conference, Oslo, vol 1, pp 123–129

Man A, Graham J (2010) Pore fluid chemistry, stress–strain behaviour, and yielding in reconstituted highly plastic clay. Eng Geol 116:296–310

Matsuo S (1957) A study of the effect of cation exchange on the stability of slopes. In: Proceedings of 4th international conference on soil mechanics and foundation engineering, London, vol 1, pp 330–333

Mazurek M (2004) Long-term used nuclear fuel waste management. Geoscientific review of the sedimentary sequence in southern Ontario. Institute of Geological Sciences, University of Bern, Technical Report TR04-01, Bern Switzerland, available from Nuclear Waste Management Organisation, Toronto, Canada
Mitchell JK (1993) Fundamentals of soil behaviour, 2nd edn. Wiley, New York
Moore R (1991) The chemical and mineralogical controls upon the residual strength of pure and natural clays. Géotechnique 41:35–47
Moore R (1992) Discussion: the chemical and mineralogical controls upon the residual strength of pure and natural clays. Géotechnique 42:151–153
Moum J, Rosenqvist IT (1961) Mechanical properties of montmorillonite and illite clays related to electrolytes of the pore water. In: Proceedings of 5th international conference on soil mechanics and foundation engineering, Paris, vol 1, pp 263–267
NWMO (2005) Choosing a forward: the future management of Canada's used nuclear fuel, final study. Annual Report, Nuclear Waste Management Organization, Toronto, Canada
Oswell JM (1991) Elastic plastic behaviour of a sand–bentonite mixture. Ph.D. thesis, Department of Civil Engineering, The University of Manitoba, Winnipeg, MB
Pearson FJ Jr (1985) Geochemical and isotopic evidence on the origin of brines in the Canadian Shield. Report by Intera Tech. Inc., Tex., for Atomic Energy of Canada Limited, WNRE, Pinawa, MB
Priyanto DG, Blatz JA, Siemens GA, Offman R, Powell JS, Dixon DA (2008) The effects of fluid composition on the one-dimensional consolidation behaviour of clay based sealing materials. Nuclear Waste Management Organization Report NWMO TR-2008-20. Toronto, Canada
Pusch R (2001) The buffer and backfill handbook, part 2: materials and techniques, SKB, TR-02-12. Stockholm
Ramiah BK, Dayalu NM, Purushothamaraj P (1970) Influence of chemicals on residual strength of silty clay. Soils Found 10:25–36
Romero E, Villar MV, Lloret A (2005) Thermo-hydro-mechanical behaviour of two heavily overconsolidated clays. Eng Geol 81:255–268
Rosenqvist ITh (1953) Considerations on the sensitivity of Norwegian quick clays. Géotechnique 3:195–200
Saadat F (1989) Consecutive modelling of the behaviour of a sand–bentonite mixture. Ph.D. thesis, Department of Civil Engineering, The University of Manitoba, Winnipeg, MB
Siddiqua S, Blatz J, Siemens G (2011a) Evaluation of the impact of pore fluid chemistry on the hydromechanical behaviour of clay-based sealing materials. Can Geotech J 48(2): 199–213
Siddiqua S, Blatz J, Siemens G (2011b) Experimental study on the performance of light and dense backfills. Can Geotech J 48(2):214–225
Siemens GA, Blatz JA (2007) A triaxial apparatus for applying liquid infiltration with controlled boundary conditions and internal suction measurement. J Geotech Geoenviron Eng 133(6):748–752
Siemens GA, Blatz JA (2009) Evaluation of the influence of boundary confinement on the behaviour of unsaturated swelling clay soils. Can Geotech J 46(3):339–356
Skempton AW, Northey RD (1952) The sensitivity of clays. Géotechnique 1:1–30
Steward HE, Cripps JC (1983) Some engineering implications of chemical weathering of pyritic shale. Q J Eng Geol Hydrogeol 16:281–289
Sun BCC (1986) Stress–strain properties in sand–clay buffer materials. M.Sc. thesis, Department of Civil Engineering, The University of Manitoba, Winnipeg, MB
Tang GX (1999) Suction characteristics and elastic–plastic modelling of unsaturated sand–bentonite mixture, Ph.D. thesis, Department of Civil Engineering, The University of Manitoba, Winnipeg, MB
Tang GX, Graham J, Blatz J, Gray M, Rajapakse RKND (2002) Suctions, stresses and strengths in unsaturated sand–bentonite. Eng Geol 64:147–156
Tang CS, Tang AM, Cui YJ, Delage P, Schroeder C, Shi B (2011) A study of the hydro-mechanical behaviour of compacted crushed argillite. Eng Geol 118:93–103
Thomas HR, Cleall PJ, Chandler N, Dixon D, Mitchell HP (2003) Water infiltration into a large-scale in situ experiment in an underground research laboratory. Géotechnique 53(2):207–224
Villar MV, S'anchez M, Gens A (2008) Behaviour of a bentonite barrier in the laboratory: experimental results up to 8 years and numerical simulation. Phys Chem Earth 33:S476–S485
Wan AWL (1996) The use of thermocouple psychrometer to measure in situ suctions and water content in compacted clays. Ph.D. thesis, Department of Civil Engineering, The University of Manitoba, Winnipeg, MB
Warkentin BP, Yong RN (1962) Shear strength of montmorillonite and kaolinite. Clays Clay Miner 9:210–218
Winterkorn HF, Moorman RBB (1941) A study of changes in physical properties of Putnam soil induced by ionic substitution. In: Proceedings of highway research board, vol 21, pp 415–434
Yin JH (1990) Constitutive modelling of time-dependent stress–strain behaviour of soils. Ph.D. thesis, Department of Civil Engineering, The University of Manitoba, Winnipeg, MB
Yong RN, Mohamed AMO, Warkentin BP (1992) Principles of contaminant transport in soils. Elsevier, Amsterdam

APPENDIX L – PUBLISHED CONFERENCE PAPERS

Lim, B.F., Siemens, G., Boyle, J.S., Remenda, V. and Take, A. 2008. Numerical analysis of expansive soil behaviour using the swell equilibrium limit. The 61st Canadian Geotechnical Conference, Edmonton, Alberta: 176-81.

Numerical analysis of expansive soil behaviour using the Swell Equilibrium Limit

Bee Fong Lim[1], Greg Siemens[1], J. Suzanne Boyle[2], Vicki Remenda[2] & Andy Take[3]
[1]*Department of Civil Engineering – Royal Military College of Canada, GeoEngineering Centre at Queen's-RMC, Kingston, Ontario, Canada*
[2]*Department of Geological Sciences & Geological Engineering – Queen's University, GeoEngineering Centre at Queen's-RMC, Kingston, Ontario, Canada*
[3]*Department of Civil Engineering – Queen's University, GeoEngineering Centre at Queen's-RMC, Kingston, Ontario, Canada*

ABSTRACT
Soil deformation in swelling clay often cause excessive ground movements and swell pressures on adjacent structures. The excessive deformation could cause adverse impacts on the integrity of a structure. Siemens and Blatz (2008a) proposed a new method to describe swelling soil behaviour which is known as the Swelling Equilibrium Limit (SEL). The proposed method captures the behaviour of expansive soil under the boundary conditions ranging from constant stress to constant volume. In the field, soil expansion is subjected to a wide influence of the boundary conditions that may be captured by the SEL. In this paper, a numerical analysis is completed to show how the SEL can be used to analyze foundations constructed in swelling soil. The numerical model is first calibrated to laboratory swell tests on Bearpaw Formation. Following calibration with the experimental data, the model is used to investigate soil deformations and induced-stresses of a basement foundation during wetting conditions. Sensitivity analysis was performed to determine the influence of model parameters.

RÉSUMÉ
La déformation des sols dans les argiles gonflantes causent souvent des pressions et des déplacements excessifs. La déformation excessive peut avoir des effets néfastes sur une structure. Siemens et Blatz (2008a) ont proposé une nouvelle méthode pour décrire le comportement des sols gonflants, connue sous le nom de Limite de Gonflement à l'Équilibre (LGE). La méthode proposée capte le comportement d'un sol gonflant sous des conditions limites allant de "contraintes constantes" à "volume constant". Sur le terrain, le gonflement est assujettis à une vaste gamme de conditions limites qui peuvent être captées par la LGE. Dans cet article, une analyse numérique est effectuée pour montrer comment la LGE peut être utilisée pour l'étude des fondations construites dans les sols gonflants. La LGE est tout d'abord calibrée contre des essais de gonflements réalisés sur du Formation de Bearpaw. Par la suite, le modèle est utilisé pour étudier les déplacements d'une fondation durant des conditions de mouillage. Une analyse de sensibilité à été réalisée pour déterminer l'influence des paramètres du modèle.

1 INTRODUCTION

Structures constructed in expansive soil can be subjected to excessive swell-induced deformation or pressure which would adversely affect the structure's integrity. Engineered design should account for swell-induced impacts in order to avoid or minimize the cost of repairing the damage caused.

The evidence of damage caused by swelling to a residential basement is demonstrated in Figure 1. Cracking of floor slab is commonly seen as evidence of neglecting swelling considerations in expansive soil. If damage caused are not taken care of in a timely manner more serious structural defects can occur.

The objective of this paper is to present a practical design analysis that includes swell-induced effects. Recent insight gained from the research in expansive soil provides a different perspective from the conventional consideration. A new relationship termed the 'Swell Equilibrium Limit' (SEL) by Siemens and Blatz (2008a) is capable of describing general swelling soil behaviour in a broader perspective. Traditionally the conventional one-dimensional oedometer test measures the swell pressure and the amount of vertical heave (ASTM 4546). Swelling behaviour between the two extreme boundaries is not normally well defined in oedometer test. The SEL provides a general limit to swelling induced stresses and displacements. In this paper an example analysis using the Finite Element Method (FEM) is performed displaying use of the SEL in the foundation design. Oedometer results are converted into the SEL framework and then the SEL is used to predict equilibrium stresses and deformations on a foundation constructed in swelling soil.

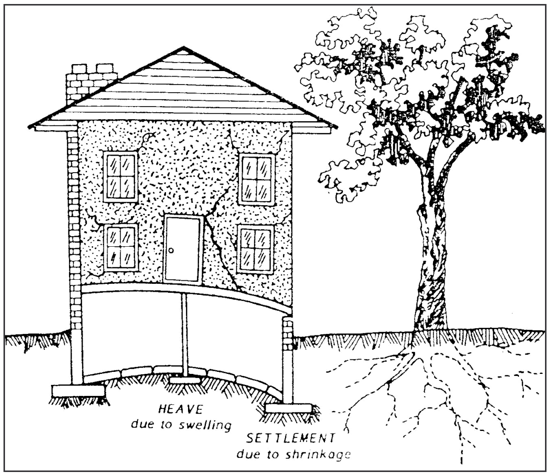

Figure 1. Damage to houses caused by ground movements of swelling soils (Domaschuk, 1986).

2 SWELL EQUILIBRIUM LIMIT (SEL)

The Swell Equilibrium Limit (SEL) forms a limit to expansion and swelling-induced stresses during wetting (Siemens and Blatz 2008a). It is a characteristic curve for each expansive soil depending on montmorillonite content and dry density. The SEL for bentonite-sand-buffer is plotted in Figure 2 in specific volume – mean stress space. It forms a limit to volume expansion and swelling-induced stress when the swell potential of the soil comes into equilibration with the imposed hydraulic and mechanical boundary conditions. The new relationship was discovered through the testing of highly expansive soil (bentonite-sand-buffer (BSB)) under the influence of controlled infiltration boundary conditions in an automated triaxial infiltration test (Siemens 2006, Siemens and Blatz 2008a). The SEL defines equilibrium swelling soil behaviour ranging from maximum expansion to maximum swelling induced stress.

2.1 Stress Paths to reach the Swell Equilibrium Limit

The conventional oedometer test captures the swell-induced response in either free swelling or constant volume conditions in the vertical direction (ASTM 4546). The soil behaviour in between these two extremes is not normally defined. The newly developed automated triaxial apparatus (Siemens and Blatz 2008a) is able to apply general boundary conditions to the tested specimen during infiltration.

A schematic plot of the stress paths in the automated triaxial test is shown in Figure 3. In the triaxial infiltration test free swell is referred to as 'constant mean stress' (CMS) where no constraint of volume change is imposed to the specimen. Fully constrained volume change in the triaxial test is termed as 'constant volume' (CV) where the specimen is subjected to high confining pressure in order to maintain the specimen's original volume. The interim condition, termed 'constant stiffness' (CS) boundary condition, acts as a flexible spring-type boundary condition under which both expansion and swelling-induced pressures are applied.

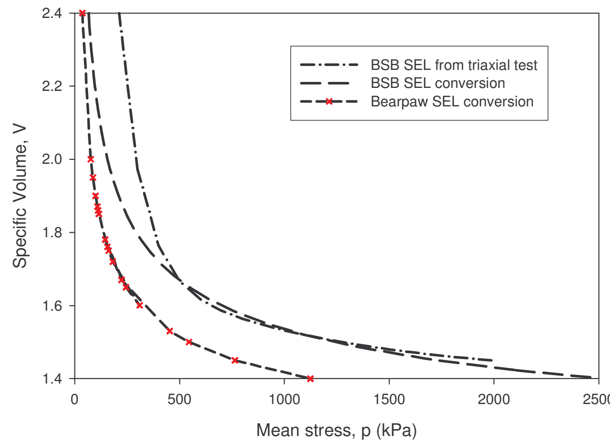

Figure 2. The Swell Equilibrium Limit (SEL) plotted in specific volume versus mean stress space.

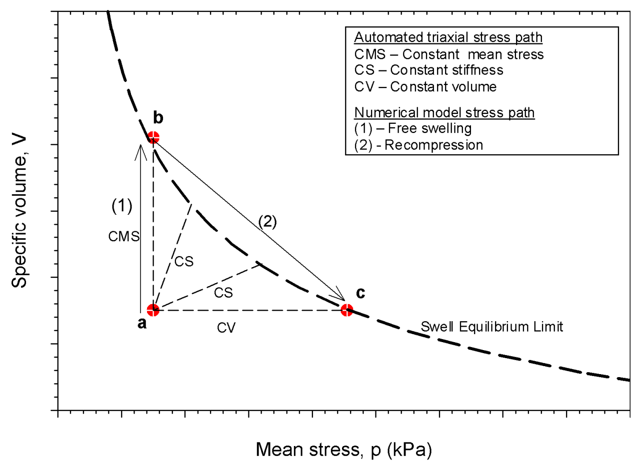

Figure 3. Boundary conditions applied in automated triaxial infiltration test and numerical model in specific volume versus mean stress space.

The SEL is directly defined by a curve fitting of all the 'end of test' experimental data points. The 'end of test' points indicate the final state of soil when the swelling potential comes into equilibrium under the imposed conditions. In addition, the SEL was shown to agree with one-dimensional swell pressure tests. Siemens and Blatz (2008a) successfully converted a swell pressure relationship given by Dixon et al. (2002) to compare with the SEL plot as shown in Figure 2. The relationship provided by Dixon et al. (2002) correlates one-dimensional swell pressures with the 'effective montmorillonite dry density' (EMDD). Siemens and Blatz (2008a) detail the process to convert the swell pressure – EMDD to an equivalent mean stress using an assumption of elasticity. The converted curve from Dixon et al. (2002) shows remarkable well comparison to the SEL curve.

The current study shows how traditional one-dimensional swell tests can be used in design in the SEL context. Traditional swell pressure tests were completed and the results used to predict swelling induced stresses and deformations on foundation footings and walls. Test data is obtained from an on-going research project (Boyle 2007) in which a series of one-dimensional swell pressure measurements have been made on samples of the Bearpaw Formation, an extensive, Cretaceous-age, clayey silt bedrock unit in southern Saskatchewan. Although examples of foundations constructed in Bearpaw are limited, the purpose of the paper is to display a design procedure for expansive soils. Using a similar process as detailed in Siemens and Blatz (2008a) and Siemens (2006), a preliminary SEL for Bearpaw was found and plotted in Figure 2. Comparing the BSB and Bearpaw SEL curves, the clay and montmorillonite content of BSB is higher than Bearpaw and it has a greater dry density (lower specific volume), hence the SEL curve of BSB is reasonably located at a higher point in the volume-stress plot. Higher swelling potential results in greater equilibrium induced-pressures and volume change. Given initial stress and volume conditions, the SEL is used to predict the swell-induced soil behaviour given initial soil conditions and boundary conditions that are defined by the foundation application.

3 NUMERICAL MODEL USING THE SWELL EQUILIBRIUM LIMIT

The finite element programs used in this paper are SIGMA/W and SEEP/W from GeoStudio 2007. The stress distribution and volume change are analysed in SIGMA/W while the pore water pressure distribution is generated in SEEP/W. The numerical analysis begins with calibration of the experimental data (oedometer) using the concept of the SEL.

3.1 Insitu Analysis

The insitu analysis step builds in the initial stresses in the model. The initial condition is set-up by axis-symmetric (half-space model) 'insitu' analysis with the boundaries applied as per the oedometer test. As the soil specimen is constrained laterally in the oedometer ring both sides of the model boundaries are constrained horizontally but allowed to move vertically. A linear elastic model with Young's Modulus, E=50 MPa (Hanna and Little, 1992) and Poisson's ratio, ν = 0.2 was used for this step. The insitu stress field is used as the initial stress condition for the subsequent free swell analysis.

3.2 Free Swell Analysis

The free swelling process is modeled by the change in pore water pressure from unsaturated (with initial suction) to saturated (hydrostatic pressure) condition. Free swell in the numerical model is comparable to 'constant mean stress' in the SEL plot. The maximum volume change can be anticipated by the SEL curve where the soil will follow a vertical stress path from point 'a' to 'b' (Figure 3) until it reaches the SEL line.

In order to allow the soil to expand to the desired volume change, the soil stiffness is varied in the model until the amount of heave matches the prediction of the SEL curve. The free swell stiffness with respect to the predicted heave in numerical model is termed '$E_{free\ swell}$'.

For the laboratory study specimens were taken from a depth of 45 to 90m and had an unknown initial suction following removal from the insitu condition. The influence of the initial pore water pressure distribution was examined by varying three different suction levels (Δsuction), namely, 600kPa, 1000kPa and 1500kPa. Interestingly, the ratio of $E_{free\ swell}/\Delta$suction obtained from the numerical model is 5 for all the three different suction levels. A constant ratio was anticipated since the same displacement was modelled for each case.

There is inadequate test results on the material properties under the influence of different suctions in the current paper. Nevertheless, the study by Blatz et al. (2002) shows that increasing suction appears to have significant influence on the initial stiffness of the material. In future tests, initial suction will be measured and the final $E_{free\ swell}$ will be known.

3.3 Recompression Analysis

The 'constant volume' stress path (from point 'a' to point 'c' in Figure 3) can not be modeled directly in this type of numerical analysis since the swell pressure is generally less than the change in suction. Therefore, a recompression step is required to compress the swelled soil back to the original volume (from point 'b to point 'c') to simulate the 'constant volume' stress path.

The objective of the recompression model is to reach the final state which is defined as point 'c' in the SEL plot. The known heave displacement from the previous free swell model is applied to the recompression model in a separate 'load/deformation' analysis. When the soil element is recompressed under hydrostatic conditions the swell-induced pressure can be related to effective vertical stress in the model. The material stiffness is varied until the effective vertical stress matches the measured swell pressure from the lab. The stiffness specified at this stage is termed as '$E_{recompression}$'.

$E_{recompression}$ from the analyses of the three different suction levels is constant ($E_{recompression}$ = 1164kPa). This is due to all recompression analyses compressing the same amount of heave under a hydrostatic pore water pressure distribution (eg, ponding).

For an initial suction value of 1500 kPa, the $E_{free\ swell}$ and $E_{recompression}$ of the expansive soil obtained from the numerical analysis is 7500kPa and 1164kPa, respectively. For the three initial suction levels applied, the ratio of $E_{free\ swell}/E_{recompression}$ is in the range of 2.6 to 6.4. A range is anticipated since the deformation amounts remain the same while the initial suction level is altered.

4 APPLICABILITY OF THE SWELL EQUILIBRIUM LIMIT IN PRACTICAL DESIGN

The applicability of the SEL in predicting the expansive soil response is shown in a basement foundation model. The soil below the basement would be under a 'constant mean stress' path because there is no significant constraint on the soil movement. Soil adjacent to the basement wall is likely to follow the 'constant stiffness' or 'constant volume' stress path. Soil movement is constrained by the stiff retaining system used in the basement wall.

Following a similar procedure as in the oedometer calibration, the SEL is used to predict vertical and horizontal deformation and swelling-induced stresses adjacent to the basement wall.

4.1 Modelling of a Basement Foundation

Swelling mechanisms induce volume change and stresses in the soil. The degree of change is observed as wall displacement and basement heave in the model. The magnitude of soil displacement indicates the amount of soil expansion when swelling occurs. The soil deformation result obtained from 'volume change' analysis assumed the pore water pressure distribution changed from unsaturated to saturated condition.

A foundation was analysed in a half space two-dimensional finite element mesh. The dimension of the basement was 2.5m in depth and 10m in total width. Initial groundwater table was assumed at 7.5m depth. Parameters including initial suction level, $E_{free\ swell}$ and $E_{recompression}$ used in the basement model were taken from the previous calibration exercise. A similar model process including insitu, free swell and recompression steps were followed.

A worst case scenario was simulated as ponding where the initial suction is lost due to the infiltration and inundation in the basement. The change in pore water pressure from dry condition (initial suction) to wet condition (saturation) simulates the swelling phenomenon in the expansive soil. This is an extreme event that could occur during an extended rainfall event or locally around the basement if proper drainage is not ensured.

Besides soil deformation, swell-induced stress on the adjacent structure (eg, basement wall) is another good indication on how much additional pressure has been exerted on the structure in addition to the mechanical loadings from the building and the retained soil. Stress and strain are the two fundamental variables in engineering design. Therefore, it is essential to look into the modelling result in these two particular aspects. The study of swelling soil behaviour in this paper is focused on the basement wall displacement, basement heave and swell-induced pressure on the wall.

4.2 Soil Deformation in Basement Foundation

When the soil in the basement swells, wall displacement and basement heave are the primary concerns in the engineered design. Structures should be checked for their deformation tolerance and serviceability limit during the functional design life.

Following definition of initial stresses and suction, a 'free swell' analysis was performed on an 'open' basement excavation. An initial suction of 1500, 1000 or 600kPa was applied at the surface and the bottom boundary condition (at the depth of 25m) was at the water table of 7.5m depth.

The unrestrained horizontal displacement due to ponding is shown in Figure 4. The highest horizontal wall displacement is estimated at 753mm at the top of the wall while the maximum basement heave is approximately 91mm at the centre of basement.

The influence of suction on soil deformation is investigated in Figure 5. A normalised plot of suction levels versus the swell-induced wall displacement is illustrated. At the lowest initial suction of 600kPa, the increase in wall displacement is close to 18% compared to the maximum wall deformation of 1500kPa initial suction. The slope of the linear relationship in the plot is 0.03. This shows the model is relatively insensitive to changes in the initial condition. This is anticipated since the $E_{free\ swell}$ value for each model was calibrated using the oedometer results.

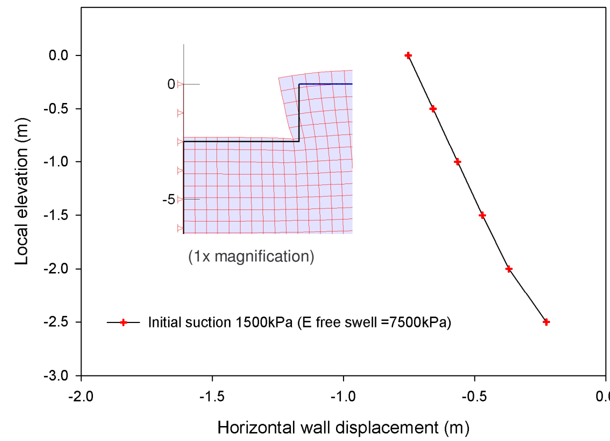

Figure 4. Horizontal wall displacement due to ponding at basement foundation.

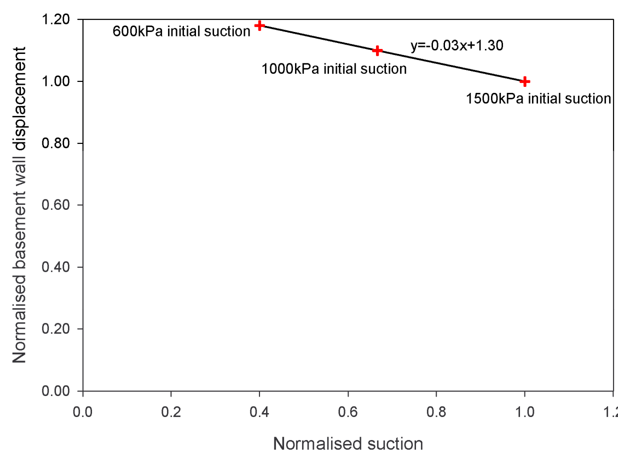

Figure 5. Normalised suction versus normalised wall displacement.

An analysis on the effects of varying depths of expansive soil layer on the amount of heave was also carried out. In Figure 6, the result of heave is normalised with respect to the heave in 25m full depth of expansive soil layer. The result shows that, as anticipated, as the depth of expansive soil layer increases the amount of heave increases. The heave of the 12.5m deep expansive layer

(50% of the full depth) is approximately 40% of the maximum heave.

Plotting the normalised depth of expansive layer versus normalised maximum vertical displacement (heave) at the basement foundation, Figure 7 shows the model behaves as expected. The positive slope of the fitted curve indicates greater deformations will occur in foundations constructed in thicker expansive layers.

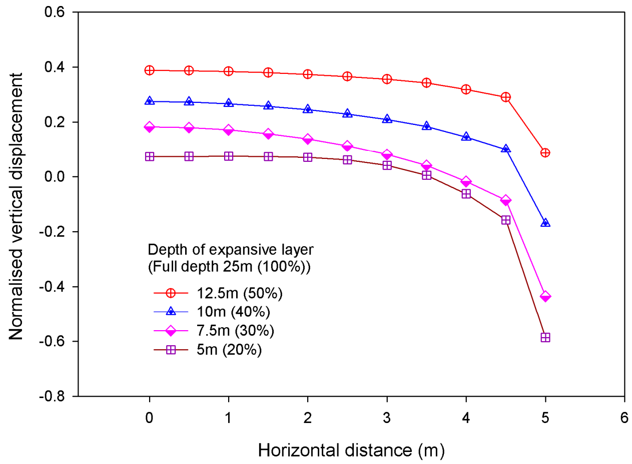

Figure 6. Normalised vertical displacement at basement foundation with respect to the vertical heave that occurs at 25m depth of expansive soil.

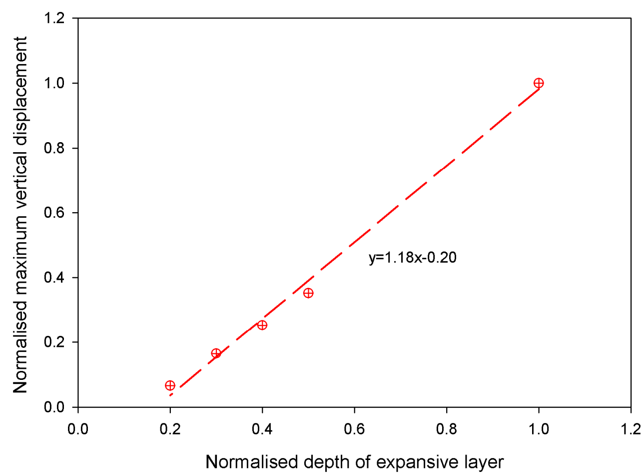

Figure 7. Normalised depth of expansive layer versus normalised maximum vertical displacement at the basement foundation.

4.3 Swell-induced Pressure and the Constant Stiffness Stress Path

The swell-induced pressure on the basement wall was investigated through the recompression model in the analysis. Commonly the basement wall would be designed with either timber or concrete materials depending on the suitability and the estimated lateral pressure on the wall. The stiffer material such as reinforced concrete will tend to have reduced displacements but corresponding increased horizontal pressures.

According to the SEL concept, the ‘constant stiffness’ stress path (Figure 3) represents different degrees of volume confinement in the soil. Recompressing the swelling soil back to the original volume is regarded as ‘full recompression’. To simulate varying confinement conditions the soil was recompressed partially back to 40% or 70% of the full displacement. As shown in Figure 3 the SEL is non-linear. Partially recompresion using a constant stiffness will therefore provide a conservative over estimation of the swelling induced stresses.

Swelling-induced stresses occur due to restrained boundary conditions. The results of swell pressure on the basement wall are presented in Figure 8. The maximum swell-induced pressure of full recompression is approximately 209kPa which is very close to the measured swell pressure obtained from the lab test.

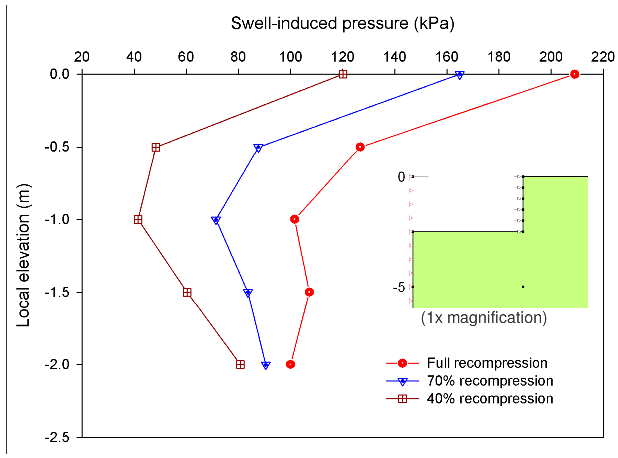

Figure 8. Swell-induced pressure on the basement wall with varying degree of recompression.

Figure 8 shows that as the degree of recompression decreases (more movement is allowed), the corresponding pressure of the wall decreases. It is a reasonable soil response since less pressure is induced when the soil deformations increase (less recompression).

The swell pressure of the basement wall was normalized to the maximum swell pressure and plotted versus varying degree of recompression. Figure 9 exhibits a linear relationship with a positive slope indicating a direct relationship between swelling induced pressure and recompression.

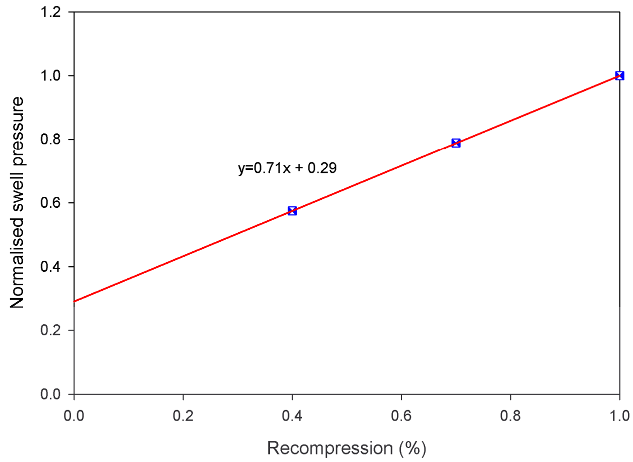

Figure 9. Normalised swell pressure versus varying degree of recompression.

With the predicted soil deformations and swell-induced pressures a better engineered structure can now be designed if the worst case condition (eg, ponding) would ever occur to the structure constructed in expansive soil.

5 CONCLUSIONS

Neglecting swelling effects in highly swelling soil will inevitably cause unforeseen maintenance costs in the future. This paper developed a method for using the Swell Equilibrium Limit for design of a foundation in swelling soil. It should be noted that this is a preliminary study and that the predicted pressures and displacements must be verified with field data.

The parameters used in this model provide realistic insight to the soil behaviour. The excessive soil deformation and swell pressure predicted by the SEL should be taken as a design consideration for structures constructed in high swelling potential ground.

Precautionary measures could include either reinforcing the structures with the anticipated deformation and stress or properly managing the drainage system in order to avoid excessive water ingress into the soil.

REFERENCES

Blatz, J.A., Graham, J. and Chandler, N.A. 2002. Influence of suction on the strength and stiffness of compacted sand–bentonite. *Canadian Geotechnical Journal, 39*, 1005-1015.

Boyle, J. S. 2007. Reassessing the current geologic model for the deposition and stress history of cretaceous clays in Southern Saskatchewan. Proceeding of *2nd Canadian Young Geotechnical Engineers and Geoscientists Conference (cYGEGC).*

Byrne, P.J.S. and Farvolden, R.N. 1959. The clay mineralogy and chemistry of the Bearpaw formation of Southern Alberta. *Research Council of Alberta, Geological Division,* Bulletin 4, 1-44.

Dixon, D.A., Chandler, N.A., and Baumgartner, P. 2002. The influence of groundwater salinity and influences on the performance of potential backfill materials. *In* Proceedings of *the 6th International Workshop on Design and Construction of Final Repositories, Backfilling in Radioactive Waste Disposal,* Brussels, March 2002. ONDRAF/NIRAS. Transactions, Session IV, paper 9.

Hanna, A. and Little, T.E. 1992. An estimate of rebound potential of the Shaftesbury Shales at a damsite in British Columbia. *Canadian Geotechnical Journal, 29*, 375-392.

Siemens, G.A. and Blatz, J.A. 2008a. Evaluation of the influence of boundary confinement on the behaviour of unsaturated swelling clay soils. *Canadian Geotechnical Journal (In review)*

Siemens, G.A. and Blatz, J.A. 2008b. Numerical modelling of shallow foundations on swelling clay soil using the Swelling Equilibrium Limit. *Submitted to* The 1st European Conference on Unsaturated Soils. (*In press*)

Siemens, G.A. 2006. The influence of boundary conditions on the hydraulic-mechanical behaviour of an unsaturated swelling soil. Ph.D. Thesis, Department of Civil Engineering, University of Manitoba, Winnipeg, MB. Available for download at http://www.collectionscanada.ca/obj/s4/f2/dsk3/MWU/TC-MWU-262.pdf

Sridharan, A., and Gurtug, Y. 2004. Swelling behaviour of compacted fine-grained soils. *Engineering Geology, 72*, 9-18.

Tripathy, S., Rao, K.S.S., and Fredlund, D.G. 2002. Water content-void ratio swell-shrink paths of compacted expansive soils. *Canadian Geotechnical Journal, 39*, 938-959.

Wong, R. C. K. 1998. Swelling and softening behaviour of La Biche Shale. *Canadian Geotechnical Journal,* (35), 206-221.